

University of Louisville

## ThinkIR: The University of Louisville's Institutional Repository

---

Electronic Theses and Dissertations

---


12-2014

# Boundary contour based surface representation.

Yong Su

*University of Louisville*

Follow this and additional works at: <https://ir.library.louisville.edu/etd>

 Part of the [Nervous System Commons](#), [Neuroscience and Neurobiology Commons](#), [Ophthalmology Commons](#), and the [Physiology Commons](#)

---

### Recommended Citation

Su, Yong, "Boundary contour based surface representation." (2014). *Electronic Theses and Dissertations*. Paper 1737.  
<https://doi.org/10.18297/etd/1737>

This Doctoral Dissertation is brought to you for free and open access by ThinkIR: The University of Louisville's Institutional Repository. It has been accepted for inclusion in Electronic Theses and Dissertations by an authorized administrator of ThinkIR: The University of Louisville's Institutional Repository. This title appears here courtesy of the author, who has retained all other copyrights. For more information, please contact [thinkir@louisville.edu](mailto:thinkir@louisville.edu).

# BOUNDARY CONTOUR BASED SURFACE REPRESENTATION

By

Yong Su

B.S. and B.E., University of Science and Technology of China, 1999

A Dissertation

Submitted to the Faculty of the

College of Arts and Sciences of the University of Louisville

in Partial Fulfillment of the Requirements

for the Degree of

Doctor of Philosophy

Department of Psychological and Brain Sciences

University of Louisville

Louisville, KY

December, 2014



# BOUNDARY CONTOUR BASED SURFACE REPRESENTATION

By

Yong Su

A Dissertation Approved on

September 30, 2014

by the following Dissertation Committee:

---

Zijiang He, Ph.D.

Dissertation Chair

---

John Pani, Ph.D.

---

Paul DeMarco, Ph.D.

---

Sandra Sephton, Ph.D.

---

Pavel Zahorik, Ph.D.

## ACKNOWLEDGMENTS

I would like to thank my mentor and dissertation committee chair, Dr. Zijiang He, for his guidance and patience over the years. I would like to thank the other committee members, Dr. John Pani, Dr. Paul DeMarco, Dr. Sandra Sephton, and Dr. Pavel Zahorik, for their assistance and supports. I would also like to thank Dr. Teng Leng Ooi, who acted as my adviser during the years when I was conducting many of my experiments at Salus University, Pennsylvania. Finally, I would like to express my thanks to my wife, Jing, for her understanding and patience. She went through those difficult times with me and always helped me sort my life out.

ABSTRACT  
BOUNDARY CONTOUR BASED SURFACE REPRESENTATION

Yong Su

Sep 30, 2014

We receive most information about our surrounding space and objects through the eyes. To reconstruct the 3D space and objects in the visual system from the 2D retinal images, surface representation must be a critical intermediate stage in the visual processing stream. It is hypothesized in the dissertation that the visual system represents textured surface by a border-to-interior strategy: boundary contours would be encoded first and then border-ownership assignments would be resolved. This process would solve the related problems such as figure-ground segregation, surface depth relationship, occlusion, transparency, etc. As a result, the boundary contours of the surfaces would be well defined and then the visual system could register the local features in different domains with the boundary contours, gradually from the adjacent areas of the boundary contours to the interior of the surfaces. To testify this hypothesis in the current proposal, a monocular boundary contour (MBC) paradigm is adapted from earlier studies by Ooi and He (2005, 2006). In Chapter 1, the boundary-contour-based hypothesis, with the MBC paradigm, is used to re-address a decade-long debate about binocular vision: whether (and how) binocular integration and inhibition coexist. In Chapter 2–5, the MBC-induced binocular suppression is systematically investigated, especially in Chapter 3 where the cortical speed of the hypothesized border-to-interior spreading is quantitatively estimated. In the end, the rules how the surface fragments are integrated to a global representation is further studied in Chapter 6 and 7, especially focusing on the role of luminance and color contrast polarities.

## TABLE OF CONTENTS

ACKNOWLEDGMENTS.....	iii
ABSTRACT.....	iv
LIST OF FIGURES.....	ix
GENERAL INTRODUCTION.....	1
CHAPTER I.....	7
INTRODUCTION.....	7
METHODS.....	11
Experiment 1.1.....	11
Experiment 1.2.....	12
Control Experiment 1.1.....	12
Experiment 1.3.....	13
Experiment 1.4.....	13
Control Experiment 1.2.....	13
RESULTS.....	14
Experiment 1.1.....	14
Experiment 1.2 and Control Experiment 1.1.....	14
Experiment 1.3.....	16
Experiment 1.4 and Control Experiment 1.2.....	16
DISCUSSION.....	17
CHAPTER II.....	20
INTRODUCTION.....	20
METHODS.....	24

Experiment 2.1.....	24
Experiment 2.2.....	28
Experiment 2.3.....	29
Experiment 2.4.....	32
RESULTS.....	33
Experiment 2.1.....	33
Experiment 2.2.....	35
Experiment 2.3.....	36
Experiment 2.4.....	37
DISCUSSION.....	38
CHAPTER III.....	41
INTRODUCTION.....	41
METHODS.....	46
Experiment 3.1.....	46
Experiment 3.2.....	51
RESULTS.....	52
Experiment 3.1.....	53
Experiment 3.2.....	55
DISCUSSION.....	57
CHAPTER IV.....	60
INTRODUCTION.....	60
METHODS.....	64
Experiment 4.1.....	65
Experiment 4.2.....	66
RESULTS.....	71
Experiment 4.1.....	71



Experiment 4.2.....	72
DISCUSSION.....	74
CHAPTER V.....	78
INTRODUCTION.....	78
METHODS.....	80
RESULTS.....	86
DISCUSSION.....	92
CHAPTER VI.....	94
INTRODUCTION.....	94
METHODS.....	99
Experiment 6.1.....	100
Experiment 6.2.....	102
Experiment 6.3.....	104
RESULTS.....	106
Experiment 6.1.....	106
Experiment 6.2.....	107
Experiment 6.3.....	108
DISCUSSION.....	108
CHAPTER VII.....	113
INTRODUCTION.....	113
METHODS.....	115
Experiment 7.1.....	116
Experiment 7.2.....	117
Experiment 7.3.....	118
Experiment 7.4.....	120
Experiment 7.5.....	121

RESULTS.....	122
Experiment 7.1.....	122
Experiment 7.2.....	123
Experiment 7.3.....	125
Experiment 7.4.....	126
Experiment 7.5.....	127
DISCUSSION.....	128
REFERENCES.....	132
APPENDIX I: FIGURES.....	152
APPENDIX II: COPYRIGHT CLEARANCE.....	198
CURRICULUM VITA.....	203

## LIST OF FIGURES

### CHAPTER I

Fig. 1.1.....	152
Fig. 1.2.....	153
Fig. 1.3.....	153
Fig. 1.4.....	154
Fig. 1.5.....	155
Fig. 1.6.....	155
Fig. 1.7.....	156

### CHAPTER II

Fig. 2.1.....	157
Fig. 2.2.....	158
Fig. 2.3.....	159
Fig. 2.4.....	160
Fig. 2.5.....	161
Fig. 2.6.....	162

### CHAPTER III

Fig. 3.1.....	163
Fig. 3.2.....	164
Fig. 3.3.....	165
Fig. 3.4.....	166
Fig. 3.5.....	167

### CHAPTER IV

Fig. 4.1.....	168
Fig. 4.2.....	169
Fig. 4.3.....	170
Fig. 4.4.....	171

### CHAPTER V

Fig. 5.1.....	172
Fig. 5.2.....	173
Fig. 5.3.....	174
Fig. 5.4.....	175
Fig. 5.5.....	176
Fig. 5.6.....	177

Fig. 5.7.....	178
Fig. 5.8.....	179
Fig. 5.9.....	180
Fig. 5.10.....	181

#### CHAPTER IV

Fig. 6.1.....	182
Fig. 6.2.....	182
Fig. 6.3.....	183
Fig. 6.4.....	183
Fig. 6.5.....	184
Fig. 6.6.....	185
Fig. 6.7.....	186
Fig. 6.8.....	187
Fig. 6.9.....	188
Fig. 6.10.....	189
Fig. 6.11.....	190

#### CHAPTER VII

Fig. 7.1.....	191
---------------	-----

Fig. 7.2.....	192
Fig. 7.3.....	193
Fig. 7.4.....	194
Fig. 7.5.....	195
Fig. 7.6.....	196
Fig. 7.7.....	197

## GENERAL INTRODUCTION

We live in such a rich environment where our eyes receive massive visual information every second about all kinds of objects surrounding us. These objects in a 3D space are all projected into our retinas as 2D images. To recognize these objects and understand their spatial relations, the visual system has to parse the 2D images to reconstruct the objects in a 3D coordinate system. Surface representation is considered as a critical intermediate stage for the transformation from retinal images to perceived objects (e.g. Nakayama, He, and Shimojo, 1995; von der Heydt, 2003). We now know in detail how the various local surface features carried by the retinal images, such as orientation, spatial frequency, binocular disparity, and so on, are processed in area V1. There, these local features are coded by various types of neurons in different feature dimensions (e.g. Barlow, Blakemore, and Pettigrew, 1967; Hubel and Wiesel, 1962, 1968, 1970; Jones and Palmer, 1987). For instance, with respect to each retinal location, a grating texture is coded by V1 neurons that prefer its orientation. In this way, the visual system generates in V1 an orientation map of the grating texture when combining different locations together. Similarly, spatial frequency and other feature maps are also constructed at this level. In addition, we know that surface edges are coded in cortical areas as early as V1 where some neurons have increased responses at the borders between different texture regions (e.g. Lamme, 1995; Nothdurft, 1992; Nothdurft, Gallant, and van Essen, 2000). However, to finally come up with a percept of the surface, the visual system has to integrate these feature maps and boundary information into a global surface representation at next stages of visual processing.

Our knowledge of surface representation is still relatively limited. Nevertheless, a variety of studies have shed some light on this subject. First of all, neurophysiological research has

found that many neurons of earlier visual cortices, such as V1 and V2, show modulations in their responses to illusory contours (e.g. Lee and Nguyen, 2001; Peterhans and von der Heydt, 1989, 1991; von der Heydt, Peterhans, and Baumgartner, 1984), figure-ground segregation (e.g. Lamme, 1995; Lamme, Super, and Spekreijse, 1998; Roelfsema, Tolboom, and Khayat, 2007), border-ownership (e.g. Qiu and von der Heydt, 2005, 2007; Zhou, Friedman, and von der Heydt, 2000), and attention (Bakin, Nakayama, & Gilbert, 2000; Qiu, Sugihara, and von der Heydt, 2007). For instance, Zhou et al. found that some neurons tend to fire more when an edge is owned by a figure on the side of receptive field and some other neurons prefer the opposite side. Indeed, these border-ownership (BO) selective neurons are fairly common in areas V2 and V4 (> 50%) and, to a lesser extent, in V1 (about 18%). Meanwhile, BO selectivity is independent of the preferences of these neurons in local feature dimensions. A recent functional magnetic resonance imaging (fMRI) study by Fang, Boyaci, and Kersten (2009) has confirmed the existence of BO selectivity in human earlier visual cortices. Traditionally, it is believed that earlier visual cortices mainly process local features. However, to solve problems like BO assignment, the neurons require information from an area much larger than their classic receptive fields. Considering that the short latency (< 25 ms) for the neurons to first demonstrate BO modulation after stimulus onset is insensitive to the size of figures, the information is not likely obtained through horizontal fibers within the same cortical area (Zhou et al., 2000). Accordingly, recent neural models have proposed that the BO selective neurons could get the information beyond their receptive fields through a hierarchical recurrent neural network from higher visual cortices to V2 or even V1 (Craft, Schutze, Niebur, and von der Heydt, 2007; Jehee, Lamme, and Roelfsema, 2007). To comply with empirical facts, these models must take factors that affect BO assignment, such as occlusion (e.g. Zhou et al., 2000), transparency (e.g. Qiu and von der Heydt, 2007), binocular disparity (e.g. Qiu and von der Heydt, 2005), and attention modulation (e.g. Fang et al., 2009; Qiu et al., 2007), into account. That is to say, such a proposed hierarchical neural network should have already been carried all information required for construction of surface representation.



This endorses a proposition that BO is critical for surface representation (e.g. Koffka, 1935; Nakayama and Shimojo, 1990; Nakayama, Shimojo, and Silverman, 1989).

Other clues come from studies on surface color, brightness, texture, and motion spreading/filling-in (e.g. Caputo, 1998; Grossberg and Mingolla, 1985; Motoyoshi, 1999; Paradiso and Nakayama, 1991; Watanabe and Cavanagh, 1991). For example, Paradiso and Nakayama found that a metacontrast mask presented inside a larger homogeneous white target dramatically suppresses the brightness of the target (2 log unit). Such a suppression effect only occurs within the area covered by the mask as if it prevents the brightness signal carried by the outer part of the target from filling into the central area. These filling-in studies support a border-to-interior hypothesis for explaining the formation of surface representation (e.g. Grossberg and Mingolla, 1985; Paradiso and Nakayama, 1991). It assumes that the visual system first encode boundary contour information and then integrate it with local texture signals from adjacent areas subsequently. For a uniform surface, the filling-in process probably solely relies on the color/brightness contrast information carried by the boundary contour and does not need local integration of the interior region since visual cortices does not receive much color/brightness information from LGN about the uniform interior surface (von der Heydt, Friedman, and Zhou, 2003). For a texture surface, however, the situation is different because the various maps of local features accounting for the interior area must be finally registered with the boundary contour. Either way, it is suggested that boundary contours play a critical role for surface representation; the same conclusion can be drawn from various other studies, especially the aforementioned neurophysiological studies (e.g. Bakin et al., 2000; Lamme, et al., 1998; von der Heydt, 2003; von der Heydt et al., 1984; Zhou et al., 2000; also see Nakayama et al., 1995; von der Heydt, 2003).

When viewing the stimulus illustrated in Fig. 1.1a with free-fusion, we experience alternating percepts of the dissimilar half-images. This phenomenon is called binocular rivalry (BR). It has been known for centuries (Porta, 1593). It was believed that BR happened when the

visual system failed to match the corresponding retinal points with the uncorrelated half-images, and thus, alternately selected one of them and suppressed the other to maintain singleness of vision. However, with the rivalry stimulus in Fig. 1.1b, we tend to perceive a rather stable vertical grating disc superimposed upon a horizontal grating (Frisby and Mayhew, 1978). The difference relies on the monocular boundary contour (MBC) carried by one of the half-images in Fig. 1.1b. This type of stimulus is referred to as the MBC rivalry stimulus. With this stimulus, the percept of the grating disc surface is surprisingly robust, without much frequent alternation that a BR stimulus would usually induce. Ooi and He (2005, 2006) have done extensive studies on this interesting phenomenon. It was revealed that the predominance of the grating disc surface can even surpass 90%, well above what would usual be measured with traditional BR stimuli like the one in Fig. 1.1a (around 50% when measured with a two-key percept-tracking method). It was generally assumed that the visual system first searches for matching local features between eyes and, when the matching fails, BR occurs because an interocular inhibitory process is triggered to suppress the image representation in one of the two eyes. However, with the MBC effect as a powerful tool, we found that such interocular suppression can still coexist with the binocular integration process (see Chapter 1 for details). To explain the coexistence of the interocular integration and inhibition, it is proposed in the current dissertation that, with a hierarchical recurrent neural network, the MBC triggers the suppression of the half-image in the fellow eye (likely through BO selective neurons) to solve the unmatched boundary contour information and construct the MBC defined textured surface while the visual system can still integrate the useful local features for binocular depth perception. To better understand the role of the MBC in interocular suppression, the magnitude and dynamics are further investigated (Chapter 2–5). Especially, our findings reinforce the notion that the visual system first registers the boundary contour and then sequentially spreads texture from the border to the interior of the image to generate the representation of the surface.

The next stage to construct the 3D objects in our surrounding space is to integrate the surfaces to a global representation. In the real world, we see objects occluding some others every moment. For example, we tend to perceive the stimulus in Fig. 7.1c as a surface occluding another one (oblique bar), instead of just unrelated smaller pieces. To recognize a partially occluded object, the visual system must be able to integrate the physically visible non-occluded fragments together and interpolate the invisible occluded parts. It is known that boundary contour plays a crucial role in the process of surface completion in such a case (e.g. Nakayama, et al., 1995). Firstly, the boundary contours of the occluding and occluded surfaces form T-junctions, which is known as an important cue for occlusion and the corresponding depth relationship between the involved surfaces (e.g. Anderson, 1997; Anderson and Julesz, 1995; Nakayama et al, 1995; von Helmholtz, 1925). Secondly, earlier studies suggested that surface completion begins in cortical areas as early as V1/V2 (e.g. Albert, 2007; Bakin, et al., 2000; Lee and Nguyen, 2001; Sugita, 1999; von der Heydt et al., 1984; von der Heydt, Zhou, and Friedman, 2003). According to Zhou et al. (2000), majority of BO selective neurons in monkey's V2 (approximately 75%) and V4 (more than 71%) are also selective to luminance and/or color CP. Possibly, when two fragments have the opposite luminance/color CP against the common background, different sets of BO units with opposite CP preferences are activated for the two fragments, respectively (Fig. 7.1f). Presumably, this causes that it is harder for the two fragments to be connected through amodal completion, which is also suggested by the Gestalt principle of similarity. Most of earlier theories postulated that surface completion should be insensitive to CP (e.g. Grossberg and Mingolla, 1985; Kellman and Shipley, 1991). However, more direct empirical evidence has shown that surface completion is actually rather weak when it happens between elements with the opposite CP (e.g. He and Ooi, 1998; Spehar, 2000). For instance, He and Ooi (1998) designed the wagon-wheel stimuli shown in Fig. 6.1a and b. Each spoke of the stimulus in Fig. 6.1a has a pair of inner and outer segments having the same luminance CP. It induces a strong illusory ring called Illusory-O. In contrast, if the inner and outer segments have

the opposite luminance CP like in Fig. 6.1b, although the stimulus is still made of the exactly same group of segments overall, the Illusory-O perceived by observers will be much weakened. In the current proposal, more experiments are conducted to further investigate on the factors affecting surface integration, including the luminance and color CP, as well as common motion and shape (Chapter 6&7).

CHAPTER I  
COEXISTENCE OF BINOCULAR INTEGRATION AND SUPPRESSION DETERMINED  
BY SURFACE BORDER INFORMATION

INTRODUCTION

The lateral separation between our eyes causes 3-D scenes to be seen from slightly different vantage points of view, providing the basis for binocular depth perception (stereopsis). The visual system ensures that the disparate images from the two eyes are experienced as a single, coherent percept predominantly through: (1) The integration process, which analyzes signals from the two eyes to create binocular representations of the images and extracts their binocular disparity for depth perception, and (2) The interocular inhibitory process, which suppresses all but one binocular image representation to provide a coherent percept. Much of our knowledge of the interocular inhibitory process comes from studies of binocular rivalry (BR).

The typical BR stimuli have two half-images of the same overall shape but whose simple features differ in orientation (Fig. 1.1a), motion direction, color, etc. This local difference in simple features prevents the fusion/stereopsis process from integrating the two half-images. If the features of the two half-images are made more similar, the BR between the two half-images is reduced and/or is replaced by the fusion phenomenon (Blake & Boothroyd, 1985). Meanwhile, Hochberg (1964) found that adding contours (grid lines) to one half-image of a correlated stereogram eliminates the depth percept. This suggests the added contours suppress the information of the other half-image. Observations like these lead to the notion that the visual system triggers the interocular inhibitory process to suppress one of the two half-images when the

integration process fails to make a match (Blake & O'Shea, 1988; O'Shea, 1987). We coin this the fusion-preceding-rivalry hypothesis. Opposing the fusion-preceding-rivalry hypothesis is what we coin the co-existence hypothesis, which claims that the integration and the interocular inhibitory processes operate independently (Blake, Westendorf, & Overton, 1980; Kaufman, 1974; Treisman, 1962; Wolfe, 1983, 1986, 1988). Support for the co-existence hypothesis includes the observations that one can perceive binocular depth even as BR is experienced. For instance, using bandpass filtered random-dot stereograms with masking noise of other spatial frequency bands, Julesz and Miller (1975) found observers simultaneously experienced stereopsis and BR. Others used half-images with dissimilar features (e.g., different colors, opposite contrast, or orthogonal grid lines) to induce BR while having correlated contours with binocular disparity to induce stereopsis (Kaufman, 1964, 1974; Ogle & Wakefield, 1967; Treisman, 1962). Although these studies provide support for the co-existence hypothesis, several arguments against them could be made. For example, the depth and BR percepts are probably carried by different spatial frequency channels (Julesz & Miller, 1975), or separately via the chromatic vs. achromatic channels (Treisman, 1962), and these percepts may not occur at the same spatial location (Julesz & Miller, 1975; Ogle & Wakefield, 1967). Thus, the fusion-preceding-rivalry hypothesis could still prevail. According to this view, that stereopsis and BR occur simultaneously at different spatial locations, or different channels, simply reflects the spatial and modular independence of visual processing.

Our study approaches the issue behind these two hypotheses, namely, how the visual system integrates information from the two eyes to support stereopsis while suppressing incompatible images, from a new perspective. We created a stereo/rivalry stimulus with one half-image having a homogeneous vertical grating (right or left, Fig. 1.1b) and the other half-image having the same vertical grating but with an additional disc in the center (middle, Fig. 1.1b). The central disc is defined by a monocular boundary contour (MBC) created by phase shifting ( $45^\circ$ ) a circular area of the vertical grating. This circular disc area, relative to the homogeneous grating

half-image also creates binocular disparity. Thus, with free fusion of the two half-images in Fig. 1.1b, one perceives a stable depth separation between the central grating disc and the surrounding grating (disc is seen behind with crossed fusion of the left and middle half-images), indicating the working of the integration process. Our first experiment quantified this observation using a simultaneous depth discrimination design. We further inserted a phaseshift between the gratings in the upper and lower half-disc areas and measured observers' ability to discriminate the relative depth of the two half-discs in two conditions (Fig. 1.1c). In a back depth condition (Fig. 1.1c, crossed fusers should fuse the left and middle half-images) the grating of the disc is seen behind the surrounding homogeneous grating, while in a front depth condition it is seen in front of the surrounding grating. Notice also (with crossed fusion), that in the back depth condition, the lower half-disc is seen in front of the upper half-disc. In the front depth condition, the upper half-disc is seen in front of the lower half-disc.

Accompanying the depth percept with the MBC phase-shift stimuli (Fig. 1.1b&c) is the observation that the perceived MBC disc is stable, suggesting that the corresponding homogeneous grating is suppressed. This observation agrees with our previous findings showing that the MBC strongly affects BR (Ooi & He, 2005, 2006; van Bogaert, Ooi, & He, 2008). For example, Fig. 1.2a (MBC from orientation-difference) shows an MBC disc in the left half-image created by an orientation difference between the central and surrounding areas. With free-fusion of the half-images, one perceives a stable vertical disc in front (Frisby & Mayhew, 1978). This is unlike the frequent alternating percepts experienced with the typical BR stimulus in Fig. 1.1a even though the central corresponding areas in both stimuli have orthogonal gratings. Thus, the MBC orientation-difference stimulus suggests the strong dominance of the MBC disc is mainly attributed to the MBC. To reveal the suppression of the homogeneous grating half-image by the MBC, our second experiment measured the contrast increment threshold of a Gabor probe on the MBC phase-shift stimulus (Fig. 1.2b). The Gabor probe was either added to the center of the left half-image with the MBC disc, or that of the right half-image with the homogeneous grating. We

found a higher threshold on the homogeneous grating. To further reveal that it is the MBC that triggers the interocular inhibition, we tested two additional conditions where both half-images have boundary contours. These are the ring/disc condition where we added a ring onto the homogeneous grating half-image (right half-image in Fig. 1.2c) to correspond to the MBC in the left half-image, and the ring/ring condition where the MBC phase-shift disc was replaced by the same ring as that in the other half-image (Fig. 1.2d). We found that with such binocular boundary contour (BBC) stimuli, thresholds on the two half-images are similar, i.e., binocular suppression is absent without the MBC.

To generalize the notion that MBC alone can induce interocular inhibition, our third experiment measured thresholds on a variant of the above stimulus (Fig. 1.3a&b). Here, the MBC and relative binocular disparities are created by a difference in spatial frequency, which renders the grating disc to be perceived as tilted in depth (Blakemore, 1970). We obtained similar threshold results as with the MBC phase-shift stimulus.

To further demonstrate the co-existence of integration and binocular suppression, our fourth experiment had observers tracked their percepts of a colored MBC phase-shift stimulus (Fig. 1.4a). With color labeling, we can readily observe the alternating dominance and suppression percepts of the two half-images. From the foregoing, we can predict that the MBC disc remains dominant most of the time while the corresponding homogeneous grating is suppressed. One can confirm this by free fusing Fig. 1.4a and observing that a stable green disc is seen most of the time. Also, one can verify that the strong green dominance is not due to a stronger perceptual salience of the green color, because a robust BR alternation between the red and green half-images occurs with the typical rivalry (red/green discs) stimulus in Fig. 1.4b. Similarly, when we tested observers with a BBC (disc/ring) stimulus (Fig. 1.4c), we found the frequency of BR alternation is almost equal. Finally, to reinforce our finding, we conducted a control experiment where observers tracked a monocular Gabor probe on grayscale MBC phase-shift stimuli (Fig. 1.4d&e). We found higher predominance for seeing the Gabor probe on the



half-image with the MBC.

## METHODS

### *Observers*

One author participated in all four main experiments, and another in Control Experiment 1.2. Fifteen naïve observers with informed consent were recruited. Four participated in Experiment 1.1, three in Experiments 1.2 and 1.3, four in Control Experiment 1.1, and the remaining four in Experiment 1.4. Three of the four naïve observers in Control Experiment 1.1 also participated in Control Experiment 1.2. All observers had normal or corrected-to-normal visual acuity and a stereoscopic resolution of 40 arcsec or better.

### *Apparatus*

*MATLAB* and *Psychophysics Toolbox* (Brainard, 1997; Pelli, 1997) on a *Macintosh* were used to present stimuli on a CRT monitor (1280 × 1024 @ 100 Hz). Observers viewed the stimuli from 75 cm away through a mirror haploscopic system attached to a chin-and-headrest.

### *Stimuli and Procedures*

#### Experiment 1.1: Relative Depth Perception

A  $0.45^\circ \times 0.45^\circ$  white nonius fixation target ( $76 \text{ cd/m}^2$ ) on a gray background ( $40 \text{ cd/m}^2$ ) preceded the  $5^\circ \times 5^\circ$  MBC half-images with grayscale vertical sinusoidal grating (2.2 cpd,  $40 \text{ cd/m}^2$ ; 90% Michelson contrast) (Fig. 1.1c). The half-image presented to the test eye had a  $1.5^\circ$  circular MBC disc, which was divided into two halves. The upper half-disc grating was phase-shifted horizontally relative to the surrounding grating by  $54^\circ$ ,  $72^\circ$ ,  $108^\circ$ , or  $126^\circ$ , while the lower half-disc grating was shifted by  $90^\circ$ . Depending on the eye viewing the MBC disc and the direction of the shift (left/right), the MBC disc grating had either positive or negative horizontal disparities relative to the background grating (-3.4, -1.7, 1.7 and 3.4 arcmin). Four binocular

green dots ( $\sim 0.1^\circ \times 0.1^\circ$ ) in the vicinity of the MBC disc aided eye alignment. A 500 ms black and white square-wave checkerboard mask ( $5^\circ \times 5^\circ$ ; 2.2 cpd;  $40 \text{ cd/m}^2$ ; 90% contrast) terminated a trial. Each test condition was run over 40 blocks of trials in four sessions [5 contrast levels  $\times$  2 eyes  $\times$  2 probe types (dominance vs. suppression)  $\times$  2 repeats]. The observer judged whether the upper or lower half-disc was perceived as nearer.

### Experiment 1.2: Contrast Increment Threshold (Phase-Shift)

The MBC phase-shift stimulus ( $4.5^\circ \times 4.5^\circ$ , Fig. 1.2b) had 3 cpd vertical sinusoidal gratings ( $72.4 \text{ cd/m}^2$ ), with the central  $1.5^\circ$  disc region of one half-image being phase-shifted by  $180^\circ$ . The contrast of the gratings was set at one of five levels (0.8, 1.0, 1.2, 1.4 and 1.6 log%). A white nonius fixation target ( $0.4^\circ \times 0.4^\circ$ ) was located  $0.91^\circ$  above the disc. A Gabor probe [full width at half-maximum (FWHM) of Gaussian kernel =  $0.75^\circ$ , 160 ms] was presented either on the half-image with the MBC disc (dominant condition) or the half-image with the homogeneous grating (suppression condition). The trial ended with a black and white checkerboard mask (500 ms, 95% contrast, 3 cpd). For the ring/disc condition (Fig. 1.2c), a  $1.5^\circ$  counterphase annulus (width =  $0.046^\circ$ ) was added to the half-image with the homogeneous grating. For the ring/ring condition (Fig. 1.2d), the half-image with the MBC disc was replaced by the half-image with the annulus and homogeneous grating. Monocular contrast increment thresholds were obtained using a 2AFC-staircase method. The Gabor probe was either presented 1 or 2 sec after the onset of the MBC stimulus. Four blocks of trials over four sessions were tested for each stimulus.

### Control Experiment 1.1

The MBC phase-shift stimulus (2.2 cpd,  $60 \text{ cd/m}^2$ , 1.5 log% contrast,  $90^\circ$  phase-shift) was centrally fixated. Four surrounding orange dots ( $0.13^\circ$ ) served as fusion lock. Monocular increment thresholds on the MBC phase-shift stimulus were compared with those on the binocular disc and binocular background conditions (Fig. 1.2e&f). The Gabor probe (Gaussian

kernel FWHM =  $0.25^\circ \times 0.43^\circ$ , 250 ms) was either presented to a location corresponding to the upper half or lower half of the MBC disc. Four blocks of thresholds were measured in each condition using a 2AFC-QUEST design.

### Experiment 1.3: Contrast Increment Threshold (Spatial-Frequency-Difference)

All aspects of the experiment were the same to those of Experiment 2 except for the MBC stimulus design (Fig. 1.3). The MBC disc was generated by a circular area of grating with a different spatial frequency from that of the surrounding grating (3 cpd vs. 3.5 cpd and vice versa).

### Experiment 1.4: Perceptual Tracking

The MBC phase-shift stimulus ( $5^\circ \times 5^\circ$ , Fig. 1.4a) comprised of 4 cpd red/black vertical sinusoidal grating ( $12.6 \text{ cd/m}^2$ , 79.7% contrast) with a central  $1^\circ$  circular region of green/black grating (phase-shift =  $180^\circ$ ,  $15.3 \text{ cd/m}^2$ , 83.4% contrast) in one half-image. For the disc/ring stimulus (Fig. 1.4c), a  $1^\circ$  gray annulus (width =  $0.05^\circ$ ,  $29.7 \text{ cd/m}^2$ ) was added to the half-image with the homogeneous red/black grating. For the red/green disc stimulus (typical BR, Fig. 1.4b),  $1^\circ$  red/black and green/black vertical grating discs with  $180^\circ$  phase difference were presented against a gray background ( $29.7 \text{ cd/m}^2$ ). All three stimuli were randomly interspersed within a block of 18 trials (2 test eyes  $\times$  3 stimulus types  $\times$  3 repeats). Each observer was tested over four blocks. A  $0.5^\circ \times 0.5^\circ$  white nonius fixation target ( $76 \text{ cd/m}^2$ ) was presented between each trial and removed 250 ms before the stimulus display of the upcoming trial, whose duration was 30 s. To eliminate the afterimages at the end of the 30-s trial, a black and white checkerboard mask (0.25 Hz anti-phase, 4 cpd,  $52.3 \text{ cd/m}^2$ , 95.1% contrast) was presented for 8 s, and followed by a 2-s blank screen. The observer reported his/her instantaneous percepts (whole disc, no disc, mixture) by continuously depressing one of three keys on the keyboard.

### Control Experiment 1.2

The MBC phase-shift stimulus was the same as that in Control Experiment 1.1. A Gabor probe (Gaussian kernel FWHM =  $0.4^\circ$ ) with variable contrast (0.1 log% interval) was presented either to the center of the MBC disc (Fig. 1.4d, dominance condition) or its corresponding area on the homogeneous grating (Fig. 1.4e, suppression condition). Observers reported either seeing or not seeing the Gabor probe throughout the 30-s stimulus duration by pressing either the left or right arrow key. At least six Gabor probe contrast levels, with four repeat trials per probe contrast, were tested on each observer.

#### *Data Analyses*

ANOVAs were performed on the data in Experiments 1.2–4 and the control experiments, using *SPSS*.

## RESULTS

### Experiment 1.1

Fig. 1.5 depicts the average responses in perceiving the relative depth between the upper and lower half-discs in the near (circles) and far conditions (triangles) in Fig. 1.1c. Clearly, observers correctly perceived the depth of the upper half-disc when it is either nearer (>50%) or farther (<50%) than the lower half-disc. This indicates they ably integrated the MBC phase-shift stimulus for binocular depth perception.

### Experiment 1.2 and Control Experiment 1.1

We measured contrast increment thresholds of monocular Gabor probes that were presented on either half-image (that acted as the pedestal for the probe) of the MBC phase-shift stimulus (Fig. 1.2b). We found contrast thresholds on the homogeneous grating half-image (filled circles, Fig. 1.6) are significantly higher than those on the MBC disc (open circles) [ $F(1,3) = 61.7$ ,  $p < 0.005$ ; ANOVA using GLM with Repeated Measures for the average data]. This

confirms that MBC alone, in the absence of locally conflicting simple features, can initiate the interocular inhibitory process to suppress the half-image with the homogeneous grating. Our data also reveal that thresholds on both half-images increase with the contrast of the pedestal grating in a similar linear pattern [ $F(4,12) = 70.1, p < 0.001$ ;  $F(4,12) = 1.40, p > 0.25$ ]. This suggests that binocular suppression does not affect the contrast gain control mechanism, just like in other types of BR stimuli (Ooi, He, & Su, 2005).

The data for the ring/disc condition show that the thresholds on the phase-shifted disc ( $0.857 \pm 0.059 \log\%$ ) and on the gray-ring disc ( $0.865 \pm 0.051 \log\%$ ) are not significantly different [ $t(9) = 0.100; p = 0.922$ , Contrasts Analysis]. These thresholds are quite close to the thresholds in the ring/ring condition, which average  $0.835 \pm 0.065 \log\%$  [ $t(9) = 0.367; p = 0.722$ , Contrasts Analysis]. Thus both conditions reveal that when the boundary contour in each half-image corresponds as a pair of BBC interocular inhibition no longer exerts its influence.

Arguably, our findings in Fig. 1.6 need not necessarily indicate interocular suppression, but rather that probe detection threshold on a figure (MBC disc grating) is lower than that on a large grating background. Presumably, the MBC disc configuration itself could cause less spatial uncertainty and/or attract stronger focal attention, leading to a lower threshold. To explore this alternative argument, we compared probe detection thresholds of the MBC phase-shift condition with two new conditions. The binocular disc condition (Fig. 1.2e) had the half-image with the disc stimulating both eyes during threshold measurement, and the binocular background condition (Fig. 1.2f) had the homogeneous background half-image stimulating both eyes. We found the average threshold in the binocular disc condition ( $0.98 \pm 0.02 \log\%$ ) to be slightly higher than that in the binocular background condition ( $0.91 \pm 0.02 \log\%$ ) [ $F(1, 3) = 37.376, p = 0.009$ ]. Clearly, this finding rejects the alternative argument. Moreover, in the MBC phase-shift condition (measured in the same test block), we found the average threshold on the MBC disc ( $0.89 \pm 0.02 \log\%$ ) lower than that on the homogeneous grating ( $1.08 \pm 0.05 \log\%$ ) [ $F(1, 3) = 12.076, p = 0.040$ ].

### Experiment 1.3

We measured contrast increment thresholds on each half-image of the MBC spatial-frequency-difference stimuli in Fig. 1.3. We found the average threshold on the 3 cpd homogeneous grating ( $1.016 \pm 0.099$  log%) higher than that on the 3.5 cpd disc ( $0.821 \pm 0.0721$  log%) [Fig. 1.3a;  $t(3) = 3.704$ ,  $p = 0.034$ ]. Similar results were found for the stimulus in Fig. 1.3b (3.5 cpd homogeneous grating:  $1.013 \pm 0.084$  log%; 3 cpd disc:  $0.792 \pm 0.069$  log%) [ $t(3) = 3.638$ ,  $p = 0.036$ ]. The higher threshold on the homogeneous grating half-image in both stimuli indicates binocular suppression, even as stereopsis is experienced, further supporting the co-existence hypothesis.

### Experiment 1.4 and Control Experiment 1.2

To reveal the binocular suppression induced by the MBC alone is sufficiently strong to prevent the homogeneous grating from perception, observers indicated their instantaneous percepts of the stimuli in Fig. 1.4a–c. For the colored-MBC phase-shift stimulus (Fig. 1.4a), the predominance (Fig. 1.7) for seeing the MBC disc (green) is much higher than for seeing the homogeneous grating [ $F(1.012, 4.407) = 10011.296$ ,  $p < 0.001$ , with Greenhouse-Geisser correction, ANOVA using GLM with Repeated Measures]. This indicates MBC induced binocular suppression causes the homogeneous grating to be unperceived most of the time. In contrast, for the red/green disc (Fig. 1.4b) and the disc/ring (Fig. 1.4c) stimuli, the predominance for seeing red, green or mixed colored disc is quite similar (red/green disc stimulus:  $F(2,8) = 0.192$ ,  $p = 0.829$ ; disc/ring stimulus,  $F(2,8) = 0.11$ ,  $p = 0.897$ ).

Instead of color labeling the MBC phase-shift stimulus to measure binocular suppression, our control experiment tagged a Gabor probe onto either half-image of the grayscale stimulus (Fig. 1.4d&e). Observers tracked the probe's visibility (seen or unseen), which reflects the dominance or suppression state of the half-images. Fig. 1.7b plots the average predominance for seeing the probe on the MBC disc (open circles) and on the homogeneous grating (filled circles)

as a function of relative probe contrast. As expected, for an extremely low contrast probe that is barely above detection threshold, or an extremely high contrast probe that is sufficiently strong to resist suppression by the MBC, the predominance for seeing the probe is similar on both half-images. But for intermediate probe contrast levels, the predominance is significantly higher on the MBC disc than on the homogeneous grating, indicating binocular suppression of the former on the latter half-image. This is confirmed by a statistical analysis of the average data [main effect of stimulus condition:  $F(1,3) = 35.103$ ,  $p = 0.010$ ; main effect of contrast:  $F(3,9) = 95.187$ ,  $p < 0.001$ ; interaction:  $F(3,9) = 6.770$ ;  $p = 0.011$ , ANOVA using GLM with Repeated Measures], further confirming the existence of interocular inhibition with the MBC phase-shift stimulus. Finally, we found the binocular suppression does not affect the stability of the perceived depth of the MBC disc, as the observers continuously experienced the depth percept throughout the 30-s stimulus interval.

## DISCUSSION

Using the MBC phase-shift stimulus, we showed both stereopsis and binocular suppression are experienced simultaneously at the same location. This suggests even as the integration process extracts binocular depth from both eyes, the interocular inhibitory process suppresses the homogeneous grating half-image leading to the selection of the MBC grating disc for perception. In general, our findings agree with the notion that the integration process and the interocular inhibitory process operate independently (co-existence hypothesis) (Blake et al., 1980; Kaufman, 1974; Treisman, 1962; Wolfe, 1983, 1986, 1988). However, we recognize that our observation does not necessarily exclude the fusion-preceding-rivalry hypothesis (Blake & Boothroyd, 1985; Blake & Camisa, 1978; Blake & O'Shea, 1988; Hochberg, 1964; O'Shea, 1987). This is because the observed binocular integration and binocular suppression are intimately related, respectively, to the surface feature (e.g. grating) and boundary contour (e.g.

MBC) information that are processed by different neural mechanisms. Specifically, with the MBC phase-shift stimulus, the interocular inhibitory process is activated when the visual system cannot find a matching boundary contour in the homogeneous grating half-image, i.e., agreeing with the fusion-preceding-rivalry hypothesis. In this regard, the two hypotheses are reconcilable when we consider that BR is processed by a distributed intercortical network (Blake & Logothetis, 2002; Ooi & He, 1999, 2003).

Equally significant, our study reveals the important role of the boundary contour. In earlier studies (Ooi & He, 2005, 2006) we showed using an MBC stimulus with conflicting local features (orthogonal gratings in Fig. 1.2a), the critical contribution of the boundary contour to BR. Here, with the MBC phase-shift stimulus, we found that the MBC can induce binocular suppression even when there are no conflicting local features (same vertical grating in Fig. 1.2b). This indicates that the MBC alone can trigger the interocular inhibitory process.

Research shows that the boundary contour representation provides the basis for representing surfaces and objects, and that boundary contours are extracted in the early visual cortices (e.g., Bakin, Nakayama, & Gilbert, 2000; Grossberg & Mingolla, 1985; Nakayama, He, & Shimojo, 1995; Lamme, Super, & Spekreijse, 1998; Mitchison & McKee, 1987; von der Heydt, 2003; von der Heydt, Peterhans, & Baumgartner, 1984; Zhou, Friedman, & von der Heydt, 2000). Importantly, single unit recording in monkeys have revealed a significant proportion of V2 cortical neurons with selectivity for the side of the contour, i.e., border ownership (BO) (Zhou et al., 2000; Qiu & von der Heydt, 2005). BO signals are critical for segregating surfaces in depth, as front (figure) or back (ground) (Driver & Baylis, 1996; Koffka, 1935; Nakayama et al. 1995; Nakayama, Shimojo, & Silverman, 1989; von der Heydt, 2003; Zhou et al., 2000). We believe the crucial role of the BO neurons is reflected in our study. It is possible that the MBC stimulus (e.g., Fig. 1.2a&b) triggers activities in the BO selective neurons, which in turn initiates the boundary contour based surface representation process to construct the MBC defined texture surface (disc). Meanwhile, the BO selective neurons also trigger the



interocular inhibitory network to suppress the homogeneous grating half-image at the corresponding retinal area. This ensures the homogeneous grating image does not interfere with the surface representation of the MBC disc.

Given the modular organization of the early visual cortices (DeYoe & Van Essen, 1988; Livingstone & Hubel, 1988), our findings also suggest that the perceived 3-D MBC disc is obtained from the binding of different modular inputs. The first is the monocular texture information within the MBC disc. The second is the quantitative binocular depth derived from the binocular disparity process (Ohzawa, DeAngelis, & Freeman, 1990). This explanation, if correct, advances our understanding of feature-binding in vision (Treisman & Gelade, 1980). Interestingly, for binocular surface perception, the visual system can bind selective features from the two retinal images based on projection geometry constraints. This reinforces the notion that the visual system can solve the feature-binding problem by relying on perceptual rules that are derived from its past experiences of interacting with the ecological environment (Nakayama & Shimojo, 1992; Purves, Lotto, Williams, Nundy, & Yang, 2001; von Helmholtz, 1925).

## CHAPTER II

### THE MAGNITUDE AND DYNAMICS OF INTEROCULAR SUPPRESSION AFFECTED BY MONOCULAR BOUNDARY CONTOUR AND CONFLICTING LOCAL FEATURES

#### INTRODUCTION

When the two eyes view dissimilar stimuli (half-images) such as the orthogonal gratings in Fig. 2.1a, one perceives an alternation between the images of the two stimuli. In this phenomenon of binocular rivalry, the stimulus whose image is momentarily perceived is referred to as the dominant stimulus, while the stimulus whose image is not perceived the suppressed stimulus. One approach to revealing the fate of the suppressed image, which is not consciously perceived, is by measuring the effect of the suppression on the detection threshold of a monocular probe. The probe detection protocol has been used by various laboratories in the past (e.g., Blake & Camisa, 1979; Fox & Check, 1972; Li, Freeman, & Alais, 2005; Makous & Sanders, 1978; Nguyen, Freeman, & Wenderoth, 2001; Norman, Norman, & Bilotta, 2000; Ooi & Loop, 1994; Paffen, Alais, & Verstraten, 2005; Smith, Levi, Manny, Harwerth, & White, 1985; Su, He, & Ooi, 2009; Wales & Fox, 1970; Watanabe, Paik, & Blake, 2004). Collectively, it is found that during binocular rivalry, the detection threshold of a probe presented to the suppressed eye is higher than that presented to the dominant eye. The elevation of the detection threshold in the suppressed eye is thought to be caused by an interocular inhibitory mechanism that inhibits signals from the suppressed eye before they reach the site(s) of visual awareness (Blake, 1989; Wilson, 2003). Depending on the property of the probe and binocular rivalry stimulus, the probe detection protocol can reveal either the general, or feature specific, characteristics of interocular

suppression (e.g., Alais & Parker, 2006; Blake, 2001; Nguyen et al., 2001; O'Shea & Crassini, 1981; Ooi & Loop, 1994; Smith, Levi, Harwerth, & White, 1982; Stuit, Cass, Paffen, & Alais, 2009).

The current study uses the probe detection protocol to extend our investigation of binocular rivalry involving monocular boundary contour (MBC, as in Fig. 2.1b). The left half-image of the binocular rivalry stimulus has a homogeneous horizontal grating while the right half-image has a vertical grating disc surrounded by horizontal grating. With free-fusion, one perceives a stable vertical grating disc floating in front of the horizontal grating (Frisby & Mayhew, 1978) rather than the typical binocular rivalry alternation. Psychophysical studies from our laboratory have revealed that the MBC formed between the vertical grating disc and the surrounding horizontal grating in the right half-image leads to a high predominance (about 90%) of perceiving the vertical grating disc (Ooi & He, 2005, 2006). Accordingly, we call the display in Fig. 2.1b an MBC rivalry stimulus to distinguish it from the more typical binocular rivalry stimulus such as the one in Fig. 2.1a, which we refer to as a BBC (binocular boundary contour) rivalry stimulus, since the boundary contours of the two half-images have the same shape and size.

The MBC rivalry stimulus provides a unique opportunity to investigate the contribution of boundary contours to binocular rivalry, and its relationship to binocular surface perception (Ooi & He, 2005, 2006; Su et al., 2009; van Bogaert, Ooi, & He, 2008; Xu, He, & Ooi, 2010). For example, Xu et al. (2010) modified the MBC rivalry stimulus into a BBC rivalry stimulus by inserting a relative phase-shift between the central and surrounding square wave gratings in the left half-image of Fig. 2.1c ( $36^\circ$  phase-shift) to create a horizontal grating disc with a boundary contour. It was found that increasing the phase-shift, which mainly enhances the boundary contour strength of the horizontal grating disc, increases the predominance of seeing the horizontal grating disc. Then in a subsequent experiment Xu et al. (2010) added a circular ring with fixed luminance (same mean luminance as the grating disc) between the horizontal grating disc and surrounding horizontal grating. This time they found that changing the relative phase-

shift did not affect the predominance of the horizontal grating disc. This is because the (constant luminance) ring now served as the boundary contour of the horizontal grating disc. Thus, this second experiment showed that the effect of phase-shift in their main experiment (Fig. 2.1c) is mainly due to the modulation of boundary contour strength caused by the phase-shift, rather than the phase-shift triggering the center-surround interaction (e.g., Alais & Blake, 1998; Fukuda & Blake, 1992; Ooi & He, 2006; Paffen et al., 2005). This result supports an earlier finding by Ooi & He (2006) that the center-surround suppression factor contributes less to binocular rivalry induced by the MBC rivalry stimulus than the boundary contour factor.

Recently, we used a threshold detection method similar to that used by Watanabe et al. (2004) to investigate whether an MBC alone can trigger the interocular inhibitory mechanism to suppress the image in the fellow eye (Su et al., 2009). Our experiments employed an MBC phase-shift rivalry stimulus similar to that in Fig. 2.1d, where the two half-images have the same vertical grating (i.e., no conflicting local features) and additionally, the right half-image has an MBC grating disc created by the phase-shift. We measured the increment threshold of detecting a monocular Gabor probe on either half-image (pedestal) as a function of the grating contrast to obtain the threshold vs. contrast (TvC) function. We found the TvC function is significantly elevated when measured on the homogeneous grating than on the MBC disc, indicating suppression of the homogeneous grating (the results are reproduced in Fig. 1.6). This finding indicates that the MBC alone can initiate interocular inhibition. Additionally, we found that the TvC functions measured on both half-images can be fitted by linear functions with similar slopes, suggesting that the contrast gain control mechanism is not affected by the interocular inhibitory mechanism (Watanabe et al., 2004).

The MBC rivalry stimulus, with either orientation-difference or phase-shifted grating, is also useful for investigating the distributed cortical processes involved in binocular rivalry. It is recognized that the cortical representation of visual surfaces includes at least two critical stages: registering surface boundary contours and spreading-in of the interior surface features (texture

and color) within the boundary contours (e.g., Caputo, 1998; Grossberg & Mingolla, 1985; Nakayama, He, & Shimojo, 1995; Paradiso & Nakayama, 1991; Su, He, & Ooi, 2011a; van Bogaert et al., 2008; von der Heydt, Friedman, & Zhou, 2003). Since the boundary contour information that is responsible for surface image segmentation is largely extracted in cortical area V2 (e.g., Bakin, Nakayama, & Gilbert, 2000; Qiu & von der Heydt, 2005; Zhou, Friedman, & von der Heydt, 2000), it is likely that the MBC initiated interocular inhibitory mechanism resides in area V2. Presumably, once triggered, the interocular inhibition could directly, or via feedback to V1, cause suppression of the image representation from the other eye. But for the MBC orientation-difference rivalry stimulus (Fig. 2.1b), it is likely that the conflicting local features activate the interocular inhibitory mechanism in area V1, in addition to the MBC triggered interocular inhibitory mechanism in area V2. On the other hand, with either the MBC orientation-difference or MBC phase-shift rivalry stimulus, it is the MBC half-image that contributes substantially to the dominant percept (Ooi & He, 2005, 2006; Su et al., 2009). This notion is reinforced in Fig. 2.1e, where the low contrast MBC vertical grating disc is predominantly perceived over the high contrast horizontal grating half-image. In contrast, with the BBC rivalry stimulus in Fig. 2.1f it is the high contrast horizontal disc that is predominantly perceived. Such an observation can lead to the argument that the interocular inhibitory mechanism in area V1, which is activated by conflicting local features, contributes little to interocular inhibition in the MBC rivalry stimulus. If this is true, we will expect the threshold elevation in the suppressed eye (homogeneous grating) to be similar when tested with either the MBC orientation-difference or MBC phase-shift rivalry stimulus. To explore this possibility, our first experiment measured the TvC functions of the MBC orientation-difference rivalry stimulus (Fig. 2.1b) using the same method and observers as in our earlier study with the MBC phase-shift rivalry stimulus (Su et al., 2009).

Our first experiment reveals that the threshold elevation due to the MBC orientation-difference rivalry stimulus is significantly higher than that with the MBC phase-shift rivalry

stimulus. This indicates the contributions of both conflicting local features and MBC to interocular suppression. Then to further explore the interocular inhibition in the MBC rivalry stimulus, our second experiment tested whether the magnitude of suppression is independent of the strength of the stimulus in the dominant eye. To do so, we measured the TvC functions of the MBC orientation-difference rivalry stimulus in which the contrast of the homogeneous grating (suppression condition) was fixed while the contrast of MBC disc (dominance condition) varied.

Our third and fourth experiments measured performance of detecting a suprathreshold Gabor probe, respectively in the MBC orientation-difference stimulus and the MBC phase-shift stimulus, at various stimulus onset asynchrony (SOA) (80–410 ms) to investigate the early dynamics of interocular inhibition. Our goal is to reveal that the interocular inhibition triggered by the MBC becomes effective before 150 ms, unlike that with a BBC rivalry stimulus (Su, He, & Ooi, 2011b; Wolfe, 1983).

## METHODS

### Experiment 2.1: The Dominance and Suppression TvC Functions with the MBC Orientation-difference Rivalry Stimulus

We measured the contrast increment threshold of seeing a monocular Gabor probe presented on the MBC orientation-difference rivalry stimulus (Fig. 2.2). The luminance contrast of the MBC rivalry stimulus was set at one of six contrast levels (5.01–50.12%). For each contrast level tested, both the right and left half-images always had the same contrast specification (see Fig. 2.3, top). This allows us to determine the threshold vs. contrast (TvC) function in the dominance and suppression conditions.

#### *Observers*

One author, and three observers who were naïve to the purpose of the study, participated in Experiment 2.1 and 2.2. For all experiments in this paper, the observers had normal or

corrected-to-normal visual acuity and a stereoscopic resolution of 20 arcsec or better. Informed consent was obtained from the naïve observers before commencing the experiment.

### *Apparatus*

A *Macintosh* computer using *MATLAB* and *Psychophysics Toolbox* software generated the stimuli (Brainard, 1997; Pelli, 1997). The images were displayed on a 19" flat cathode ray tube (CRT) screen with a 100 Hz vertical scanning rate. The stimuli were viewed with a mirror haploscopic system attached to a head-and-chin rest from a viewing distance of 75 cm.

### *Stimuli*

The MBC orientation-difference rivalry stimulus ( $6^\circ \times 6^\circ$ ) was presented upon a gray background with the same mean luminance ( $87 \text{ cd/m}^2$ ). One half-image had a homogeneous sinusoidal grating (3 cpd). The other half-image also had the same sinusoidal grating but with an additional  $2^\circ$  sinusoidal grating disc (3 cpd) with an orthogonal orientation (vertical vs. horizontal). A white nonius fixation target ( $0.4^\circ \times 0.4^\circ$ ) was located  $0.85^\circ$  above the grating disc and its corresponding region in the other half-image. The luminance contrast of the MBC rivalry stimulus was set at one of six levels: 5.01%, 7.94%, 12.59%, 19.95%, 31.62% and 50.12% (equivalent log % contrast levels of 0.7, 0.9, 1.1, 1.3, 1.5 and 1.7, respectively).

During each trial, a Gabor probe was presented either on the center of the grating disc of one half-image (dominance condition; see example in Fig. 2.2a), or on the center of the homogeneous grating of the other half-image (suppression condition; see example in Fig. 2.2b).

The probe was specified by the following formula:

$$L(x, y) = L_m \left\{ 1 + c \cdot \sin(2\pi\omega x) \cdot \left[ 1 + a \cdot \exp\left(-\frac{x^2 + y^2}{2\sigma^2}\right) \right] \right\}.$$

In the formula,  $L(x, y)$  represents the luminance at a specified location  $(x, y)$ . The  $x$ -axis is orthogonal to the orientation of the probe's pedestal grating while the  $y$ -axis is parallel with the grating orientation; the origin overlaps the center of the probe.  $L_m$  is the mean luminance ( $87$

$\text{cd/m}^2$ );  $c$  is the contrast of the grating;  $a$  is the peak contrast increment ratio of the probe;  $\omega$  is the spatial frequency of the grating (3 cpd); and  $\sigma$  is the standard deviation of the Gaussian function in the Gabor kernel (set to  $0.42^\circ$ ). The trial ended with the presentation of a binocular checkerboard mask. The spatial frequency of the mask was 3 cpd; its mean luminance was  $87 \text{ cd/m}^2$  and its contrast was 96.5%.

### *Procedures*

The dominance condition was tested with the probe presented on the half-image with the grating disc (pedestal), while the suppression condition was tested with the probe presented on the half-image with the homogeneous grating (pedestal). The probe was always presented to the observer's dominant eye. To control for the effect of orientation, the orientation of the disc and homogeneous grating square were counter-balanced (vertical vs. horizontal). Effectively, this gave rise to four stimulus combinations. Fig. 2.2a and b illustrate two of the four stimulus combinations where the probe was, respectively, presented on the grating disc half-image (dominance condition) and on the homogeneous grating half-image (suppression condition).

Observers were tested in four separate sessions (2 repeats  $\times$  2 pedestal orientations) with its order counter-balanced. Each session consisted of 12 blocks with the same pedestal orientation, of which six blocks had the grating disc half-image as the pedestal (dominance condition) and the other six blocks had the homogeneous grating half-image as the pedestal (suppression condition). Each block measured the contrast increment threshold for one of the six pedestal contrast levels.

We used a 2AFC-staircase design to determine the contrast threshold of the Gabor probe (Fig. 2.2c). To begin a trial, the observer steadied himself/herself on a head-and-chin rest and maintained eye alignment on the nonius fixation. He/she then pressed the spacebar on the computer keyboard to present the MBC rivalry stimulus. One (interval-1) or 2 s (interval-2) after the onset of the MBC stimulus, a Gabor probe (duration = 0.16 s) was presented on one half-



image (pedestal) of the MBC stimulus. Two brief tones, each presented at 1 and 2 s, were used to aid the observers in discriminating between the two separate intervals. The 2AFC trial ended with the presentation of a 0.5-s checkerboard mask. The observer's task was to press one of two keys on the computer keyboard to indicate whether the probe was seen at the first or second interval. No feedback regarding the response accuracy was given to the observer.

Once a trial was completed, the observer would press the space bar to initiate the next trial. The probe contrast in the subsequent trial was determined based on an adaptive 3-down/1-up rule. At the beginning of each block, the relative intensity (contrast increment ratio) of the probe was set at 50% (i.e., at its peak, the probe enhanced the contrast of the stimulus by 50%). The step size of the contrast change was 15% after the second reversal and 30% before the second reversal. In the rare event (< 1%) where the grating disc of the MBC stimulus was suppressed from perception during the trial, the observer would abort the trial by pressing the down-arrow key. A test block ended after nine reversals. To calculate the contrast increment threshold for data analysis, the probe contrast levels (in log contrast unit) from the last six reversals were averaged.

It should be noted that the threshold measured by this staircase procedure was slightly different from the threshold at 79.4% correct that was usually reported by other studies using the transformed 3-down/1-up staircase method. This is because the step upward (+15%, i.e., 0.0607 log unit) and the step downward (-15%, i.e. -0.0706 log unit) in our experiment was slightly different when analyzed in logarithmic scale. The equilibrium condition (Kaernbach, 1991) for this weighted step size is:

$$S_{down}P^3 = S_{up}(1 - P^3).$$

Effectively, we have an  $S_{down}$  that equals to 0.0706 log unit and a  $S_{up}$  of 0.0607 log unit. Therefore, the threshold reflects the 77.3% correct point on the psychometric function.

#### *Data Analyses*

The contrast increment threshold data from the dominance and suppression conditions were averaged from those measured on the horizontal and vertical pedestals.

### Experiment 2.2: Effect of the Contrast of the Dominant Half-image of the MBC Orientation-difference Rivalry Stimulus on the Suppression TvC Function

We investigated whether the contrast increment threshold in the suppressed eye is a function of the grating contrast in the dominant eye. Assuming that the increment threshold of the suppressed eye reflects the stimulus strength required for the putative “visual switch” to disengage its selection from the currently dominant image representation to the suppressed one, this experiment will inform whether the selection change depends on the contrast of the stimulus (saliency) in the dominant eye. Experiment 2.1 above could not reveal this because we varied the grating contrast equally in both the dominant and suppressed half-images (see Fig. 2.3, top). Therefore, in this experiment we varied only the contrast of the grating disc in the dominant half-image while keeping the contrast of the remaining components of the MBC orientation-difference rivalry stimulus constant (Fig. 2.4, top).

#### *Stimuli and Procedures*

We employed the same stimuli as in Experiment 2.1 except for the manipulation of the contrast of the grating disc in one of five levels (7.94%, 12.59%, 19.95%, 31.62% and 50.12%), while the contrast of the remaining stimulus components was fixed at 19.95%.

The test procedures were similar to that of the first experiment except for a minor adjustment to the staircase protocol. We adjusted the step size of the probe contrast change in the staircase to 0.0667 log unit after the second reversal, and 0.1333 log unit before the second reversal. This led to a theoretical threshold at 79.3% correct, which was slightly different from that of the first experiment (77.3%).

### Experiment 2.3: The Effect of SOA on Probe Detection with the MBC Orientation-difference Rivalry Stimulus

Wolfe (1983) made an intriguing discovery of the effect of presentation duration on the perception of the typical binocular rivalry (BBC) stimulus with vertical and horizontal gratings. His observers reported seeing the gratings as plaid/checkerboard or piecemeal when the stimulus duration was shorter than 150 ms, but beyond 150 ms, the observers saw global dominance of either vertical or horizontal grating. This led to the conclusion that interocular inhibition takes longer than 150 ms to fully assert its influence (Wolfe, 1983). We used a similar method to investigate whether interocular inhibition requires the same duration to assert its influence on the MBC orientation-difference rivalry stimulus. We found that, consistent with Wolfe (1983), observers rarely saw global dominance with presentation durations shorter than 150 ms for the typical BBC rivalry stimulus. With the MBC rivalry stimulus, however, our observers perceived the MBC grating disc, i.e., global dominance percept, for stimulus durations shorter than 150 ms.

To further investigate our finding with the MBC rivalry stimuli, we tested observers' performance in detecting a suprathreshold monocular Gabor probe in Experiments 2.3 and 2.4 below. If the interocular inhibitory mechanism is effective before 150 msec (after the onset of the MBC rivalry stimulus), we should expect the rate of detecting a monocular probe on the MBC grating disc (dominance condition) to be higher than that on the homogeneous grating (suppression condition). We tested this prediction by measuring both the percentage correct and response time, in detecting a monocular Gabor probe at various SOAs between the probe and the MBC rivalry stimulus. Experiment 2.3 tested with the MBC orientation-difference rivalry stimulus and Experiment 2.4 tested with the MBC phase-shift rivalry stimulus.

#### *Observers*

One author and four new naïve observers participated in the experiment.

#### *Stimuli*

The apparatus and display settings were the same as in Experiment 2.1 except for the dimension of the CRT monitor being 21 inch. At the beginning of each trial, a white  $0.45^\circ \times 0.45^\circ$  nonius fixation cross ( $73.1 \text{ cd/m}^2$ ) was presented in the middle of a  $5^\circ \times 5^\circ$  black frame fusion lock ( $5 \text{ cd/m}^2$ ). The MBC orientation-difference rivalry stimulus (Fig. 2.5) was modified after the one used in Experiment 2.1 as follows: (i) the mean luminance of the stimulus and gray background was  $63.1 \text{ cd/m}^2$ ; (ii) the luminance contrast of the grating was fixed at 39.8%; (iii) the overall size of the MBC rivalry stimulus was  $4.5^\circ \times 4.5^\circ$  while and the MBC disc diameter was  $1.5^\circ$ . During a trial, a monocular Gabor probe ( $L_m = 63.1 \text{ cd/m}^2$ ,  $c = 39.8\%$ ,  $\sigma = 0.24^\circ$ ) was presented either in the center of the MBC grating disc (dominance condition), or in the center of the homogeneous grating half-image (suppression condition). The probe was always presented to the dominant eye. Each trial terminated with a  $4.5^\circ \times 4.5^\circ$  black-and-white random-dot mask (dot size =  $0.1^\circ \times 0.1^\circ$ ; contrast = 95%).

#### *Determination of the Gabor Probe*

The contrast increment of the Gabor probe for this and the following experiment was determined separately for each observer. To do so, a monocular vertical grating pedestal ( $4.5^\circ \times 4.5^\circ$ , 3 cpd,  $63.1 \text{ cd/m}^2$ , 39.8% contrast) upon a homogeneous gray background was presented to the eye to be stimulated with the Gabor probe. The fellow eye viewed the same gray background (without the stimulus). This was followed, after a 100 ms SOA, by the Gabor probe (10 ms). The observer reported whether he/she detected the probe. The goal was to find the weakest probe strength (contrast increment) that led to a detection rate of no less than 86.7%. Thus, a series of mini-experimental blocks with various probe strengths were run. Each experimental run tested 3–4 blocks of different probe strengths (15 trials per probe strength). The probes were varied by a step of approximately 4%, within a contrast range of 15.92–39.81%. The probe strength that led to a detection rate of at least 13 out of 15 hits (86.7% detection) was used for Experiment 2.4.

Since the suppression with the MBC-orientation-difference rivalry stimulus is significantly larger, we added ~10% higher in increment contrast to the probe for use in the current experiment.

### *Procedures*

The Gabor probe, whose increment contrast level was determined above, was presented on either half-image of the MBC orientation-difference rivalry stimulus. For each test trial, the probe duration was 20 ms and its onset relative to the onset of the MBC orientation-difference rivalry stimulus (SOA) was 80, 120, 180, 270, or 410 ms. This allowed us to measure the detection rate and response time to detect the probe in the dominance and suppression conditions. To check for the reliability of the observer's responses, we also included catch trials in which the MBC orientation-difference rivalry stimulus was presented without the probe. The catch trials and test trials were intermingled within a block of 240 trials {[5 SOAs  $\times$  2 test conditions (dominance and suppression)  $\times$  2 probe orientations (horizontal and vertical)  $\times$  10 repeats] + 40 catch trials}. The trials were semi-randomized with the provision that no more than three consecutive trials had exactly the same combination of test condition and probe orientation. In all, six blocks of trials were conducted over two sessions for each observer.

To begin a trial, the observer aligned his/her eyes with the nonius fixation and pressed the spacebar on a computer keyboard. This led to the removal of the nonius fixation (the surrounding square fusion lock remained) and 250 ms later, the presentation of the MBC rivalry stimulus. Depending on the type of trial (test or catch), the probe could be added at the appropriate SOA. The observer's task was to respond as quickly as possible by pressing the right arrow key of the keyboard if he/she saw the Gabor probe. Once the response was made, the trial terminated with the presentation of the mask (250 ms). If no response was made (because the probe was either not detected or absent), the MBC rivalry stimulus would be removed after 1.5 s and the trial terminated with the presentation of the mask. If no probe was detected, the observer should not press any key.

Several precautionary measures were implemented. In the rare event ( $< 1\%$ ) where the MBC disc disappeared (suppressed) during the trial, or had its texture seen in plaid/piecemeal, the observer would abort the trial by pressing the down-arrow key. The trial would then be repeated. Audio feedbacks with different tones were given to convey two possible types of false alarms: (i) responding to a catch trial, and (ii) responding less than 100 ms upon the probe onset (anticipatory response). Trials with anticipatory responses ( $< 0.1\%$ ) would be repeated. A third audio feedback accompanied the “regular” test trials where probe detection were made. In this way, the observer could monitor the reliability of his/her responses. For each block of trials, the observer was allowed to make a maximum of four false alarms (10%) when responding to the catch trials. If a fifth false alarm was made, the test program would abort and the observer would have to repeat the entire block of trials. Furthermore, a 1-min rest period was inserted after every 40 trials to reduce the possibility of observer fatigue during the 240-trial block.

The data from the six blocks of trials were pooled for analysis of reaction time data. To increase data reliability, responses whose reaction times deviated from the mean by larger than three standard deviations were excluded from analysis. This rarely occurred ( $< 0.1\%$ ).

#### Experiment 2.4: The Effect of SOA on Probe Detection with the MBC Phase-shift Rivalry Stimulus

The results of Experiment 2.3 reveal effective interocular inhibition of MBC orientation-difference rivalry stimulus as early as 80 ms after its onset. Since interocular suppression in the MBC orientation-difference rivalry stimulus can be contributed by both the local conflicting features and the MBC, it is important to investigate if the interocular inhibition initiated by the MBC alone can be effective earlier than 150 ms. Thus, we used the same method as in Experiment 2.3 to measure the effect of SOA on the percentage correct and reaction time of detecting the monocular Gabor probe with the MBC phase-shift stimulus (Fig. 2.6).

#### *Observers*

One author and three naïve observers, who also participated in Experiment 2.3, participated in the current experiment. In addition, two new naïve observers were tested.

### *Stimuli*

The stimulus parameters were the same as those in Experiment 2.3, but with two key exceptions. One, the MBC disc was created by a 90° phase-shift between the central and surrounding vertical grating (MBC phase-shift stimulus) (Fig. 2.6). Two, unlike Experiment 2.3 that tested both vertical and horizontal orientation (for the purpose of counterbalancing), we only tested the vertical orientation. The increment contrast of the Gabor probe was determined individually for each observer with the method described in Experiment 2.3.

### *Procedures*

All aspects of the experimental procedures were similar to those in Experiment 2.3, except for the following. While each observer was still tested over two experimental sessions, the total number of blocks was twelve. This is because each block now comprised 120 trials {[5 SOAs (80, 120, 180, 270, and 410 ms) × 2 test conditions (dominance and suppression) × 10 repeats] + 20 catch trials}. To maintain the same false alarm rate (10%) for penalty (aborting the entire block of trials), the observer was only allowed to make a maximum of two false alarms (responding to catch trials) in each block of trials.

## RESULTS

### Experiment 2.1

We obtained the TvC functions for the dominance (circles) and suppression (squares) conditions by plotting the probe increment contrast threshold versus the pedestal contrast in a log-log coordinate in Fig. 2.3. Fig. 2.3a depicts the four observers' average data while Fig. 2.3b that of a representative naïve observer. By applying a ANOVA using GLM with Repeated

Measures to the average data, we found that the contrast increment thresholds are significantly higher for the suppression condition than for the dominance condition with an average elevation of 0.3–0.4 log unit [ $F(1, 3) = 31.734, p < 0.025$ ]. This indicates there is a meaningful elevation of the contrast increment threshold in the suppression condition compared to that in the dominance condition. Fig. 2.3 also shows that for both the dominance and suppression conditions, the (log) contrast increment threshold increases significantly with the pedestal contrast [ $F(2.472, 7.416) = 57.837, p < 0.001$ , with the Greenhouse–Geisser correction], and they have a similar slope (regression line for the dominance condition:  $y = 0.521x + 0.157$ ; regression line for the suppression condition:  $y = 0.418x + 0.643$ ) [ $F(2.284, 6.853) = 1.020, p = 0.420$ , with the Greenhouse–Geisser correction for the interaction effect of dominance/suppression by pedestal-contrast]. This suggests the interocular inhibitory mechanism activated by the conflicting local features and MBC does not have a significant impact on the contrast gain control of the MBC rivalry stimulus. The trend of our current results resembles those found in two previous studies, respectively, by Watanabe et al. (2004) (with typical BBC rivalry) and ourselves (with MBC phase-shift rivalry; Su et al., 2009).

Indeed, the similarity in trend facilitates our comparison between the MBC orientation-difference (Fig. 2.3) and MBC phase-shift rivalry stimuli (Fig. 1.6). Overall, the average elevation of the TvC function on the homogeneous grating half-image of the MBC orientation-difference stimulus is larger than that with the MBC phase-shift rivalry stimulus (the same four observers participated in both experiments). Specifically, the average difference in the magnitude of suppression between the two types of MBC rivalry stimuli is about 0.146 log contrast [ $F(1, 8) = 74.641, p < 0.001$ , ANOVA using GLM with Repeated Measures]. Thus, assuming the MBCs in both stimuli have equal strengths, the larger interocular inhibition in the MBC orientation-difference rivalry stimulus compared to the MBC phase-shift rivalry stimulus is very likely contributed by its local conflicting features (orthogonal gratings).



## Experiment 2.2

Similar to Experiment 2.1, we plotted the data of the dominance (circles) and suppression (squares) conditions as TvC functions in a log–log coordinate. Fig. 2.4a shows the average data of the four observers and Fig. 2.4b the data of the same naïve observer whose data were shown in Fig. 2.3b (Experiment 2.1). Clearly, the dominant TvC function has a similar trend to that of the dominance condition in Experiment 2.1 (regression line:  $y = 0.473x + 0.305$ ) [ $F(4, 15) = 5.48, p < 0.01$ , ANOVA using GLM with Repeated Measures]. However, the suppression TvC function does not change significantly with the contrast of the grating disc (regression line:  $y = 0.047x + 1.090$ ) [ $F(4, 15) = 0.19, p > 0.9$ ]. This finding indicates that the contrast increment threshold of the suppressed eye depends only on the contrast of the half-image stimulating it, and not on the contrast of the half-image (MBC disc) stimulating the fellow eye. In other words, changing the contrast of the MBC grating disc to vary both the strength of the MBC and the local feature within the disc (grating) in the dominant half-image, has little impact on the suppression threshold in the contralateral half-image. This finding has a significant implication. Suppose that the contrast increment threshold of the suppressed eye reflects the minimal strength of the probe stimulus in the suppressed eye required for the visual process to switch its selection from the currently dominant image representation to the suppressed one. In this regard, our finding (Fig. 2.4) suggests that no matter how salient the dominant half-image is during binocular rivalry, it is the saliency of the perturbing signals (probe) in the suppressed eye that modulates the putative visual switch. On the other hand, a transient probe that augments the signals of the dominant image representation can prevent it from being unselected (Chong & Blake, 2006; Hering, 1879/1942; Kamphuisen, van Wezel, & van Ee, 2007; Lack, 1978; Levelt, 1965; Mitchell, Stoner, & Reynolds, 2004; Ooi & He, 1999; von Helmholtz, 1925; Walker 1978).

Our finding with the MBC rivalry stimulus parallels that with the BBC rivalry stimulus. For example, Blake and Camisa (1979) conducted a similar study with the typical BBC rivalry stimulus (conflicting local features only). In their experiment, they presented a circular flash of

light (probe) with fixed intensity on a grating half-image. They found that when the grating half-image was suppressed, the percentage correct in detecting the probe did not vary with the contrast of the half-image in the fellow (dominant) eye. Although their study measured the percentage correct performance, rather than threshold, it is gratifying that both studies arrive at the same conclusion.

### Experiment 2.3

Fig. 2.5a and b show, respectively, the average detection data of five observers and the data of a representative naïve observer. The percentage correct in detecting the monocular Gabor probe is plotted as a function of SOA for both conditions. As predicted, detection is significantly higher in the dominance condition (circles) than in the suppression condition (squares) [ $F(1, 4) = 57.467, p = 0.002$ ; 2-way ANOVA with repeated measures]. The percentage correct detection in both conditions does not vary significantly with SOA [SOA main effect:  $F(4, 16) = 1.159, p = 0.365$ ; interaction between condition and SOA:  $F(1.885, 7.541) = 0.388, p = 0.680$ , with Greenhouse–Geisser correction]. This indicates that interocular inhibition becomes effective as early as 80 ms after the onset of the MBC orientation-difference rivalry stimulus. The tendency of the magnitude of suppression to be largely constant over the various SOAs appears consistent with previous studies using the BBC rivalry stimulus that tested thresholds at longer test durations (Fox & Check, 1972; Norman et al., 2000). For example, Norman et al. (2000) measured the percentage correct of detecting a probe presented to either the dominant or suppressed eye after the observer indicated perceiving global dominance of the BBC rivalry stimulus. They found the reduction of the percentage correct in the suppressed eye was constant.

Our conclusion is also confirmed by the reaction time data in Fig. 2.5c (average) and d (same naïve observer). The average reaction time is shorter in the dominance condition (circles) than in the suppression condition [ $F(1, 4) = 11.821, p = 0.026$ ]. Reaction times decrease significantly with SOA [ $F(1.657, 6.627) = 7.526, p = 0.022$ , with Greenhouse–Geisser correction].

The difference in reaction time between the two conditions does not change significantly with SOA [ $F(4, 16) = 0.929, p = 0.472$ ].

#### Experiment 2.4

Fig. 2.6a and b, respectively, depict the average detection data of six observers and the data of one representative naïve observer. The percentage correct in detecting the monocular Gabor probe is plotted as a function of SOA. Similar to Experiment 2.3 (Fig. 2.5a&b), the detection rate is significantly higher in the dominance condition (circles) than in the suppression condition (squares) [ $F(1, 5) = 30.043, p = 0.003$ , ANOVA using GLM with Repeated Measures]. The detection rate in the two conditions does not change significantly with SOA [ $F(1.680, 8.402) = 2.398, p = 0.153$ , with Greenhouse–Geisser correction]. Overall, the finding indicates that the interocular inhibition triggered by the MBC begins as early as 80 ms after the onset of the stimulus.

The reaction time results in Fig. 2.5c (average) and d (naïve observer) show a similar trend. The average reaction time is shorter in the dominance condition (circle symbols) than in the suppression condition [ $F(1, 5) = 9.821, p = 0.026$ ]. The difference in reaction time between the two conditions do not change significantly with SOA [ $F(1.166, 5.832) = 0.084, p = 0.818$ , with Greenhouse–Geisser correction]. Similarly, the reaction time for each condition does not change significantly with SOA [ $F(1.181, 5.907) = 2.874, p = 0.143$ , with Greenhouse–Geisser correction].

To summarize, this experiment together with Experiment 2.3, reveal interocular inhibition begins as early as 80 ms when locally measured with a Gabor probe. This finding supports the results of our earlier study with the MBC orientation-difference rivalry stimulus, which found that the global dominance percept can be obtained before 150 ms (Su et al., 2011b). But we wish to point out a critical difference between the two studies. That is, measuring local dominance/suppression with the probe method only gauges the event at the probed area of the

stimulus. Whereas, measuring global percept gauges the overall event after surface integration of like (dominant) features has occurred. Thus, it is reasonable to assume that it would take a longer time to achieve global dominance than local dominance. As such, it is possible that if measured locally, BBC rivalry stimuli might exhibit interocular inhibition earlier than 150 ms.

## DISCUSSION

In summary, to understand how the suppressed image of the MBC rivalry stimulus is processed, we first measured the dominance (probe on the MBC grating disc) and suppression (probe on homogeneous grating) TvC functions of the MBC orientation-difference rivalry stimulus. We found the TvC function for the suppression condition is elevated compared to that for the dominance condition, although both functions have similar slopes. While the trend of the TvC functions is similar to that found with the MBC phase-shift rivalry stimulus (Su et al., 2009), the magnitude of suppression with the MBC orientation-difference rivalry stimulus is larger. This comparison allows us to distinguish between the extent of interocular inhibition caused by the MBC alone (Su et al., 2009), and the extent caused by both the MBC and local conflicting features together. Our second experiment showed that for the MBC orientation-difference rivalry stimulus, the contrast increment threshold on the suppressed half-image (the homogeneous grating) is independent of the contrast of the dominant half-image (MBC grating disc). Our third and fourth experiments measured both the percentage correct and reaction time of detecting a monocular Gabor probe and showed that the MBC initiated interocular inhibition becomes effective as early as 80 ms after stimulus onset. In all, the current findings obtained with the probe detection protocol provide a different perspective on the mechanisms underlying the perception of the MBC rivalry stimulus, compared to our previous studies using the perceptual tracking method (Ooi & He, 2005, 2006; van Bogaert et al., 2008).

It is now well established that binocular rivalry is mediated by a distributed cortical neural network (Andrews, Sengpiel, & Blakemore, 2005; Blake & Logothetis, 2002; Fang & He, 2005; Lee & Blake, 2004; Lee, Blake, & Heeger, 2007; Leopold, Wilke, Maier, & Logothetis, 2005; Nguyen, Freeman, & Alais, 2003; Ooi & He, 1999, 2003; Papathomas, Kovacs, & Conway, 2005; Suzuki & Grabowecky, 2002, 2007; Tong & Engel, 2001; Tong, Meng, & Blake, 2006). Along this cortical network, the visual system implements a sequence of actions that include the processing of local features, surface boundary contours, and surface/object representation. For example, a number of psychophysical studies have demonstrated that image properties that are largely processed in the extrastriate cortices can significantly affect binocular rivalry (e.g., Alais & Blake, 1999; Kovacs et al., 1996; Ooi & He, 2003, 2006; Paffen et al., 2005; Shimojo & Nakayama, 1990; Sobel & Blake, 2002; Su et al., 2009; van Bogaert et al., 2008; van der Zwan & Wenderoth, 1994; Xu et al., 2010). Binocular rivalry is thus the collective outcomes of these sequential processes that lead to binocular surface representation. Along this line of thinking, Ooi and He (2005), based on the possible projection geometry of the BBC and MBC rivalry stimuli, proposed that the visual system represents a stimulus beginning at the boundary contours, with the interocular inhibitory mechanism playing a role in representing the interior surface.

We further speculate that in natural viewing, the interocular inhibitory mechanism is involved in representing binocular surfaces at, and beyond, the horopter. For surfaces near the horopter, the interocular inhibitory mechanism primarily eliminates the false matches of the retinal images to achieve a single, 3-D surface representation. For surfaces far beyond the horopter (outside the binocular fusional zone), their half-images fall on vastly non-corresponding areas. In other words, corresponding retinal areas receive dissimilar half-images, which largely are unmatchable. Evidently, from the phenomenon of binocular rivalry, we can surmise that the visual system adopts the strategy of selecting one half-image (and suppressing the other) at a time for perception, instead of superimposing the two dissimilar half-images for perception. A

possible reason is that sampling one half-image is more informative than sampling a mixture of two half-images. The dynamic characteristics of binocular rivalry ensure that both half-images are alternately sampled over time. What is sampled depends on both bottom-up and top-down visual processes. In this respect, the boundary-contour-based, bottom-up mechanism plays a significant role as a pictorial cue. When the (local) corresponding area receives one homogeneous half-image (without boundary contour) and one half-image with boundary contour (i.e., an MBC rivalry stimulus), it is more likely the former is treated as a part of a larger background surface whereas the latter as part of an object surface (i.e., figure). This biases the visual system to select the half-image with the boundary contour for surface representation (hence, dominance). The outcomes of these local interactions will then be integrated for global surface representation (e.g., Alais & Blake, 1999; Kovacs et al., 1996; Ooi & He, 2003, 2006; van Bogaert et al., 2008).

Thus, for the MBC rivalry stimulus, the visual system preferentially selects the MBC and the monocular feature attached to the MBC (in the same eye) for representation, leading to the interocular inhibitory mechanism suppressing the feature information from the other eye. On the other hand, for the BBC rivalry stimulus that carries the same boundary contour in each eye, the visual system represents the interior texture images beginning from the boundary contour in each eye. [The 3-D projection geometry of the BBC rivalry stimulus corresponds to a natural scene where the two eyes view two different texture surfaces through an aperture (Ooi & He, 2005).] Consequently, a local competition between the conflicting features (e.g., orthogonal orientation) ensues, with the winning feature being integrated into a global surface (dominant percept). Accordingly, it takes a longer time to achieve a global surface representation (dominance) with the BBC rivalry stimulus than with the MBC rivalry stimulus. Hence, the effect of interocular inhibition can be observed earlier with the MBC rivalry stimulus ( $< 80$  ms) than with the BBC rivalry stimulus ( $> 150$  ms).

## CHAPTER III

### SEEING GRATING-TEXTURED SURFACE BEGINS AT THE BORDER

#### INTRODUCTION

We live and interact in an environment where most objects in the natural scenes are defined by surfaces, and are themselves often supported by larger background surfaces. This suggests a significant amount of visual processing must be devoted to representing surfaces (Gibson, 1950; Nakayama, He, & Shimojo, 1995; von der Heydt, 2003). Although we have learned a great deal about how retinal images are coded locally by the early visual processors to obtain simple feature information, we know less about how the local simple feature information is integrated into a global surface representation. For example, for texture regions comprising of lines with different orientations, V1 neurons whose preferred orientation corresponds to the line orientation of either texture region will respond strongly to those lines. There are also some V1 neurons whose activities increase at the border between the texture regions, which reveals an early form of texture boundary contour representation (e.g., Lamme, 1995; Nothdurft, 1992; Nothdurft, Gallant, & Van Essen, 2000). It is, however, not entirely clear how V1 and the extrastriate cortices subsequently process the texture information to ultimately construct the global surface representation that supports our perception of texture surfaces. There are reasons to believe that the surface integration process is not an exclusively data driven operation but one that relies on a number of intrinsic assumptions. These assumptions, or perceptual rules, are largely derived from the regularities embedded in our ecology (niche) (Albert & Hoffman, 2000; Geisler, 2008; Gibson, 1950; Nakayama & Shimojo, 1992; Ooi, Wu & He, 2001; Purves, Lotto,

Williams, Nundy & Yang, 2001; Schwarzkopf & Kourtzi, 2008). Thus, an important approach in research of visual surface representation is discovering the rules that are shaped by the statistical properties of natural images, projection geometry, and visual-motor interactions.

The study reported in this paper tested and extended the proposal that the visual system relies on a border-to-interior strategy to represent texture surfaces (Grossberg & Mingola, 1985; Paradiso & Nakayama, 1991). With this strategy, the surface boundary contour (BC) of the texture image is first coded, followed by the texture region adjacent to the BC. Presumably, the surface texture adjacent to the BC is then sequentially integrated with the local texture signals of the interior image. The time required to integrate the local texture signals for global surface representation depends on the complexity of the texture. In this way, the particular properties of the texture determine the overall speed of surface representation.

It should be noted that the process of representing a texture surface is probably different from the filling-in process for representing a uniform color/achromatic surface. Unlike the representation of a texture surface, the filling-in operation for a uniform surface is mainly based on the color/brightness contrast information at the BC and does not include the local integration of the uniform region enclosed by the BC (von der Heydt et al, 2003). This is because the primary visual cortex receives only either very weak or no signals from the LGN neurons regarding the color/light intensity of the interior uniform region.

An argument for adopting the border-to-interior strategy is related to the fact that surface BCs are crucial cues for surface separation, and they are represented in the early visual cortices (e.g., Bakin, Nakayama & Gilbert, 2000; Grossberg & Mingola 1985; Lamme, 1995; Nakayama et al, 1995; Nothdurft, Gallant, & Van Essen, 2000; von der Heydt, 2003; Zhou, Friedman & von der Heydt, 2000). Furthermore, since rich depth information (T-junctions, etc.) are found in the vicinity of surface BCs, representing 3-D surfaces from 2-D images beginning at the BCs can help overcome some depth ambiguity inherent in the interior surface regions with similar texture information. Thus, we hypothesize that for the display in Fig. 3.1, the BC of the disc (Fig. 3.1a)



will be represented first, followed by the spreading-in of the vertical grating texture from the BC (Fig. 3.1b). This contrasts with a pixel-by-pixel strategy that locally integrates individual image patches with the same surface feature (vertical grating) to form a global surface representation (vertical grating disc).

The current study is also motivated by the early theoretical and empirical studies of perceptual fading and filling-in of uniformly-colored surfaces and scotoma (e.g., Friedman, Zhou & von der Heydt, 2003; Gerrits & Timmerman, 1969; Gerrits & Vendrik, 1970; Huang & Paradiso, 2008; Komatsu, 2006; Komatsu, Kinoshita & Murakami, 2000; Krauskopf, 1963; Meng, Ferneyhough, & Tong, 2007; Riggs, Ratliff, Cornsweet & Cornsweet, 1953; Sasaki & Watanabe, 2004; Troxler, 1804; von der Heydt, Friedman & Zhou, 2003; Walls, 1954; Yarbus, 1967). For example, when the BC of a uniformly colored figure is stabilized on the retina, the contrast signals at its border/edge become weak. This causes the color of the interior of the figure to fade away, to be replaced (“filling-in”) by the color of the larger surface external to the figure’s border/edge. It is thus hypothesized that the visual system relies on the color contrast signals at the border/edge to fill in the color of the interior region (Cohen & Grossberg, 1984; Gerrits & Vendrik, 1970). Separately, studies have also demonstrated perceptual fading and filling-in of texture patterns for stabilized images and scotoma (De Weerd, Desimone & Ungerleider, 1998; De Weerd, Gattass, Desimone & Ungerleider, 1995; Ramachandran & Gregory, 1991; Spillmann & Kurtenbach, 1992; Watanabe & Cavanagh, 1991).

There are also empirical studies other than with perceptual fading and filling-in performances that support the border-to-interior strategy (e.g., Caputo, 1998; Davey, Maddess & Srinivasan, 1998; DeValois, DeValois & Lingelbach, 1986; Motoyoshi, 1999; Paradiso & Hahn 1996; Paradiso & Nakayama 1991; Rossi & Paradiso, 1996). More direct and straightforward support for the border-to-interior strategy comes from studies that measured how the perceived image changes over time after the stimulus onset using a masking paradigm (Caputo, 1998; Motoyoshi, 1999; Paradiso & Nakayama, 1991; Stoper & Mansfield, 1978). For example,

Paradiso & Nakayama (1991), in one of their experiments, presented the observers with a homogeneous white disc (target) on a black background for 16 ms, followed after a variable ISI, with a small white ring (annular mask) on a black background for 16 ms. Their observers perceived the brightness of the central area concentric with the annulus changed from black to white as the ISI increased from 0 to 126 ms. According to the border-to-interior strategy, the visual system first codes the BC of the disc after the onset of the white disc, and then spreads the edge contrast signal (brightness) inward until it meets another edge. Thus, in Paradiso and Nakayama's experiment, when the inter-stimulus interval (ISI) is sufficiently short, the white ring stops the brightness-spreading wave resulting in the central region being seen as black. This explanation predicts that when the spatial separation between the white disc and masking ring is increased (i.e., with larger diameter white disc), it will take a longer time for the spreading wave to reach the location of the white masking ring. This is because the spreading wave, which originates from the BC of the white disc, now has to travel a longer distance before reaching the masking ring. Therefore, a longer ISI is expected to produce the same quality of brightness perception. This was exactly what Paradiso and Nakayama (1991) found. Using a similar masking paradigm, Caputo (1998) and Motoyoshi (1999) presented a texture surface in one eye and an annular or square frame mask in the other eye to reveal the characteristics of texture spreading.

The current study provides further evidence that the visual system follows the border-to-interior strategy for representing textured surfaces using a new psychophysical method that measures the texture spreading during surface representation. This method allows us to directly measure the perceived position of the leading-front of the spreading texture. Thus, when measured as a function of time after the stimulus onset we can derive the speed of the spreading wave. Notably, our method of measuring texture spreading, where the judgment depends on the leading-front of the spreading wave over time, differs from the masking method (Paradiso & Nakayama, 1991; Caputo, 1998; Motoyoshi, 1999). The masking method is more indirect

because it derives the spatio-temporal characteristics of a hypothetical spreading wave based on the perceived brightness within a masking ring. Specifically, its spatio-temporal characteristics are derived from manipulations of the ISI between the target stimulus and the masking ring, and the BC distance between the masking ring and the target stimulus. While the outcomes of these studies using the masking method are consistent with the hypothesis that the brightness of a target stimulus spreads inward from the BC, they can also be explained by an alternative hypothesis that the brightness of the entire surface of the target stimulus is represented simultaneously. According to the latter hypothesis, the spatio-temporal characteristics of the perceived brightness inside the masking ring reflect the contour interaction between the masking ring and the target stimulus, which also depends on the BC distance and the ISI (Cornelissen et al, 2006; von der Heydt et al, 2003).

Our investigation begins with the phenomenological observations of the textured surfaces in Fig. 3.1c–e, which suggest that the visual system employs the border-to-interior strategy. One can free fuse the dichoptic stimuli in Fig. 3.1c–e to qualitatively verify the important role of the BC in surface representation. With Fig. 3.1c, one perceives a vertical grating disc floating above the surrounding horizontal grating (Ooi & He, 2006; Su, He & Ooi, 2009). This demonstrates the visual system preferentially selects an image (vertical grating) with a BC over a competing image (horizontal grating) without the BC for perception. Such a significant role of the BC cannot be explained by a strategy based on a pixel-by-pixel representation, which predicts the vertical and horizontal gratings in the two eyes have equal chance to be represented. Therefore, it is not surprising that when the half-images of Fig. 3.1d and e carry BCs of similar strengths both the orthogonal gratings associated with the BCs are represented, resulting in perceptual competition between the two gratings.

In a related study (Su, He, & Ooi, 2011b), we showed the advantage of the BC by comparing the stimulus duration required to achieve global dominance with the MBC (Fig. 3.1c) and BBC (Fig. 3.1d or e) stimuli. We presented each stimulus at various durations (30–150 ms)

and asked the observers to report their percepts in three categories: global dominance of the grating disc, piecemeal, or plaid. We found that global dominance is perceived as early as 30 ms for the MBC stimulus, whereas it is hardly perceived even at 150 ms for the BBC stimuli. The latter finding is consistent with the report by Wolfe (1982) who tested a BBC stimulus with similar procedure. On the other hand, our finding with the MBC stimulus clearly demonstrates the visual system preferentially selects an image (vertical grating) with a BC over a competing image (horizontal grating) without the BC for perception. This paper takes advantage of the uniqueness of the MBC stimulus to study the early dynamics of texture spreading.

## METHODS

### Experiment 3.1: Measuring the Speed of Texture Spreading in a Dichoptic Stimulus

We sought evidence that the representation of the interior surface spreads inward from the MBC, as shown schematically in Fig. 3.1f. (This differs from the dichoptic stimulus with binocular BCs in Fig. 3.1g.) We created a dichoptic stimulus with a rectangular monocular boundary contour (MBC) containing horizontal grating (Fig. 3.2a). To restrict spreading along the lateral direction, the upper and lower edges of the rectangle were blurred. The stimulus was presented at various durations (30–500 ms). Please refer to Fig. 3.2b and the supplementary movie for the predicted (simulated) percepts as a function of time. It is predicted that at the shortest stimulus duration, a plaid, i.e., mixture of horizontal and vertical gratings, is seen (Wolfe, 1983). Next, the left and right edges of the rectangle are filled with horizontal grating while much of the central region is filled with plaid. We refer to the length of the plaid region as the “gap size”. With longer stimulus duration, as more horizontal grating texture spreads inward from the left and right BCs, the region filled with plaid (gap size) becomes smaller.

As mentioned above, we presented the dichoptic stimulus in Fig. 3.2a at various durations (30–500 ms) during the experiment. For each trial, observers reported the perceived plaid region

(gap size,  $G$ ) using a proportional scale from 0–6. From  $G$ , we obtained the average length of the perceived spread of the horizontal grating texture from one side of the rectangle,  $S_{ret}$  [ $S_{ret} = (L - G) / 2$ , where  $L$  is the total MBC rectangle length and  $S_{ret}$  denotes the distance spread in retinal domain]. We tested MBC rectangles of three different lengths ( $L = 1.50^\circ, 2.00^\circ, 2.67^\circ$ ).

### *Observers*

One author participated in all experiments. Six naïve observers with informed consent participated (three in Experiment 3.1 and three in Experiment 3.2). All observers had normal or corrected-to-normal visual acuity, stereopsis ( $<20$  sec arc), and no significant sensory eye dominance (Ooi & He, 2001).

### *Apparatus*

Stimuli generated with *MATLAB* and *Psychophysics Toolbox* (Brainard, 1997; Pelli, 1997) on a *Macintosh* were presented on a flat-screen CRT ( $1280 \times 1024$  pixels @ 100 Hz). A mirror haploscopic system attached to a chin-and-head rest aided fusion (viewing distance = 75 cm).

### *Stimuli and Procedures*

The dichoptic MBC stimulus ( $4.14^\circ \times 4.14^\circ$ ) had 4cpd sinusoidal grating ( $40.3 \text{ cd/m}^2$ , 29.1% contrast) surrounded by black ( $2.77 \text{ cd/m}^2$ ) and white ( $153 \text{ cd/m}^2$ ) square-framed fusion lock ( $5.23^\circ \times 5.23^\circ$ , width =  $0.23^\circ$ ) (Fig. 3.3a). One half-image had vertical grating and the other the same vertical grating and an additional rectangular region of horizontal grating (MBC target). The upper and lower horizontal boundaries of the MBC target were blurred with a Gaussian kernel whose full width at half-maximum (FWHM) was  $0.6^\circ$ . The MBC target length was  $1.50^\circ$ ,  $2.00^\circ$  or  $2.67^\circ$ .

The experiment comprised 18 blocks (2 eyes  $\times$  3 MBC lengths/conditions  $\times$  3 repeats). Each block had 8 warm-up, and 50 test trials (5 durations  $\times$  10 repeats). A trial began with the observer aligning his/her eyes on a  $0.91^\circ \times 0.91^\circ$  nonius fixation target ( $153 \text{ cd/m}^2$ ). Then he/she

pressed the spacebar to remove the nonius fixation target. Fifty ms later, the MBC stimulus was presented for 30, 60, 120, 250, or 500 ms, followed by a blank field. The observer indicated the perceived gap size within the MBC rectangle using the numbered keys (0–6). This psychophysical paradigm allows us to directly measure the actual surface spread.

#### *Prior training for Experiments 3.1 and 3.2*

Observers practiced rating simulated gap sizes (Fig. 3.2b) before the experiments to stabilize their gap-size rating criterion. They were shown seven simulated gaps paired with 0–6 digits, and scaled according to the proportion of the gap width relative to the overall horizontal length of the MBC rectangle. At the extremes, “0” indicates seeing horizontal grating and “6” seeing a mixture of vertical and horizontal gratings (plaid) over the entire length of the MBC stimulus, while numbers 1–5 represent various gap sizes.

Once the observers were familiar with the rating scale, they rated the simulated gap sizes with the accompanying numeric values removed. To reinforce learning, feedback was given after each trial. A block of trials would end after the observer scored eight consecutive correct responses. For Experiment 3.1, the training trials were run for each of the three MBC rectangle lengths used. In this and Experiment 3.2’s training, the viewing duration of the simulated gap stimuli was unrestricted.

We implemented two other training paradigms on the naïve observers before Experiment 3.2. First, we randomly timed the stimulus duration of the simulated gap between 30-500 ms. In this way, a gap size of “0” could be presented for 30 ms and a gap size of “6” could be presented for 500 ms, etc. This ensured that the observers did not learn to associate smaller gap sizes with longer stimulus durations. The clarity of the simulated gap stimuli was also varied to alter the difficulty of the task (achieved by manipulating the contrast and horizontal-vertical mix ratio of the texture pattern of the gap). Within every single training block, each combination of gap size and stimulus duration was tested ten times. The trials within a block were fully randomized so

that no more than three consecutive trials were the same. The binocular and monocular viewing conditions were conducted in separate blocks. The second training paradigm had “catch trials”, in which the test stimuli were intermingled with the simulated gap stimuli. As in the above, the stimulus duration of the simulated gap stimulus was randomized (30–500 ms). The ratio between the number of catch trials and test trials was fixed at 1:3. Therefore, in each block, four catch trials were employed for each level of stimulus duration, while 12 test trials with the same stimulus duration were tested. The performance of the observers was evaluated by both their average simulated gap size rating errors and percentages of correct answers in the catch trials. Formal testing (Experiment 3.2) only began when the observer’s performance stabilized at a reasonably good level (e.g., average errors across all levels of presentation duration should be less than  $0.1^\circ$  after conversion to the perceived spread in visual angle).

*Data Analyses of the Perceived Gap Size Data: Transforming between Retinal and Cortical Domains*

From the observers’ perceived gap size ( $G$ , in degree of visual angle) data, we calculated the average spreading from one side of the horizontal grating rectangle (length =  $L$ , in degree) in the retinal domain ( $S_{ret}$ , in degree):

$$S_{ret} = 0.5(L - G).$$

The derived average  $S_{ret}$  is then plotted as a function of stimulus duration ( $D$ ) in Fig. 3.2c and 4a, respectively, for Experiments 3.1 and 3.2. To estimate the average spreading in the cortical domain ( $S_{cor}$ ), we used the V1 cortical magnification factor,  $M = 15.87 E^{-1}$ , where  $E$  is eccentricity in degree. This factor is taken from Engel, Glover, and Wandell (1997) fMRI study of the retinotopic organization of the human visual cortex between  $2^\circ$  and  $12^\circ$  of eccentricity

$$S_{cor} = \int_{0.5L - S_{ret}}^{0.5L} M dE = 15.87 [\ln(0.5L) - \ln(0.5L - S_{ret})].$$

The function above allows us to transform the retinal spreading results in Fig. 3.2c and 4a to cortical spreading in Fig. 3.2d and 4b, respectively. Note that to obtain a reliable estimate of the spreading speed; we omitted the data points that reached the asymptote, i.e. those with stimulus presentation durations longer than 250 ms and 150 ms, in Experiments 3.1 and 3.2, respectively. For Experiment 3.2 (Fig. 3.4b), we only used data up to 150 ms because two observers reported completion of spreading earlier (200 ms) in the monocular stimulus condition with the preceding vertical grating pedestal (Mono-pre condition).

We then used the method of least squares to fit the data in Fig. 3.2d and 3.4b with regression lines that pass through the origin. Clearly, the good fit suggests a constant cortical spreading speed ( $V$ , the slopes of the regression lines). From the regression lines, we can, in turn, model the original spreading data in the retinal domain with the following function:

$$S_{estret} = 0.5L - \exp[\ln(0.5L) - 0.063VD].$$

The predicted retinal spreading is plotted as solid curves in Fig. 3.2c and 3.4a, for Experiments 3.1 and 3.2, respectively.

For the graphs shown in Fig. 3.3 and 3.5 (for V1 and V2), we also performed similar analyses based on the cortical magnification factors derived from another fMRI study of human cortical magnification for areas V1, V2, V3v and V4v between 0.5° and 12° of eccentricity (Serenó, Dale, Reppas, Kwong, Belliveau, Brady, Rosen, & Tootell, 1995):

$$M_{V1} = 20.05(E + 0.08)^{-1.26},$$

$$M_{V2} = 25.19(E + 0.09)^{-1.53},$$

$$M_{V3v} = 18.28(E + 0.24)^{-1.75},$$

$$M_{V4v} = 18.17(E + 0.24)^{-1.55}.$$

We thus obtained the cortical spreading functions for areas V1–V4 as follows:

$$S_{V1cor} = 77.12[(0.5L - S_{V1ret} + 0.08)^{-0.26} - (0.5L + 0.08)^{-0.26}],$$



$$S_{V2cor} = 47.53[(0.5L - S_{V2ret} + 0.09)^{-0.53} - (0.5L + 0.09)^{-0.53}],$$

$$S_{V3vcor} = 24.37[(0.5L - S_{V3vret} + 0.24)^{-0.75} - (0.5L + 0.24)^{-0.75}],$$

$$S_{V4vcor} = 33.04[(0.5L - S_{V4vret} + 0.24)^{-0.55} - (0.5L + 0.24)^{-0.55}].$$

The average results are shown in Fig. 3.3 (Experiment 3.1) and Fig. 3.5 (Experiment 3.2). Clearly, this analysis also indicates a constant cortical spreading speed (linear regression lines). Accordingly, using the estimated cortical velocities (slopes of the regression lines) we can model the retinotopic data with the following functions:

$$S_{estV1ret} = 0.5L + 0.08 - [0.013VD + (0.5L + 0.08)^{-0.26}]^{-3.85},$$

$$S_{estV2ret} = 0.5L + 0.09 - [0.021VD + (0.5L + 0.09)^{-0.53}]^{-1.89},$$

$$S_{estV3vret} = 0.5L + 0.24 - [0.041VD + (0.5L + 0.24)^{-0.75}]^{-1.33},$$

$$S_{estV4vret} = 0.5L + 0.24 - [0.030VD + (0.5L + 0.24)^{-0.55}]^{-1.82}.$$

Note: Fig. 3.3 and 3.5 do not include the fittings for V3v and V4v, which also suggest constant velocity.

### Experiment 3.2: Measuring the Speed of Texture Spreading in a Monocular Stimulus

Up till now our findings support the border-to-interior strategy for texture surface representation, which is consistent with the conclusion by Caputo (1998) and Motoyoshi (1999) based on the dichoptic stimuli (Caputo used a monocular target and binocular mask while Motoyoshi presented the target and mask in different eyes). However, since dichoptic stimuli trigger binocular competition (Ooi & He, 2006; Su et al., 2009), it is possible that our conclusion and those of Caputo (1998) and Motoyoshi (1999) are limited to binocular surface representation that involves binocular inhibitory interaction. To generalize our conclusion, we next tested with a monocular stimulus that only carries the right MBC half-image of Fig. 3.2a while the other half-image is a homogeneous gray field. We first, following the same test protocol of Experiment 3.1,

only observed a moderate trend of surface spreading for representing the rectangular region with horizontal grating (triangles, mono condition Fig. 3.4a). But this seemingly rapid surface representation cannot be easily revealed with our current method (we address this issue further in the Discussion section). We thus modified the test protocol by presenting a homogeneous vertical grating pedestal for 200 ms before the MBC test stimulus (horizontal grating rectangle) is presented. Presumably, at the initial stage of processing, the iconic memory of the prior vertical grating pedestal fuses with the signals of the horizontal grating to generate a plaid pattern. This then retards the spreading wave for representing the MBC grating rectangle.

### *Stimuli and Procedures*

There were four conditions: Mono, Dichoptic, Mono-Pre and Dichoptic-Pre. The suffix “pre” indicates trials where a homogeneous vertical pedestal grating was presented for 200 ms before the MBC stimulus was presented. The basic stimulus parameters were the same as in Experiment 3.1, except the contrast was 40% and the MBC rectangle target length was  $2.67^\circ$ . The stimulus was displayed either dichoptically (similar to Fig. 3.2a), or monocularly. With the monocular presentation, only the half-image containing the MBC target was presented while the other eye viewed a homogenous gray field. A  $0.4^\circ \times 0.4^\circ$  green fixation cross ( $6.6 \text{ cd/m}^2$ , CIE: [0.281, 0.484]) was presented either to both eyes (dichoptic conditions) or to the test eye (monocular conditions). The MBC stimulus duration was 30, 50, 100, 150, 200, 250, or 500 ms. The dichoptic conditions were re-tested here for the purpose of verification and comparison.

The four conditions were tested in different blocks. Each test block consisted of four warm-up trials and 70 randomized test trials (7 durations  $\times$  10 repeats). The test procedure was the same as in Experiment 3.1 except for the prior presentation of the vertical pedestal grating in the “pre” conditions.

## RESULTS

### Experiment 3.1

Fig. 3.2c shows for each  $L$ ,  $S_{ret}$  increases with the stimulus duration [ $F(1.104, 3.311) = 13.54$ ,  $p = 0.029$ , with Greenhouse-Geisser correction] and asymptotes around 250 ms. This result provides direct evidence that surface representation spreads inward from the BCs.

Assuming the texture spreading activities involve cortical area V1 and/or beyond, we scaled the average lengths in Fig. 3.2c according to the cortical distances in V1 based on the cortical magnification factor obtained from a human fMRI study (Fig. 3.2d) by Engel et al. (1997). Please refer to the Appendix for details of the data analysis and fitting. Remarkably, the data from all three MBC conditions with different horizontal rectangular lengths follow the same linear trajectory ( $R^2=0.937$ ), suggesting a constant spreading speed (28.7 cm/s) of surface representation within V1. We also applied cortical magnification factors of V1, V2, V3v and V4v from a different fMRI study by Sereno et al. (1995) and found the data could be fitted with linear functions, suggesting constant spreading speeds in visual cortex (V1: 29.5 cm/s,  $R^2 = 0.914$ ; V2: 48.0 cm/s,  $R^2 = 0.927$ ; V3v: 21.2 cm/s,  $R^2 = 0.903$ ; V4v: 18.6 cm/s,  $R^2 = 0.891$ ). Fig. 3.3 depicts the transformed data according to the V1 and V2 cortical magnification factors.

We further compared our derived speed with those from two other psychophysical studies, albeit with different paradigms and parameters. We first examined the finding by Paradiso and Nakayama (1991) who presented the target (uniform disc) and mask (ring) dichoptically. They estimated the speed of brightness filling-in activities in V1 in the range of 15–40 cm/s. This estimation is close to what we observed above. Second, we applied a model of 3-D depth spreading (Nishina, Yazdanbakhsh, Watanabe & Kawato, 2007) to fit the first 4 data points of our results (before the data asymptote). The estimated speed based on their model is  $\sim 30$  deg/s, which is slower than the depth propagation of the illusory (neon-color) surface ( $\sim 95$ – $117$  deg/s) studied by Nishina et al. The slower speed we found with our data is likely due to the task and stimulation difference between the two studies. Whereas we measured texture surface representation, Nishina et al measured spreading of 3-D homogeneous surface (neon-color).

There are no directly comparable physiological studies for us to verify our estimate of the spreading speeds from V1 to V4. However, we can make an indirect comparison based on an optical imaging recording study by Grinvald, Lieke, Frostig & Hildesheim (1994) in the monkey. They observed the speeds of spreading activities that originated from the stimulus location to be 0.10–0.25 m/s for area V1. These speeds are just slightly slower than our estimates for V1 (from our human observers). Likely, with optical imaging or single unit recording, future research can verify our speculation that surface representation activities travel in the visual cortex (V1 and extrastriate cortices) at a constant speed. Further, having a constant speed suggests the homogeneity of the cortical neural network in constructing the representation of surfaces.

The average results in Fig. 3.2c show that more than 90% of the MBC grating surface area is represented by 150 ms (stimulus duration). This is comparable with the study we mentioned in the Introduction (Su et al, 2006) where we measured the time to achieve global dominance in MBC and BBC stimuli. In that study, we found that with a stimulus size of  $1.9^\circ$  and at a stimulus duration of 150 ms, the percentage of seeing global dominance was about 80% with the MBC stimulus, but less than 10% with the BBC rivalry stimulus.

Finally, we consider another important factor that could influence our observation. It has been shown that the speed of visual information processing along the early visual pathway increases with retinal eccentricity (e.g., Carrasco et al, 2003; De Valois and De Valois, 1988). This “eccentricity factor” could arguably have contributed to the observed spreading effect in Fig. 3.2c, because the middle section of the horizontal MBC rectangle was imaged on the fovea while its left and right sides were imaged on the peripheral retina. However, such an eccentricity factor could not be the sole contributor. If it were, we would have found that the (measured) perceived gap sizes were the same regardless of the different lengths of the MBC rectangle. Refuting this, our data show a significant effect of the length of the MBC rectangle on the perceived gap size [main effect of length:  $F(1.061, 19.103) = 32.302, p < 0.001$ ; interaction effect between the presentation duration and length:  $F(1.061, 19.103) = 12.961, p = 0.002$ , with Greenhouse-Geisser

correction; ANOVA using GLM with Repeated Measures]. The two gray square symbols in Fig. 3.2c show example predictions of the eccentricity factor. (Note the graph plots the perceived length of the horizontal grating from one side, which is derived from the perceived gap size.) To make the prediction, we used the measured perceived gap size for the MBC rectangle of  $1.5^\circ$  length, and calculated the hypothetical perceived horizontal grating length per side  $[(\text{MBC length} - \text{gap size}) / 2]$  for the MBC rectangle of  $2.67^\circ$  length. The two gray squares would overlap with the corresponding actual data (blue) if they had the same perceived gap sizes. However, they do not overlap, thus ruling out the eccentricity factor as the sole factor causing the spreading-in results in Fig. 3.2c.

### Experiment 3.2

As predicted, we found the representation of the horizontal grating (rectangle) takes a longer time and exhibit the characteristic surface spreading from the BCs (Fig. 3.4a, mono-pre, pink circles). This indicates the border-to-interior strategy is implemented for monocular surfaces. For comparison, we also tested the same observers using the dichoptic MBC stimulus (Fig. 3.2a) with a preceding binocular vertical grating pedestal, and without a preceding vertical grating pedestal (the latter is essentially the same as in Experiment 3.1). The average results (dichoptic and dichoptic-pre in Fig. 3.4a) show a similar trend as Experiment 3.1 (Fig. 3.2c). We then converted the data in Fig. 3.4a to V1 cortical distance (Fig. 3.4b) to estimate the spreading speeds within V1 based on the human fMRI study by Engel et al. (1997). We found with the preceding vertical grating pedestal, the spreading speed for the monocular stimulus is 53.9 cm/s ( $R^2 = 0.850$ ), which is faster than the speed for the dichoptic-pre stimulus (35.2cm/s,  $R^2 = 0.891$ ). The speed of the dichoptic stimulus, 32.1 cm/s ( $R^2 = 0.810$ ), is quite similar to that of the dichoptic-pre stimulus. We attribute the slower speeds with the dichoptic and dichoptic-pre stimuli to the local interocular competition between the orthogonal gratings. This is because the orthogonal gratings (conflicting local features) at corresponding retinal locations will initiate

interocular inhibition. At each local area, the dichoptic gratings have equal chance to compete for representation. As such, along its inward path, the horizontal grating spreading wave will encounter a locally dominant image representation, which can be either a horizontal or vertical grating. If it is a horizontal grating, the texture integration will be quick, whereas if it is vertical, it will be slower as time is needed for that local patch of retinal area to revert to horizontal grating dominance. The latter operation requires additional processing and thus extra time, which does not occur in the mono and mono-pre stimulus conditions. Fig. 3.5 provides the same analysis based on the fMRI study by Sereno et al. (1995), for cortical areas V1 and V2 (V1: Mono-pre, 49.5 cm/s,  $R^2 = 0.886$ ; Dichoptic, 36.2 cm/s,  $R^2 = 0.828$ ; Dichoptic-pre: 40.4 cm/s,  $R^2 = 0.894$ ; V2: Mono-pre, 78.3 cm/s,  $R^2 = 0.865$ ; Dichoptic, 54.2 cm/s,  $R^2 = 0.798$ ; Dichoptic-pre: 61.1 cm/s,  $R^2 = 0.886$ ). We also obtained the fitting lines (not shown in the figure) according to the human V3v and V4v cortical magnification factors (V3v: Mono-pre, 35.6 cm/s,  $R^2 = 0.864$ ; Dichoptic, 26.6 cm/s,  $R^2 = 0.803$ ; Dichoptic-pre: 29.9 cm/s,  $R^2 = 0.865$ ; V4v: Mono-pre, 32.6 cm/s,  $R^2 = 0.799$ ; Dichoptic, 24.9 cm/s,  $R^2 = 0.748$ ; Dichoptic-pre: 27.8 cm/s,  $R^2 = 0.795$ ).

We now address the possible factors causing the faster surface representation in the mono condition than mono-pre condition (Fig. 3.4a). We recognize that the mono condition resembles the viewing condition where one first views a blank field and then shifts gaze to a texture surface, whereas the mono-pre condition is similar to the viewing condition of gaze shift from one texture surface to another texture surface. In the mono-pre condition, the test grating signals may initially integrate with the iconic memory signals from the preceding grating to form a plaid neural image representation. With time, the spreading wave of the horizontal test grating originating from the BC overcomes the plaid signals to form the global (test) grating representation. Thus, the integration operation in the mono-pre condition requires extra time compared to the mono condition, which does not generate an initial plaid representation. Similarly, as mentioned in the previous paragraph, the spreading wave from the BC in the dichoptic conditions needs to integrate with the local texture signals in the interior. However, one

key difference between the mono-pre and dichoptic conditions is that the plaid signals in the interior region are generated as a result of temporal interaction (forward masking) in the former but spatial interaction (binocular rivalry) in the latter.

Finally, since the average data from the mono condition are quite close to 100% (spreading) completion at the 30 ms stimulus duration (Fig. 3.4a), one might question whether the monocular surface is represented according to the border-to-interior strategy. We believe our behavioral method may not be quick enough to reveal the rapid surface spreading in the mono condition for all observers. This is because we noticed that at the shortest stimulus duration tested (30 ms), two of our four observers in the current study (Experiment 3.2) reliably reported seeing gaps in the MBC rectangle, i.e., the surface representation of the MBC rectangle for these observers was not complete at 30 ms. Our calculations revealed the percentages of incomplete surface representation for these two observers were, respectively,  $21.27 \pm 2.32\%$  and  $5.02 \pm 1.50\%$ . Separately, we have found several other observers showing an incomplete surface representation at 30 ms in an unreported experiment. This thus reflects individual difference in the speed of surface representation.

## DISCUSSION

In sum, we provide strong evidence the visual system employs a border-to-interior strategy to represent (grating) textured surfaces after the onset of the image. This finding dovetails with the results of earlier studies using different experimental paradigms (e.g., Caputo, 1998; Davey et al. 1998; DeValois et al. 1986; Motoyoshi, 1999; Paradiso & Hahn 1996; Paradiso & Nakayama 1991; Rossi & Paradiso, 1996). The border-to-interior strategy may be driven by the fact that most natural surfaces are smooth, with abrupt surface discontinuation or curvature changes mainly occurring at the surface border. This being the case, most crucial information regarding image segmentation is found at the boundary contour (Grossberg &

Mingolla, 1985; Nakayama et al., 1995). Moreover, the color and texture of the surface region adjacent to the BC usually provides a good estimate of the entire surface, as the interior of most natural surfaces have common optical properties (color and texture) (Elder & Goldberg, 2002; Fine et al., 2003; Yang & Purves, 2003). There is evidence our visual system capitalizes on such regularities to represent uniform colored surfaces (Attneave, 1954; Barlow, 1961). With the lateral inhibition mechanism implemented early in the retina, retinal ganglion cells produce vigorous responses to luminance changes (edge contrasts) of the stimulus but little responses to the interior, uniform luminance area of the stimulus (Kuffler, 1953). For representing a textured surface, a similar lateral inhibition mechanism is also implemented at the visual cortex that causes the neurons to be more sensitive to the BC of the textured surface than to the interior textured region of the surface (Knierim & van Essen, 1992; Lamme, 1995; Kourtzi, Tolias, Altmann, Augath, & Logothetis, 2003; Nothdurft, Gallant & Van Essen, 2000; Sillito, Grieve, Jones, Cuderio & Davis, 1995). Thus, by relatively strengthening the surface BC signals early on, the visual system can facilitate the later surface representation process to select the BC. For example, in Fig. 3.1c, the lateral inhibition mechanism could enhance the monocular BC signal in the left half-image. This then facilitates the MBC disc to be selected for surface representation over the homogeneous grating in the other half image.

The notion of strong BC signals complements our findings that the visual system uses the border-to-interior strategy to represent a grating texture surface. Since we used a psychophysical method that measures the position of the leading-front of the surface-spreading wave at various durations, our findings provide the first direct and explicit behavioral evidence that a spreading-in operation (the isomorphic theory) is involved in textured surface representation.

The observed spreading wave in our study reveals a fundamental operation of surface representation. We speculate two possible underlying neural mechanisms supporting this operation. The first possible mechanism, which was briefly described in the Introduction, establishes the BC as a reference (Bakin et al, 2000; von der Heydt et al., 2003; Zhou et al, 2000),



and then uses the local texture region adjacent to the BC to sequentially integrate with the remaining local texture signals (in the interior image) from the early cortical neurons (with similar selectivity) to form a global surface representation. An advantage of using the BC, which carries rich 3-D surface layout information as a reference, is that the visual system can reduce some 3-D ambiguity when integrating the local texture information (Mitchison & McKee, 1987; He, Wu, Ooi, Yarbrough, & Wu, 2004; Wu, Ooi & He, 2004). The second possible mechanism is related to a high-level interpolation process that modally creates a texture surface “image” based on the texture information at the BC. The image needs to be created because the interior homogeneous texture signals at the early level are suppressed by lateral inhibition, and thus, do not contribute to the later surface representation stage. An implication of this process is that the textured surface we perceive in the real world is actually an estimate of the global surface whose information is largely contributed by the signals near the BC. At first blush, this conjecture appears to be at odds with our normal experience of seeing a textured surface where we are able to scrutinize the rich, local structures of the surface in detail. But it does not need to be, as we propose that to see the local surface structures requires focal attention to be directed to the early local features. With attention, the lateral inhibition on the local texture signals is reduced, thus allowing its contribution to texture surface representation to be realized.

CHAPTER IV  
REVEALING BOUNDARY-CONTOUR BASED SURFACE REPRESENTATION  
THROUGH THE TIME COURSE OF INTEROCULAR INHIBITION

INTRODUCTION

Our ability to perceive single, 3-D surfaces from the 2-D retinal images is the product of binocular visual processing comprising of binocular integration and interocular inhibition. The latter process, which suppresses false matches and ecologically invalid-image representations, is assumed to play a critical role in the perception of single objects and surfaces. An important approach to understanding interocular inhibition in the laboratory is by studying binocular suppression when the two eyes are presented with dissimilar images (Blake, 1989; Fox, 1991). Fig. 4.1a illustrates a typical binocular rivalry (BR) stimulus with similar surface boundary contour (BC) information (circular outlines framing the discs) in the two half-images but with different surface feature information (orthogonal grating orientation). With fusion, one experiences perceptual alternation between the percepts of the vertical and horizontal grating discs over time. Presumably, this reflects the visual system's momentary selection of one half-image for surface representation while suppression of the other half-image through the interocular inhibitory process. One also experiences a similar alternating percept with the BR stimulus in Fig. 4.1b, where the BC of the horizontal grating disc in the right half-image is created by a relative spatial phase-shift between the central and surrounding gratings. By using such stimuli, or their variants, researchers have been able to reveal the characteristics of interocular inhibition (e.g., Alais and Blake, 1998; Kaufman, 1974; Kovács, Papathomas, Yang, and Fehér, 1996; Lee &

Blake, 2004; Nguyen, Freeman, and Alais, 2003; Ooi and He, 2005; Ooi and Loop, 1994; Papatomas, Kovács, and Conway, 2005; Shimojo and Nakayama, 1990; Smith, Levi, Harwerth, and White, 1982; Su, He, and Ooi, 2009; Suzuki and Grabowecky, 2002, 2007; Watanabe, Paik, and Blake, 2004; Wolfe, 1983).

Wolfe (1983) made an important observation regarding the influence of stimulus duration on the perception of the typical BR stimulus (similar to the stimulus in Fig. 4.1a). He found that at short stimulus durations ( $< 150$  ms) observers reported seeing the superimposition of the dichoptic orthogonal gratings (plaid or checkerboard). Only with stimulus durations of 150 ms or longer did the observers begin to report seeing either piecemeal rivalry or the entire image of a grating that belonged to one eye (i.e., global dominance percept). This empirical finding has been taken to suggest that the interocular inhibitory process asserts its influence after a relatively long delay ( $> 150$  ms) and that before BR's onset the two half-images are abnormally fused. Here, we consider an alternative explanation based on the broader consideration that the global dominance percept, i.e., global surface representation, of the typical BR stimulus (Fig. 4.1a) is the outcome of binocular surface representation where processes of surface integration and interocular inhibition are jointly involved (Ooi and He, 2005; Su et al., 2009). At each local binocular corresponding area the conflicting orientation signals from the two eyes compete via the interocular inhibitory process, which selects one orientation as the "winner" for perception (dominant) and suppresses the other. The local "winner" then integrates with adjacent local "winners" with similar orientation to form a larger surface patch of the same orientation. With further spatial integration, a global surface representation of the grating is formed endowing the observer with the global dominance percept. This analysis thus argues that the time required to form a global dominance percept depends on both the latency of the local interocular inhibitory process and the time required for global surface integration of like surface texture signals. Therefore, the long duration ( $> 150$  ms) required for global perceptual dominance observed by

Wolfe (1983) might also be attributed to the slowness of global surface integration with the typical BR stimulus (Su, He, and Ooi, 2011a).

The boundary contours of the BR stimuli (outlines of the stimuli in Fig. 4.1a&b) may play a crucial role in the time required for the visual system to achieve global surface representation. Various empirical findings have led to the proposal that the visual system relies on a border-to-interior strategy to represent global surfaces (Caputo, 1998; Grossberg and Mingola, 1985; Motoyoshi, 1999; Paradiso and Nakayama, 1991; Su et al., 2011; Watanabe and Cavanagh, 1991). With this strategy, the visual system represents a texture surface from the BC of the texture image. Specifically, the visual system first codes the BC of the texture image and a sample of the surface feature adjacent to the BC (Lamme, 1995; Nothdurft, Gallant, and van Essen, 2000; Qiu and von der Heydt, 2005; Zhou, Friedman, and von der Heydt, 2000). The sample is then used to sequentially integrate with the more interiorly located, local texture signals to form the global texture surface (Su et al., 2011). The time required to achieve a global representation of the texture surface depends on the texture structure and perceptual saliency.

We assume the visual system represents the BR stimulus using a similar border-to-interior strategy that involves surface integration in addition to interocular inhibition (Ooi and He, 2005, 2006; Su, He, and Ooi, 2009, 2010c, 2011; van Bogaert, Ooi, and He, 2008; Xu, He, and Ooi, 2010). Please refer to Fig. 4.1c for the predicted percepts of the BR stimuli in Fig. 4.1a and b. Note the surface texture feature (oriented grating) adjacent to the BC of each paired half-image is different (orthogonal). The dissimilar texture features between the paired half-images instigate the interocular inhibitory process, whereby one feature orientation is momentarily selected for representation while the other is suppressed. Both the relative strengths of the BC and texture features between the two eyes can affect the dominance selection process. According to the border-to-interior strategy, from the initial representation of the surface texture adjacent to the BC of each half-image, the visual system spreads the surface representation wave inward. On its inward path from each BC, the spreading wave interacts with the local “winners” emerging

from local binocular competition between the dichoptic orthogonal gratings. The spreading wave integrates with the local “winners” if they have the same feature (e.g., orientation). If they have different features, the spreading wave is halted until the same feature wins again in the local binocular competition. Because the spreading waves from the two half-images have different surface features (orientation) but similar saliency, they compete for global dominance when they meet (Fig. 4.1c). Consequently, a relatively longer time is required for global dominance. This theoretical analysis based on the border-to-interior strategy thus raises the possibility that a delay in local interocular inhibition may not be the sole factor causing the long duration to perceive global dominance with the typical BR stimulus (Su et al., 2011). To test it, we investigated the perception of the monocular boundary contour (MBC) rivalry stimulus shown in Fig. 4.1d (Ooi and He, 2005, 2006).

When one free fuses the two half-images of the MBC rivalry stimulus in Fig. 4.1d, one perceives a vertical grating disc surrounded by horizontal grating. The vertical grating disc percept is relatively stable despite its corresponding area being stimulated by horizontal grating (Frisby and Mayhew, 1978; Ooi and He, 2005). The strong predominance of the MBC disc is mainly attributed to the visual system’s preference to select the MBC formed between the vertical and horizontal gratings over the image with no boundary contour for surface representation (Ooi and He, 2005). To do so according to the border-to-interior hypothesis (and reiterating the above for emphasis), the visual system begins by representing the MBC and a sample of the texture adjacent to it in the same eye. Then bit-by-bit the process continues with the immediate texture area adjacent to the sample being integrated, until the entire monocular disc image is represented (see predicted percepts in Fig. 4.1e; also refer to the movie demonstration). Importantly, in contrast to the typical BR stimuli (Fig. 4.1a&b), the spreading wave of surface representation does not encounter another with a different grating texture from the other eye (half-image), particularly when the MBC disc has a small diameter. This is because the local homogeneous grating texture in the other half-image (without the BC) is not selected for surface representation

and is suppressed. Thus, without resistance from a competing wave, the time required to represent and perceive the MBC disc is predicted to be shorter, compared to the time required to perceive global dominance with the typical BR stimuli with binocular boundary contour (BBC) (Fig. 4.1a&b). On the other hand, if a delayed onset of local interocular inhibition is the main factor causing the long stimulus duration to obtain global dominance, both the MBC and typical BR stimuli should produce a similar relationship between the percentage of seeing global dominance and the stimulus duration. Our first experiment provides support for the former prediction.

Our second experiment sought further evidence for the border-to-interior hypothesis by measuring the detection of a monocular Gabor probe superimposed on the center of the MBC rivalry stimulus (Fig. 4.1d; also see examples of stimuli with probes in Fig. 4.4). With binocular suppression, the chance of detecting the probe is higher in the eye viewing the MBC disc than in the eye viewing the homogeneous grating (Su et al., 2009, 2010). Thus, consistent with the observations from the first experiment, we should be able to reveal binocular suppression in the central region of the disc at very short stimulus duration ( $< 150$  ms). Furthermore, according to the border-to-interior hypothesis, because global surface representation starts from the MBC, we expect to find the time to achieve dominance in the central disc area to increase with the diameter of the MBC disc. This predicts that interocular suppression will be observed at an earlier time with an MBC rivalry stimulus with a small disc diameter, than one with a large disc diameter. These predictions are confirmed by our experiment.

## METHODS

### *Observers*

One author and five naïve observers participated in Experiment 4.1. Four other naïve observers, who did not participate in Experiment 4.1, participated in Experiment 4.2. The naïve

observers provided their informed consent before the experiments. All observers had normal or corrected-to-normal visual acuity, stereopsis ( $\leq 40$  arcsec), and no significant eye dominance.

### *Apparatus*

Stimuli generated with *MATLAB* and *Psychophysics Toolbox* (Brainard, 1997; Pelli, 1997) on a *Macintosh*, were presented on a flat-screen CRT ( $1280 \times 1024$  pixels @ 100 Hz). A mirror haploscopic system attached to a chin-and-head rest aided fusion from a viewing distance of 75 cm.

## Experiment 4.1: Perception of MBC and BBC Rivalry Stimuli as a Function of Stimulus Duration

### *Stimuli and Procedures*

Each stimulus (Fig. 4.1a, b or d) was surrounded by a  $4.1^\circ \times 4.1^\circ$  square-frame fusion lock (width =  $0.4^\circ$ ). The fusion lock was filled with black ( $4.0 \text{ cd/m}^2$ ) and white ( $154.8 \text{ cd/m}^2$ ) texture pattern. The vertical and horizontal sinusoidal gratings (4cpd,  $79.4 \text{ cd/m}^2$ ) of each stimulus had 95% contrast. In the MBC condition (Fig. 4.1d), one half-image had a vertical grating disc surrounded by horizontal grating while the other half-image had only horizontal grating. The outermost dimension (size) of each square half-image was  $3.0^\circ \times 3.0^\circ$ . We used two variants of the typical BR stimulus with BBC. The stimulus in the typical BR-b condition (Fig. 4.1b) was similar to that in the MBC condition, except that a disc was created in the horizontal grating half-image at a region corresponding to the disc in the fellow half-image. This horizontal grating disc was created by a  $180$  deg phase shift between the designated disc area and the surrounding horizontal grating. In the typical BR-a condition (Fig. 4.1a), the grating disc in each half-image was surrounded by a homogeneous gray field ( $79.4 \text{ cd/m}^2$ ) (instead of horizontal grating). For each condition, the diameter of the grating disc in each half-image was fixed at one of four predetermined values ( $1.0^\circ$ ,  $1.3^\circ$ ,  $1.6^\circ$  or  $1.9^\circ$ ). The half-image with the vertical grating disc was always presented to the dominant eye.

To begin a trial, the observer aligned his/her eyes on the nonius fixation target ( $0.91^\circ \times 0.91^\circ$ ,  $153 \text{ cd/m}^2$ ). He/she then pressed the spacebar to remove the nonius fixation target. Fifty ms later, the test stimulus was presented for 30, 50, 100 or 150 ms. A  $3^\circ \times 3^\circ$  mask (250 ms,  $45^\circ$  oblique plaid, 1.33cpd,  $79.4 \text{ cd/m}^2$ , 12% contrast) followed to terminate the trial. The observer pressed one of four keys that corresponded to the percept of the disc area: global dominance (vertical or horizontal grating), piecemeal, plaid or unsure. The criterion for selecting dominance was strictly when the entire disc was filled with either vertical or horizontal grating. If any region within the disc  $> 0.5^\circ$  (across 2 cycles) had a plaid pattern, the percept qualified as plaid. If the disc had grating and plaid patterns ( $< 0.5^\circ$ ), the observer reported “piecemeal”. The unsure response (rare) was made when the percept was uncertain.

For each condition, 16 combinations of variables were tested (4 durations  $\times$  4 disc diameters). Each combination was tested 20 times. Two experimental sessions, each comprising of 12 blocks (3 stimulus conditions  $\times$  4 disc diameters), were run. Each block consisted of 40 semi-randomized trials (4 durations  $\times$  10 repeats).

#### Experiment 4.2: Performance in Detecting a Monocular Gabor Probe on MBC Rivalry Stimuli with Small ( $1.5^\circ$ ) versus Large ( $3.0^\circ$ ) Disc Diameter

##### *Stimuli*

A  $0.45^\circ \times 0.45^\circ$  white nonius fixation target ( $73.1 \text{ cd/m}^2$ ) and a  $5^\circ \times 5^\circ$  black square fusion lock frame ( $5 \text{ cd/m}^2$ ) were used to achieve proper eye alignment before the trial. During the trial, the nonius fixation cross was removed, while the black frame remained to surround the MBC rivalry stimulus ( $4.5^\circ \times 4.5^\circ$ ). The MBC disc ( $1.5^\circ$  or  $3.0^\circ$ ) in one half-image was created by having a  $90^\circ$  grating orientation difference between the central circular area and the surrounding area of the half-image (either vertical grating disc vs. horizontal grating surround or horizontal grating disc vs. vertical grating surround). The grating orientation of the other half-image adopted the orientation of the surround grating of the fellow half-image. T o



counterbalance the effect of stimulus orientation, we designed two pairs of MBC rivalry stimuli for each disc diameter condition (1.5° or 3.0°), in which one pair had a vertical grating disc and the other pair had a horizontal grating disc. Thus, we tested four stimulus combinations: 1.5° MBC with vertical grating disc, 1.5° MBC with horizontal grating disc, 3.0° MBC with vertical grating disc and 3.0° MBC with horizontal grating disc rivalry stimuli. Fig. 4.2a shows an example of a 1.5° MBC with vertical grating disc stimulus and Fig. 4.2b shows a 3° MBC with horizontal grating disc stimulus. All stimuli had 3 cpd sinusoidal grating (39.8% Michelson contrast) and were presented against a gray background of the same mean luminance (63.1 cd/m<sup>2</sup>). A 4.5° × 4.5° black-and-white random-dot mask (dot size: ~ 0.1° × 0.1°; 92.1% contrast, 250 ms) was employed at the end of the stimulus presentation.

During a trial, the monocular Gabor probe (20 ms) was presented either in the center of the MBC grating disc (dominance condition), or in the center of the homogeneous grating half-image (suppression condition). (See the examples in the upper panel of Fig. 4.4.) The definition of the probe was given by the formula,

$$L(x, y) = L_m \left\{ 1 + c \cdot \sin(2\pi\omega x) \cdot \left[ 1 + a \cdot \exp\left(-\frac{x^2 + y^2}{2\sigma^2}\right) \right] \right\}.$$

In the above formula,  $L(x, y)$  represents the luminance at a specified location  $(x, y)$ .  $L_m$  is the mean luminance (63.1 cd/m<sup>2</sup>);  $c$  is the grating contrast (39.8%);  $\omega$  is the spatial frequency (3 cpd);  $a$  is the peak increment contrast ratio of the probe (observer-specific, see section 2.4.2 below);  $\sigma$  is the standard deviation of the Gaussian kernel (0.24°). The probe was always presented to the observer's dominant eye.

#### *Procedures of Determining the Gabor Probe Strength*

The increment contrast ratio ( $a$ ) of the Gabor probe used in the proper experiment was determined separately for each observer to control for individual differences in sensitivity. To do so, we measured the increment contrast threshold (at 79.4% correct) of a monocular Gabor probe

while the observer experienced global perceptual dominance, or suppression, with the MBC rivalry stimulus. The probe was always presented to the observer's dominant eye. The parameters of the MBC rivalry stimulus were the same as those in the proper experiment; however, only the MBC rivalry stimuli with the  $1.5^\circ$  discs were used for the contrast threshold measurements.

We used a 2-temporal AFC design to determine the contrast threshold of the Gabor probe on the MBC rivalry stimulus. To begin a trial, the observer steadied himself/herself on a head-and-chin rest and maintained eye alignment on the nonius fixation and fusion lock. He/she then pressed the spacebar on the computer keyboard to present the MBC rivalry stimulus, which was displayed 250 ms after the removal of the nonius fixation target. Five hundred ms (interval-1) or 1000 ms (interval-2) after the onset of the MBC stimulus, a monocular Gabor probe (20 ms) was presented on one half-image (pedestal) of the MBC stimulus. Two brief tones, each presented at 500 and 1000 ms after the onset of the MBC stimulus, were used to aid the observers in discriminating between the two separate intervals. After the second interval, the MBC stimulus was displayed for another 500 ms. A 250 ms random-dot mask followed to terminate the trial. The observer's task was to press one of two keys to indicate whether the probe was seen on the first or second interval. No feedback regarding the response accuracy was given to the observer.

Once a trial was completed, the observer would press the space bar to initiate the next trial. The probe contrast in the subsequent trial was determined by the QUEST procedure. To ensure that the observer only responded to trials with total (global) dominance or suppression, he/she was instructed to abort trials where either parts, or all, of the MBC disc was suppressed, or where piecemeal rivalry was experienced. This was done by pressing the right-arrow key.

Pairs of dominance and suppression thresholds were measured for detecting both horizontal and vertical probes over three days. We then took the average threshold over the three days. From this, we determined the contrast of the vertical and horizontal probes to be used in the proper RT experiment using the following criteria: (i) if the observer had an average dominance

threshold of at least 0.2 log unit lower than his/her average suppression threshold, the probe contrast in the proper test would be set to 0.4 log unit above the average dominance threshold; (ii) if the average dominance threshold was less than 0.2 log unit lower than his/her average suppression threshold, the probe contrast would be set to 0.1 log unit above the average suppression threshold. We set these criteria based on the assumption that the typical observer has a depth of suppression of about 0.3 log unit during BR. Doing so ensures that the probe contrast was suprathreshold. With these criteria, two observers used probes that were 0.4 log unit above their dominance thresholds, and one observer used probes that were 0.1 log unit above the suppression thresholds, in the proper experiment. The last observer had an orientation specific asymmetry; thus, her vertical probe was 0.4 log unit above the dominance threshold while her horizontal probe was 0.1 log unit above the suppression threshold.

#### *Procedures of Measuring Probe Detection Performance and Reaction Time*

The Gabor probe, whose increment contrast level was determined above, was presented on either half-image of the MBC rivalry stimulus (see examples on the top panel of Fig. 4.4). For each test trial, the probe duration was 20 ms and its onset relative to the onset of the MBC rivalry stimulus (SOA, stimulus onset asynchrony) was 30, 50, 80, or 120 ms. We measured both the hit and false alarm rates, as well as the response time to detect the probe in the dominance and suppression conditions. To check for the reliability of the observer's responses, we also included catch trials in which the MBC rivalry stimulus was presented without the probe. The catch trials and test trials were intermingled within a block of 180 trials {[4 SOAs  $\times$  2 test conditions (dominance and suppression)  $\times$  2 probe orientations (horizontal and vertical)  $\times$  10 repeats] + 20 catch trials}. The trials were semi-randomized with the provision that no more than three consecutive trials had exactly the same combination of test condition and probe orientation. Additionally, four warm-up trials were provided at the beginning of each block of trials. The

stimuli used for the warm-up trials were randomly chosen by the computer. In all, each observer was tested over 12 blocks (2 disc sizes  $\times$  6 repeats) of trials.

To begin a trial, the observer aligned his/her eyes with the nonius fixation target and pressed the spacebar of the computer keyboard. This led to the removal of the nonius fixation (while the surrounding square fusion lock remained) and 250 ms later, the presentation of the MBC rivalry stimulus. Depending on the type of trial (test or catch), the monocular probe could be added at the appropriate SOA. The probe was always presented to the observer's dominant eye. The observer's task was to respond as quickly as possible by pressing the right arrow key of the keyboard if he/she saw the Gabor probe. Once the response was made, the trial terminated with the presentation of a mask (250 ms). If no response was made (because the probe was either not detected or absent), the MBC rivalry stimulus would be removed after 1.5 sec and the trial terminated with the presentation of the mask. If no probe was detected, the observer should not press any key. Unlike the threshold measurements to determine the probe contrast (see the previous section), observers need not abort a trial if the MBC disc was not seen in global dominance. However, the observer was instructed to abort the trial if the contour of the MBC disc either disappeared or was perceived as broken. This never occurred with either the 1.5° or 3.0° MBC rivalry stimulus.

In addition, several precautionary measures were implemented. Audio feedbacks with different tones were given to convey two possible types of false alarms: (i) responding to a catch trial, and (ii) responding less than 100 ms upon the probe onset (anticipatory response). Trials with anticipatory responses ( $< 0.1\%$ ) would be repeated. A third audio feedback accompanied the "regular" test trials where probe detection were made. In this way, the observer could monitor the reliability of his/her responses. For each block of trials, the observer was allowed to make a maximum of four false alarms (20%) when responding to the catch trials. If a fifth false alarm was made, the test program would abort and the observer would have to repeat the entire block of

trials. Furthermore, a one-minute rest period was inserted after every 40 trials to reduce the possibility of observer fatigue during the 180-trial block.

The data from the 12 blocks of trials from each observer were pooled for analysis of reaction time data. To increase data reliability, responses whose reaction times deviated from the mean by larger than three standard deviations were excluded from analysis. This rarely occurred (< 0.1%).

We estimated  $\hat{d}'$ , the sensitivity index for detecting the Gabor probe, from the hit rate ( $h$ ) and the false alarm rate ( $f$ ) according to the formula,  $\hat{d}' = Z(h) - Z(f)$ . We combined the  $\hat{d}'$  values of the two probe orientations, horizontal and vertical, in the final data presentation because they are not statistically different.

## RESULTS

### Experiment 4.1

The observer viewed a briefly presented MBC or BBC rivalry stimulus (Fig. 4.1a, b or d). He/she then reported the perceived grating pattern (global dominance, piecemeal, or plaid), or that he/she was unsure of the percept (average occurrence rate < 1%), by pressing one of four keys. The full-stacked area plots in Fig. 4.3 show the average percentages of seeing the four percepts as a function of stimulus duration for the three conditions (Fig. 4.3a–c) and disc diameters. We found that the global dominance percept is experienced as early as 30 ms [ $t(5) \geq 2.874, p < 0.05$ ] for all four MBC stimuli with different disc sizes/diameters (Fig. 4.3a). Notably, since the MBC rivalry stimuli have conflicting texture features that activate the interocular inhibitory mechanism, this finding indicates the onset of interocular inhibition has a short latency. The percentage of seeing global dominance increases with stimulus duration in a manner that is opposite to the trend of seeing piecemeal and plaid patterns [ $F(1.558, 7.789) = 15.503, p = 0.003$ , with Greenhouse-Geisser correction, ANOVA using GLM with Repeated Measures].

Furthermore, the percentage of perceiving global dominance is significantly higher with the MBC rivalry stimuli with small disc sizes compared to those with large disc sizes [ $F(3, 15) = 5.467, p < 0.01$ ]. This supports the prediction of the border-to-interior surface representation hypothesis that it takes longer time for the spreading wave from the border to cover the entire surface area (Fig. 4.1e).

In contrast, for the typical BR (BBC) s stimuli (Fig. 4.3b&c), the percentages of seeing global dominance are not significantly different from zero even for the longest stimulus duration tested (150 ms) [ $t(5) \leq 1.536, p \geq 0.185$ ]. This confirms the previous observations by Wolfe (1983). This finding, when compared to that of the MBC rivalry stimulus (Fig. 4.3a), does not indicate that the interocular inhibitory mechanism has a long latency. Instead, it is more likely related to the extra time required for global surface representation of BR stimuli with BBC (Fig. 4.1c).

#### Experiment 4.2

Fig. 4.4a and b, respectively, show the average  $\hat{d}'$  for detecting the monocular Gabor probes on the 1.5° and 3.0° diameter MBC rivalry stimuli. As predicted, the  $\hat{d}'$  difference between the dominance (circles) and suppression (squares) conditions, i.e., the suppression effect, is affected by the diameter of the MBC disc. With the small disc (1.5°), the overall suppression effect is strong [ $F(1, 14) = 13.852, p = 0.002$ , ANOVA with repeated measures] and increases with SOA [ $F(1, 14) = 6.783, p = 0.021$ ]. However, with the large MBC disc (3.0°), the overall suppression effect is only marginally significant [ $F(1, 14) = 4.365, p = 0.055$ ] although it also increases significantly with SOA [ $F(1, 14) = 33.913, p < 0.001$ ].

Similar to the results of the first experiment with the MBC rivalry stimuli above, binocular suppression is observed at 30 ms SOA for the small MBC disc stimulus [ $F(1, 3) = 21.961, p = 0.018$ ]. The suppression effect for the large MBC disc stimulus, however, is not significant even by 50 ms SOA [ $F(1, 3) = 2.483, p = 0.213$ ], and only reaches significance at 80

ms SOA [ $F(1, 3) = 14.550, p = 0.032$ ]. This indicates at least 50 ms is required for the central region of the  $3.0^\circ$  MBC disc to become dominant (i.e., for completion of global surface representation). These findings confirm the prediction of the border-to-interior hypothesis that the larger the MBC disc the longer is the time needed for the spreading wave to travel from the boundary contour to reach the center of the disc (Fig. 4.1e).

We should emphasize that the finding of similar detection performance in the dominance and suppression conditions at 30 ms SOA with the  $3^\circ$  MBC rivalry stimulus simply reveals there is no consistent dominance or suppression in the central region. It does not, however, necessarily indicate the lack of local interocular inhibition. This is because our psychophysical measurement does not distinguish between an equal amount of local interocular inhibition between the two eyes or the absence of local interocular inhibition.

The average reaction times (RT) reveal a similar effect of MBC disc size on binocular suppression (Fig. 4.4c&d). For the small MBC rivalry stimulus ( $1.5^\circ$ ), RT is significantly longer for detecting the probe on the suppressed half-image (squares) than on the dominant half-image (circles) and is evident as early as 80 ms SOA [ $F(1, 3) = 15.808, p = 0.028$ ]. Such RT difference between the suppression and dominance conditions reveals the effect of binocular suppression (O'Shea and Crassini, 1981). In contrast, for the large MBC rivalry stimulus ( $3^\circ$ ), the RT difference at 80 ms SOA is smaller and fails to reach the statistically significant level of 0.05 [ $F(1, 3) = 8.121, p = 0.065$ ]. The RT difference becomes significant only at 120 ms SOA [ $F(1, 3) = 23.432, p = 0.017$ ].

The difference in RT between the dominance and suppression conditions increases significantly with SOA for the small ( $1.5^\circ$ ) MBC rivalry stimulus [ $F(1, 14) = 9.076, p = 0.009$ , interaction effect]. But the effect of SOA is only moderate for the large ( $3.0^\circ$ ) MBC rivalry stimulus [ $F(1, 14) = 2.751, p = 0.119$ , interaction effect]. In addition, re 4c and 4d reveal the overall RT is longer with the large MBC rivalry stimulus than with the small MBC rivalry

stimulus, for both the dominance [ $F(1, 14) = 15.604, p = 0.001$ , ANOVA using GLM with Repeated Measures] and suppression conditions [ $F(1, 14) = 15.113, p = 0.002$ ].

Finally, we describe here a related phenomenon that we observed in this and previous studies (e.g., Su et al., 2010). This pertains to an observation we encountered when measuring the contrast threshold for detecting the monocular Gabor probe in the suppressed eye. We noticed that when the monocular probe in the suppressed eye was detected, one sometimes observed the suppressed half-image surrounding the probe also became dominant. Sometimes the dominant grating pattern (surface) expanded from the probe region much like a spreading wave. This phenomenon reminds us of the traveling wave in BR reported by Wilson, Blake, and Lee (2001), and also of the common observation where a transient increase in contrast energy (“contour strength”) breaks BR suppression (Hering, 1879/1942; Levelt, 1965; von Helmholtz, 1925). Since the monocular Gabor probe used in our experiment had a weak BC strength, the dominance switch it triggered can mainly be attributed to the local saliency of its surface feature. This observation thus reinforces the proposal that both the BC strength and surface feature saliency determine binocular surface representation in BR (Ooi and He, 2005; Su et al., 2009, 2010; Xu et al., 2010).

## DISCUSSION

Our study confirms Wolfe’s (1983) observations that longer stfigmulus duration ( $> 150$  ms) is required to obtain global dominance in the typical BR stimuli with BBC (Fig. 4.1a&b). However, we found that when the BR stimulus has an MBC (Fig. 4.1c), global dominance is perceived as early as 30 ms after stimulus onset. This finding indicates that the interocular inhibitory mechanism does not require a long processing period (delay) to produce effective binocular suppression. Furthermore, by measuring performance in detecting a monocular Gabor probe at the center of the MBC rivalry stimulus, we were able to observe reliable binocular



suppression as short as 30 ms after stimulus onset when the MBC disc is small ( $1.5^\circ$  in diameter). In contrast, there is a significant delay in observable binocular suppression when the MBC disc is large ( $3.0^\circ$  in diameter). This supports the hypothesis that the visual system employs a border-to-interior strategy to represent the MBC disc, wherein the representation of the MBC disc begins at the MBC (border) and spreads inward (Fig. 4.1e). Because it takes time for the surface-spreading wave to travel from the border, the representation of an MBC rivalry stimulus with a larger disc diameter ( $3.0^\circ$ ) takes longer.

The current findings complement those of our recent study (Su et al., 2011), which provided evidence for the border-to-interior surface representation hypothesis using a different approach. We measured the spreading speed of the surface representation wave of a MBC rivalry stimulus. To facilitate our measurements, we employed an MBC surface in the shape of a rectangle with horizontal grating texture. Our observers viewed the MBC rivalry stimulus, presented for various durations (30-500 ms), and reported the perceived grating texture pattern within the MBC rectangle. With sufficiently long stimulus duration, observers perceived an MBC rectangle completely filled with horizontal grating. But with very short stimulus duration, observers perceived a wide area of plaid pattern (superimposition of horizontal and vertical grating textures from the two eyes) at the center of the MBC rectangle, flanked by horizontal grating texture on its left and right sides. This percept supports the prediction of the border-to-interior hypothesis, where the surface representation of the horizontal grating texture spreads from the left and right borders of the MBC. Most importantly, the proportion of the represented horizontal grating area expanded inward while the plaid area shrank as the stimulus duration increased. This indicates an inward spreading of surface representation with time. Based on the perceived proportion of the horizontal grating texture within the rectangular MBC as a function of the stimulus duration, we were able to estimate the presumed neural spreading speeds of the surface representation wave from the right and left borders according to the cortical magnification factors (V1, V2, V3v and V4v). We found the cortical speed is more or less constant over the

cortical distance traveled by the surface representation wave. Furthermore, we measured the spreading speed of surface representation with a monocular stimulus that does not instigate local interocular competition (i.e., one eye views a blank field and the other eye views the half-image with the rectangular MBC stimulus). We obtained similar results, except the estimated neural spreading speed is faster probably due to the absence of local interocular inhibition.

Finally, the current finding that effective interocular inhibition occurs after a relatively short duration of binocular processing augments the notion that binocular integration and interocular inhibition co-exist to construct binocular surface perception (e.g., Blake, Westendorf, and Overton, 1980; Kaufman, 1974; Su et al., 2009; Treisman, 1962; Wolfe, 1983, 1986, 1988). In fact, this adds to our findings on the co-existence theory (Su et al., 2009). For instance, in that study the observer viewed one half-image with a vertical grating disc on a larger phase-shifted vertical grating surround and the other half-image with a homogeneous vertical grating (i.e., an MBC phase-shift stimulus). We were able to reveal this stimulus causes the observer to simultaneously experience both global stereo depth and binocular suppression. Specifically, the grating disc was seen as separated in depth from the surrounding grating, indicating the involvement of the binocular integration process in computing binocular disparity from the relative phase shift of the dichoptic gratings. Also, the observer's contrast threshold for detecting a monocular Gabor probe at the center of the MBC grating disc was lower than that on the homogeneous grating in the fellow eye, indicating some degree of binocular suppression of the homogeneous grating half-image. Our current study adds to the Su et al. (2009) study by revealing that the interocular inhibitory mechanism functions quite early and is thus likely to work in conjunction with the binocular integration process at a relatively early temporal phase of binocular information processing.

### *Conclusions*

It is proposed that processes of interocular inhibition (resolving conflict between locally dissimilar features) and global surface integration determine the global dominance percept of a BR stimulus. Supporting this, we found that the surface boundary contour properties of the BR stimuli can affect the stimulus duration required to achieve global dominance. Specifically, global dominance is perceived as early as 30 ms when the BR stimulus has an MBC, whereas it takes 150 ms or longer to perceive global dominance when the BR stimulus has a BBC. In addition, we found that binocular suppression (thus, the representation of the dominant surface) is observed earlier at a location closer to the MBC. This confirms the notion that the global surface integration process begins at the boundary contour.

## CHAPTER V

### BOUNDARY CONTOUR AFFECTS TEMPORAL DYNAMICS IN BINOCULAR RIVALRY

#### INTRODUCTION

Our previous studies have revealed that, in addition to the local feature, the boundary contour of a target plays a critical role in the binocular rivalry perception (Ooi & He, 2006; Su et al., 2010, 2011a&b). For examples, for the monocular boundary contour (MBC) rivalry display where an MBC is presented in one eye (Fig. 5.1a&b), the grating disc enclosed by the MBC has a strong predominance during a period of time (e.g. 90 s). This is in contrast to a typical binocular rivalry (BR) stimulus where the boundary contours are presented in both eyes and cause equal predominance of the two discs with orthogonal orientations (Fig. 5.1c). Further studies using a monocular probe detection method have showed that the detection threshold of a small monocular Gabor probe target is lower when it is added on the MBC grating disc than when on the homogeneous grating in the fellow eye, which has no boundary contour corresponding to the MBC (Su et al., 2010). This shows the binocular suppression of the homogeneous grating. Along with other empirical observations, these findings have led to the following proposal: to represent a large surface image, the visual system first forms the boundary contour and then represents its texture (feature) information within the boundary contour (Ooi & He, 2005; Su et al., 2011a&b). Accordingly, for the MBC display, the visual system has a preference to represent the MBC grating disc over the grating without a corresponding boundary contour in the fellow eye, and causes the suppression of the latter. Furthermore, representation of MBC disc begins at the MBC and then spreads or fills-in grating texture towards the center area (Su et al., 2011a).

However, for the typical binocular rivalry stimulus, the boundary contours in both eyes are represented, and the visual system tries to represent the texture patterns within them equally which leads to perceptual alternation of the two texture patterns.

To further reveal the role of boundary contour in binocular rivalry perception, the current experiment investigates how it affects temporal dynamics of the binocular rivalry perception. Recall that in a previous study by Ooi and He (2006), observers were asked to track the global perception of grating targets (disc) for 30 s, and the tracking data for the entire 30 s were analyzed. In the current study, the traditional procedure is modified to reveal more details of the temporal dynamics of the binocular rivalry perception. First, we modify the displays by adding a small monocular Gabor probe in either eye and ask observers to track the perception of the probe. With such a probe-tracking protocol, we can learn the binocular inhibition at the local region that is also affected by the global dominance. It also differs from the global dominance tracking protocol on the MBC display (e.g. Ooi and He, 2006), which can be influenced by high level object representation. When the MBC disc is dominant, the high-level object representation registers the MBC disc. When the observer tracks the MBC disc, the top-down system may help stabilize the MBC disk representation. When the homogeneous grating in the fellow eye is dominant, where no “disc” object representation exists, the top-down advantage is little or none. With the monocular Gabor probe protocol, when the small probe is represented, both eyes should be equal in terms of the top-down influence associated with the local region of the probe.

The current study also performs more detailed analyses on the data collected during a longer track period (90 s). First, instead of examining the average tracking performance for the entire tracking period, we look into more detailed tracking changes with higher temporal resolutions (2-s and 10-s). This allows us to learn the finer dynamics of the binocular rivalry perception (predominance and duration as a function of the tracking time). First, we can find out whether the impact of MBC on the predominance of the MBC disc fades over time. Second, since representation of MBC disc begins at the MBC and then spreads or fills-in grating texture

towards the center area (Su et al., 2011a), it is expected that the dominance perception at the center area of MBC disc depends on the distance between the disc center and the MBC (i.e. the disc size). It is thus predicted that the MBC effect on the dynamics of the probe percept at the center will decrease with the MBC disc size. Third, by evaluating its prediction that the current status of the *dominance/suppression* does not affect the characteristics of the subsequent dominance phase, we can test the hypothesis that the local perceptual alternation is mediated by a random oscillation process. For example, when the probe is perceived (dominant) in the left eye, whether is its dominance duration affected by the preceding suppression duration when the probe is suppressed? If the underlying mechanism is a purely random oscillation process, there should be no such a “priming” effect. Alternatively, the priming effect, if exists, may be related to contrast adaptation mechanism during binocular rivalry. It is possible that the eye in dominance phases may have a stronger contrast adaptation than being in suppression phases in spite of the same stimulus presentation. Accordingly, it predicts that a longer dominance phase would be following a longer suppression phase, or vice versa.

## METHODS

### *Observers*

Three naïve observers and one author participated in this experiment. All observers had normal or corrected-to-normal visual acuity and a stereoscopic resolution of 20 arcsec or better. Informed consent was obtained from the naïve observers before commencing the experiment.

### *Apparatus*

Stimuli were all generated by using *MATLAB* and *Psychophysics Toolbox* (Brainard, 1997; Pelli, 1997) on a *Mac Pro* workstation. A 21" CRT monitor was used for stimulus presentation. Its display resolution was set to 1280 × 1024 at a refresh rate of 100 Hz. The *Mac Pro* was equipped with a graphics card featuring a 10-bit per channel DAC, which allowed the

output of the monitor to be linearized without sacrificing the number of usable grayscale levels. Observers viewed the stimuli dichoptically through a mirror haploscope attached to a chin- and headrest from a viewing distance of 75 cm. The monitor screen was split into two half-screens by a partition board. Its actual luminance outputs were measured with a *Minolta LS-100* photometer.

### *Stimuli*

A  $0.45^\circ \times 0.45^\circ$  gray nonius fixation ( $70 \text{ cd/m}^2$ ) was used to achieve proper eye alignment before the stimulus presentation in each trial. There were three types of stimuli employed in this experiment (MBC, BBC, and BR; as shown in Fig. 5.1). Each of the MBC stimuli ( $4.5^\circ \times 4.5^\circ$ ) was comprised of two half-images: one having a homogeneous ( $45^\circ$  or  $135^\circ$ ) sinusoidal grating, while the other additionally having an orthogonal grating disc that was concentrically surrounded by the formal grating. For BBC stimuli, both half-images contained the surrounding grating and the orthogonal grating disc, while BR stimuli had only the grating disc. Three levels of disc size were tested [ $1.5^\circ$  (small),  $2.25^\circ$  (medium), and  $3^\circ$  (large)]. A suprathreshold Gabor contrast increment probe was always presented monocularly in the sensory dominant eye (Ooi and He, 2001). Especially, with the MBC stimuli, it was at the center of either the grating disc (MBC-disc condition) or the homogeneous grating in the contralateral half-image (MBC-grating condition). The probe was defined by the following formula:

$$L(x, y) = L_m \left\{ 1 + c \cdot \sin(2\pi fx) \cdot \left[ 1 + \frac{\Delta c}{c} \cdot \exp\left(-\frac{x^2 + y^2}{2\sigma^2}\right) \right] \right\}$$

$L(x, y)$  here is the luminance of the stimulus at a specified location  $(x, y)$ . The  $x$ -axis is orthogonal to the orientation of the grating pedestal (i.e. the  $y$ -axis) and the origin resides at the probe center.  $L_m$  is the mean luminance of the gratings ( $60 \text{ cd/m}^2$ );  $c$  stands for the grating contrast ( $1.5 \log\%$ );  $\Delta c$  represents the contrast increment at the probe center (i.e. the probe intensity; see *Procedures*);  $f$  is the spatial frequency of the gratings ( $2.2 \text{ cpd}$ );  $\sigma$  is the standard deviation of the Gaussian kernel ( $0.4^\circ$ ). Four orange fusion dots ( $0.13^\circ$  in diameter) were added

on each half-image to facilitate fusion and the spacing between adjacent dots was the same as the disc diameter. A  $4.5^\circ \times 4.5^\circ$  black-and-white random-dot mask (dot size: approximately  $0.1^\circ \times 0.1^\circ$ , contrast: 91.7%) was employed at the end of the stimulus presentation.

### *Procedures*

The task for observers was to track whether they could perceive the probe by pressing and holding the left (probe perceived) and right (probe not perceived) arrow keys on a computer keyboard. The 90-s stimulus presentation was automatically ended by a 1-s mask presentation. Each observer was tested with a constant probe intensity (of 1.2, 1.4, or 1.6 log% contrast, depending on observer). Preliminary track trials were tested with various probe intensities and the one that led to around 50% predominance of perceiving-probe in BR conditions was finally selected for each individual observer. And then he/she was tested in four test sessions in a counterbalanced manner. Within each session, all of the three levels of disc size were tested with each combination of stimulus condition and probe orientation. In total, 96 tracking trials were conducted on each observer [4 stimulus conditions (BBC, BR, MBC-disc, and MBC-grating)  $\times$  2 probe orientations ( $45^\circ$  and  $135^\circ$ )  $\times$  3 disc sizes (small, medium, and large)  $\times$  4 repeats]. Between every pair of consecutive trials, there was an interval of at least 90 s for the visual system to rest.

### *Data Analyses*

We evaluated the tracking data by comparing various measurements, including the predominance (i.e. the percentage of time when the observer perceived the probe), the average duration of dominance phases (i.e. the period of time when the probe was continuously perceived), the average duration of suppression phases (i.e. the period of time when the probe could not be perceived), and the frequency of probe being perceived. All statistical analyses were done in *SPSS* and *MATLAB*.

#### *1) Average results over the three tracking durations (0-30 s; 30-60 s; and 60-90 s)*



We first conducted a series of ANOVAs and contrasts analyses using the general linear model (GLM) with repeated measures. In these analyses, stimulus condition was taken as a fixed factor of four levels (BBC, BR, MBC-disc, and MBC-grating). Disc size and tracking time were treated as covariates since they are scalar factors. We conducted these analyses for all of the four measurements: predominance, average duration of dominance phases, average duration of suppression phases, and frequency, which were, as shown in Fig. 5.2, summarized upon three 30-s windows (0-30, 30-60, and 60-90 s, counted since tracking started).

2) Further analyses of finer dynamics of predominance and average duration of dominance phases

To reveal more details of the dynamic changes in predominance, we shortened the time window for calculating predominance data to 10 s in a further analysis. By moving the window along the elapsed tracking time by a step of 0.2 s, we could get a series of dynamic predominance data (Fig. 5.3). To assess the dynamic data statistically, ANOVAs using GLM with Repeated Measures and contrasts analyses were conducted. In these statistical tests, only predominance data calculated from nine selected time windows (0-10, 10-20, ..., and 80-90 s) were used to prevent violating the data independence assumption of these tests. For the ANOVA, we employed a model similar to the one used in the previous analyses: stimulus condition as a fixed factor while disc size and tracking time as covariates (see *Average results over the three tracking durations* above), but the BBC condition was excluded since the predominance in that condition barely changed.

We also applied a dynamic analysis on the average duration of the probe dominance phases (Fig. 5.4). To learn the characteristics of the binocular rivalry in a relative short period, we adopted the method used for predominance data with modifications. This time we pinned the data using a 2-s, instead of 10-s, time window: each data point represented the average duration of all probe dominant phases that started within the specific 2-s window (as illustrated in Fig. 5.5,

where only the probe dominance phases rendered in red counted for the given 2-s window). In this way, the data points were mathematically independent of one another so that we could conduct linear regressions and ANOVAs, as we previously did for the dynamic analysis on predominance. As in the dynamic analysis on predominance, we did not include the BBC condition. The model for the ANOVAs and contrast analyses was similar to that in dynamic predominance analysis: stimulus condition as a fixed factor of three levels (BR, MBC-disc, and MBC-grating); disc size and tracking time as covariates.

### 3) Probability density of the dominance duration and gamma distribution

To further investigate the detailed temporal dynamics, we pursued Gamma fitting on the duration data that we collected in this experiment. We fitted the dominance duration data with Gamma distribution PDFs (probability density functions) for each combination of stimulus condition, disc size, and time (using the same time windows as in the GLM analyses), respectively. For each observer, the data collected from all test trials in the same condition were pooled together and normalized by dividing each data point with the sample mean. Subsequently, the normalized data were pooled together across probe orientation and observers. The normalization was to reduce biases caused by observers' possible orientation asymmetry and between-subject variation. Then, the data were binned (bin size: 0.2) and fitted with the Gamma distribution PDF by using the least squares method in MATLAB with Optimization Toolbox. Gamma PDF is given by the following formula:

$$y = \frac{\lambda^k}{\Gamma(k)} x^{k-1} e^{-x\lambda},$$

where  $\Gamma(k)$  represents gamma function:

$$\Gamma(k) = \int_0^{\infty} e^{-t} t^{k-1} dt .$$

For all of the aforementioned Gamma fittings, the goodness of fit was evaluated by calculating the adjusted  $R^2$ :

$$R_{adj}^2 = 1 - \frac{SS_{error}}{SS_{total}} \cdot \frac{n-1}{n-m-1},$$

where  $n$  is the number of bins (i.e. the number of observations for the fitting process) and  $m$  is equal to 2 (because here're 2 regressors, i.e. the 2 parameters of a Gamma distribution).  $SS_{error}$  is the residual sum of squares:

$$SS_{error} = \sum_i (y_i - \hat{y}_i)^2,$$

while  $SS_{total}$  is the total sum of squares:

$$SS_{total} = \sum_i (y_i - \bar{y})^2.$$

In the above definitions of sums of squares,  $y_i$  represents the value of the  $i$ th bin,  $\bar{y}$  is their mean, and  $\hat{y}_i$  stands for the estimate of the same data point according to the fitted Gamma distribution. Fitting data were presented in Fig. 5.6–8 and the fitted Gamma parameters were also plotted against tracking time (Fig. 5.9).

#### 4) The relation between the dominance duration and its preceding suppression duration

Finally, for each observer, we plotted the durations of probe dominance phases against the durations of their immediate preceding probe suppression phases in each stimulus condition (Fig. 5.10). Correlation analyses were conducted to investigate whether the preceding suppression phases had any priming effect on the successive dominance phases. Assuming the “priming” mechanism underlying the binocular alternation, despite different disc sizes, be the same in each stimulus condition, we did not split the data into different disc size groups. Moreover, to improve the reliability of the data, we selected the dominance phases and their preceding suppression phases that were both at least 400 ms long, since tracking the short (< 400 ms) phases can be significantly affected by the variability of human visual-motor reaction time

during key-pressing. Outliers with deviations greater than 3 SD were also excluded from the analyses.

## RESULTS

### *1) Average results over the three tracking durations (0-30 s; 30-60 s; and 60-90 s)*

Fig. 5.2 depicts the average predominance, dominance duration, suppression duration and frequency over three tracking periods (0-30, 30-60, and 60-90 s). Overall, the predominance, dominance and suppression duration data exhibit clear effects of stimulus type, tracking time and disc size, whereas the frequency data are less clear. For example, the MBC-disc (green triangles) has a stronger predominance and longer average dominance duration, and shorter suppression duration than the BR condition (red squares). This effect of MBC on rivalry perception is largely in agreement with the previous observation using *global dominance tracking protocol* with 30 s tracking duration (Ooi & He, 2006). Other than using a different probe-tracking protocol, the current observations expand to revealing the impacts of tracking time and disc size. For instance, Fig. 5.2a shows that in the MBC-disc condition (green triangles) the predominance decreases with the tracking time while in the MBC-grating condition (blue triangles) it shows an opposite trend. If we take the differences between the two MBC conditions as a measure of the effect of MBC, we can notice that the effect of MBC decreases with tracking time. This is in contrast to the BR condition where the predominance (red squares) shows little change over the tracking period. We can also notice that the effect of MBC decreases as the size of MBC disc increases. We next performed statistical analysis over the average results in Fig. 5.2 (GLM with Repeated Measures, see *Data Analyses* for detailed explanations).

For the predominance results, the main effect of the stimulus conditions is found significant [ $F(2.384, 78.686) = 64.581, p < 0.001$ , with Greenhouse-Geisser correction], whereas the two covariates, tracking time and disc size, are insignificant ( $p > 0.05$ ). The contrast effect

between the MBC-disc and BR conditions [ $F(1, 33) = 57.369, p < 0.001$ ] as well as the contrast effect between MBC-grating and BR conditions [ $F(1, 33) = 59.844, p < 0.001$ ] are significant. There exist significant interaction effect between the stimulus condition and tracking time [ $F(3, 99) = 3.507, p = 0.018$ ] and significant interaction effect between stimulus condition and disc size [ $F(3, 99) = 16.341, p < 0.001$ ].

For the dominance duration results (Fig. 5.2b), the main effect of the stimulus condition [ $F(1.039, 34.275) = 22.185, p < 0.001$ , with Greenhouse-Geisser correction] is significant, whereas the two covariates (tracking time and disc size) fail to reach a significant level ( $p > 0.05$ ). There is a significant contrast effect between MBC-disc and BR conditions [ $F(1, 33) = 23.689, p < 0.001$ ]; and a significant contrast effect between MBC-grating and BR conditions [ $F(1, 33) = 8.513, p = 0.006$ ]. There exist significant interaction effect between the stimulus condition and tracking time [ $F(2, 66) = 4.345, p = 0.017$ ] and significant interaction effect between stimulus condition and disc size [ $F(2, 66) = 8.861, p < 0.001$ ].

For the average suppression durations (Fig. 5.2c), we found significant effect of the stimulus condition [ $F(1.196, 39.455) = 2.466, p < 0.001$ , with Greenhouse-Geisser correction], but the two covariates (tracking time and disc size) fail to reach a significant level ( $p > 0.05$ ). There is a significant contrast effect between the MBC-disc and BR conditions [ $F(1, 33) = 5.572, p = 0.024$ ]; and between the MBC-grating and BR conditions [ $F(1, 33) = 27.902, p < 0.001$ ]. There exists significant interaction effect between stimulus condition and disc size [ $F(2, 66) = 11.494, p < 0.001$ ], but not the interaction effect between the stimulus condition and tracking time [ $F(2, 66) = 0.079, p = 0.924$ ].

For the average frequency results (Fig. 5.2d), the main effect of the stimulus condition [ $F(1.486, 49.034) = 8.395, p = 0.002$ , with Greenhouse-Geisser correction] is found significant, but the two covariates (tracking time and disc size) and their interaction effects fail to reach a significant level ( $p > 0.05$ ). There are significant contrast effects: one between MBC-disc and BR

conditions [ $F(1, 33) = 27.806, p < 0.001$ ] and another one between MBC-grating and BR conditions [ $F(1, 33) = 23.573, p < 0.001$ ].

### *2a) Further analysis of dynamics of predominance*

The average predominance data over 30 s tracking period in Fig. 5.2a reveal that the effect of MBC decays with the tracking time. To reveal its finer dynamics, Fig. 5.3 plots the average data with time windows shorter than 30 s. Specifically, each data point in a curve represents predominance in a 10 s window centered at it; and separation between two adjacent data points is 0.2 s. Reasons to choose the 10-s window length are that it is long enough to avoid excessive noises and short enough to be sensitive to reflect dynamic changes with sufficient detail.

In the BBC condition (brown curves) the Gabor probe could be perceived for most of the time (predominance always above 90%) within the entire 90-s tracking period. The high predominance indicates lack of binocular inhibition on the probe, although the occasionally Troxler's fading (Troxler, 1804) might have caused it less than 100%. In the BR condition (red curves), predominance always stays below 60% for almost half of the time, indicating strong binocular suppression of the Gabor probe. By comparison, in the MBC-disc condition when the probe is presented on the MBC disc, the predominance is high (80-90%) initially and decreases to an asymptotic level (green curves), which is still above that in the BR condition. On the other hand, the predominance in the MBC-grating condition when the probe is on the homogenous grating in the opposite eye of the MBC disc, the predominance dynamic curves (blue) are below 50% and appear roughly symmetry to that of the MBC-disc (green curves), indicating strong suppression of the homogenous grating. The differences between the two MBC conditions (separations between green and blue curves) that reflect the MBC effect decreases with the tracking time. Note specifically that the effect of MBC peaks right when tracking started and decays gradually over the first 15 s after that, and then becomes rather stable. It is also clear that the MBC effect reduces as the MBC disc size increases.

We performed statistical analyses (GLM with Repeated Measures) on the average data over nine time windows within the 90-s tracking period (0-10 s; 10-20 s; ...; 80-90 s). The main effect of stimulus condition is found significant [ $F(1.198, 40.734) = 87.067, p < 0.001$ , with Greenhouse-Geisser correction], whereas the main effects of the two covariates (tracking time and disc size) are not significant. The interaction effect among all three factors is significant [ $F(3.645, 123.943) = 2.972, p = 0.026$ , with Greenhouse-Geisser correction]. Further analysis reveals that the interaction effect between stimulus condition and disc size [ $F(4, 136) = 22.510, p < 0.001$ ] and the interaction effect between stimulus condition and tracking time [ $F(1.198, 40.734) = 7.057, p = 0.008$ , with Greenhouse-Geisser correction] are significant. The predominance for the BR condition is significantly smaller than the MBC-disc stimulus condition [ $F(1, 34) = 23.690, p < 0.001$ ] but larger than the MBC-disc condition [ $F(1, 34) = 12.000, p = 0.001$ ].

#### *2b) Further analysis of dynamics of dominance duration*

We summarize the average dominance durations with a narrower time window (rather than 30 s) in Fig. 5.4. Specifically, each data point in a curve represents duration in a 2 s window centered at it (for detail refer *Methods* and Fig. 5.5). Overall, the dynamics of the duration results show similar trends as the predominance results in Fig. 5.3. For example, exists a descending order of dominance durations from the MBC-disc (green), to the BR (red), and to the MBC-grating (blue) conditions. The duration differences between the two MBC conditions vary with both the tracking time and disc size.

We first performed statistical analyses using GLM with Repeated Measures on the average data in Fig. 5.4. The main effect of stimulus condition [ $F(1.261, 586.423) = 109.914, p < 0.001$ , with Greenhouse-Geisser correction] is significant. Specifically, the dominance duration for the BR stimulus condition is significantly smaller than the MBC-disc condition [ $F(1, 465) = 108.606, p < 0.001$ ] but larger than the MBC-grating condition [ $F(1, 465) = 13.716, p < 0.001$ ]. The dominance duration is also significantly affected by the disc size [ $F(1, 465) = 5.236, p =$

0.023]. The impact of the stimulus condition on the dominance duration decreases as the disc size increases [ $F(1.261, 586.423) = 39.537, p < 0.001$ , with Greenhouse-Geisser correction]. The dominance duration decreases with the tracking time [ $F(1, 465) = 9.324, p = 0.002$ ], which is consistent with a previous study from our lab using the global dominance tracking protocol (Xu et al., 2010). The dominance duration differences among the stimulus conditions decreases with the tracking time [ $F(1.261, 586.423) = 25.72, p < 0.001$ , with Greenhouse-Geisser correction]. To further reveal how the dominance duration is affected by the tracking time in each condition, we performed linear regressions on each set of data in Fig. 5.4 over the 90-s tracking period. We only found a linear trend of a significant negative slope for the  $1.50^\circ$  disc size in the MBC-disc condition [ $-0.0474, t(43) = -4.523, p < 0.001; R^2 = 0.322$ ] and the BR condition [ $-0.0063, t(43) = -2.162, p = 0.036; R^2 = 0.098$ ]. The rest sets of the data do not show significant slope ( $p > 0.05$ ).

### 3) Probability density of the dominance duration and gamma distribution

A typical binocular rivalry stimulus such as the one in Fig. 5.1c often causes perceptual alternation between entire images from the two eyes. Previous studies, using *the global dominance tracking protocol* that monitors an entire image from each eye, have shown that the probability density of the dominance duration can be fit with a gamma distribution, suggesting a stochastic process underlying the temporal oscillation of spatially coherent percept (Fox & Hermann, 1967; Levelt, 1965, 1966, 1967).

During binocular rivalry, other than the percept of an entire image, observer occasionally experiences patchwork coming from the images in both eyes. Thus, the results from studies using the protocol of tracking the entire image may not reveal the exact dynamics at a local area within a target disc. The probe-tracking protocol used in the current experiment can overcome this problem and allows us to find out whether the probability density of the dominance duration at local area can also be fitted with a Gamma distribution.



The Gamma fitting curves were drawn in Fig. 5.6–8. The corresponding distribution parameters  $\alpha$  (shape) and  $\beta$  (rate) are indicated in each graph. We conducted Kolmogorov-Smirnov nonparametric tests to evaluate the fitting results and found that in general the data can be well fitted by Gamma distribution, indicating that the perceptual dynamics in local region is mediated by a stochastic process. Fig. 5.9 depicts the averaged fitted  $\alpha$  and  $\beta$  under the BR, MBC-disc, and MBC-grating conditions. In the BR condition, there is no clear effect of the disc size and tracking time on the two parameters (ANOVA,  $p > 0.05$ ). In the MBC-disc condition, for  $\alpha$ , there is a moderate significant effect of disc size [ $F(1, 32) = 3.387, p = 0.075$ ] and tracking time [ $F(1, 32) = 4.017, p = 0.054$ ], whereas their interaction effect fails to reach significant [ $F(1, 32) = 2.363, p = 0.134$ ]; for  $\beta$ , there is significant effect of disc size [ $F(1, 32) = 4.733, p = 0.037$ ] and moderate significant tracking effect of tracking time [ $F(1, 32) = 3.258, p = 0.08$ ], whereas the interaction effect is not significant [ $F(1, 32) = 1.574, p = 0.219$ ]. This trend is consistent with the average dominance duration results of the MBC-disc condition depicted in Fig. 5.2, where the dominance duration decreases with both the disc size and tracking time. In the MBC-grating condition, the ANOVA results do not reveal either significant main effect of disc size and tracking time, or their interaction effects.

#### 4) The relation between the dominance duration and its preceding suppression duration

If the binocular alternation during BR is driven merely by random oscillation mechanism, the dominance duration of a probe should be independent of the duration of the preceding suppression. This predicts no significant correlation between them. However, there is a possibility that there is a meaningful positive correlation between them. This is because that during binocular rivalry, the suppressed eye-channel is likely to exhibit weaker contrast adaptation than the dominant eye-channel (e.g. Blake et al., 2006). To verify the two predictions, we performed correlation analyses between the dominance duration and the duration of the preceding suppression phases. The correlation coefficients are presented in the Table 5.1 below.

**Table 5.1**Correlation between Dominance Duration and Preceding Suppression Duration

	S1		S2		S3		S4	
	<i>r</i>	<i>p</i>	<i>r</i>	<i>p</i>	<i>r</i>	<i>p</i>	<i>r</i>	<i>p</i>
BR	0.013	0.759	0.302	<0.001	0.190	<0.001	0.092	0.010
MBC-disc	-	0.118	0.207	0.007	0.176	0.001	-	0.150
MBC-grating	0.152	0.001	0.184	0.006	-	0.443	-	0.003

In the BR condition three (S2, S3, and S4) of the four observers showed significant positive correlations between the durations of the dominance phases and their preceding suppression phases. Such a priming effect, that longer suppression duration leads longer dominance duration, suggests that the binocular alternation in BR is not purely driven by a random oscillation mechanism. For the MBC-disc condition, S2 and S3 showed significant positive correlations whereas the other two observers did not. In the MBC-grating condition, however, between observer variation was larger: two (S1 and S2) of them had significant positive correlations while the other two had negative correlations, although only one (S4) of them was significant. Take together, the results from the three stimulus conditions do not support that the perceptual alternation is purely mediated by a random oscillation mechanism.

## DISCUSSION

We employed a novel probe tacking protocol to investigate the dynamics of perceptual alternation at a local area inside of typical BR, MBC-disc and MBC-grating stimuli. We found that for all the three stimulus conditions, probability densities of the dominance duration can be well fit by Gamma distribution. There exist quantitative differences in perceptual dynamics due to the impact of the MBC and disc size. Consider predominance for example. In the MBC-disc condition, the predominance reaches its peak immediately after the stimulus onset and then decreases gradually to a stable level within 15 s or so, and stays there to the end of 90 s tracking period. This differs from the typical BR condition that exhibits little change over the tracking

period. Further, the predominance in the MBC-disc condition is higher than the typical BR condition for the entire tracking period. We also observed that such effect of MBC decreases as the disc size increases. These findings reinforce the notion that the visual system relies on boundary contour signals to construct a global representation of binocular surface from the boundary contour towards interior area. The further correlation analyses on the relationship between the dominance duration and its preceding suppression duration suggests that the perceptual alternation during binocular rivalry is not purely mediated by a random oscillation mechanism.

## CHAPTER VI

### SURFACE COMPLETION AFFECTED BY LUMINANCE CONTRAST POLARITY AND COMMON MOTION

#### INTRODUCTION

Surface occlusion that occurs frequently in the external visual scene presents a special challenge to the surface representation process. A partially occluded surface does not have its occluded parts imaged on the retina, while the same surface's non-occluded parts are imaged on the retina as separated image patches. Thus to represent a partially occluded surface, the visual system has to fill-in the occluded parts of the surface and piece them together with the separated, non-occluded parts of the surface (amodal surface completion). Broadly speaking, the visual system can use two classes of cues to construct the occluded surface. The first is related to the surface relationship between the occluding and occluded surfaces, e.g., the various contour junctions, relative motion parallax, relative binocular disparity, etc. The second class of cues is related to the surface relationship between the non-occluded parts of the surface, which includes their geometric relationship and surface feature similarity. The geometric relationship pertains to, for example, whether the visible (non-occluded) surface patches have similar surface curvature, or whether they are aligned and could potentially form a smooth continuous surface (e.g., Kanizsa, 1979; Kellman, Garrigan & Shipley, 2005; Kellman & Shipley, 1991; Nakayama & Shimojo 1990; Nakayama, Shimojo & Silverman, 1989; Sekuler & Palmer, 1992). The surface feature cue is concerned with whether the non-occluded surface patches have similar surface feature properties such as texture, color, luminance, etc. Whereas much perception research has shown

that elements with similar surface image properties tend to group together, few studies have demonstrated that this Gestalt principle (similarity) applies to amodal surface integration (e.g., Yin, Kellman & Shipley, 1997; 2000). In fact, the lack of such empirical evidence has led most theories of surface representation to assign a modest role to surface features in the surface completion process (Grossberg, 1994; Grossberg & Mingolla, 1985; Kellman & Shipley, 1991). Given this, a goal of our paper is to investigate whether luminance contrast polarity, a fundamental surface feature property, plays a significant role in the representation of a partially occluded surface.

Our investigation begins by considering the display shown in Fig. 6.1a in which the inner and outer rectangular spokes along the same radial direction have the same luminance contrast polarity (He & Ooi, 1998). When one fixates at the center of the display, one perceives an illusory ring (illusory-O) occluding one longer rectangular spoke. Even though the perceived longer rectangular spoke is made up of two separated shorter spokes, it is as if the two separated spokes are now joined beneath the illusory-O occluder. To account for the perception of the illusory-O, He and Ooi (1998) proposed that the visual system amodally completes the aligned inner and outer spokes as a single, long rectangle, and modally constructs an illusory-O (ring surface) to occlude the long rectangle. The basic concept is illustrated in Fig. 6.1c with a pair of rectangular spokes in the horizontal radial direction. The corners of the rectangular segments (L-junctions) separated by the gap are now treated as implicit T-junctions. Studies have shown that the T-junction cue is a monocular cue for amodal surface completion (Anderson & Julesz, 1995; Guzman, 1969; Nakayama et al, 1995; Rubin, 2001; Stoner & Albright, 1996). As such, the two smaller white rectangles are amodally completed as one longer rectangle, with a modal surface (illusory-O) perceptually created to occlude the longer rectangular surface. To reveal the constraint of same contrast polarity, He and Ooi (1998) designed Fig. 6.1b where the inner and outer rectangular spokes along the same radial direction have opposite luminance contrast

polarity. They found that having an opposite luminance contrast polarity prevents the formation of illusory-O; instead an illusory disc (not ring) is seen.

But one might argue that He and Ooi's findings only provided an indirect evidence for the role of luminance contrast polarity in amodal surface completion. This is because they only measured the perception of the illusory-O (modal surface), and not the perceived amodal surface completion (occluded surface) between the inner and outer rectangular spokes.

To directly examine the role of luminance contrast polarity in amodal surface completion, our investigation in this paper explores the perception of object motion behind an occluder. Fig. 6.2a schematically depicts a gray rectangle moving horizontally behind two black vertical rectangles (occluders). The two vertical occluders essentially divide the gray rectangle into three smaller rectangular segments: two outer rectangles and one middle rectangle. Furthermore, owing to the absence of texture information within the rectangular segments, the local motion signals can only be found at the vertical edges/terminals of the two outer rectangles (arrows in Fig. 6.2a) and not in the middle rectangle. How does the visual system obtain global motion from these two local motion signals, which are ambiguous? It has been shown that to derive global motion from local motion information at the surface's edges, the visual system often utilizes the spatial configuration cues (Adelson & Movshon, 1984; Duncan, Albright & Stoner, 2000; He & Nakayama, 1994; Lorenceau & Shiffrar, 1992; Shimojo, Silverman & Nakayama, 1989; Stoner & Albright, 1996; Watanabe, 1997; Watamaniuk & McKee, 1995). An important spatial configuration cue is derived from the assignment of border ownership to the surface's edge (Shimojo, et al, 1989). Fig. 6.2c, which provides an analysis of the motion condition in Fig. 6.2a, elaborates on this. Notice that the right outer rectangular segment has a right edge that carries the local, leftward motion signal, and a left edge that is shared with the vertical black rectangle. Now, if the left edge is deemed to own the border, a stationary or no motion signal will be attached to the left terminal edge of the right rectangular segment. This will lead the visual system to interpret the rectangular segment as being compressed leftward while its left edge remains

stationary. However, if the border ownership is assigned to the black vertical rectangle and not the left edge of the right outer rectangle, the visual system may not necessarily interpret the left edge of the right rectangle as stationary, but instead as part of a longer rectangle moving behind the black vertical rectangle that occludes it. Thus, depending on how the visual system integrates the three rectangular segments (given the available visual cues), there are two possible perceptual interpretations of the motion display in Fig. 6.2a. Let us further consider this issue below.

As mentioned earlier, the visual system can use two classes of cues to represent overlapping surfaces. One cue, which exists between the occluding and occluded surfaces is the T-junction cue. The circles drawn onto the display in Fig. 6.2d indicate the T-junctions formed between the gray rectangular segments and black vertical rectangles. The particular configuration of the T-junctions leads the visual system to assign the border ownership to the black vertical rectangles and not the gray rectangular segments. Then the alignment between the left and right pairs of T-junctions (alignment is a factor in the second class of cues related to the surface features between the non-occluded parts of the surface) facilitates amodal surface integration between the middle rectangle and the two outer rectangles (Fig. 6.2d vs. 6.2e) (e.g., He & Ooi, 1998, 1999; Kellman & Shipley, 1991; Rubin, 2001). Another factor in the second class of cues for amodal surface completion is whether the aligned T-junction stems (the horizontal edges of the separated rectangular segments) have the same contrast polarity (He & Ooi, 1998). For the motion display in Fig. 6.2a, all three rectangular segments are lighter than the background and thus all the aligned junction stems have the same positive luminance contrast polarity. On the other hand, for the motion display in Fig. 6.2b, the contrast polarity of the middle rectangular segment (positive) is opposite to that of the two outer rectangular segments (negative). If the visual system has a preference to group or integrate separated segments with the same contrast polarity into one common surface, the observer will be less likely to perceive all three rectangular segments with opposite contrast polarity in Fig. 6.2b as one longer gray rectangle occluded by the black vertical rectangles. Thus, for Fig. 6.2a where surface completion is possible, we can predict

that motion signals from the two outer rectangles propagate to the middle stationary rectangle, leading to one perceiving a strong global motion of the long rectangle moving leftward. But for the display in Fig. 6.2b, one only perceives independent motion of the terminals of the two outer rectangular elements, which results in a leftward expansion of the left rectangle and a synchronous compression of the right rectangle, while the middle rectangle remains stationary. Our first experiment tested these predictions using the displays in Fig. 6.5.

One might wonder why our experiment measured the perceived global motion patterns rather than use the task of subjective rating to subjectively rate the perceived amodal surface of the rectangle in Fig. 6.1a. The latter task has frequently been used to measure the perceived illusory contours, such as in the study of the illusory-O perception by He and Ooi (1998). The main reason is that the representation of an occluded surface is invisible even as it produces a perceptual impression of being occluded. Thus, observers cannot reliably report this impression, as it could be confused with the impression of perceptual grouping between the visible rectangular segments that occurs even when there is no amodal surface integration between them. This is in contrast to the representation of an illusory contour (modal integration) whose image properties, such as contour sharpness, are visible and can be reliably used in a perceptual judgment task. Therefore, one has to use an indirect psychophysical method to measure the perceptual quality that is a consequence of amodal surface integration.

Our second experiment was also motivated by the study of illusory-O formation (He & Ooi, 1998). We examined whether the same contrast polarity constraint applies to motion displays with illusory occluding surfaces (Fig. 6.3). In contrast to Fig. 6.2a, the motion display in Fig. 6.3a does not have the two black vertical rectangles to physically serve as the occluders. Local, leftward motion signals are now rendered to the edges/terminals of the two gaps (arrows in the Fig. 6.3a). On the basis of the study of the illusory-O display (Fig. 6.1) we can predict that the visual system amodally completes the outer gray rectangular segments with the middle rectangular segment into a single longer horizontal rectangle (Fig. 6.3a). Furthermore, because



the left edge of the left outer rectangle and right edge of the right outer rectangle do not carry local motion signals, the amodally completed rectangle is not perceived as moving. Meanwhile, the gaps are now modally completed as illusory vertical occluders, and they move leftward as a unit (since the illusory rectangular edges demarcating the gaps carry the local motion signals). On the other hand, for the motion display in Fig. 6.3b, amodal surface completion does not occur because the middle and the two outer rectangular segments have opposite luminance contrast polarity. All the terminal edges of the rectangular segments at the gaps now own the borders and thus, carry the local motion signals. Consequently, one perceives only the middle rectangle moving leftward, while the left outer rectangle compresses and right outer rectangle expands leftward. These predictions are confirmed in our second experiment using the displays in Fig. 6.8.

Our third experiment extended the observations of the second experiment by manipulating the shape of the terminals of the rectangular segments adjacent to the gaps (Fig. 6.10b). We found that when arrowhead-shaped terminals were used, amodal surface completion between the outer and middle rectangular segments became weaker and observers were less likely to see them as an integrated unit.

## METHODS

### *Observers*

Two authors and four naïve observers participated in all experiments. All observers had normal or corrected-to-normal visual acuity and a stereoscopic resolution of 40 arcsec or better. Informed consent was obtained from the naïve observers before commencing the experiment.

### *Apparatus*

A *Macintosh* computer running *MATLAB* and *Psychophysics Toolbox* (Brainard, 1997; Pelli, 1997) were used to generate and present the visual stimuli on a 17" flat-screen CRT monitor.

The resolution of the monitor was set to  $1024 \times 768$  pixels at a refresh rate of 100 Hz. A chin-and-headrest was used to stabilize the seated observer from a viewing distance of 75 cm.

### Experiment 6.1: Physical Occluder

Fig. 6.4a and b illustrate two motion stimuli modified, respectively, from Fig. 6.2a and b. In both displays, the black diamond frame (real, physical occluder) and the gray X-shaped elements within the diamond frame are stationary while the outer oblique rectangles carry the local motion signals depicted by the arrows. In Fig. 6.4a, the stationary X-shaped elements and the outer oblique rectangles have the same luminance contrast polarity and they are expected to be amodally completed behind the black diamond frame. It is predicted that the observer will perceive the display as two longer oblique rectangles sliding over one another behind the black diamond frame (arrows) (global motion). In Fig. 6.4b, the outer oblique rectangles are darker than the background while the X-shaped elements (inner oblique rectangles) are lighter than the background. This sets up a condition where the outer rectangles have an opposite contrast polarity relative to the background compared to the inner rectangles. According to the same contrast polarity constraint, no amodal surface completion will occur between the inner and outer rectangles. This leads to the prediction that the inner rectangles within the black diamond frame will be seen as stationary while the outer rectangles along each oblique axis compress and expand in synchrony (arrows), i.e., no motion integration.

To test these predictions, we used the four types of displays shown in Fig. 6.5. Fig. 6.5a and b are the same as those in Fig. 6.4, while Fig. 6.5c and d have the stimulus background luminance increased so that both the outer and inner rectangles have the same negative contrast polarity. We predict that all displays except that in Fig. 6.5b will induce the perception of sliding motion (global motion). It is noteworthy that in Fig. 6.5d, even though the outer and inner rectangles have different luminance levels, they have the same (negative) contrast polarity relative to the background. Thus if luminance contrast polarity (sign), rather than luminance level

itself, is critical for amodal surface completion between the rectangular elements, amodal surface completion is expected to occur in Fig. 6.5d as in Fig. 6.5c. Fig. 6.5e depicts the stimulus dimensions used in our experiment. We used two different sizes of the occluding diamond frame and three different frame thickness.

### *Stimuli*

The stimulus (Fig. 6.5) comprised two oblique bars (orientation =  $\pm 45^\circ$ , length =  $2.5^\circ$ , width =  $0.33^\circ$ ) that were arranged in an X-shape formation, and a black diamond frame ( $0.1 \text{ cd/m}^2$ ) that acted as the occluder. The occluder effectively divided each oblique bar into three rectangular segments: two outer rectangles and one inner rectangle. The outermost edges of the outer rectangles were rendered with a terminal velocity of  $0.6 \text{ deg/s}$  (along its motion direction), with a maximum displacement of  $0.57^\circ$ . The entire stimulus was presented above a black fixation target ( $0.4^\circ \times 0.4^\circ$ ). The distance of the fixation target from the center of the stimulus was  $1.88^\circ$ .

Two aspects of the diamond frame occluder were varied (Fig. 6.5e). The first was the occluder width (4.0, 10.1 or 20.2 min), which effectively varied the gap size of the stimulus. The second was the overall size of the occluder, being either  $2.0^\circ$  or  $2.5^\circ$  (as measured along the axis of the diamond).

To manipulate the contrast polarity of the inner and outer rectangles with respect to the background, we fixed the luminance of the inner rectangles at a constant level ( $21.6 \text{ cd/m}^2$ ) while varied the luminance levels of both the outer rectangles ( $4.9 \text{ cd/m}^2$  or  $21.6 \text{ cd/m}^2$ ) and the homogeneous background ( $12.5 \text{ cd/m}^2$  or  $61.9 \text{ cd/m}^2$ ). With such an arrangement, the inner and outer rectangles had an opposite contrast polarity relative to the background only when they were presented against the darker background (Fig. 6.5b: opposite contrast polarity condition). When the brighter background was employed, the inner and outer rectangles had the same contrast polarity with respect to the background. Therefore, the influence of contrast polarity can be distinguished from that of luminance.

## *Procedures*

To begin a trial, the observer first stabilized his eye fixation at the fixation target and then pressed the space bar of the computer keyboard to present the stimulus. He was instructed to maintain good eye alignment with the fixation target throughout the entire 1.5-s stimulus presentation duration. The observer was instructed to respond to seeing either one of two percepts. The first is, of two partially occluded oblique bars sliding over each other back and forth (global motion when motion integration occurred; see the prediction in Fig. 6.4a). The second is, of the four outer rectangles expanding and contracting while the inner rectangles remained stationary (when motion integration failed; see the prediction in Fig. 6.4b). To report the percept, the observer pressed the left or right arrow key on the keyboard, respectively, for the first or second percept.

Each test block had 96 trials, which included four repeats of the 24 stimulus combinations (2 luminance levels of the outer rectangles  $\times$  2 background luminance levels  $\times$  3 gap sizes  $\times$  2 occluder sizes). For each observer, six such blocks were conducted during the test session. The first two blocks were treated as familiarization blocks, and only data from the last four blocks (i.e., 16 trials for each stimulus combination) were used for analysis. In all, three same luminance contrast polarity conditions and one opposite luminance contrast polarity condition were tested.

### Experiment 6.2: Illusory Occluder

To investigate whether the same contrast polarity constraint applies to the perception of illusory surfaces and global motion, we first considered the two displays in Fig. 6.7. For the display with the same contrast polarity (Fig. 6.7a, left), the aligned rectangular elements separated by the two gaps along the same oblique axis amodally complete as a single longer rectangle. Then, further facilitated by the parallel edges of the gap (see Experiment 6.3 for detailed explanation), (modal) illusory surface patches are formed at each gap (as described in Fig. 6.3a).

Consequently all four illusory surface patches are integrated into an illusory diamond frame that moves rightward (global motion) over the amodally completed rectangles (Fig. 6.7a, right). Meanwhile, the two amodally completed rectangles are perceived as stationary. However, when the outer rectangular elements are darker than the background (Fig. 6.7b, left), they have opposite luminance contrast polarity relative to the background compared to that of the inner rectangular elements. Thus, according to the same contrast polarity constraint, the visual system can no longer amodally complete the rectangular elements, nor create an illusory diamond frame in front. Without the illusory diamond frame formation, one sees the inner rectangles sliding over each other, instead of remaining stationary (Fig. 6.7b, right).

We tested the predictions above using the four types of displays in Fig. 6.8. Fig. 6.8a and b are the same as those in Fig. 6.7, while Fig. 6.8c and d have a lighter background that causes all the rectangular elements to have the same (negative) contrast polarity relative to the background. Similar to Experiment 6.1 above, we varied the gap sizes of the display. Also, we varied the distance between each pair of opposing gaps (inter-gap distance, Fig. 6.8e), which is similar to changing the overall size of the occluder in Experiment 6.1.

### *Stimuli*

The general design of the stimulus (Fig. 6.8) was similar to that used in Experiment 6.1. That is, the X-shaped stimulus with an overall size of roughly  $3^\circ \times 3^\circ$ , was formed by two intersecting oblique bars (orientation =  $\pm 45^\circ$ , length =  $3.91^\circ$ , width =  $0.33^\circ$ ). Two gaps were inserted into each oblique bar, essentially breaking the oblique bar into three rectangular segments. The spaces of the gaps were filled with the same gray level as the background. The boundaries of each gap, i.e., the inner edge of the outer rectangle and the outer edge of the adjacent inner rectangle, were rendered with back-and-forth motion along the long axis of the rectangle (0.6 deg/s, maximum displacement =  $0.57^\circ$ ). Thus, an expansion of one outer rectangle

was synchronized with a contraction of the adjacent inner rectangle along the same direction, essentially, causing the gap between the rectangles to move along.

Considered in its entirety, and at any given moment, all four gaps of the X-shaped stimulus would have the same horizontal motion component so that it was possible to conceive them as parts of an illusory diamond occluder translating horizontally. To stabilize eye alignment, a  $0.4^\circ \times 0.4^\circ$  black fixation target was located  $1.2^\circ$  below the center of the stimulus during the entire stimulus presentation of a test trial.

As in Experiment 6.1, luminance contrast polarity was manipulated by changing the luminance of the background ( $12.5 \text{ cd/m}^2$  or  $61.9 \text{ cd/m}^2$ ) and/or that of the outer rectangles ( $4.9 \text{ cd/m}^2$  or  $21.6 \text{ cd/m}^2$ ), while keeping that of the inner rectangles constant ( $21.6 \text{ cd/m}^2$ ). Thus, we have three same luminance contrast polarity conditions (Fig. 6.8a, c, & d) and one opposite luminance contrast polarity condition (Fig. 6.8b). The width of the gap size was also varied (4.0, 10.1 or 20.2 min), as was the distance between each pair of opposing gaps (inter-gap distance). The two inter-gap distances used were  $1.41^\circ$  and  $1.77^\circ$ .

### *Procedures*

The same test procedure as in Experiment 6.1 was adopted. The observers' task was to report their percepts of the stimuli, which were either: (i) two inner rectangles remaining stationary, or (ii) two inner rectangles sliding over each other. The observers pressed the left arrow key of the keyboard for percept (i) and the right arrow key for percept (ii).

Each observer was tested in an experimental session comprising six test blocks. Each block had 96 trials, i.e., four repeats of 24 stimulus combinations (2 luminance levels of the outer rectangles  $\times$  2 background luminance levels  $\times$  3 gap sizes  $\times$  2 inter-gap distances). The first two blocks of trials were taken as familiarization trials. Data from the last four blocks (i.e., 16 trials for each condition combination) were used for analysis.

### Experiment 6.3: Terminal Shape

The goal of this experiment is to further test the explanation that in Experiment 6.2, surface completion plays a critical role in determining the global motion percept of the rectangles. We changed the terminal shape of the rectangular elements from flat (Fig. 6.10a&c) to arrowhead (Fig. 6.10b&d), which is an invalid shape for amodal surface completion between two separated elements. Research has shown that for the terminal shape to be valid (Fig. 6.10a&c), the terminal edges of the two juxtaposed rectangular elements have to be parallel to each other. This is because the visual system has a tendency to treat parallel edges as opposite sides of an object/surface (Albert, 1993; Rock, 1983). This tendency leads to a bias for forming an illusory surface patch that owns the two parallel borders/edges. Furthermore, this illusory surface patch is interpreted as occluding the inner and outer rectangles (Fig. 6.10f), causing both the rectangles to yield their borders to the occluding illusory surface patch, which facilitates their amodal surface integration. In contrast, in the shape-invalid display where the terminal shape of the juxtaposed rectangles is arrowhead rather than flat (parallel), amodal surface completion between the juxtaposed rectangles is less likely to occur. Accordingly, for the four displays in Fig. 6.10, we can predict that little or no perception of moving illusory diamond frame will be seen in Fig. 6.10b, unlike in Fig. 6.10a, even though the elements have the same contrast polarity. We can also predict that no moving illusory diamond frame will be observed for the displays in Fig. 6.10c&d due to their having opposite contrast polarity.

### *Stimuli*

Two terminal shape conditions (flat vs. arrowhead) were tested (Fig. 6.10). The stimuli for the flat-terminal condition were the same as a subset of the stimuli used in Experiment 6.2. Specifically, only the larger stimuli with an inter-gap distance of  $1.77^\circ$ , a gap size of 12.6 min and displayed against the darker background ( $12.5 \text{ cd/m}^2$ ) were employed. The stimuli for the arrowhead-terminal condition were modified from those in the flat-terminal condition by “sharpening” the terminal endings. Doing so altered the shape of the gap from parallel to

arrowhead. The width of the arrowhead gap at its narrowest location in the middle was 4 min, and at its widest locations on the sides was 20.2 min. These dimensions were chosen so that the average width of the arrowhead gap was similar to that of the parallel gap (12.6 min).

### *Procedures*

The same test procedure and task as in Experiment 6.2 were adopted, except that only four stimulus combinations were tested (2 luminance levels of outer rectangle  $\times$  2 terminal shapes). A test block comprised 64 trials (i.e., 16 repetitions per stimulus combination). Each observer was tested over 4 blocks of trials, with the first two blocks being taken as familiarization blocks. Data collected from the last two blocks were used for analysis (i.e., 32 trials per stimulus combination).

## RESULTS

### Experiment 6.1

Fig. 6.6 illustrates the average percentages of perceiving motion integration as a function of gap sizes for the small (upper graph) and large occluder sizes (lower graph). Clearly, the percentages of perceiving integrated motion are very low (almost zero) in the opposite contrast polarity condition (Fig. 6.5b), unlike those in the same contrast polarity conditions. The p-values of one-sample t-test for all data points in the opposite contrast polarity condition range between 0.076 to 0.363, and overall, the data points are significantly lower than those in the three same contrast polarity conditions (Fig. 6.5a, c, & d) [ANOVA with Contrasts Analysis:  $F(1, 5) = 67.427, p < 0.001$ ]. Furthermore, the data of the two same contrast polarity conditions with the lighter background (Fig. 6.5c&d) are similar to the data of the same contrast polarity condition with the darker background (Fig. 6.5a) [ $F(1, 5) = 1.194, p = 0.324$ ;  $F(1, 5) = 3.324, p = 0.128$ ]. This suggests that neither the luminance difference between the elements (Fig. 6.5c vs. 6.5d) nor the luminance of the background (Fig. 6.5a vs. 6.5c) can account for the poor motion integration



of the opposite contrast polarity condition (Fig. 6.5b). Thus the results support the prediction that the visual system can only amodally complete elements with the same luminance contrast polarity to achieve a global motion percept (Fig. 6.4).

The gap size factor also has a significant main effect on motion integration [ $F(1.037, 5.187) = 20.903, p = 0.005$ , with Greenhouse-Geisser correction; ANOVA using GLM with Repeated Measures] and an interaction with contrast polarity [ $F(2.216, 11.081) = 12.971, p = 0.001$ , with Greenhouse-Geisser correction]. As described earlier, motion integration is almost absent in the opposite contrast polarity condition regardless of the gap size. However, when the inner and outer rectangles of the stimulus has the same contrast polarity, increasing the gap size results in significantly less motion integration. Yet changing the occluder size does not significantly affect motion integration [ $F(1, 5) = 3.644, p = 0.115$ ]. One possibility is that the two occluder-sizes were not sufficiently large to reveal an effect on amodal surface completion.

### Experiment 6.2

The average data are plotted in Fig. 6.9. The percentages of perceiving global motion (motion integration) in the opposite contrast polarity condition are only slightly above zero (onesample t-test for every combination of gap size and occluder size:  $p > 0.175$ ), which are significantly lower than those in the three same contrast polarity conditions [ $F(1, 5) = 28.836, p = 0.003$ ; ANOVA with Contrasts Analysis]. There is also an interaction effect between contrast polarity and gap size [ $F(2.607, 13.035) = 6.031, p = 0.010$ , with Greenhouse-Geisser correction]. This finding confirms that the same contrast polarity constraint applies both to amodal surface completion between separated elements and modal surface completion (illusory surface formation).

Additionally, for all the three same contrast polarity conditions, motion integration decays with increasing gap size [ $F(1.116, 5.578) = 11.998, p = 0.014$ , with Greenhouse-Geisser

correction]. As in Experiment 6.1, there is no significant effect of inter-gap distance on motion perception [ $F(1, 5) = 0.033, p = 0.863$ ].

We also noticed that when the illusory diamond shape is perceived as a unique moving object, the perceptual impression of the diamond shape is stronger than when the display is not rendered with local motion signals. This suggests that a common motion signal facilitates the integration of the illusory elements to become a single illusory figure (Anderson & Barth, 1999; Kellman and Cohen, 1984; Yonas, Craton and Thompson, 1987).

### Experiment 6.3

Fig. 6.11 depicts the average results. As in the previous experiments, the percentages of perceiving integrated motion are higher in the same contrast polarity condition than in the opposite contrast polarity condition [ $F(1, 5) = 18.187, p = 0.008$ ; ANOVA using GLM with Repeated Measures]. In addition, when the juxtaposed rectangles had the arrowhead terminals (invalid shape), observers saw less motion integration compared to when they had flat (parallel) terminals (valid shape) [ $F(1, 5) = 6.820, p = 0.048$ ]. This confirms the prediction that the shape factor that affects surface completion between separated elements also influences the global motion perception.

## DISCUSSION

In summary, we first revealed that elements with the same luminance contrast polarity but physically separated by a real occluding surface are amodally integrated and perceived as moving together (global motion). The global motion percept is not experienced when the separated elements have opposite luminance contrast polarity. Second, we showed that even without a real occluding surface image, separated elements with the same luminance contrast polarity are amodally integrated and an illusory occluding (modal) surface is perceived along with the integrated motion (global motion). This finding extends the observation of the illusory-

O display of He and Ooi (1998). Third, we found that an invalid terminal shape degrades both surface integration and global motion perception. In all, these experiments suggest that motion signals can propagate along the visible as well as the invisible parts (amodal) of a partially occluded surface, leading to the partially occluded surface being perceived as moving together as a single entity.

As mentioned in the Introduction, the observation of the illusory-O display (Fig. 6.1) provides a clear demonstration that luminance contrast polarity plays a critical role in surface completion. This led He and Ooi (1998) to put forward the idea that the formation of the illusory-O is contingent on the inner and outer rectangular segments being amodally integrated, which occurs only when they have the same luminance contrast polarity. This contingency idea is consistent with the notion that the main casual factor for illusory surface (modal) completion is the visual system's tendency to amodally complete separated elements (Kanizsa, 1955). Together, Experiments 6.1 and 6.2 in this paper provides a more direct support for this notion. First, Experiment 6.1 shows that amodal surface interpolation, in the presence of a real occluding surface, is subjected to the same contrast polarity constraint. Then Experiment 6.2 shows that when the visual system is confronted with geometric cues valid for amodal and modal surface completion, there is a tendency to amodally interpolate only when the separated elements have the same luminance contrast polarity.

We need to point out that the same contrast polarity constraint does not affect the formation of an illusory surface that is not driven by amodal surface integration between two elements. For example, it has been shown that the Kanizsa illusory square is perceived even when neighboring pac-man elements have opposite contrast polarity (Prazdny 1983; Shapley & Gordon, 1985). This is because the formation of the Kanizsa illusory square is not driven by the amodal surface integration between the neighboring pac-men (He & Ooi, 1998). In fact, when one perceives the Kanizsa illusory square, one also has an impression of each pac-man being amodally completed as a disc in back. Consistent with this explanation, Spehar and Clifford

(2003) reported that when each pac-man is made of one-half white and one-half black sector (opposite contrast polarity), which cannot to be amodally completed as an occluded disc, the perception of the illusory square is degraded.

The observation of the Kanisza illusory square with opposite contrast polarity elements motivates the proposal that the brain has a Contour Boundary system that is responsible for surface completion (Grossberg & Mingolla, 1985; Kellman & Shipley, 1991; Shipley & Gordon, 1987; Williams & Hanson, 1996). The Contour Boundary system is insensitive to luminance contrast polarity, and codes the contrast edge. To represent a texture-free surface, the Contour Boundary system first constructs the borders (outlines) of the surface. Then from the borders, a Feature Contour system, which carries the luminance and color contrast polarities at the border, fills the interior surface with brightness and hue (e.g., Grossberg & Mingolla, 1985; Grossberg, 1994). Accordingly, it is the Contour Boundary system that determines whether two elements can be completed. Since the Contour Boundary system is insensitive to luminance contrast polarity, it is expected to complete separated elements with opposite contrast polarity such as those displays in Fig. 6.1b, 6.2b, 6.5b, and 6.8b.

However, our current results and those of He and Ooi (1998) demonstrate a strong influence of luminance contrast polarity (a surface feature cue) on surface completion. This suggests that computational models of surface representation need to more heavily weight the contributions of surface feature cues in surface completion. There are two possible ways to do so. The first way is to include feedback interactions in the model (e.g., Albert, 2007). For example, the initially integrated boundary contour representation can be inhibited or vetoed by the Feature Contour system if the latter system detects an opposite contrast polarity between separated elements. The second way is for the Feature Contour system to detect both the contour and contrast polarity, and represent the surface. In this way, the Feature Contour system can integrate surface segments when their aligned contours have the same contrast polarity. Several neurophysiological studies of early visual cortical neurons have shown that form (e.g., orientation

and edge location) and color/luminance contrast polarity information are often coded by the same neurons (e.g., Friedman, Zhou & von der Heydt, 2003; Gegenfurtner et al, 1996; Leventhal et al, 1995; Zhou, Friedman & von der Heydt, 2000). In particular, Zhou et al (2000) found that the majority of neurons in V2 and V4 code both the border ownership (BO) and the local luminance contrast polarity (CP) information. These border ownership selective neurons are crucial for representing surface separation (surface limit/extension), which is likely to contribute to surface completion (Baylis & Driver, 1995; Fang, Boyaci & Kersten, 2009; Koffka, 1935; Nakayama et al, 1995; Nakayama & Shimojo, 1990; Qiu & von der Heydt, 2005; Zhou et al, 2000).

While it is beyond the scope of this paper, we recognize the future need to investigate whether the same contrast polarity constraint can be generalized to more complex images. Our studies have thus far used relatively simple displays wherein the element's luminance contrast polarity can be easily defined, as all elements are viewed against a background with the same luminance specification. Such simple displays allow us to explain our results based, presumably, on an early and local surface contour process. But how does the visual system represent more complex surface layouts? For instance, when separated gray surface segments are seen against a background surface with locally abrupt changes in luminance levels? In this case, it is not easy to define the overall luminance contrast polarity of the contours. This scenario leads us to speculate that since the goal of amodal surface completion is to specify a large surface entity, a higher level of global surface representation process must be involved in amodal surface integration. The higher level would ensure that for complex surface layouts the similarity of the overall lightness of the surface segments would be the determining factor used for surface integration. To be precise, we speculate that the later stage of global surface representation process could override the same contrast polarity constraint of the early and local surface contour process, if the later process identifies two surface segments as having a similar overall lightness. The simple stimuli employed in our experiments are able to show the same luminance contrast polarity constraint because with the same homogeneous background used, the local contrast polarity (negative vs.

positive) is consistent with the perceived global lightness of the surface segments (black vs. white).

## CHAPTER VII

### BOUNDARY CONTOUR BASED SURFACE INTEGRATION AFFECTED BY COLOR

#### INTRODUCTION

The visual system often needs to represent partially occluded surfaces by filling in the occluded fragments and integrating the visible fragments. Surface boundary contours play a major role in this process of surface completion (Nakayama et al 1995). The surface completion process probably begins as early as in cortical areas V1 and V2 where orientation and contour/edge are represented (e.g., Bakin et al 2000; Sugita 1999; von der Heydt et al 1984, 2003). Zhou et al (2000) discovered that V2 neurons are selective for the side of the boundary contour of a region (border ownership, BO). A pair of BO selective neurons with opposite directions of BO preference comprises a functional BO unit. Presumably, in response to Fig. 7.1a where an oblique segment intersects a horizontal rectangle, the functional BO units at the intersection would signal that the horizontal rectangle owns the border (arrows), while the oblique segment does not leading to its amodal extrapolation in back. The ellipse in Fig. 7.1b depicts one functional BO unit at the intersection; it has black and white halves indicating its contrast polarity preference. It follows that with two oblique segments juxtaposing the horizontal rectangle as in Fig. 7.1c, the functional BO units (two ellipses at horizontal edges in Fig. 7.1d) provide consistent information for amodal surface completion to occur between the two oblique segments. Note also, the functional BO units at the oblique edges in Fig. 7.1d signal that the oblique segments own the borders.

Most theories assume that the boundary contour-based surface completion process is

insensitive to contrast polarity (CP) (e.g., Grossberg and Mingolla, 1985; Kellman and Shipley, 1991). Accordingly, these theories predict completion would occur (as in Fig. 7.1c) between the two oblique segments with opposite CP in Fig. 7.1e. Fig. 7.1f schematically depicts the functional BO units that are activated by the stimulus in Fig. 7.1e. It shows functional BO units at the horizontal borders selective for the same CP direction being activated, signaling that the horizontal rectangle owns the borders. At the same time, these functional BO units, together with the functional BO units along the oblique edges, signal that the two oblique segments at the opposite sides of the horizontal rectangle have opposite luminance contrast polarity. According to the Gestalt principle of similarity, completion between the two oblique segments is less likely to occur owing to the inconsistent contrast polarity (black vs. white). In fact, there is evidence that completion between elements with opposite CP is rather weak (He and Ooi, 1998; Spehar, 2000; Su, He, & Ooi, 2010a). He and Ooi (1998) found using the stimuli in Fig. 6.1a and b, that the Illusory-O (ring) percept is stronger when the aligned rectangles have the same luminance CP. That the visual system creates an occluding Illusory-O in Fig. 6.1a suggests a preference for integrating rectangles of the same CP. In a recent study using a global motion paradigm (Fig. 6.5a) where only the terminals of the two oblique rectangles carry local motion signals, we found that each oblique rectangle – including the stationary segment surrounded by the diamond frame - is perceived as moving (Su et al., 2010). But when segments of the oblique rectangles have opposite CP (Fig. 6.5b), negating amodal surface integration, the terminal endings are perceived as moving independently while the segments surrounded by the frame remain stationary.

Besides luminance CP, does color CP affect surface completion? While the color system contributes to form perception, many psychophysical studies found equiluminous stimuli do not induce illusory contours (Cavanagh, 1987, 1991; Gegenfurtner et al, 1997; Gregory 1977; Li and Guo, 1995; Livingstone and Hubel, 1988). Yet, Zhou et al (2000) found some BO neurons carrying both luminance and color CP information. This implies surface completion could be sensitive to color CP. Confirming this, we revealed in this paper that one can perceive the



Illusory-O (ring) when aligned inner and outer rectangles have the same color CP, including when the yellow background is at equiluminance (Fig. 7.2a top row, middle stimulus). But the Illusory-O becomes weaker when aligned rectangles have opposite color CP (bottom row), and is barely seen when the rectangles and background are equiluminous (middle stimulus). With the opposite color CP stimuli, an illusory disc formed from the inner terminals of the outer rectangles, rather than the Illusory-O (ring), is seen instead. This phenomenological observation is confirmed by a perceptual rating experiment. We then employed two objective paradigms based on shape discrimination and global motion perception to show that color contributes to surface completion. Altogether, our psychophysical findings demonstrate that the visual system can rely on color information to represent surface layouts. Our findings also ascribe a crucial role to the color sensitive BO-neurons that are predominantly found in cortical areas V2 and above.

## METHODS

### *Observers*

The three authors and nine naïve observers participated in the various experiments. All had normal or corrected-to-normal visual acuity. All aspects of this study were approved by Salus University Institutional Review Board. Informed consent was obtained from the naïve observers before commencing the experiments.

### *Heterochromatic Flicker Photometry Method*

Equiluminance was determined individually for each observer with the heterochromatic flicker photometry (HFP) method. During an HFP trial, a  $2^\circ$  circular disc target on a black background ( $2.9 \text{ cd/m}^2$ ) was alternated at 20 Hz between a red reference color and a test color (green or yellow). For all experiments with colored displays except Experiment 7.3, the red reference was  $25 \text{ cd/m}^2$  (CIE: [0.563, 0.346]). For Experiment 7.3, the red reference was  $20 \text{ cd/m}^2$  (CIE: [0.554, 0.347]). The observer adjusted the luminance of the test color with key

presses until the disc target appeared at minimum flicker. The HFP procedure was repeated 12 times and the average luminance setting was taken as the point at which the test color was equiluminous with the red reference color.

### Experiment 7.1: Perception of Color Illusory-O - Perceptual Rating Task

#### *Apparatus*

*MATLAB* and *Psychophysics Toolbox* (Brainard, 1997; Pelli, 1997) on a *Macintosh* computer were used to present visual stimuli on a 21" flat CRT monitor. An *ATI Radeon 9000 Pro* graphics card with 10-bit per channel DACs was used to provide 10 bits color-depth. The resolution of the monitor was set to  $1152 \times 864$  pixels at a vertical scanning rate of 120 Hz. The same hardware/software setup was also applied to Experiment 7.3–7.5, except that a longer viewing distance (105 cm) was used in Experiment 7.3 instead of the one (75 cm) in Experiment 7.1, 7.4, and 7.5.

#### *Stimuli*

The length and width of individual inner and outer rectangular spokes of the stimuli (Fig. 7.2) were  $0.35^\circ \times 0.15^\circ$ . The inner edge of the inner rectangle was  $0.4^\circ$  from the center of the stimulus, and the gap size between the inner and outer rectangles was  $0.1^\circ$ . The entire stimulus display had a diameter of  $2.4^\circ$ . The luminance of the red rectangles was  $25 \text{ cd/m}^2$  (CIE: [0.563, 0.346]), and the green rectangles was individually set to be equiluminous with red. The luminance of the yellow background was set to one of seven levels: equiluminance (0%),  $\pm 16\%$ ,  $\pm 32\%$  and  $\pm 64\%$  Weber contrast relative to equiluminance.

#### *Procedure*

A typical perceptual rating task was used to measure the perceived strength of Illusory-O of the stimuli in Fig. 7.2 (e.g., He and Ooi, 1998). Paired stimuli with the same and opposite color CP, were used in conjunction with four sets of background (Weber) contrast levels (0%,

$\pm 16\%$ ,  $\pm 32\%$ ,  $\pm 64\%$ ). Three sets of paired stimuli ( $-16\%$ ,  $0\%$ ,  $+16\%$ ), ( $-32\%$ ,  $0\%$ ,  $+32\%$ ), and ( $-64\%$ ,  $0\%$ ,  $+64\%$ ), were tested by sequentially presenting each set on the flat CRT screen. For each set of stimuli, the observer rated the strength of the perceived Illusory-O from a scale of 0 (no illusion) to 10 (very strong illusion). During the test, the observer first rated the paired stimuli at equiluminance, then the stimuli with positive contrast and negative contrast, respectively. Then a second rating response was obtained by having the observer rate the three stimuli with the same color CP across the different contrast background, followed by the rating of the stimuli with opposite color CP. The various rating data obtained for each condition were averaged and taken for data analysis.

#### Experiment 7.2: Orientation Discrimination Task with Grayscale Illusory-O - Validating Method

##### *Apparatus*

The visual stimuli were similarly generated as in Experiment 7.1, but displayed on a 17" flat CRT monitor. The resolution of the monitor was set to  $1024 \times 768$  pixels at a vertical scanning rate of 100 Hz. The viewing distance was 105 cm.

##### *Stimuli*

An example of an elliptical Illusory-O stimulus is illustrated in Fig. 7.3a (top left). The luminance levels of the gray background, the black and the white rectangular spokes were, respectively, 40, 4 and 76  $\text{cd/m}^2$ . The display consisted of radially arranged rectangular spokes. The diameter of the circular profile from the outer spokes was  $2.4^\circ$  and that from the inner spokes was  $0.8^\circ$ . The width of each spoke was  $0.17^\circ$ . The gap sizes between pairs of aligned spokes were variable ( $0.09^\circ$ – $0.11^\circ$ ) with an average size of  $0.1^\circ$ . The elliptical Illusory-O was oriented at either  $45^\circ$  or  $135^\circ$ , with the long and short axes being approximately  $1.7^\circ$  and  $1.5^\circ$ , respectively (aspect ratio=1.136). Between trials, the center of the elliptical Illusory-O was randomly deviated away from the center of the entire display by about  $0.04^\circ$  in one of four possible radial directions ( $45^\circ$ ,  $135^\circ$ ,  $225^\circ$ , or  $315^\circ$ ).

### *Procedures*

Each observer was tested over two sessions. A session consisted of two sections separated by a 15 min break. Six test blocks, each with 50 trials and one of six predetermined stimulus durations (20, 50, 80, 110, 140 or 200 ms), were conducted within a section. A test block began with two warm-up trials followed by 48 test trials. The two test conditions (same and opposite luminance CPs) were randomly intermingled within the test block (24 trials per condition). The six test blocks within a section were conducted in a successive order, either from 20 to 200 ms, or the reverse. In total, the entire experiment was conducted with 12 stimulus combinations (2 CP conditions  $\times$  6 stimulus durations). Across the two test sessions, each test condition was run over four blocks (2 sections  $\times$  2 sessions) of 96 trials (4 blocks  $\times$  24 trials) each.

An orientation discrimination task in a 2AFC design was performed (Fig. 7.3c). To begin a trial, the observer pressed the space bar of a computer keyboard while maintaining eye alignment on a  $0.27^\circ \times 0.27^\circ$  fixation cross ( $10 \text{ cd/m}^2$ ). The first stimulus ( $45^\circ$  or  $135^\circ$  orientation) was then presented concentric to the fixation, which was followed by a black-and-white random dot mask (mean luminance =  $40 \text{ cd/m}^2$ ; contrast = 90%; dot size =  $0.07^\circ$ ) for 500 ms. A 500 ms blank screen ( $40 \text{ cd/m}^2$ ) followed, before the second stimulus with an orientation orthogonal to the first stimulus was displayed. The same mask was then presented for 500 ms to terminate the trial. The observer reported the perceived orientation of the first stimulus by pushing either the left (for  $135^\circ$ ) or right arrow key (for  $45^\circ$ ).

### Experiment 7.3: Perception of Color Illusory-O - Orientation Discrimination Task

#### *Stimuli*

The spatial configuration of the color stimuli (Fig. 7.4a&b) was similar to the gray ones in Experiment 7.2. The diameter of the circular profile from the rectangular outer spokes was  $2.4^\circ$  and that from the inner rectangular spokes was  $0.8^\circ$ . The width of each spoke was  $0.15^\circ$ .

The gap sizes between pairs of aligned spokes were variable ( $0.09^{\circ}$ – $0.11^{\circ}$ ) with an average size of  $0.1^{\circ}$ . The elliptical Illusory-O was oriented at either  $45^{\circ}$  or  $135^{\circ}$ , with the long and short axes being approximately  $1.7^{\circ}$  and  $1.5^{\circ}$ , respectively (aspect ratio=1.07). Between trials, the center of the elliptical Illusory-O was randomly deviated away from the center of the entire display by about  $0.04^{\circ}$  in one of four possible radial directions ( $45^{\circ}$ ,  $135^{\circ}$ ,  $225^{\circ}$ , or  $315^{\circ}$ ). The red spokes were  $20 \text{ cd/m}^2$  (CIE: [0.554, 0.347]), and similar to Experiment 7.1, the luminance of the green spokes, yellow background, and gray fixation cross (at equiluminance) were individually determined by HFP. The contrast levels of the yellow backgrounds were 0%,  $\pm 16\%$  and  $\pm 32\%$ . The mask comprised of red and green random dots ( $20 \text{ cd/m}^2$ ).

### *Procedure*

Our main goal in this experiment was to reveal the performance difference between the same and opposite color CP stimuli and how it is affected by the luminance contrast of the yellow background. As such, we conducted a pilot test to estimate each observer's optimal stimulus presentation duration at which the advantage of the same color CP stimulus over the opposite color CP stimulus was maximum. In the test, observers performed the 2AFC-orientation discrimination task at equiluminance using a protocol similar to that shown in Fig. 7.3c, but with the stimuli in color. The stimulus duration varied from 91.7 ms to 141.7 ms in an 8.3 ms step. The same and opposite color CP stimuli were tested in the same block, and the observer's task was the same as in Experiment 7.2. From the data, we obtained each observer's optimal stimulus presentation duration for use in the proper experiment (Observer 1: 99.6 ms, Observers 2 & 3: 116.2 ms, and Observer 4: 132.8 ms).

The proper experiment was conducted over two sessions. In each session, testing was run in two sections separated by a 15 min break. Within a section, five test blocks corresponding to the five different luminance levels of the yellow background (Weber contrast of stimuli = -32%, -16%, 0, 16%, or 32%) were tested. Each block comprised of 50 trials, with the first two trials

being treated as warm-up trials. The two stimulus conditions (same and opposite color CP) were randomly intermingled within the block (24 trials per condition). Overall, there were 96 test trials for each stimulus condition (2 sections  $\times$  2 sessions  $\times$  24 trials).

#### Experiment 7.4: Color Effect on Amodal Surface Completion - Global Motion Task

##### *Stimuli*

The test stimulus (Fig. 7.5c) comprised two oblique bars (orientation =  $\pm 45^\circ$ ; length =  $3.7^\circ$ ; width =  $0.39^\circ$ ) that were arranged in an X-shape formation, and a black-and-white random dot textured diamond frame (mean luminance =  $56.5 \text{ cd/m}^2$ ) that acted as the occluder (the overall size of the occluder being  $3.0^\circ$  as measured along the axis of the diamond). Three occluder widths (6.4, 12.7 or 22.3 min), or gap sizes, were used. The occluder effectively divided each oblique bar into three segments: one inner and two outer rectangles. The outermost edges of the outer rectangles were rendered with a terminal velocity of  $1.06 \text{ deg/s}$  (along its motion direction) and a maximum displacement of  $0.91^\circ$ . The red oblique rectangles were  $25 \text{ cd/m}^2$  (CIE: [0.563, 0.346]) and the green ones were equiluminous with the red rectangles (obtained using the HFP method). The yellow background had five luminance Weber contrast levels (0,  $\pm 32\%$  and  $\pm 64\%$ ) with respect to equiluminance. There were four stimulus conditions. In the two opposite color CP conditions, the colors of the inner and outer rectangles were green and red, respectively, or vice versa (Fig. 7.5b). In the two same color CP conditions, the inner and outer rectangles were either red, or green, in color (Fig. 7.5a). The entire stimulus was presented concentric to a gray ( $22 \text{ cd/m}^2$ ) fixation target ( $0.47^\circ \times 0.47^\circ$ ) that was removed 500 ms before the presentation of the test stimulus (duration = 1.8 s).

##### *Procedures*

The same task used in Su et al. (2010a) was adopted for this experiment. To begin a trial, the observer first stabilized his/her gaze at the fixation target and then pressed the space bar of the computer keyboard to present the stimulus. He/she was instructed to respond to seeing either one

of two percepts. The first is, of two partially occluded oblique bars sliding over each other back and forth (global motion when motion integration occurred among three segments; see the prediction in Fig. 7.5a). The second is, of the four outer rectangles expanding and contracting while the inner rectangles remained stationary (when motion integration failed; see the prediction in Fig. 7.5b). The observer responded by pressing the left or right arrow key, respectively, for the first or second percept. Each test block had 96 trials, which included eight repeats of 12 stimulus combinations {4 stimulus conditions: [2 same color CP (red-red spokes, green-green spokes) + 2 opposite color CP (red-green spokes, green-red spokes)]  $\times$  3 gap sizes}. For each observer, 20 such blocks were conducted over two test sessions. A session had two sections separated by a 15-min break. Per section, five blocks comprising different background luminance (Weber contrast: 0,  $\pm 32\%$  and  $\pm 64\%$ ) were tested.

#### Experiment 7.5: Color Effect on Illusory Surface Formation - Global Motion Task

##### *Stimuli*

The general design of the stimuli (Fig. 7.6a&b, left) were similar to those used in Experiment 7.4. That is, the X-shaped stimulus with an overall size of roughly  $3.5^\circ \times 3.5^\circ$ , was formed by two intersecting  $45^\circ$  oblique bars ( $4.6^\circ \times 0.39^\circ$ ). Two gaps were inserted into each oblique bar, essentially breaking it into three rectangular segments. The spaces of the gaps were filled with the same luminance level as the background. The boundaries of each gap, i.e., the inner edge of the outer rectangle and the outer edge of the adjacent inner rectangle, were rendered with back-and-forth motion along the long axis of the rectangle at a speed of 1.06 deg/s with a maximum displacement of  $0.78^\circ$ . Thus, an expansion of one outer rectangle was synchronized with a contraction of the adjacent inner rectangle along the same direction, essentially, causing the gap between the rectangles to move along. Considered in its entirety, and at any given moment, all four gaps of the X-shaped stimulus would have the same horizontal motion component so that it was possible to conceive them as parts of a larger illusory diamond occluder

translating horizontally. To stabilize eye alignment, a  $0.35^\circ \times 0.35^\circ$  gray fixation target ( $22 \text{ cd/m}^2$ ) was located  $1.4^\circ$  below the center of the stimulus during the entire stimulus presentation (1.5 s) of a test trial. As in Experiment 7.4, color CP was manipulated by setting the inner and outer rectangular spokes with the same color (red or green), or different color (red-green or green-red). The width of the gap size was also varied (6.4, 12.7 or 22.3 min). The inter-gap distance was  $2.1^\circ$ .

### *Procedures*

The same test procedure as in Experiment 7.4 was adopted. That is, each test block had 96 trials, which included eight repeats of 12 stimulus combinations {4 stimulus conditions: [2 same color CP (red-red spokes, green-green spokes) + 2 opposite color CP (red-green spokes, green-red spokes)]  $\times$  3 gap sizes}. For each observer, 20 such blocks were conducted over two test sessions. In each session, 2 sections separated by a 15 min break were conducted. Each section tested 5 blocks comprising of different background luminance (Weber contrast: 0,  $\pm 32\%$  and  $\pm 64\%$ ). The observers' task was to report their percepts of the stimuli, which were either: (i) two inner rectangles remaining stationary (Fig. 7.6a, right), or (ii) two inner rectangles sliding over one another (Fig. 7.6b, right). The observers pressed the left arrow key of the keyboard for percept (i) and the right arrow key for percept (ii).

## RESULTS

### Experiment 7.1

We measured the perceived strength of the Illusory-O in the color stimuli in Fig. 7.2a using the typical perceptual rating task. The average rating results ( $n = 8$ , Fig. 7.2b) show that at equiluminance, observers rated the strength of the Illusory-O much higher for the same color CP stimulus (red circles) than for the opposite color CP stimulus (blue triangles). This trend continues beyond the equiluminance point (with yellow background of higher and lower Weber



contrast levels), where the boundary contours of the rectangular elements carry both luminance contrast [ $F(6,42) = 12.697, p < 0.001$ ; ANOVA using GLM with Repeated Measures] and color contrast [ $F(1,7) = 162.300, p < 0.001$ ] signals. Thus our results indicate that color information contributes to amodal surface integration and illusory surface formation, and its impact can be observed even when there exists a luminance boundary contour signal. Noticeably, both the same and opposite color CP rating functions exhibit a V-shape with its base at the equiluminance point [for the data with Weber contrast  $\leq 0$ :  $F(1,30) = 242.586, p < 0.001$ ; for the data with Weber contrast  $\geq 0$ :  $F(1,30) = 191.687, p < 0.001$ , Weber contrast as covariate]. This largely reveals the influence of luminance boundary contour signals on surface completion. There is also a significant interaction effect between the color and luminance boundary contour factors [ $F(6, 42) = 5.050, p = 0.001$ ]. (Please note the color stimulus demonstrations in this paper might not be optimal since individuals have different equiluminance settings.)

### Experiment 7.2

Another approach to investigating perceived surface completion is to use a surface shape discrimination task, a task whose methodology is considered more objective (e.g., Gold et al, 2000; Kellman et al, 1998; Ringach and Shapley, 1996). But up till now, most studies using the shape discrimination task have used grayscale stimuli and none has tested with the Illusory-O stimulus. Thus, to adapt this task to our colored stimuli, the current experiment first established and validated a shape discrimination paradigm to reveal the advantage of the Illusory-O surface (surface completion) by using grayscale Illusory-O stimuli. Then our following experiment will reveal the advantage of the same color CP stimuli over opposite color CP stimuli.

Our objective task requires the observer to detect the orientation of either an elliptical Illusory-O or an illusory-disc. As shown in Fig. 7.3a, we created elliptical Illusory-O with its long axis oriented at  $45^\circ$  (or  $135^\circ$ , not shown) by varying the relative terminal positions of the inner and outer rectangles. Complementary stimuli with opposite luminance CP that lead to an

illusory-disc (e.g., Fig. 7.3b) were also created. Then, using a 2AFC method we presented a 45° and a 135° oriented stimuli in two intervals (both stimuli always had either the same or opposite CP), and asked the observer to report the orientation of the stimulus seen in the first interval (Fig. 7.3c). The stimulus duration was 20, 50, 80, 110, 140, or 200 ms. Fig. 7.3d plots the average percentage correct as a function of stimulus duration. Clearly, the overall performance increases with the stimulus duration [ $F(1,22) = 129.826$ ,  $p < 0.001$ , duration as covariate]. Most importantly, the performance is better for the same (circles) than opposite luminance CP condition [ $F(1,22) = 13.046$ ,  $p = 0.002$ ], particularly over the intermediate stimulus durations. This finding complements the previous finding by He and Ooi (1998) using the perceptual rating task.

To quantify the dynamics of the orientation discrimination performance, we fitted the data with a Weibull distribution function. We first estimated the probability of correct detection from the percentage correct. Since the observer was exposed to two stimuli with orthogonal orientation (45° vs 135°) during the 2AFC trial, he/she could perform correctly as long as the orientation of one stimulus is perceived. Assuming the probability of detecting the stimulus in the first interval is  $p_1$  and in the second interval  $p_2$ , the estimated percentage correct made by the observer can be inferred as:

$$\begin{aligned} \%correct &= p_1 \times 100 + (1 - p_1) \times p_2 \times 100 + (1 - p_1) \times (1 - p_2) \times 50 \\ &= 50 + (p_1 + p_2 - p_1 \times p_2) \times 50 \\ &= 50 + p' \times 50 \end{aligned}$$

where,  $p'$  is the effective probability of combining the two orientation discrimination opportunities. Accordingly,  $p'$  can be derived from the percentage correct data as:

$$p' = \frac{(\%correct - 50)}{50}$$

This allows us to fit the average  $p'$  values with a Weibull distribution function:

$$p' = Weibull\_CDF(t - t_0; k, \lambda)$$

$$= 1 - \exp\left(-\left(\frac{t - t_0}{\lambda}\right)^k\right)$$

From the above,  $k$  and  $\lambda$ , respectively, are the shape parameter and the scale parameter of the Weibull distribution function. Further,  $t_0$  can be considered as the visual system's latency for accomplishing the orientation discrimination task. We found that the function fits the data for both stimulus conditions remarkably well (solid curves, Fig. 7.3c) [same CP:  $R^2 = 0.911$ ; opposite CP:  $R^2 = 0.877$ ]. From the fit, we can deduce that the observers had a shorter latency in the same CP ( $t_0 = 41.697$  msec) than opposite CP ( $t_0 = 49.930$  ms) condition. The fitting results also reveal that the same CP curve rises more steeply than the opposite CP curve ( $k$ : 1.168 versus 1.430;  $\lambda$ : 40.236 versus 74.450). In addition, for both conditions, the shape parameter  $k$  is much closer to 1 (whereby a Weibull distribution can be simplified as an exponential distribution) than to 3.4 (whereby a Weibull distribution corresponds to a normal distribution).

### Experiment 7.3

Using the shape discrimination paradigm established above, we now tested the color Illusory-O stimuli against a yellow background with one of five predetermined luminance levels (Fig. 7.4a). Fig. 7.4b plots the average orientation discrimination performance as a function of the Weber luminance contrast of the yellow background. The two curves show a similar trend as the subjective rating results in Experiment 7.1 (Fig. 7.2b). Performance is better with the same color CP (circles) than with the opposite color CP (triangles) stimuli [ $F(1,3) = 10.107$ ,  $p = 0.05$ ], confirming that color contributes to surface completion. Performance is also affected by luminance contrast [ $F(1.702, 5.105) = 17.406$ ,  $p = 0.006$ , with Greenhouse-Geisser correction] and exhibits a V-shape with its minimum occurring at the equiluminance point [for the data with Weber contrast  $\leq 0$ :  $F(1,10) = 39.596$ ,  $p < 0.001$ ; for the data with Weber contrast  $\geq 0$ :  $F(1,10) = 47.332$ ,  $p < 0.001$ , ANOVA with repeated measures (Weber contrast as covariate)]. The

performance difference between the two conditions is largest at equiluminance, with the V-shape for the opposite color CP being deeper than that for the same color CP condition [ $F(1.302, 3.905) = 12.602, p = 0.023$ , with Greenhouse-Geisser correction].

#### Experiment 7.4

It has been shown that the visual system utilizes spatial configuration cues, as well as color and luminance contrast information, to derive global motion from local motion information (Adelson and Movshon, 1982; Cavanagh and Anstis, 1991; Dobkins and Albright, 1994; Duncan et al, 2000; Gegenfurtner et al, 1994; He and Nakayama, 1994; Lorenceau and Shiffrar, 1992; Nakayama and Silverman, 1985; Shimojo et al, 1989; Stoner and Albright, 1996, 1998; Su et al., 2010a). Thus, to further investigate the contribution of the color system to surface completion, we tested observers in a motion paradigm for surface integration (Su et al, 2010a) in this and the next experiment. We employed motion stimuli in the same and opposite color CP conditions (Fig. 7.5a&b, respectively) with the prediction that more global motion will be observed in the same color CP condition owing to surface integration (amodal surface completion) between the oblique rectangular segments separated by the diamond-shaped occluder. Fig. 7.5d and e plot the average percentages ( $n = 4$ ) of perceiving global motion in both conditions as a function of the Weber luminance contrast of the yellow background. Confirming our prediction, the percentage of seeing global motion is larger in the same color CP condition (Fig. 7.5d) than in the opposite color CP condition (Fig. 7.5e) [ $F(1,3) = 174.724; p = 0.001$ ]. The percentage of seeing global motion also reduces with the width of the diamond frame (gap size) [ $F(1.021, 3.064) = 38.178; p = 0.008$ , with Greenhouse-Geisser correction], and this occluder width effect is stronger in the same color CP condition [ $F(2, 6) = 14.707; p = 0.005$ ]. This indicates amodal surface integration becomes less effective as the area (length) required for integration increases. There is a small, though not reliable, overall effect of background luminance (Weber contrast) on the perceived global motion [ $F(1.355, 4.066) = 2.316; p = 0.208$ , with Greenhouse-Geisser correction]. Global

motion perception is also stronger for the same color CP stimuli not only at equiluminance, but also on non-equiluminous yellow background, indicating that the impact of color on amodal surface integration is effective even in the presence of the luminance contour information.

### Experiment 7.5

We now investigated the contribution of color to both amodal surface completion and illusory surface formation in the absence of an explicit occluding surface (Fig. 7.6a&b). Without the explicit occluder (thus no T-junctions), the visual system has to transform L-junctions at the terminals of the rectangles to implicit T-junctions for amodal surface completion and to create the illusory “occluder”. Specifically, in Fig. 7.6a (left) (same color CP condition), if each pair of juxtaposed inner and outer rectangular segments adjacent to the gap amodally completes and yields their borders to the spaces between the gap (i.e., the rectangle no longer owns the border), an illusory oblique bar as occluding surface will be perceived. Then, the illusory oblique bar, not the rectangular segments, will carry the local motion signals. Thus, with the four gaps (occluding surface) and local motion signals in the stimulus, an illusory diamond frame will be perceived as moving rightward in global motion (Fig. 7.7a, right) while the rectangular segments appear stationary. However, we predict the tendency for amodal completion will be less in the opposite color CP stimulus (Fig. 7.6b, right). So instead of seeing the global motion of an illusory diamond occluder, the inner oblique rectangles will be seen as sliding over one another. Confirming this, the average results ( $n=4$ ) show significantly larger percentages of seeing global motion in the same color CP condition (Fig. 7.6d) than in the opposite color CP condition (Fig. 7.6e) [ $F(1, 3) = 32.064$ ;  $p = 0.011$ ]. There is also an effect of gap size on the global motion perception [ $F(2,6) = 66.514$ ;  $p < 0.001$ ], with the gap size effect being larger for the same color CP condition [ $F(2,6) = 20.811$ ;  $p = 0.002$ ]. And different from Experiment 7.4 with the random-dot defined diamond-shaped occluder, we found a significant effect of the yellow background

luminance (Weber contrast) on the perceived global motion [ $F(2.054, 6.162) = 13.703$ ;  $p = 0.005$ , with Greenhouse-Geisser correction].

## DISCUSSION

The present study uses three different psychophysical tasks to demonstrate the visual system has a preference to amodally integrate fragments of the same color CP to create representations of occluding and partially occluded surfaces. This finding, together with previous observations of the role of luminance contrast polarity (He and Ooi, 1998; Spehar, 2000; Su et al., 2010a), reveals that surface features are processed by the boundary contour-based surface completion mechanism. It also underscores the notion that the surface representation process ably utilizes the regularity of real world natural images, whereby two image patches are more likely to have the same luminance and color CP when they belong to the same surface than to two different surfaces (Elder and Goldberg, 2002; Fine et al, 2003; Geisler and Perry, 2009; Ruderman et al, 1998).

Our finding departs from a number of previous discoveries, which used Kanizsa-like illusory contour stimuli whose background is equiluminous with the inducing element (e.g., Cavanagh, 1987, 1991; Cavanagh, et al, 1987; Gegenfurtner et al, 1997; Gregory, 1977; Li and Guo, 1995; Livingstone and Hubel, 1987, 1988). Those studies found that observers were unable to perceive the illusory contours at equiluminance. An explanation given for this is that the color and form information is processed in parallel in the early visual cortical level (e.g. DeYoe and Van Essen, 1985; Livingstone and Hubel, 1987; Zeki, 1983). This explanation however, needs to be rethink as subsequent research in monkeys has found a large proportion of color sensitive neurons in areas V1 and V2 that are also orientation selective (Friedman et al, 2003; Gegenfurtner et al, 1996; Horwitz et al., 2007; Johnson et al, 2001, 2008; Leventhal et al, 1995; Solomon et al, 2004; Thorell et al, 1984. Yoshioka and Dow, 1996). Friedman et al (2003) recorded from

neurons in the upper layers of areas V1 and V2 of awaked monkeys, and found more color neurons that are selective for edges and orientations (“edge cells”) than those without selectivity for orientation (“surface cells”). The authors suggest the edge cells, rather than the surface cells, play a role in representing the color of homogeneous surface images (Friedman et al, 1999, 2003; Qiu and von der Heydt, 2007; von der Heydt et al, 2003). Thus, it is possible that the edge cells are responsible for the boundary contour-based surface integration. Meanwhile the surface cells are likely responsible for the non-boundary contour-based, surface feature completion phenomena, such as those reported by Yin et al (1997, 2000). Furthermore, Zhou et al (2000) found numerous edge cells not only being BO selective, but is color or luminance contrast polarity sensitive. These cells could be crucial for the boundary contour-based surface integration finding reported in this paper (see the schematic BO units depicted in Fig. 7.1).

Let us consider the behaviors of the functional BO units when stimulated with a luminance-defined pacman element (Fig. 7.7a) from a Kanizsa square stimulus. The pacman’s figural configuration (L-junctions) activates functional BO units at both the horizontal and vertical edges, signaling that the pacman owns the borders (arrows). The visual system thus treats the pacman as a figure in the foreground. To account for the illusory percept of the Kanizsa square in Fig. 7.7b, it is proposed the BO directions can be affected by the surface images surrounding the pacman. In Fig. 7.7b, the edge alignment between the pacman elements can cause the BO direction (arrows) to reverse. When this occurs, the boundary contours of each pacman image are no longer treated as the image’s intrinsic edges, but are caused, or owned, by an occluding surface. This is an important first step in the surface completion process that amodally completes the pacman as a disc and modally constructs the illusory square.

In parallel with the single unit recording studies, human psychological and fMRI investigations have shown the color system can contribute to form perception (e.g., Cavanagh, 1987, 1991; Cavanagh et al, 1987; Clifford et al, 2003; Engel, 2005; Gegenfurtner et al, 1997; Li and Guo, 1995; Losada and Mullen, 1994; Switkes et al, 1988; Troscianko et al, 1991).

Cavanagh and his colleagues (1987, 1991) examined various visual percepts at equiluminance and found that shape-from-shadow and illusory contour percepts are the only two that failed. With regard to this failure, Cavanagh (1991) made an insightful observation of equiluminous stimuli: *“In general, surfaces are not easily linked together across equiluminous chromatic borders. A red and green surface appears as red patches floating on a green background (or vice versa), not as a single, red and green surface.”*

By extension, we propose that the extremely weak perception of the illusory contours at equiluminance in earlier studies [e.g., the Kanizsa square (Fig. 7.7c)] is because the color-BO selective neurons are less affected by contextual information than the luminance-BO selective neurons. This proposal is consistent with the growing evidence showing that the early visual cortical neurons can be modulated by contextual information (Albright and Stoner, 2002). More specifically, at equiluminance, the BO direction at the pacman is less likely to be reversed by the surrounding elements. This cell property could be attributed to an important difference between color and luminance boundary contours in the real world. Compared to luminance-based boundary contours, color-based boundary contours in the natural scene are more likely caused by the intrinsic borders of an object’s surface (Cavanagh, 1991). But luminance edges can also be caused by shadows or shading. Thus, to extract a surface representation from luminance-based boundary contours the visual system must discount these factors (shadows and shading) by utilizing contextual information.

Effectively, we suggest that the color-BO selective neurons receive a relatively small weight, rather than absolutely no input, from the surrounding surface images. As such, amodal surface completion and illusory contours can occur for equiluminous stimuli as long as the contextual signals are sufficiently strong. Consequently, the reason one perceives the Illusory-O (Fig. 7.7d), but barely sees the Kanizsa illusory contours (Fig. 7.7c) at equiluminance is because the contextual information for amodal surface completion is stronger in the Illusory-O stimulus than in the Kanizsa square stimulus (two pairs of aligned edges vs. one pair). Whether the



contextual factor differentially affects luminance-BO and color-BO neurons can be revealed by future neurophysiological research.

## REFERENCES

- Adelson, E.H., & Movshon, J.A. (1982). Phenomenal coherence of moving visual patterns. *Nature*, **300**: 523–525.
- Adelson, E.H. & Movshon, J.A. (1984). Binocular disparity and the computation of twodimensional motion. *Journal of the Optical Society of America*, **1**: 1266.
- Albert, M.K. (1993). Parallelism and the perception of illusory contours. *Perception*, **22**(5): 589–595.
- Albert, M.K. (2007). Mechanisms of modal and amodal interpolation. *Psychological Review*, **114**: 455–468.
- Albert, M.K. & Hoffman, D.D. (2000). The generic-viewpoint assumption and illusory contours. *Perception*, **29**: 303–312.
- Albright, T.D. & Stoner, G.R. (2002). Contextual influences on visual processing. *Annual Review of Neuroscience*, **25**: 339–379.
- Anderson, B.L. (1997). A theory of illusory lightness and transparency in monocular and binocular images: the role of contour junctions. *Perception*, **26**: 419–453.
- Anderson, B.L. & Barth, H.C. (1999). Motion-based mechanisms of illusory contour formation. *Neuron*, **24**: 433–441.
- Anderson, B.L. & Julesz, B. (1995). A theoretical analysis of illusory contour formation in stereopsis. *Psychological Review*, **102**: 705–743.
- Andrews, T.J., Sengpiel, F., & Blakemore, C. (2005). From contour to object-face rivalry: Multiple neural mechanisms resolve perceptual ambiguity. In *Binocular Rivalry*. Alais & Blake (eds.). MIT Press: Cambridge, MA. pp. 187–210.

- Alais, D. & Blake, R. (1998). Interactions between global motion and local binocular rivalry. *Vision Research*, **38**: 637–644.
- Alais, D. & Blake, R. (1999). Grouping visual features during binocular rivalry. *Vision Research*, **39**: 4341–4353.
- Alais, D. & Parker, A. (2006). Independent binocular rivalry processes for motion and form. *Neuron*, **52**: 911–920.
- Attneave, F. (1954). Informational aspects of visual perception. *Psychological Review*, **61**: 183–193.
- Bakin, J.S., Nakayama, K., & Gilbert, C.D. (2000). Visual responses in monkey areas V1 and V2 to three-dimensional surface configurations. *Journal of Neuroscience*, **20**: 8188–8198.
- Barlow, H.B. (1961). Possible principles underlying the transformation of sensory messages. In *Sensory Communication*. Rosenblith (ed.). MIT Press: Cambridge, MA. pp. 217–235.
- Barlow, H.B., Blakemore, C., & Pettigrew, J.D. (1967). The neural mechanism of binocular depth discrimination. *The Journal of Physiology*, **193**: 327–342.
- Baylis, G.C. & Driver, J. (1995). Obligatory edge assignment in vision: The role of figure and part segmentation in symmetry detection. *Journal of Experimental Psychology: Human Perception and Performance*, **21**(6): 1323–1342.
- Blake, R. (1989). A neural theory of binocular rivalry. *Psychological Review*, **96**: 145–167.
- Blake, R. (2001). A primer on binocular rivalry, including current controversies. *Brain and Mind*, **2**: 5–38.
- Blake, R. & Boothroyd, K. (1985). The precedence of binocular fusion over binocular rivalry. *Perception & Psychophysics*, **37**: 114–124.
- Blake, R. & Camisa, J. (1978). Is binocular vision always monocular? *Science*, **200**: 1497–1499.
- Blake, R. & Camisa, J. (1979). On the inhibitory nature of binocular rivalry suppression. *Journal of Experimental Psychology: Human Perception and Performance*, **5**(2): 315–323.
- Blake, R. & Logothetis, N.K. (2002). Visual competition. *Nature Reviews Neuroscience*. **3**:

13–21.

- Blake, R. & O'Shea, R.P. (1988). "Abnormal fusion" of stereopsis and binocular rivalry. *Psychological Review*, **95**: 151–154.
- Blake, R., Tadin, D., Sobel, K., Chong, S.C., & Raissian, R. (2006) Strength of early visual adaptation depends on visual awareness. *Proceedings of the National Academy of Sciences (USA)*, **103**: 4783–4788.
- Blake, R., Westendorf, D.H., & Overton, R. (1980). What is suppressed during binocular rivalry? *Perception*, **9**: 223–231.
- Blakemore, C. (1970). A new kind of stereoscopic vision. *Vision Research*, **10**: 1181–1199.
- Brainard, D.H. (1997). The Psychophysics Toolbox. *Spatial Vision*, **10**: 433–436.
- Caputo, G. (1998). Texture brightness filling-in. *Vision Research*, **38**: 841–851.
- Carrasco, M., McElree, B., Denisova, K., & Giordano, A.M. (2003). The speed of visual information processing increases with eccentricity. *Nature Neuroscience*, **6**(7): 669–670.
- Cavanagh, P. (1987). Reconstructing the third dimension: interactions between color, texture, motion, binocular disparity and shape. *Computer Vision, Graphics and Image Processing*, **37**: 171–195.
- Cavanagh, P. (1991). Vision at equiluminance. In *Vision and Visual Dysfunction: Limits of Vision*. Kulikowski & Walsh (eds.). CRC Press: Boca Raton, FL. pp. 234–250.
- Cavanagh, P. & Anstis, S. (1991). The contribution of color to motion in normal and color-deficient observers. *Vision Research*, **31**: 2109–2148.
- Cavanagh, P., Shhioiri, S., and MacLeod, D.I.A. (1987). Is the achromatic form pathway based on brightness or luminance? *Invest. Ophthalmol. Vis. Sci. Suppl.* 28, 362.
- Chong, S.C. & Blake, R. (2006). Exogenous attention and endogenous attention influence initial dominance in binocular rivalry. *Vision Research*, **46**: 1794–1803.
- Clifford, C.W., Spehar, B., Solomon, S.G., Martin, P.R., & Zaidi, Q. (2003). Interactions between color and luminance in the perception of orientation. *Journal of Vision*, **3**: 106–115.

- Cohen, M.A. & Grossberg, S. (1984). Neural dynamics of brightness perception: Features, boundaries, diffusion, and resonance. *Perception & Psychophysics*, **36**: 428–456.
- Cornelissen, F.W., Wade, A.R., Vladusich, T., Dougherty, R.F., & Wandell, B.A. (2006). No functional magnetic resonance imaging evidence for brightness and color filling-in in early human visual cortex. *Journal of Neuroscience*, **26**: 3634–3641.
- Craft, E., Sc hütze, H., Niebur, E., & von der Heydt, R. (2007). A Neural Model of Figure–Ground Organization. *Journal of Neurophysiology*, **97**: 4310–4326.
- Davey, M.P., Maddess, T., & Srinivasan, M.V. (1998). The spatiotemporal properties of the Craik–O’Brien–Cornsweet effect are consistent with “filling-in”. *Vision Research*, **38**: 2037–2046.
- De Valois, R.L. & De Valois, K.K. (1988). *Spatial Vision*. Oxford University Press: New York, NY.
- De Valois, R.L., Webster, M.A., DeValois, K.K., & Lingelbach, B. (1986). Temporal properties of brightness and color induction. *Vision Research*, **26**, 887–897.
- De Weerd, P., Desimone, R., & Ungerleider, L.G. (1998). Perceptual filling-in: A parametric study. *Vision Research*, **38**: 2721–2734.
- De Weerd, P., Gattass, R., Desimone, R., & Ungerleider, L.G. (1995). Responses of cells in monkey visual cortex during perceptual filling-in of an artificial scotoma. *Nature*, **377**: 713–734.
- DeYoe, E.A. & Van Essen, D.C. (1988). Concurrent processing streams in monkey visual cortex. *Trends in Neurosciences*, **11**: 219–226.
- Dobkins, K.R. & Albright, T.D. (1994). What happens if it changes color when it moves?: the nature of chromatic input to macaque visual area MT. *Journal of Neuroscience*, **14**: 4854–4870.
- Driver, J. & Baylis, G. (1996). Edge-assignment and figure-ground segmentation in short-term visual matching. *Cognitive Psychology*, **31**: 248–306.
- Duncan, R.O., Albright, T.D., & Stoner, G.R. (2000). Occlusion and the interpretation of visual motion: Perceptual and neuronal effects of context. *J Neuroscience*, **20**: 5885–5897.

- Elder, J.H. & Goldberg, R.M. (2002). Ecological statistics for the Gestalt laws of perceptual organization of contours. *Journal of Vision*, **2**: 324–353.
- Engel, S.A. (2005). Adaptation of oriented and unoriented color-selective neurons in human visual areas. *Neuron*, **45**: 613–623.
- Engel, S.A., Glover, G.H., & Wandell, B.A. (1997). Retinotopic organization in human visual cortex and the spatial precision of functional MRI. *Cerebral Cortex*, **7**, 181–192.
- Fang, F., Boyaci, H., & Kersten, D. (2009). Border ownership selectivity in human early visual cortex and its modulation by attention. *Journal of Neuroscience*, **29**(2): 460–465.
- Fang, F. & He, S. (2005). Cortical responses to invisible objects in the human dorsal and ventral pathways. *Nature Neuroscience*, **10**: 1380–1385.
- Fine, I., MacLeod, D.I.A., & Boynton, G.M. (2003). Surface segmentation based on the luminance and color statistics of natural scenes. *Journal of the Optical Society of America A*, **20**: 1283–1291.
- Fox, R., (1991). Binocular rivalry. In *Vision and Visual Dysfunction Vol. 9: Binocular Vision*. Regan (ed.). Macmillan: London, UK. pp. 93–110.
- Fox, R., & Check, R. (1972). Independence between binocular rivalry suppression duration and magnitude of suppression. *Journal of Experimental Psychology*, **93**: 283–289.
- Fox, R. & Herrmann, J. (1967). Stochastic properties of binocular rivalry alternations. *Perception and Psychophysics*, **2**(9): 432–436.
- Friedman, H.S., Zhou, H., & von der Heydt, R. (1999). Color filling-in under steady fixation: behavioral demonstration in monkeys and humans. *Perception*, **28**: 1383–1395.
- Friedman, H.S., Zhou, H., & von der Heydt, R. (2003). The coding of uniform color figures in monkey visual cortex. *The Journal of Physiology*, **548**: 593–613.
- Frisby, J.P. & Mayhew, J.E. (1978). The relationship between apparent depth and disparity in rivalrous-texture stereograms. *Perception*, **7**: 661–678.
- Fukuda, H. & Blake, R. (1992). Spatial interactions in binocular rivalry. *Journal of Experimental Psychology: Human Perception and Performance*, **18**: 362–370.

- Gegenfurtner, K.R., Brown, J.E., & Rieger, J. (1997). Interpolation processes in the perception of real and illusory contours. *Perception*, **26**: 1445–1458.
- Gegenfurtner, K.R., Kiper, D.C., Beusmans, J.M.H., Caradini, M., Zaidi, Q., & Movshon, J.A. (1994). Chromatic properties of neurons in macaque MT. *Visual Neuroscience*, **13**: 455–466.
- Gegenfurtner, K.R., Kiper, D.C., & Fenstemaker, S.B. (1996). Processing of color, form, and motion in macaque area V2. *Visual Neuroscience*, **13**: 161–172.
- Geisler, W.S. (2008). Visual perception and the statistical properties of natural scenes. *Annual Review of Psychology*, **59**: 167–192.
- Geisler, W.S. & Perry, J.S. (2009). Contour statistics in natural images: grouping across occlusions. *Visual Neuroscience*, **26**: 109–121.
- Gerrits, H.J. & Timmerman, G.J. (1969). The filling-in process in patients with retinal scotomata. *Vision Research*, **9**: 439–442.
- Gerrits, H.J. & Vendrik, A.J.H. (1970). Simultaneous contrast, filling in process and information processing in man's visual system. *Experimental Brain Research*, **11**: 411–430.
- Gibson, J.J. (1950). *The Perception of the Visual World*. Houghton Mifflin: Boston, MA.
- Gold, J.M., Murray, P.J., Bennet, P.J., & Sekuler, A.B. (2000). Deriving behavioral receptive fields for visually completed contours. *Current Biology*, **10**: 663–666.
- Gregory, R.L. (1977). Vision with isoluminant contour contrast: 1. a projection technique and observations. *Perception*, **6**: 113–119.
- Grinvald, A., Lieke, E.E., Frostig, R.D., & Hildesheim, R. (1994). Cortical point-spread function and long-range lateral interactions revealed by real-time optical imaging of macaque monkey primary visual cortex. *Journal of Neuroscience*, **14**, 2545–2568.
- Grossberg, S. (1994). 3-D vision and figure-ground separation by visual cortex. *Perception and Psychophysics*, **55**: 48–120.
- Grossberg, S. & Mingolla, E. (1985). Neural dynamics of form perception: boundary completion, illusory figures, and neon color spreading. *Psychological Review*, **92**: 173–211.

- Guzman, A. (1969). Decomposition of a visual scene into three-dimensional bodies. In *Automatic Interpretation and Classification of Images*. Grasselli (ed.). Academic Press: New York, NY. pp. 243–276.
- York: Academic Press.
- He, Z.J. & Nakayama, K. (1994). Apparent motion determined by surface layout not by disparity or 3-dimensional distance. *Nature*, **367**: 173–175.
- He, Z.J. & Ooi, T.L. (1998). Illusory contour formation affected by luminance contrast polarity. *Perception*, **27**: 313–335.
- He, Z.J. & Ooi, T.L. (1999). Perceptual organization of apparent motion in Ternus display. *Perception*, **28**: 877–892.
- He, Z.J., Wu, B., Ooi, T.L., Yarbrough, G., & Wu, J. (2004). Judging egocentric distance on the ground: occlusion and surface integration. *Perception*, **33**: 789–806.
- Hering, E. (1879/1942). *Spatial sense and movements of the eye*. English translation by Radde. American Academy of Optometry: Baltimore, MD.
- Hochberg, J. (1964). Depth perception loss with local monocular suppression: A problem in the explanation of stereopsis. *Science*, **145**: 1334–1336.
- Horwitz, G.D., Chichilnisky, E.J., & Albright, T.D. (2007). Cone inputs to simple and complex cells in V1 of awake macaque. *Journal of Neurophysiology*, **97**: 3070–3081.
- Huang, X., & Paradiso, M.A. (2008). V1 response timing and surface filling-in. *Journal of Neurophysiology*, **100**: 539–547.
- Hubel, D.H. & Wiesel, T.N. (1962). Receptive fields, binocular interaction and functional architecture in the cat's visual cortex. *Journal of Physiology*, **160**: 106–154.
- Hubel, D.H. & Wiesel, T.N. (1968). Receptive fields and functional architecture of monkey striate cortex. *Journal of Physiology*, **195**: 215–243.
- Hubel, D.H. & Wiesel, T.N. (1970). Stereopsis vision in the macaque monkey. *Nature*, **225**: 41–42.



- Jehee, J.F.M., Lamme, V.A.F., & Roelfsema, P.R. (2007). Boundary assignment in a recurrent network architecture. *Vision Research*, **47**: 1153–1165.
- Jones, J.P. & Palmer, L.A. (1987). An evaluation of the two-dimensional Gabor filter model of simple receptive fields in cat striate cortex. *Journal of Neurophysiology*, **58**: 1233–1258.
- Johnson, E.N., Hawken, M.J., & Shapley, R. (2001). The spatial transformation of color in the primary visual cortex of the macaque monkey. *Nature Neuroscience*, **4**: 409–416.
- Johnson, E.N., Hawken, M.J., & Shapley, R. (2008). The orientation selectivity of color-responsive neurons in macaque V1. *Journal of Neuroscience*, **28**: 8096–8106.
- Julesz, B. & Miller, J.E. (1975). Independent spatial-frequency-tuned channels in binocular fusion and rivalry. *Perception*, **4**: 125–143.
- Kaernbach, C. (1991). Simple adaptive testing with the weighted up-down method. *Perception & Psychophysics*, **49**: 227–229.
- Kamphuisen, A.P., van Wezel, R.J.A., & van Ee, R. (2007). Inter-ocular transfer of stimulus cueing in dominance selection at the onset of binocular rivalry. *Vision Research*, **47**: 1142–1144.
- Kanisza G. (1955). Margini quasi percettivi in campi con stimolazione omogenea. *Rivista di Psicologia* 497-30. Translation by Gerbino, 1987, In *The Perception of Illusory Contours*. Petry & Meyer (eds.). Springer: New York, NY. pp. 40–49.
- Kanizsa, G. (1979). *Organization in vision: Essays on Gestalt Perception*. Praeger: New York, NY.
- Kaufman, L. (1964). Suppression and fusion in viewing complex stereograms. *American Journal of Psychology*, **77**: 193–205.
- Kaufman, L. (1974). *Sight and Mind*. Oxford University Press: New York, NY.
- Kellman, P.J. & Shipley, T.F. (1991). A theory of visual interpolation in object perception. *Cognitive Psychology*, **23**: 141–221.
- Kellman, P.J. & Cohen, M.H. (1984). Kinetic subjective contours. *Perception and Psychophysics*, **35**: 237–244.

- Kellman, P.J., Garrigan, P., & Shipley, T.F. (2005). Object interpolation in three dimensions. *Psychological Review*, **112**: 586–609.
- Kellman, P.J. & Shipley, T.F. (1991). A theory of visual interpolation in object perception. *Cognitive Psychology*, **23**: 141–221.
- Kellman, P.J., Yin, C., & Shipley, T.F. (1998). A common mechanism for illusory and occluded object completion. *Journal of Experimental Psychology: Human Perception and Performance*, **24**: 859–869.
- Knierim, J.J. & van Essen, D.C. (1992). Neuronal responses to static texture patterns in area V1 of the alert macaque monkey. *Journal of Neurophysiology*, **67**: 961–980.
- Koffka, K. (1935). *Principles of Gestalt Psychology*. Brace and Company: Harcourt, NY.
- Komatsu, H. (2006). The neural mechanisms of perceptual filling-in. *Nature Reviews Neuroscience*, **7**: 220–231.
- Komatsu, H., Kinoshita, M., & Murakami, I. (2000). Neural responses in the retinotopic representation of the blind spot in the macaque V1 to stimuli for perceptual filling-in. *Journal of Neuroscience*, **20**: 9310–9319.
- Kourtzi, Z., Tolias, A.S., Altmann, C.F., Augath, M., & Logothetis, N.K. (2003). Integration of local features into global shapes: monkey and human fMRI studies. *Neuron*, **37**: 333–346.
- Kovács, I., Papathomas, T.V., Yang, M., & Fehér, Á. (1996). When the brain changes its mind: Interocular grouping during interocular rivalry. *Proceedings of the National Academy of Sciences (USA)*, **93**: 15508–15511.
- Krauskopf, J. (1963). Effect of retinal image stabilization on the appearance of heterochromatic targets. *Journal of the Optical Society of America*, **53**: 741–744.
- Kuffler, S. W. (1953). Discharge patterns and functional organization of the mammalian retina. *Journal of Neurophysiology*, **16**: 37–68.
- Lack, L. (1978). *Selective attention and the control of binocular rivalry*. Mouton Publishers: The Hague, The Netherlands.

- Lamme, V.A. (1995). The neurophysiology of figure-ground segregation in primary visual cortex. *Journal of Neuroscience*, **15**: 1605–1615.
- Lamme, V.A.F., Super, H., & Spekreijse, H. (1998). Feedforward, horizontal, and feedback processing in the visual cortex. *Current Opinion in Neurobiology*, **8**: 529–535.
- Lee, S.H. & Blake, R. (2004). A fresh look at interocular grouping during binocular rivalry. *Vision Research*, **44**(10): 983–991.
- Lee, S.H., Blake, R., & Heeger, D. (2007). Hierarchy of cortical responses underlying binocular rivalry. *Nature Neuroscience*, **10**: 1048–1054.
- Lee, T.S. & Nguyen, M. (2001). Dynamics of subjective contour formation in the early visual cortex. *Proceedings of the National Academy of Science (USA)*, **98**: 1907–1911.
- Leopold, D., Wilke, M., Maier, A., & Logothetis, N. K. (2005). Binocular rivalry and the illusion of monocular vision. In *Binocular Rivalry*. Alais & Blake (eds.). MIT Press: Cambridge, MA. pp. 231–259.
- Levelt, W. (1965). *On binocular rivalry*. Royal Van Gorcum: Assen, The Netherlands.
- Levelt, W. (1966). The alternation process in binocular rivalry. *British Journal of Psychology*, **57**(3): 225–238.
- Levelt, W. (1967). Note on the distribution of dominance times in binocular rivalry. *British Journal of Psychology*, **58**(1): 143–145.
- Leventhal, A.G., Thompson, K.G., Liu, D., Zhou, Y., & Ault, S.J. (1995). Concomitant sensitivity to orientation, direction, and color of cells in layers 2, 3, and 4 of monkey striate cortex. *Journal of Neuroscience*, **15**: 1808–1818.
- Li, D., Freeman, A., & Alais, D. (2005). Contrast sensitivity of form and motion discrimination during binocular rivalry. *Vision Research*, **45**: 1255–1263.
- Li, C.Y. & Guo, K. (1995). Measurements of geometric illusions, illusory contours and stereo-depth at luminance and colour contrast. *Vision Research*, **35**: 1713–1720.
- Livingstone, M.S. & Hubel, D.H. (1987). Psychophysical evidence for separate channels for the perception of form, color, movement, and depth. *Journal of Neuroscience*, **7**: 3416–3468.

- Livingstone, M.S. & Hubel, D.H. (1988). Segregation of form, color, movement, and depth: anatomy, physiology, and perception. *Science*, **240**: 740–749.
- Lorenceau, J. & Shiffrar, M. (1992). The influence of terminators on motion integration across space. *Vision Research*, **32**, 263–273.
- Losada, M.A. & Mullen, K.T. (1994). The spatial tuning of chromatic mechanisms identified by simultaneous masking. *Vision Research*, **34**: 331–341.
- Makous, W. & Sanders, R.K. (1978). Suppressive interactions between fused patterns. In *Visual Psychophysics and Physiology*. Armington, Krauskopf, & Wooten (eds.). Academic Press: New York, NY. pp. 167–179.
- Meng, M., Ferneyhough, E., & Tong, F. (2007). Dynamics of perceptual filling-in of visual phantoms revealed by binocular rivalry. *Journal of Vision*, **7**(13), 1–15.
- Mitchell, J.F., Stoner, G.R., & Reynolds, J.H. (2004). Object-based attention determines dominance in binocular rivalry. *Nature*, **429**: 410–413.
- Mitchison, G.J. & McKee, S.P. (1987). The resolution of ambiguous stereoscopic matches by interpolation. *Vision Research*, **27**: 285–294.
- Motoyoshi, I. (1999). Texture filling-in and texture segregation revealed by transient masking. *Vision Research*, **39**: 1285–1291.
- Nakayama, K., He, Z.J., & Shimojo, S. (1995). Visual surface representation: A critical link between lower-level and higher-level vision. In *An Invitation to Cognitive Science: Visual Cognition*. Kosslyn & Oshershon (eds.). MIT Press: Cambridge, MA. pp 1–70.
- Nakayama, K., & Shimojo, S. (1990). Toward a neural understanding of visual surface representation. *Cold Spring Harbor Symposia on Quantitative Biology*, **55**: 911–924.
- Nakayama, K. & Shimojo, S. (1992). Experiencing and perceiving visual surfaces. *Science*, **257**: 1357–1363.
- Nakayama, K., Shimojo, S., & Silverman, G. H. (1989). Stereoscopic depth: its relation to image segmentation, grouping, and the recognition of occluded objects. *Perception*, **18**: 55–68.
- Nakayama, K., & Silverman, G.H. (1985). Detection and discrimination of sinusoidal grating

- displacements. *Journal of the Optical Society of America*, **2**: 267–274.
- Nguyen, V., Freeman, A., & Alais, D. (2003). Increasing depth of binocular rivalry suppression along two visual pathways. *Vision Research*, **43**: 2003–2008.
- Nguyen, V., Freeman, A., & Wenderoth, P. (2001). The depth and selectivity of suppression in binocular rivalry. *Perception & Psychophysics*, **63**: 348–360.
- Nishina, S., Yazdanbakhsh, A., Watanabe, T. & Kawato, M. (2007). Depth propagation across an illusory surface. *Journal of the Optical Society of America A*, **24**: 905–910.
- Norman, H.F., Norman, J.F., & Bilotta, J. (2000). The temporal course of suppression during binocular rivalry. *Perception*, **29**, 831–841.
- Nothdurft, H.C. (1992). Feature analysis and the role of similarity in preattentive vision. *Perception and Psychophysics*, **52**(4): 355–375.
- Nothdurft, H.C., Gallant, J.L., & van Essen, D.C. (2000). Response profiles to texture border patterns in area V1. *Visual Neuroscience*, **17**: 421–436.
- Ogle, K.N. & Wakefield, J.M. (1967). Stereoscopic depth and binocular rivalry. *Vision Research*, **7**: 89–98.
- Ohzawa, I., DeAngelis, G.C., & Freeman, R.D. (1990). Stereoscopic depth discrimination in the visual cortex: neurons ideally suited as disparity detectors. *Science*, **249**: 1037–1041.
- Ooi, T.L. & He, Z.J. (1999). Binocular rivalry and visual awareness: The role of attention. *Perception*, **28**: 551–574.
- Ooi, T.L. & He, Z.J. (2001). Sensory eye dominance. *Journal of the American Optometric Association*, **72**: 168–178.
- Ooi, T.L. & He, Z.J. (2003). A distributed intercortical processing of binocular rivalry: Psychophysical evidence. *Perception*, **32**: 155–166.
- Ooi, T.L. & He, Z.J. (2005). Surface representation and attention modulation mechanisms in binocular rivalry. In *Binocular Rivalry*. Alais & Blake (eds.). MIT Press: Cambridge, MA. pp 117–135.

- Ooi, T.L. & He, Z.J. (2006). Binocular rivalry and surface-boundary processing. *Perception*, **35**: 581–603.
- Ooi, T.L., He, Z.J., & Su, Y. (2005). Binocular rivalry is affected by surface boundary contours. *Journal of Vision*, **5**: 5a.
- Ooi, T.L. & Loop, M.L. (1994). Visual suppression and its effect upon color and luminance sensitivity. *Vision Research*, **34**: 2997–3003.
- Ooi, T.L., Wu, B., & He, Z.J. (2001). Distance determined by the angular declination below the horizon. *Nature*, **414**: 197–200.
- O’Shea, R.P. (1987). Chronometric analysis supports fusion rather than suppression theory of binocular vision. *Vision Research*, **27**: 781–791.
- O’Shea, R.P., & Crassini, B. (1981). The sensitivity of binocular rivalry suppression to changes in orientation assessed by reaction-time and forced-choice techniques. *Perception*, **10**: 283–293.
- Paffen, C.L.E., Alais, D., & Verstraten, F.A.J. (2005). Center-surround inhibition deepens binocular rivalry suppression. *Vision Research*, **45**: 2642–2649.
- Papathomas, T.V., Kovács, I., & Conway, T. (2005). Interocular grouping in binocular rivalry: Attributes and combinations. In *Binocular Rivalry*. Alais & Blake (eds.). MIT Press: Cambridge, MA. pp 155–168.
- Paradiso, M.A. & Hahn, S. (1996). Filling-in percepts produced by luminance modulation. *Vision Research*, **36**: 2657–2663.
- Paradiso, M.A. & Nakayama, K. (1991). Brightness perception and filling-in. *Vision Research*, **31**: 1221–1236.
- Pelli, D.G. (1997). The VideoToolBox software for visual psychophysics: transforming numbers into movies. *Spatial Vision*, **10**: 437–442.
- Peterhans, E. & von der Heydt, R. (1989). Mechanisms of contour perception in monkey visual cortex: II. Contours bridging gaps. *Journal of Neuroscience*, **9**: 1749–1763.
- Peterhans, E. & von der Heydt, R. (1991). Subjective contours – Bridging the gap between

- psychophysics and physiology. *Trends in Neurosciences*, **14**: 112–119.
- Prazdny, K. (1983). Illusory contours are not caused by simultaneous brightness contrast. *Perception and Psychophysics*, **34**: 403–404.
- Porta, J.B. (1593). *De refractione. Optices parte. Libri novem*. Salviani: Naples, Italy.
- Purves, D., Lotto, R.B., Williams, S.M., Nundy, S., & Yang, Z. (2001). Why we see things the way we do: Evidence for a wholly empirical strategy of vision. *Philosophical Transactions of the Royal Society B*, **356**: 285–297.
- Qiu, F.T., Sugihara, T., & von der Heydt, R. (2007). Figure–ground mechanisms provide structure for selective attention. *Nature Neuroscience*, **10**: 1492–1499.
- Qiu, F.T. & von der Heydt, R. (2005). Figure and ground in the visual cortex: V2 combines stereoscopic cues with Gestalt rules. *Neuron*, **47**: 155–166.
- Qiu, F.T. & von der Heydt, R. (2007). Neural representation of transparent overlap. *Nature Neuroscience*, **10**: 283–284.
- Ramachandran, V.S. & Gregory, R.L. (1991). Perceptual filling in of artificially induced scotomas in human vision. *Nature*, **350**: 699–702.
- Riggs, L.A., Ratliff, F., Cornsweet, J.C., & Cornsweet, T.N. (1953). The disappearance of steadily fixated visual test objects. *Journal of the Optical Society of America*, **43**, 495–500.
- Ringach, D.L. & Shapley, R. (1996). Spatial and temporal properties of illusory contours and amodal boundary completion. *Vision Research*, **36**: 3037–3050.
- Rock, I. (1983). *The Logic of Perception*. MIT Press: Cambridge, MA.
- Roelfsema, P.R., Tolboom, M., & Khayat, P.S. (2007). Different Processing Phases for Features, Figures, and Selective Attention in the Primary Visual Cortex. *Neuron*, **56**: 785–792.
- Rossi, A.F. & Paradiso, M.A. (1996). Temporal limits of brightness induction and mechanisms of brightness perception. *Vision Research*, **36**: 1391–1398.
- Rubin, N. (2001). The role of junctions in surface completion and contour matching. *Perception*,

30: 339–366.

- Ruderman, D.L., Cronin, T.W., & Chiao, C. (1998). Statistics of cone responses to natural images: implications for visual coding. *Journal of the Optical Society of America A*, **15**: 2036–2045.
- Sasaki, Y. & Watanabe, T. (2004). The primary visual cortex fills in color. *Proceedings of the National Academy of Sciences (USA)*, **101**: 18251–18256.
- Schwarzkopf, D.S. & Kourtzi, Z. (2008). Experience shapes the utility of natural statistics for perceptual contour integration. *Current Biology*, **18**: 1162–1167.
- Sekuler, A. & Palmer, S. (1992). Perception of partly occluded objects: A microgenetic analysis. *Journal of Experimental Psychology, General*, **121**: 95–111.
- Sereno, M.I., Dale, A.M., Reppas, J.B., Kwong, K.K., Belliveau, J.W., Brady, T.J., Rosen, B.R., & Tootell, R.B. (1995). Borders of multiple human visual areas in humans revealed by functional MRI. *Science*, **268**: 889–893.
- Shapley, R. & Gordon, J. (1985). Nonlinearity in the perception of form. *Perception and Psychophysics*, **37**: 84–88.
- Shapley, R. & Gordon, J. (1987). The existence of interpolated illusory contours depends on contrast and spatial separation. In *The Perception of Illusory Contours*. Petry & Meyer (eds.). Springer: New York, NY.
- Shimojo, S., & Nakayama, K. (1990). Real world occlusion constraints and binocular rivalry. *Vision Research*, **30**: 69–80.
- Shimojo, S., Silverman, G.H., & Nakayama, K. (1989). Occlusion and the solution to the aperture problem for motion. *Vision Research*, **29**: 619–626.
- Sillito, A.M., Grieve, K.L., Jones, H.E., Cudério, J., & Davis, J. (1995). Visual cortical mechanisms detecting focal orientation discontinuities. *Nature*, **378**, 492–495.
- Smith, E.L., Levi, D.M., Harwerth, R.S., & White, J.M. (1982). Color vision is altered during the suppression phase of binocular rivalry. *Science*, **218**(4574): 802–804.



- Smith, E.L., Levi, D.M., Manny, R.E., Harwerth, R.S., & White, J.M. (1985). The relationship between binocular rivalry and strabismic suppression. *Investigative Ophthalmology & Visual Science*, **26**: 80–87.
- Sobel, D. & Blake, R. (2002). How context influences predominance during binocular rivalry. *Perception*, **31**: 813–824.
- Solomon, S.G., Peirce, J.W., & Lennie, P. (2004). The impact of suppressive surrounds on chromatic properties of cortical neurons. *Journal of Neuroscience*, **24**: 148–160.
- Spehar, B. (2000). Degraded illusory contour formation with non-uniform inducers in Kanizsa configurations: the role of contrast polarity. *Vision Research*, **40**: 2653–2659.
- Spehar, B. & Clifford, C.W.G. (2003). When does illusory contour formation depend on contrast polarity? *Vision Research*, **43**: 1915–1919.
- Spillmann, L. & Kurtenbach, A. (1992). Dynamic noise backgrounds facilitate target fading. *Vision Research*, **32**: 1941–1946.
- Stoner, G.R. & Albright, T.D. (1996). The interpretation of visual motion: Evidence for surface segmentation mechanisms. *Vision Research*, **36**: 1291–1310.
- Stoner, G.R. & Albright, T.D. (1998). Luminance contrast affects motion coherency in plaid patterns by acting as a depth-from-occlusion cue. *Vision Research*, **38**: 387–401.
- Stoper, A.E. & Mansfield, J.G. (1978). Metacontrast and paracontrast suppression of a contourless area. *Vision Research*, **18**: 1669–1674.
- Stuit, S.M., Cass, J., Paffen, C.L.E., & Alais, D. (2009). Orientation-tuned suppression in binocular rivalry reveals general and specific components of rivalry suppression. *Journal of Vision*, **9**(11): 1–15.
- Su, Y., He, Z.J., & Ooi, T.L. (2009). Coexistence of binocular integration and suppression determined by surface border information. *Proceedings of the National Academy of Sciences (USA)*, **106**: 15990–15995.
- Su, Y., He, Z.J., & Ooi, T.L. (2010). Surface completion affected by luminance contrast polarity and common motion. *Journal of Vision*, **10**(3): 1–14.

- Su, Y., He, Z.J., & Ooi, T.L. (2010). Boundary contour-based surface integration affected by color. *Vision Research*, **50**(18): 1833–1844.
- Su, Y., He, Z.J., & Ooi, T.L. (2010). The magnitude and dynamics of interocular suppression affected by monocular boundary contour and conflicting local features. *Vision Research*, **50**(20): 2037–2047.
- Su, Y., He, Z.J., & Ooi, T.L. (2011). Seeing grating-textured surface begins at the border. *Journal of Vision*, **11**(1): 1–14.
- Su, Y., He, Z.J., & Ooi, T.L. (2011). Revealing boundary-contour based surface representation through the time course of binocular rivalry. *Vision Research*, **51**(11): 1288–1296.
- Sugita, Y. (1999). Grouping of image fragments in primary visual cortex. *Nature*, **401**: 269–272.
- Suzuki, S. & Grabowecky, M. (2002). Evidence for perceptual “trapping” and adaptation in multistable binocular rivalry. *Neuron*, **36**: 143–157.
- Suzuki, S. & Grabowecky, M. (2007). Long-term speeding in perceptual switches mediated by attention-dependent plasticity in cortical visual processing. *Neuron*, **56**: 741–753.
- Switkes, E., Bradley, A., and De Valois, K.K. (1988). Contrast dependence and mechanisms of masking interactions among chromatic and luminance gratings. *Journal of the Optical Society of America A*, **5**: 1149–1162.
- Thorell, L.G., De Valois, R.L., & Albrecht, D.G. (1984). Spatial mapping of monkey V1 cells with pure color and luminance stimuli. *Vision Research*, **24**: 751–769.
- Tong, F. and Engel, S.A. (2001). Interocular rivalry revealed in the human cortical blind-spot representation. *Nature*, **411**: 195–199.
- Tong, F., Meng, M., & Blake, R. (2006). Neural bases of binocular rivalry. *Trends in Cognitive Science*, **10**: 502–511.
- Treisman, A. (1962). Binocular rivalry and stereoscopic depth perception. *The Quarterly Journal of Experimental Psychology*, **14**: 23–37.
- Treisman, A. & Gelade, G. (1980). A feature-integration theory of attention. *Cognitive Psychology*, **12**: 97–136.

- Troscianko, T., Montagnon, R., Le Clerc, J., Malbert, E., & Chanteau, P.L. (1991). The role of colour as a monocular depth cue. *Vision Research*, **31**: 1923–1929.
- Troxler, I.P.V. (1804). Über das verschwinden gegebener gegenstände innerhalb unseres Gesichtskreises. *Ophthalmologische Bibliothek*, **2**: 1–53.
- van Bogaert, E.A., Ooi, T.L., & He, Z.J. (2008). The monocular-boundary-contour mechanism in binocular surface representation and suppression. *Perception*, **37**: 1197–1215.
- van der Zwan, R., & Wenderoth, P. (1994). Psychophysical evidence for area V2 involvement in the reduction of subjective contour tilt aftereffects by binocular rivalry. *Visual Neuroscience*, **11**: 823–830.
- von der Heydt, R. (2003). Image parsing mechanisms of the visual cortex. In: *The Visual Neurosciences*. Werner & Chalupa (eds.). MIT Press: Cambridge, MA. pp 1139–1150.
- von der Heydt, R., Friedman, H.S., & Zhou, H. (2003). Searching for the neural mechanisms of color filling-in. In *Filling-in: From perceptual completion to cortical reorganization*. Pessoa & De Weerd (eds.). Oxford University Press: Oxford, UK. pp. 106–127.
- von der Heydt, R., Macuda, T., & Qiu, F.T. (2005). Border-ownership-dependent tilt aftereffect. *Journal of the Optical Society of America A*, **22**: 2222–2229.
- von der Heydt, R., Peterhans, E., & Baumgartner, G. (1984). Illusory contours and cortical neuron responses. *Science*, **224**: 1260–1262.
- von der Heydt, R., Zhou, H., and Friedman, H.S. (2003). Neural coding of border ownership: implications for the theory of figure-ground perception. In *Perceptual Organization in Vision: Behavioral and Neural Perspectives*. Behrmann, Kimchi, & Olson (eds.). Lawrence Erlbaum Associates: Hillsdale, NJ. pp. 281–304.
- von Helmholtz, H. (1925). *Treatise on Physiological Optics, Vol. III*. Dover: New York, NY.
- Wales, R. & Fox, R. (1970). Increment detection thresholds during binocular rivalry suppression. *Perception & Psychophysics*, **8**: 90–94.
- Walker, P. (1978). Binocular rivalry: central or peripheral selective processes? *Psychological Bulletin* **85**: 376–389.

- Walls, G.L. (1954). The filling-in process. *American Journal of Optometry & Archives of American Academy of Optometry*, **31**: 329–341.
- Watamaniuk, S.N.J. & McKee, S.P. (1995). Seeing motion behind occluders. *Nature*, **377**: 720–730.
- Watanabe, T. (1997). Velocity decomposition and surface decomposition–reciprocal interactions between motion and form processing. *Vision Research*, **37**: 2879–2889.
- Watanabe, T. & Cavanagh, P. (1991). Texture and motion spreading, transparency and the aperture problem. *Perception & Psychophysics*, **50**: 459–464.
- Watanabe, K., Paik, Y., & Blake, R. (2004). Preserved gain control for luminance contrast during binocular rivalry suppression. *Vision Research*, **44**: 3065–3071.
- Williams, L.R., & Hanson, A.R. (1996). Perceptual completion of occluded surfaces. *Computer Vision and Image Understanding*, **64**: 1-20.
- Wilson, H. R. (2003). Computational evidence for a rivalry hierarchy in vision. *Proceedings of the National Academy of Sciences (USA)*. **100**: 14499–14503.
- Wilson, H.R., Blake, R., & Lee, S. (2001). Dynamics of travelling waves in visual perception. *Nature*, **412**: 907–910.
- Wolfe, J.M. (1983). Influence of spatial frequency, luminance, and duration on binocular rivalry and abnormal fusion of briefly presented dichoptic stimuli. *Perception*, **12**: 447–456.
- Wolfe, J. M. (1986). Stereopsis and binocular rivalry. *Psychological Review*, **93**: 269–282.
- Wolfe, J.M. (1988). Parallel ideas about stereopsis and binocular rivalry: A reply to Blake and O’Shea. *Psychological Review*, **95**: 155–158.
- Wu, B., Ooi, T.L., & He, Z.J. (2004). Perceiving distance accurately by a directional process of integrating ground information. *Nature*, **428**: 73–77.
- Xu, J., He, Z.J., & Ooi, T.L. (2010). Surface boundary contour strengthens image dominance in binocular competition. *Vision Research*, **50**: 155–170.
- Yang, Z. & Purves, D. (2003). Image/source statistics of surfaces in natural scenes. *Network*:

*Computation in Neural Systems*, **14**: 371–390.

Yarbus, A.L. (1967). *Eye Movements and Vision*. Plenum Press: New York, NY.

Yin, C., Kellman, P.J., & Shipley, T.F. (1997). Surface completion complements boundary interpolation. *Perception*, **26**, 1459–1479.

Yin, C., Kellman, P.J. & Shipley, T.F. (2000). Surface integration influences depth discrimination. *Vision Research*, **40**: 1969–1978.

Yonas, A., Craton, L.G., & Thompson, W.B. (1987). Relative motion: kinetic information for the order of depth at an edge. *Perception and Psychophysics*, **41**: 53–59.

Yoshioka, T. & Dow, B.M. (1996). Color, orientation and cytochrome oxidase reactivity in areas V1, V2 and V4 of macaque monkey visual cortex. *Behavioral Brain Research*, **76**: 71–88.

Zeki, S. (1983). Colour coding in the cerebral cortex: the response of wavelength-selective and colour-coded cells in monkey visual cortex to changes in wavelength composition. *Neuroscience*, **9**: 767–781.

Zhou, H., Friedman, H.S., & von der Heydt, R. (2000). Coding of border ownership in monkey visual cortex. *Journal of Neuroscience*, **20**: 6594–6611.

## APPENDIX I

### FIGURES

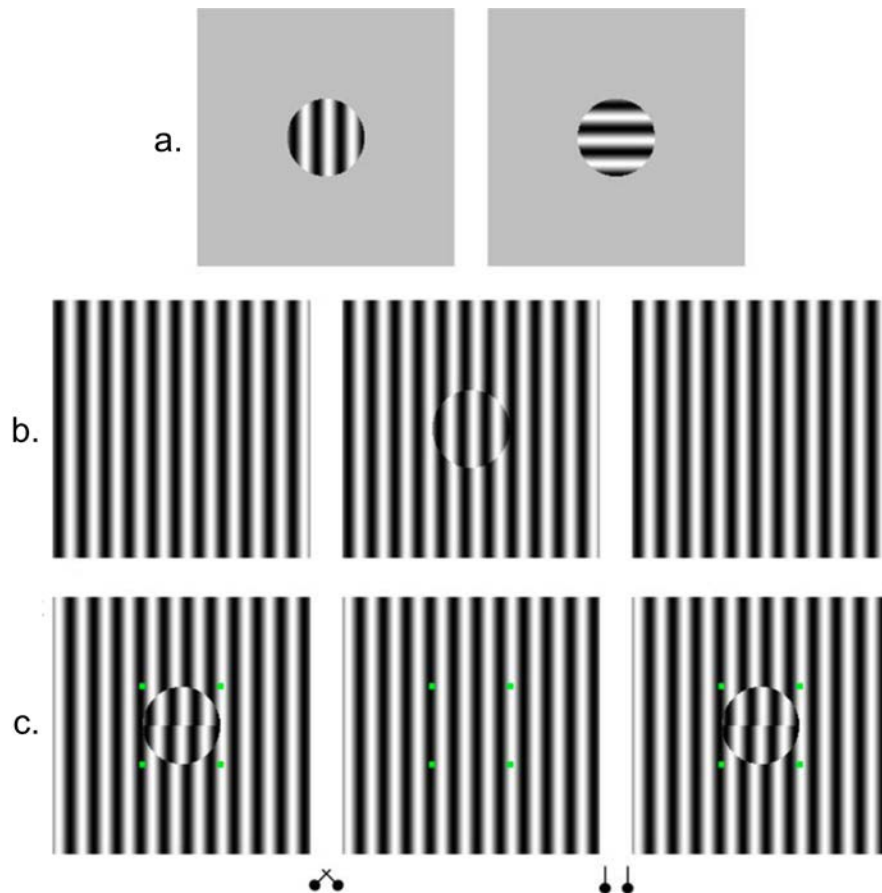


**Fig. 1.1.** (a) Typical BR stimulus. (b) MBC phase-shift stereo/rivalry stimulus. The half-image with the disc grating is phase-shifted  $45^\circ$  relative to the surrounding background grating. With crossed fusion of the left and middle half-images, one perceives the grating within the disc as behind the surrounding grating. (c) The stimulus used in Experiment 1.1, where observers judged the relative depth between the upper and lower half-discs. With crossed fusion of the left and middle half-images, the grating within the disc is seen behind the surrounding grating (far condition) while the lower half-disc is seen in front of the upper half-disc. And by crossed fusion of the right and middle half-images, the entire disc grating is seen in front of the surrounding grating, with the upper half-disc being seen in front of the lower half-disc.

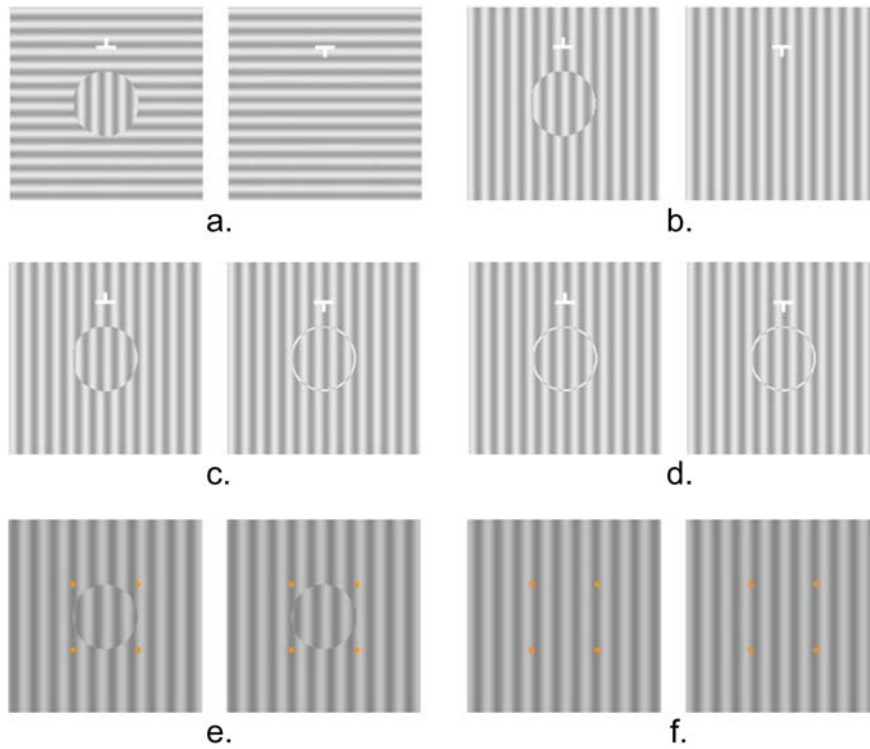


**Fig. 1.2.** (a) MBC stimulus created by orientation difference between the grating disc and surrounding grating. The stimuli used in Experiment 1.2 and Control Experiment 1.1: (b) MBC phase-shift, (c) ring/disc, (d) ring/ring, (e) binocular disc, and (f) binocular background.

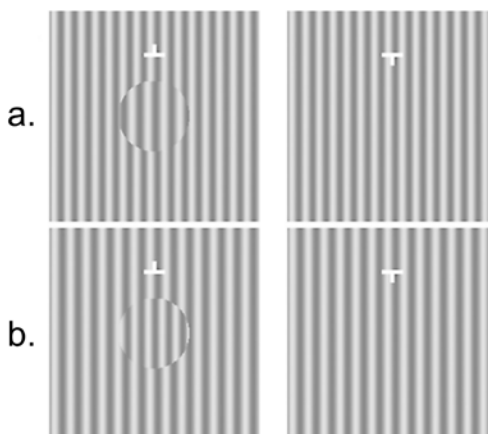


**Fig. 1.3.** MBC spatial-frequency-difference stimuli used in Experiment 1.3. The spatial frequency difference between the disc grating and the corresponding grating in the other half-image [3.5 cpd vs. 3 cpd in (a) and 3 cpd vs. 3.5 cpd in (b)] creates a gradient binocular disparity. With crossed fusion, the MBC disc in stimulus (a) is seen as rotated around the vertical axis with the right side in back. The MBC disc in stimulus (b) is seen as rotated around the vertical axis with the left side in back.

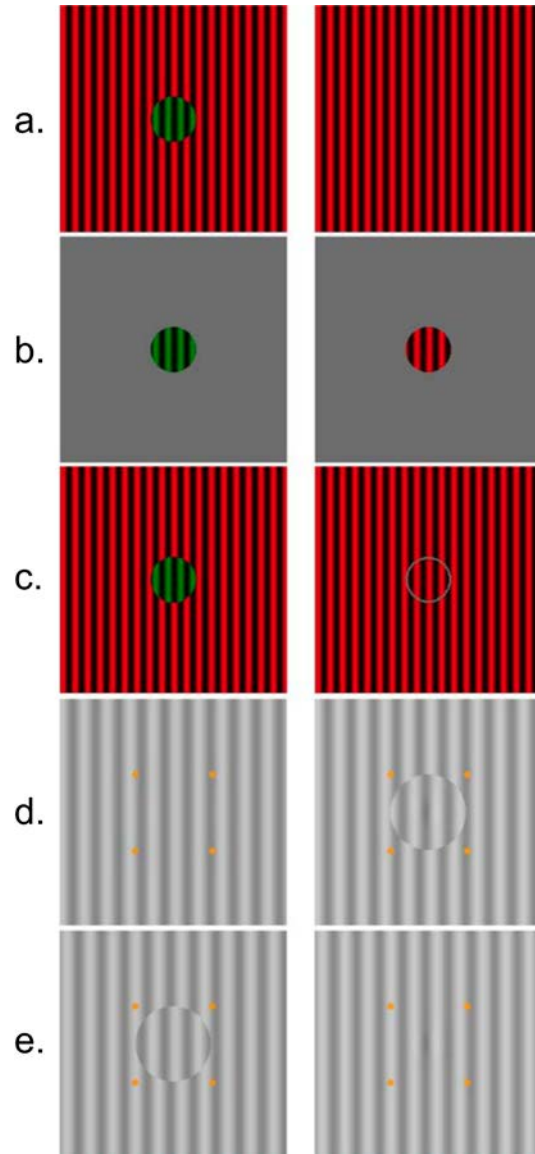


Fig. 1.4. Stimuli used in Experiment 1.4: (a) MBC phase-shift stimulus with a green MBC disc; (b) Typical BR stimulus with red/green discs; (c) Similar to (a) except a gray ring is added to the half-image with the homogeneous grating. Control Experiment 2: The MBC phase-shift stimuli in (d, dominance condition) and (e, suppression condition) each has a Gabor probe in the center.



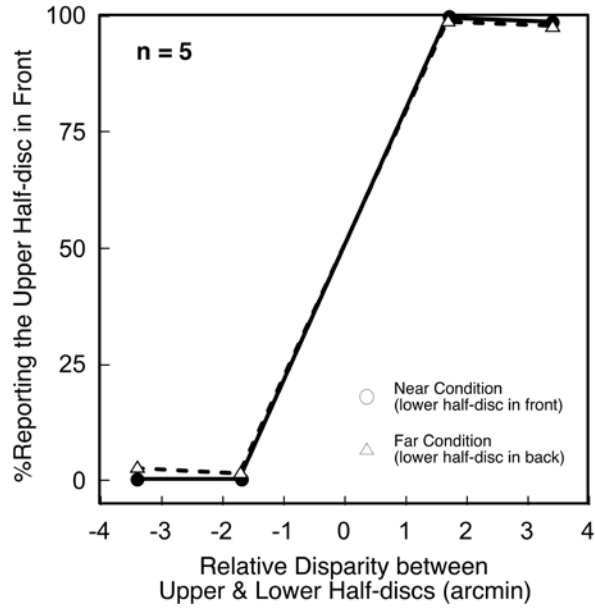


Fig. 1.5. Results of Experiment 1.1.

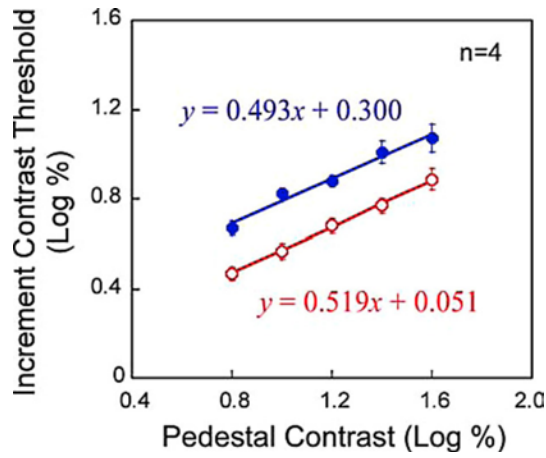
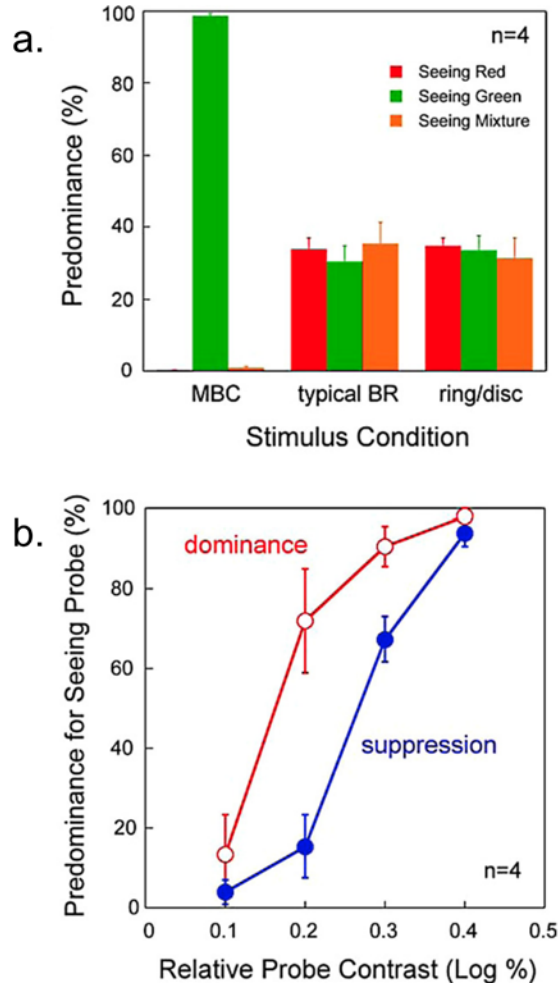
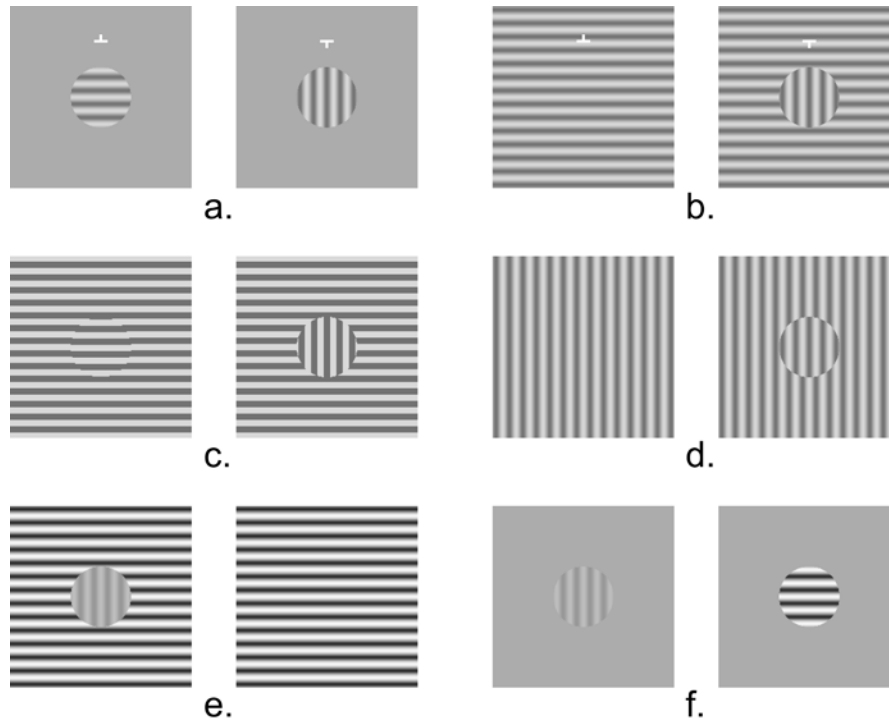


Fig. 1.6. Results of Experiment 1.2.



**Fig. 1.7.** Results of Experiment 1.4. (a) The average predominance for the stimuli in Fig. 1.4a–c. (b) The average predominance as a function of relative probe contrast for seeing the monocular Gabor probe for the stimuli in Fig. 1.4d&e. Due to individual differences, we aligned all four observers’ data at the probe contrast with the maximum predominance difference between the two stimulus conditions (this occurred at 1.2 log% for two observers, and 1.1 log% and 1.0 log%, respectively, for the remaining two observers).



**Fig. 2.1.** (a) A typical binocular rivalry stimulus that stimulates the two eyes with grating discs comprising of orthogonal orientation. We refer to this stimulus as the binocular boundary contour (BBC) rivalry stimulus because the boundary contour of each disc corresponds in the two eyes. (b) An MBC orientation-difference rivalry stimulus in which only one half-image carries the monocular boundary contour (grating disc). The vertical grating disc corresponds to a retinal area in the fellow eye receiving the homogeneous horizontal grating. Yet, when free-fused, one seldom experiences the alternation of binocular rivalry as in (a) above, but a relatively stable percept of the vertical grating disc. (c) A BBC rivalry stimulus with a weak boundary contour (horizontal grating disc) in the left half-image, which is created by phase-shifting the central and surround horizontal grating by  $36^\circ$ . The vertical grating disc with the strong boundary contour predominates in perception. (d) An MBC phase-shift rivalry stimulus, created with  $180^\circ$  phase-shift. (e) MBC orientation-difference rivalry stimulus. The vertical grating within the disc has a low contrast. (f) BBC rivalry stimulus. The vertical grating within the disc also has a low contrast. Yet, when compared between (e) and (f), the vertical grating disc predominates in (e) but not (f).

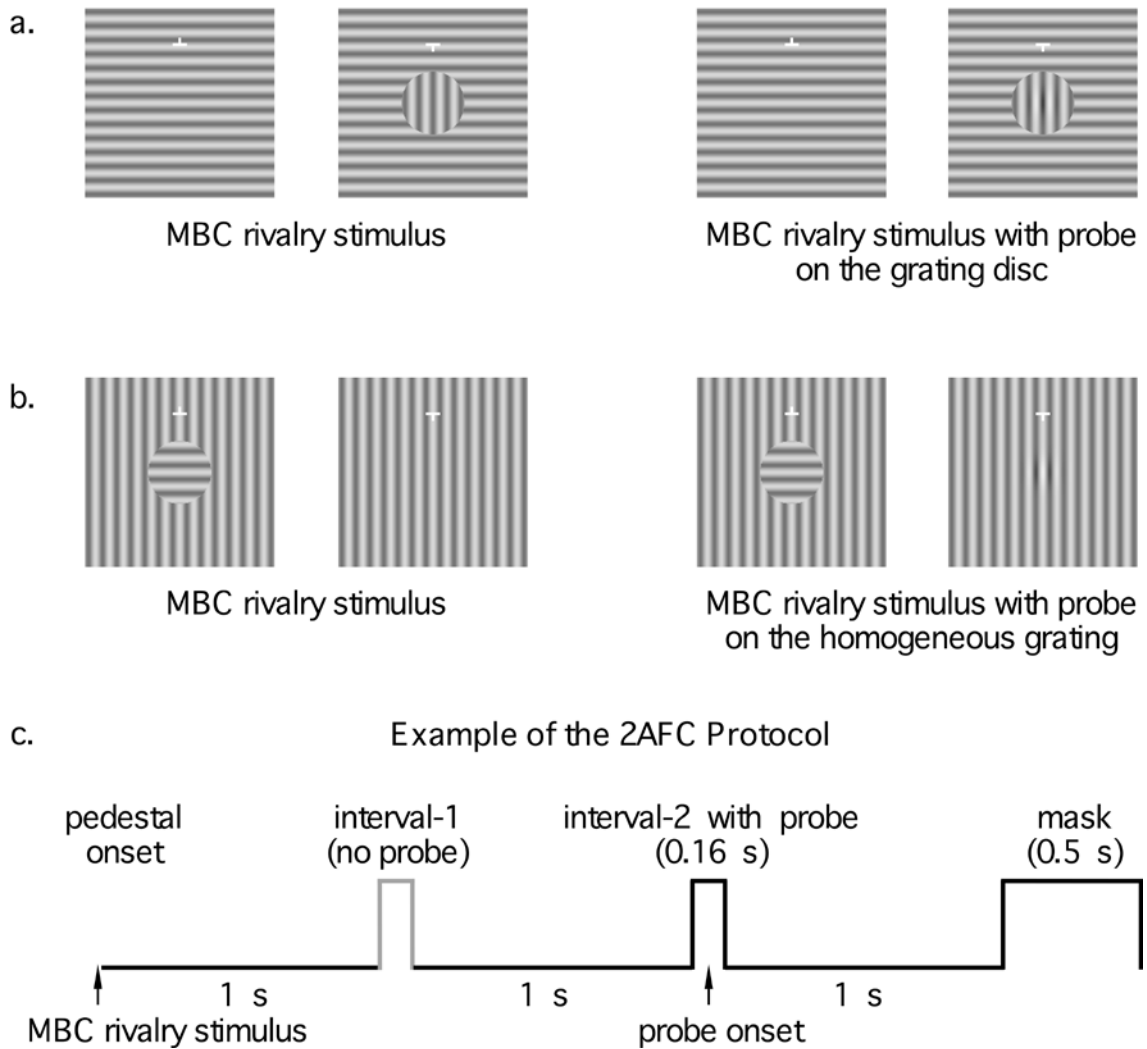


**Fig. 2.2.** (a) An example of a dominance condition. Left: the MBC orientation-difference rivalry stimulus with a vertical grating disc in the right half-image with a horizontal grating disc in the left half-image. Right: a Gabor probe is superimposed on the grating disc (pedestal) to measure the contrast threshold for detecting the probe in the dominant eye. (b) An example of the suppression condition. Left: the MBC orientation-difference rivalry stimulus. Right: the Gabor probe is superimposed on the homogeneous grating half-image (pedestal) to measure the contrast threshold for detecting the probe in the suppressed eye. To counterbalance the effect of grating orientation, dominance and suppression thresholds were also tested with horizontal Gabor probe upon a horizontal grating pedestal (not shown). (c) An example of the 2-alternative-forced-choice (2AFC) method. One sec after the onset of the MBC orientation-difference rivalry stimulus (pedestal), a brief tone is presented. This is followed, 1 s later, by another brief tone that is accompanied by the Gabor probe (0.16 s). The trial ended 1 s later with the presentation of a mask (0.5 s). The observer's task was to indicate whether the probe accompanied the first or second tone.

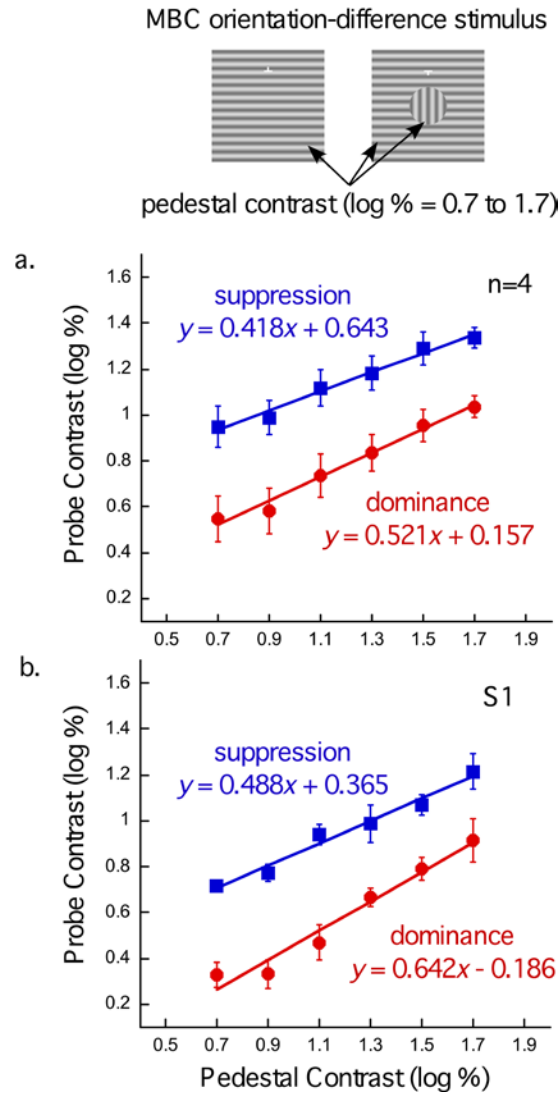


**Fig. 2.3.** Results of Experiment 2.1: the contrast of the MBC orientation-difference rivalry stimulus was set at one of six levels. (a) The average results of all observers in the dominance (circles) and suppression (squares) conditions. While the slopes of the TvC functions for both conditions are not significantly different, the threshold for detecting the Gabor probe is elevated in the suppression condition. The error bars in the graph indicate 1 S.E. (b) The results of a representative naive observer also show an elevated suppression threshold and no significant difference between the slopes of the TvC functions in the two conditions.

MBC orientation-difference stimulus

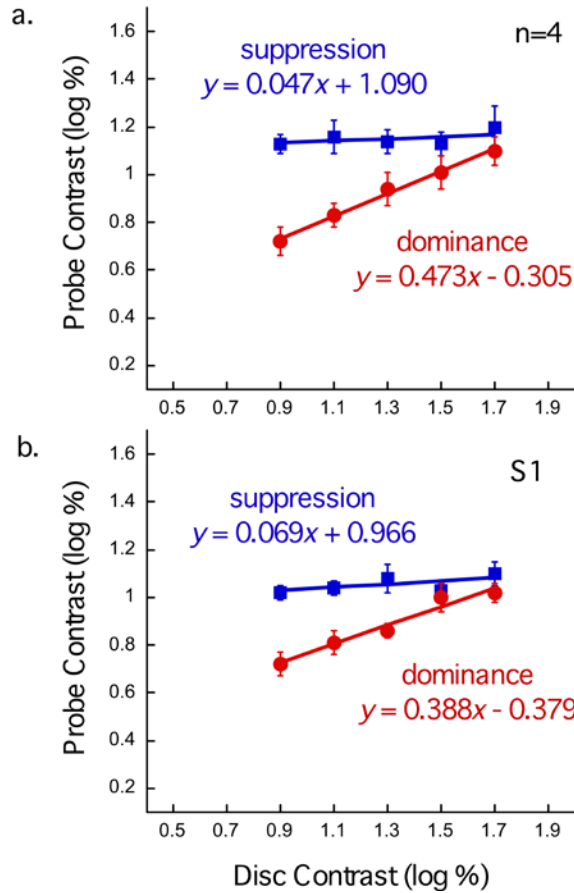
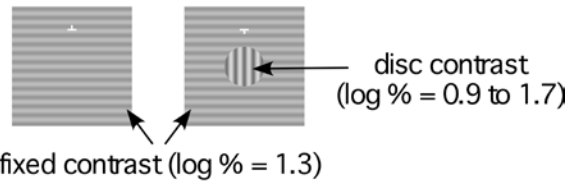
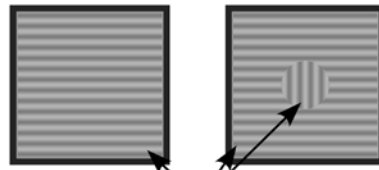


**Fig. 2.4.** Results of Experiment 2.2: the contrast of the grating disc was set at one of five different levels while the remaining components of the MBC orientation-difference rivalry stimulus was fixed at 19.19% contrast level. (a) The average results of all observers in the dominance (circles) and suppression (squares) conditions. The slope of the TvC function for the suppression condition is almost flat, while the slope of the dominance condition is steep. The error bars in the graph indicate 1 S.E. (b) The results of the same representative naive observer whose data are shown in Experiment 2.1.

MBC orientation-difference stimulus



pedestal contrast (log % = 1.6)

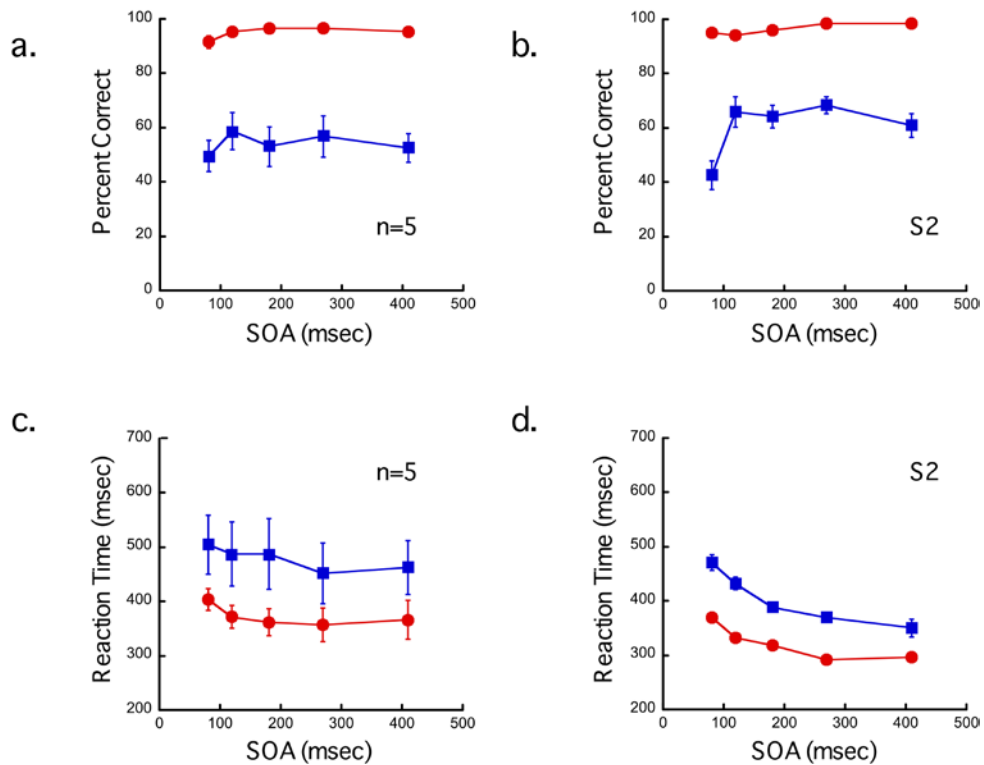
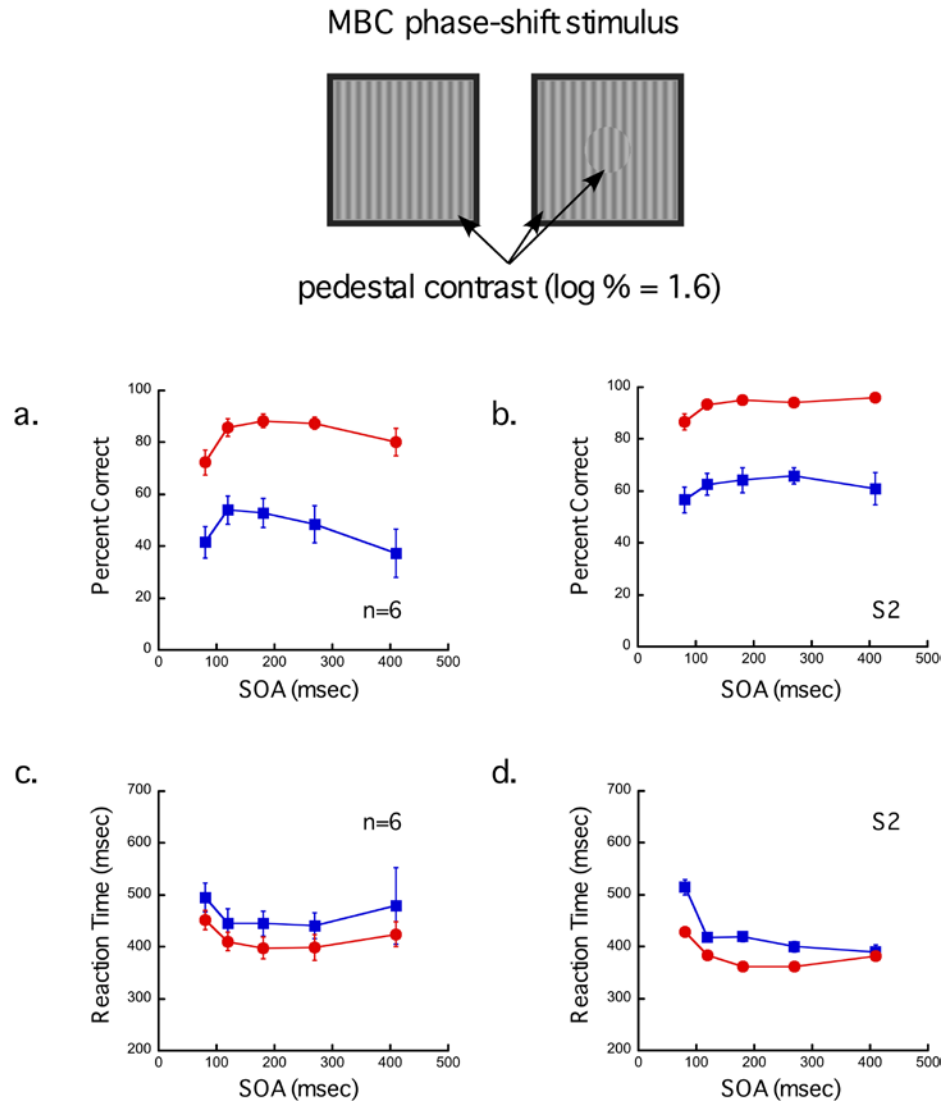
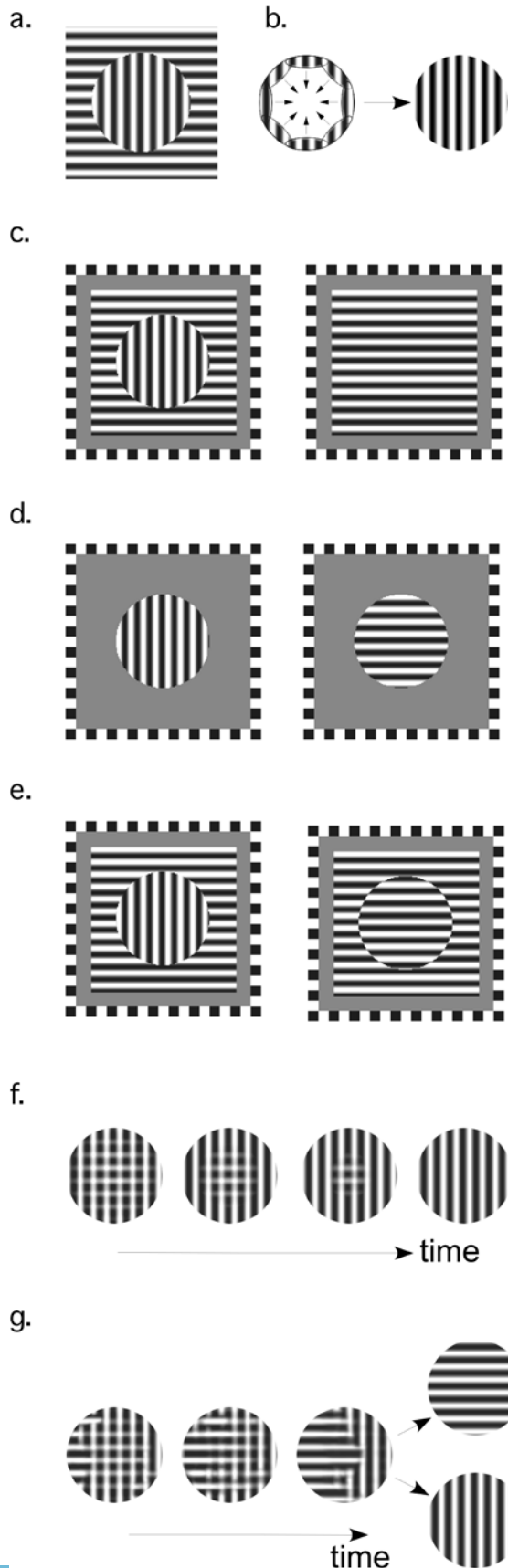


Fig. 2.5. Results of Experiment 2.3 with the MBC orientation-difference rivalry stimulus. (a) The average percentage correct detection of all observers is higher in the dominance (circles) than suppression (squares) condition. (b) The detection data of a representative naive observer show a similar trend. (c) The average reaction time for responding to seeing the Gabor probe is shorter in the dominance (circles) than suppression (squares) condition. (d) The reaction time data of the same representative naive observer. The error bars in the graphs indicate 1 S.E.



**Fig. 2.6.** Results of Experiment 2.4 with the MBC phase-shift rivalry stimulus. (a) The average percentage correct detection of all observers is higher in the dominance (circles) than suppression (squares) condition. (b) The detection data of the same representative naive observer tested in Experiment 2.3 show a similar trend. (c) The average reaction time for responding to seeing the Gabor probe is shorter in the dominance (circles) than suppression (squares) condition. (d) The reaction time data of the same representative naive observer. The error bars in the graphs indicate 1 S.E.





**Fig. 3.1.** Stimuli and percepts. (a) A grating disc surrounded by orthogonal grating. (b) The border-to-interior strategy predicts the representation of the grating disc spreads inward from the BC. (c) Dichoptic stimulus with MBC. When the half-images are fused, one perceives a stable vertical grating disc in front of the horizontal grating background. (d) and (e): Dichoptic stimuli with BBC. For each stimulus, free-fusion leads to frequent perceptual alternation between the vertical and horizontal gratings. (f) Time-sequence illustrations of the representation of the MBC grating disc for the MBC stimulus, and (g) for the BBC stimuli.

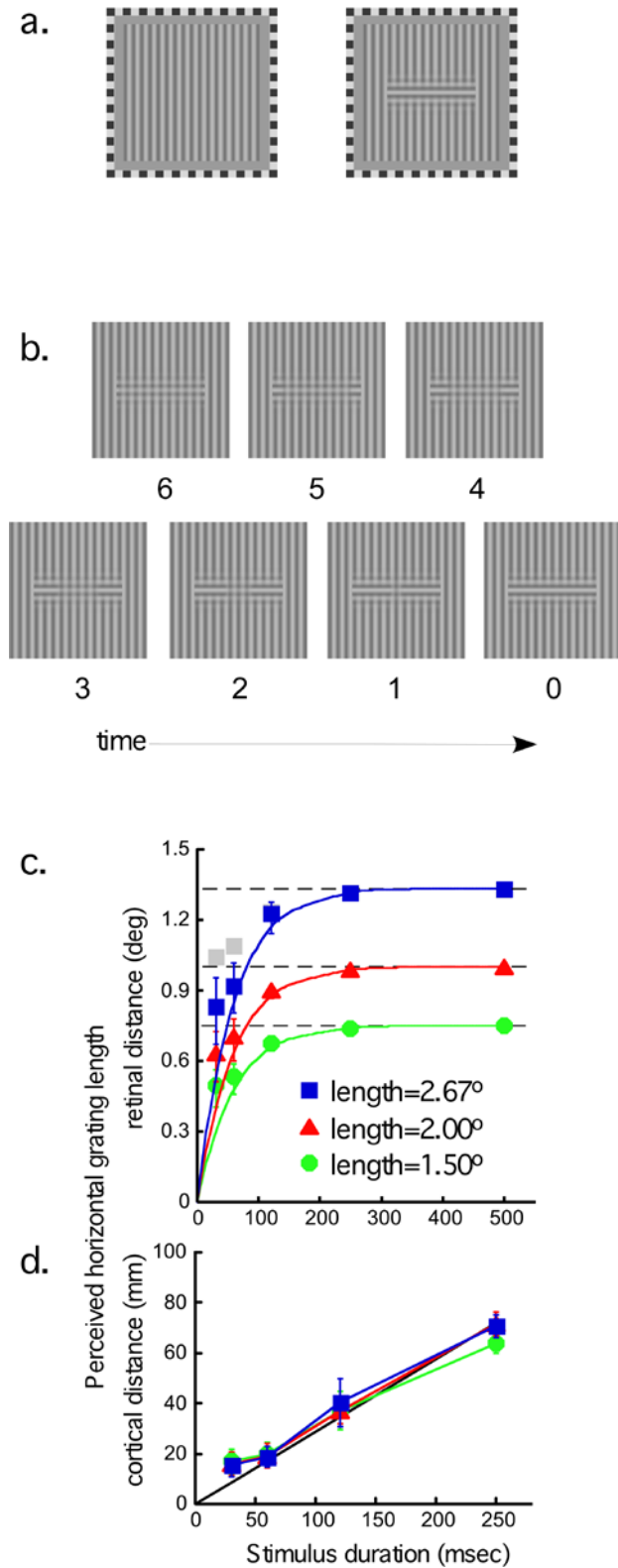


**Fig. 3.2.** Experiment 3.1. (a) The dichoptic MBC stimulus used. The left half-image has a homogeneous vertical grating and the right half-image has a rectangular area filled with horizontal grating (MBC stimulus) and surrounded by vertical grating. (b) Time-sequence illustration of the spreading-in percepts. In the beginning, a mixture of horizontal and vertical gratings (plaid) is seen. Soon after, only the left and right edges of the rectangle are filled with horizontal grating. The region spanned by the horizontal grating increases with time. Spreading is complete when the entire rectangle is represented by the horizontal grating. Seven simulated percepts are shown with the respective gap size scale provided below each example. (c) Results showing the perceived spreading (gap size) in retinal distance as a function of stimulus duration for the three MBC rectangle length conditions (blue square = 2.67°; red triangle = 2.00°; green circle = 1.50°). The curves fitting the data are based on the corresponding linear regression lines plotted in (d). The two gray squares are the predicted data for the MBC rectangle with the 2.67° length if the data were solely contributed by the eccentricity factor (see text for details). (d) The data in (c) are plotted according to the cortical distance in area V1 based on a human fMRI study by Engel et al. (1997). The linear regression line (gray) that passes through the origin ( $y = 0.287x$ ;  $R^2 = 0.937$ ) is derived from the data from all three MBC length conditions.

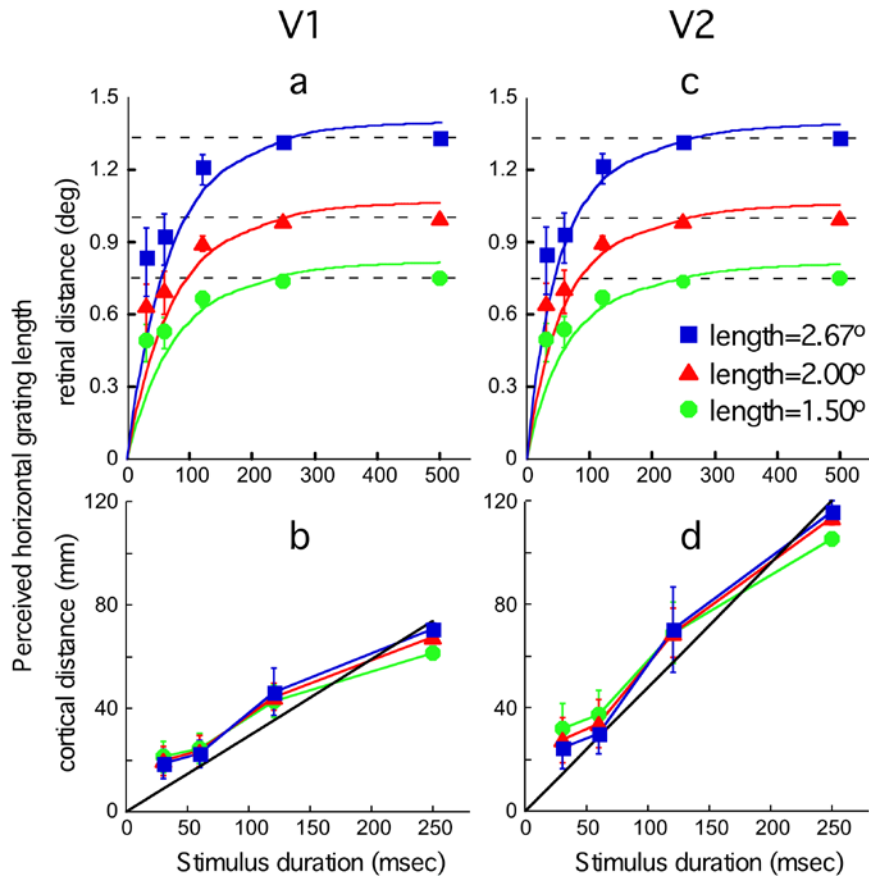


**Fig. 3.3.** The average results of Experiment 3.1 are plotted in a similar manner as in Fig. 3.2c and d. The data points in (a) and (c) plot the spreading (gap size) in retinal distance as a function of stimulus duration for the three MBC rectangle length conditions tested (blue square =  $2.67^\circ$ ; red triangle =  $2.00^\circ$ ; green circle =  $1.50^\circ$ ). The curves fitting the data are based on the corresponding linear regression lines plotted in (b) and (d), respectively, according to the cortical distance in area V1 and area V2 derived from a human fMRI study by Sereno et al. (1995). The linear regression lines (black) in (b) and (d) that pass through the origin are derived from the data from all three MBC length conditions (V1:  $y = 0.295x$ ,  $R^2 = 0.914$ ; V2:  $y = 0.480x$ ,  $R^2 = 0.927$ ).

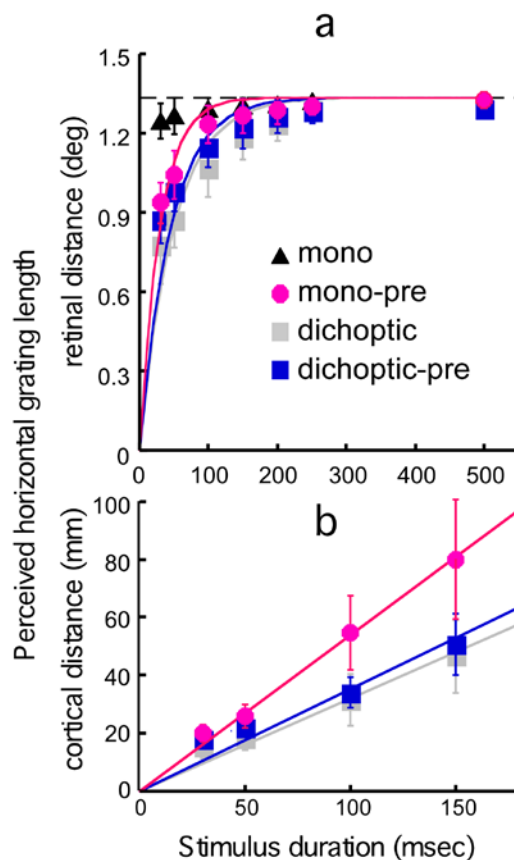


**Fig. 3.4.** Experiment 3.2 (MBC rectangle length =  $2.67^\circ$ ). (a) Results showing the perceived spreading (gap size) in retinal distance as a function of stimulus duration for the four conditions (Mono = black triangle; Dichoptic = gray square; Mono-pre = pink circle; Dichoptic-pre = blue square). The three curves, fitted for the Mono-pre (pink), Dichoptic-pre (blue) and Dichoptic (gray) conditions are based on the corresponding linear regression lines plotted in (b). (b) The average data in (a), except for the mono condition [black triangle in (a)], are plotted according to the cortical distance in area V1 based on a human fMRI study by Engel et al. (1997). The data from the remaining three conditions were fitted by linear regression lines that pass through the origin (Dichoptic:  $y = 0.321x$ ,  $R^2 = 0.810$ ; Mono-pre:  $y = 0.539x$ ,  $R^2 = 0.850$ ; Dichoptic-pre:  $y = 0.352x$ ,  $R^2 = 0.891$ ).

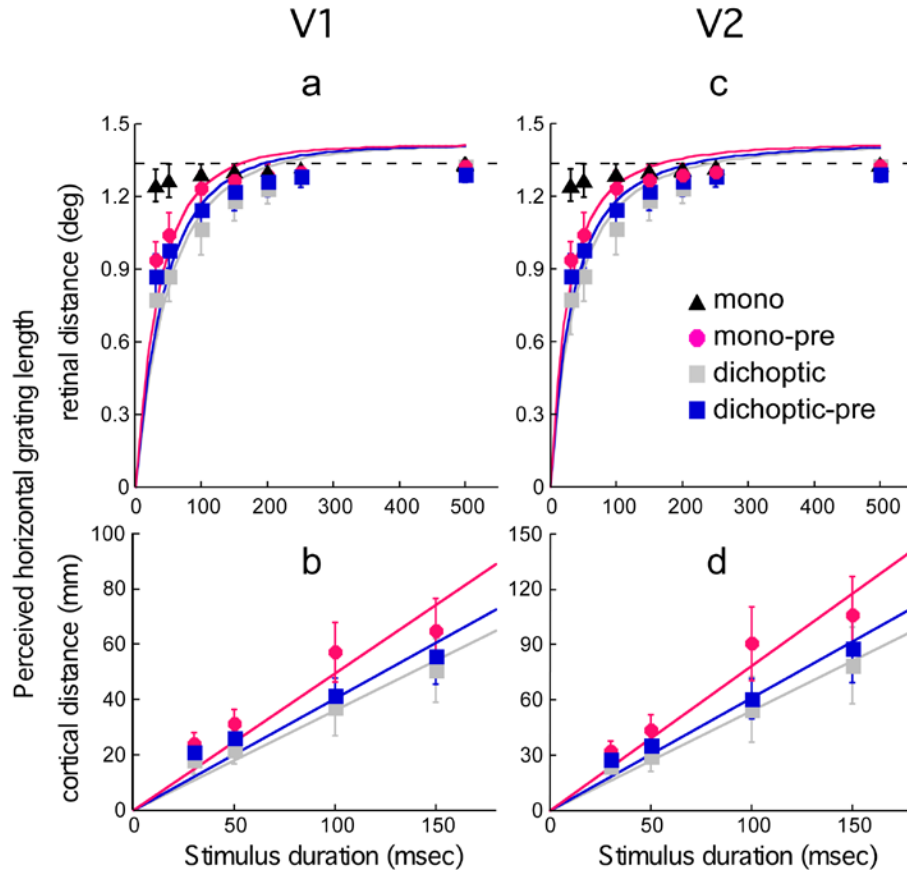


**Fig. 3.5.** The average results of Experiment 3.2 (MBC rectangle length =  $2.67^\circ$ ) are plotted in a similar manner as in Fig. 3.4a and b. The data points in (a) and (c) plot the perceived spreading (gap size) in retinal distance as a function of stimulus duration for the four conditions tested (mono = black triangle; dichoptic = gray square; mono-pre = pink circle; dichoptic-pre = blue square). The three curves, fitted for the mono-pre (pink), dichoptic-pre (blue) and dichoptic (gray) conditions are based on the corresponding linear regression lines plotted in (b) and (d). As in Fig. 3.3, the data fitting are analyzed according to the cortical distance in area V1 and area V2 based on a human fMRI study by Sereno et al. (1995). The colored linear regression lines in (b) and (d) that pass through the origin are derived from the data of each of the three stimulus conditions (V1: Mono-pre,  $y = 0.495x$ ,  $R^2 = 0.886$ ; Dichoptic,  $y = 0.362x$ ,  $R^2 = 0.828$ ; Dichoptic-pre:  $y = 0.404x$ ,  $R^2 = 0.894$ ; V2: Mono-pre,  $y = 0.783x$ ,  $R^2 = 0.865$ ; Dichoptic,  $y = 0.542x$ ,  $R^2 = 0.798$ ; Dichoptic-pre:  $y = 0.611x$ ,  $R^2 = 0.886$ ).

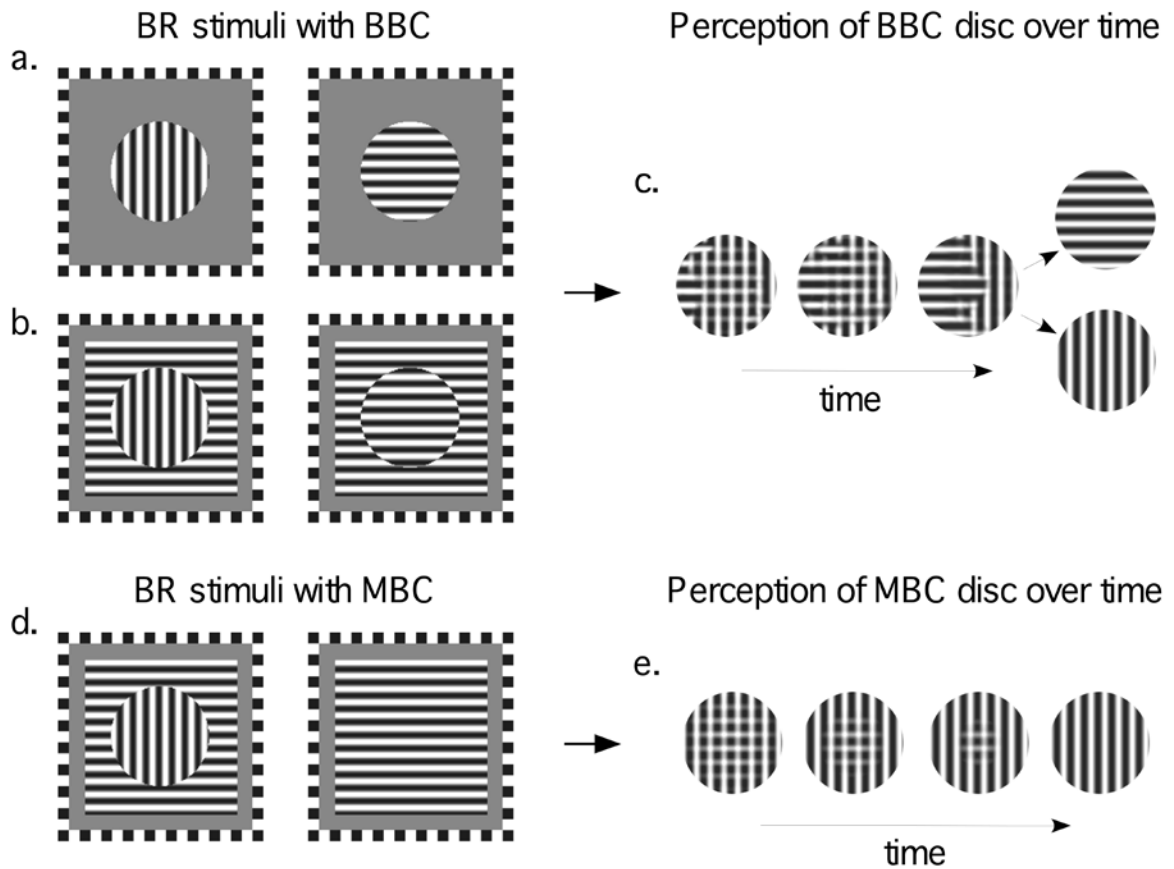


**Fig. 4.1.** Stimuli used in Experiment 4.1 and the predicted percepts. (a) A binocular rivalry (BR) stimulus typically used in the laboratory. Note the disc in each half-image is clearly delineated by a boundary contour. We thus coin this stimulus a BR stimulus with binocular boundary contour (BBC). (b) A variant of a BR stimulus with BBC. Here, the boundary contour of the right half-image is produced by a phase shift of  $180^\circ$  between the central and surrounding gratings. (c) The predicted percepts of the BBC rivalry stimulus (disc) from its onset to the development of global dominance. (d) A BR stimulus with monocular boundary contour (MBC), where only the left half-image has a boundary contour delineating the vertical grating disc. The right half-image has horizontal grating but no boundary contour at the corresponding retinal area. (e) The predicted percepts of the MBC rivalry stimulus (disc) from its onset to the development of global dominance.

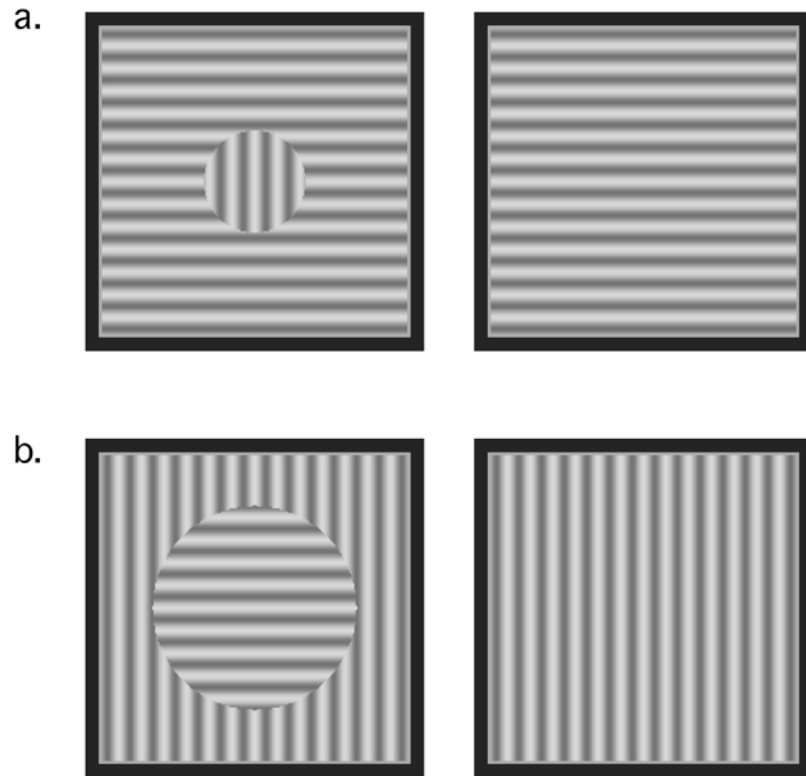


Fig. 4.2. Two examples of MBC stimuli used in Experiment 4.2. (a) A  $1.5^\circ$  MBC rivalry stimulus with vertical grating disc. (b) A  $3.0^\circ$  MBC rivalry stimulus with horizontal grating disc. Not shown at the counterparts of these stimuli, namely, a  $1.5^\circ$  MBC rivalry stimulus with horizontal grating disc and a  $3.0^\circ$  MBC rivalry stimulus with vertical grating disc. All four stimulus conditions were tested.

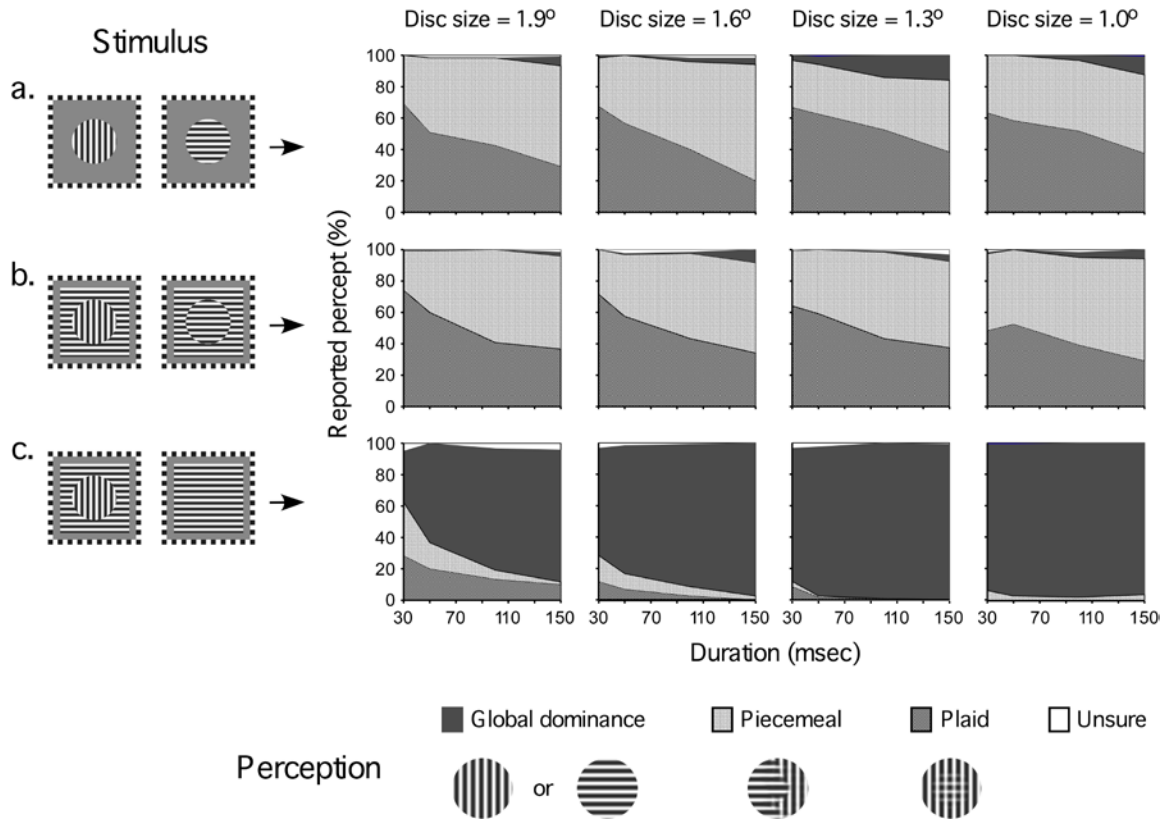


Fig. 4.3. Results of Experiment 4.1. Percentages of seeing the four percepts as a function of stimulus duration for the BBC rivalry stimuli (rows a and b) and MBC rivalry stimulus (row c). The four columns of graphs plot the data from the four disc sizes (diameters) tested. The percentage of perceiving global dominance is evident at 30 ms, increases with stimulus duration, and is significantly earlier and higher with the MBC rivalry stimulus. In contrast, with the BBC rivalry stimuli, the percentage of perceiving global dominance is not significantly different from zero even at 150 ms.



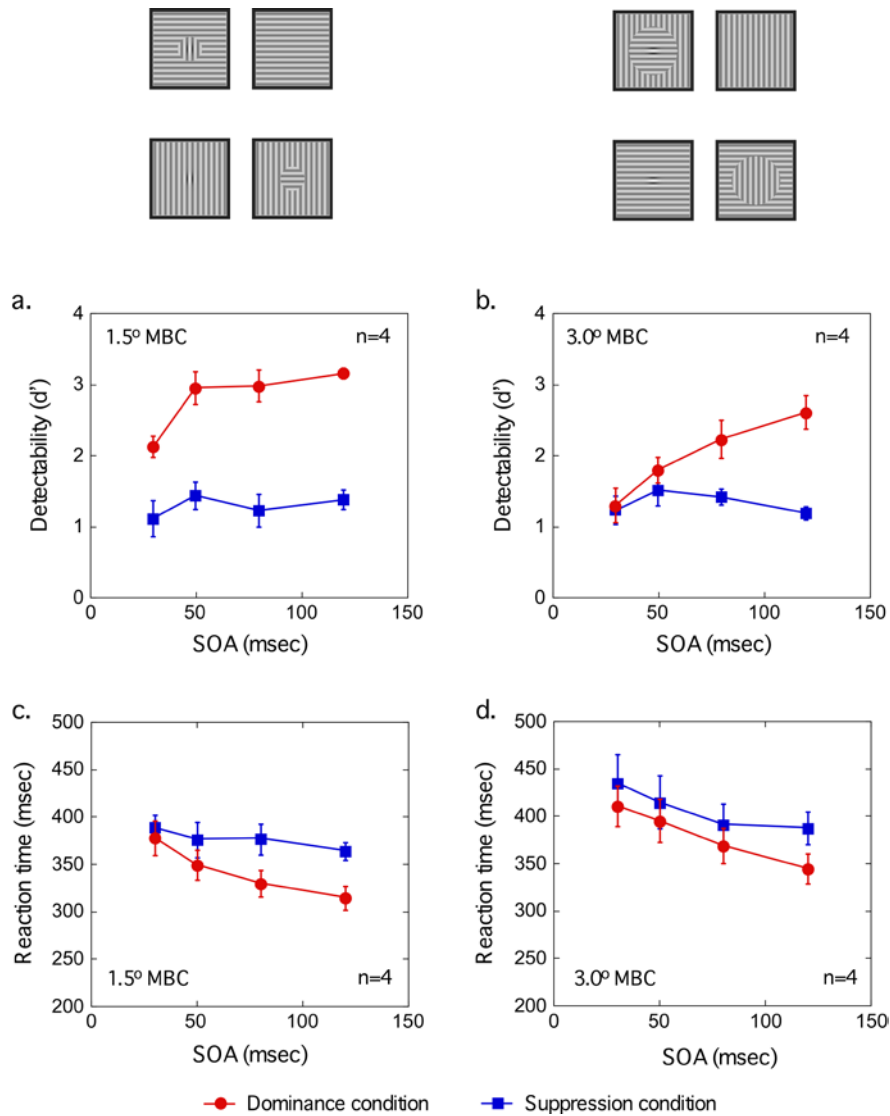
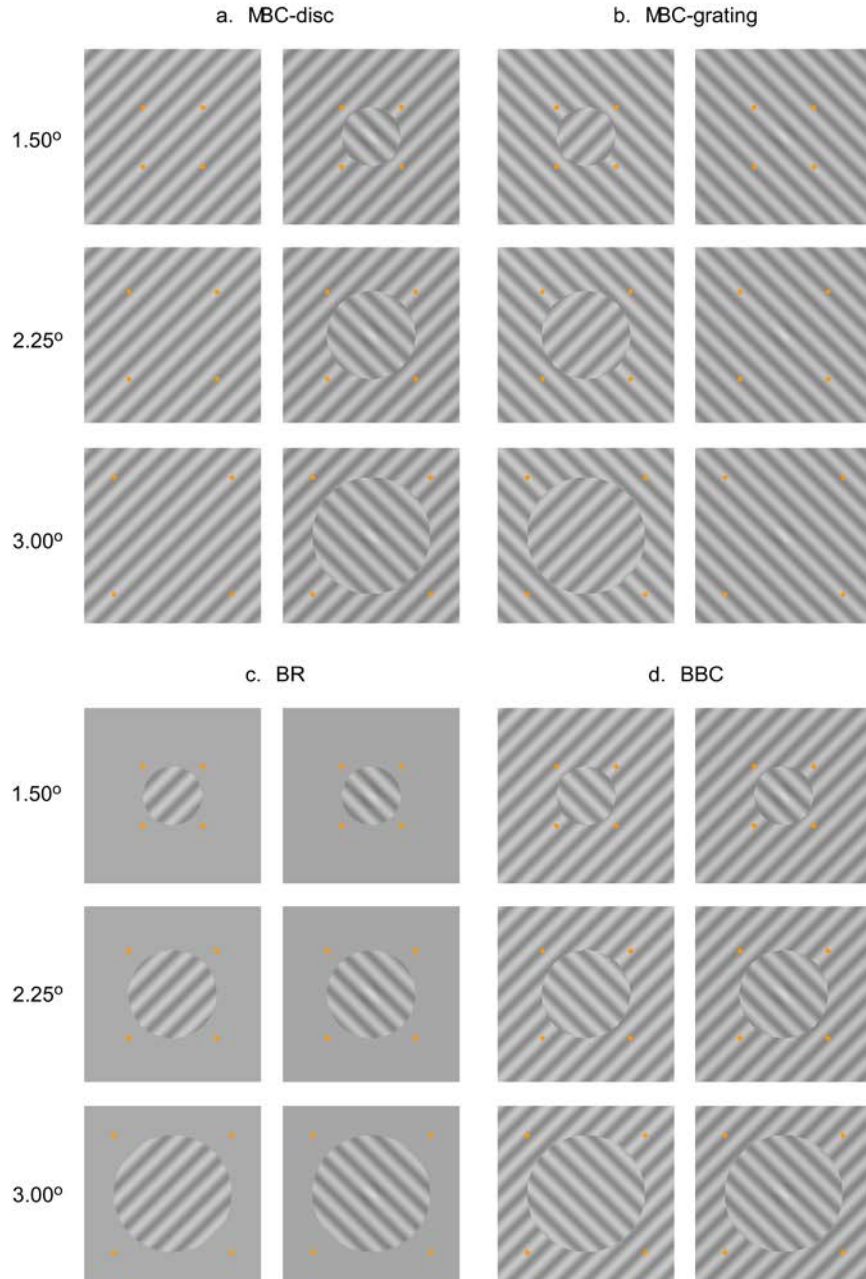
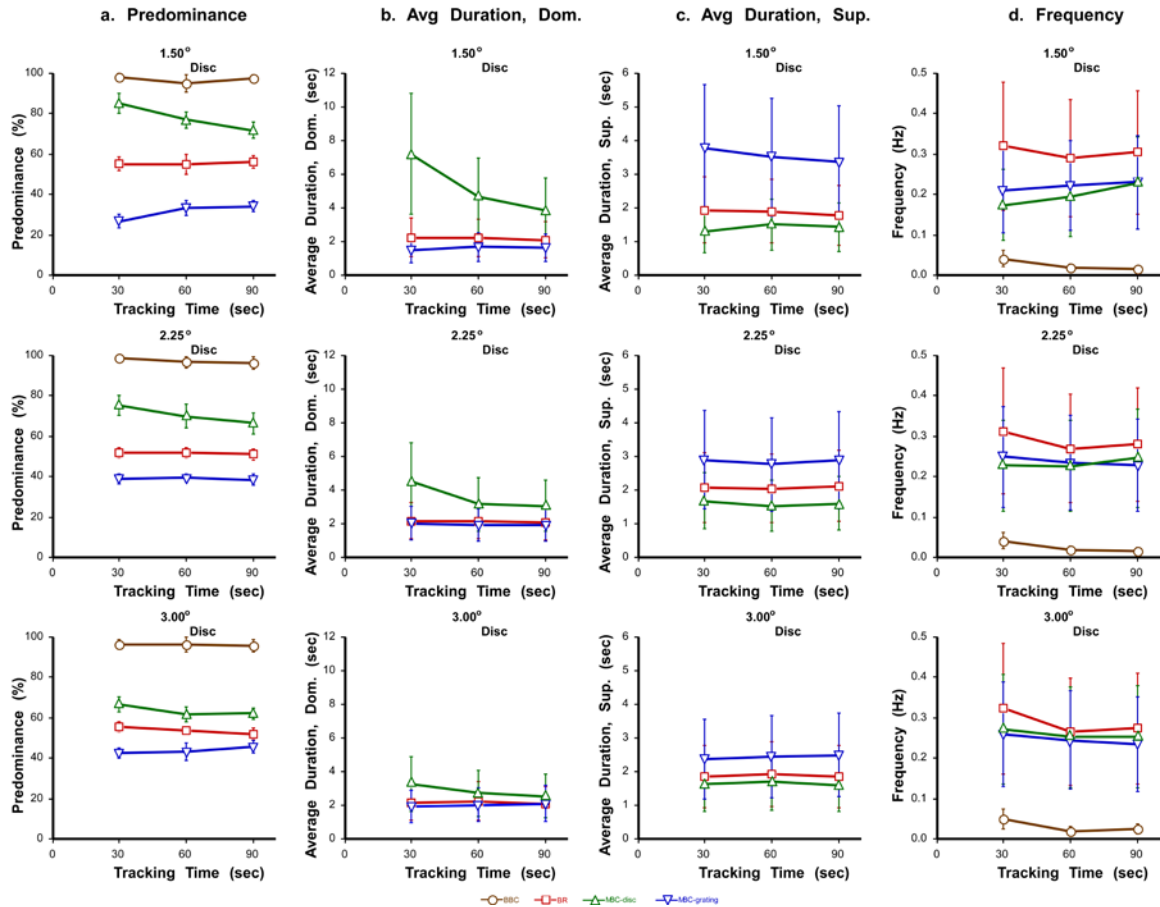


Fig. 4.4. Results of Experiment 4.2. The top panel above the graphs illustrates examples of stimuli tested in the dominance and suppression conditions, for the 1.5° (left) and 3.0° (right) MBC rivalry stimuli. The monocular Gabor probe is presented on the MBC disc half-image in the dominance condition, while it is presented on the homogeneous grating half-image in the suppression condition. Graphs (a) and (b) plot the sensitivity index  $d'$  for detecting the Gabor probe in the dominance and suppression conditions as a function of SOA, respectively, for the 1.5° and 3.0° MBC rivalry stimuli. For each SOA,  $d'$  for the dominance condition is higher for the 1.5° MBC rivalry stimulus. Furthermore, significant binocular suppression is observed as early as 30 ms with the 1.5° MBC rivalry stimulus but not until 80 ms with the 3.0° MBC rivalry stimulus. Graphs (c) and (d) plot the reaction time to detect the Gabor probe. For the 1.5° MBC rivalry stimulus, RT is longer for detecting the probe in the suppressed than dominance condition and is evident as early as 80 ms. Such RT difference between the suppression and dominance conditions reveals the effect of binocular suppression. In contrast, for the 3.0° MBC rivalry stimulus, the RT difference becomes significant only at 120 ms SOA.



**Fig. 5.1.** (a) Stimuli employed in the MBC-disc condition. Only one eye receives a monocular boundary contour (MBC) that encloses a grating disc (right half-image), which is orthogonal to the surrounding grating and the homogenous grating in the fellow eye (left half-image). A monocular Gabor probe is presented at the disc center. Three pairs of such stimuli are presented from the top to the bottom, each with a disc diameter of  $1.50^\circ$ ,  $2.25^\circ$ , or  $3.00^\circ$ , respectively. (b) Stimuli in the MBC-grating condition. Similar to (a), but the probe is presented on the homogenous grating opposing to the MBC disc. (c) Stimuli in the binocular rivalry (BR) condition. Both eyes receive the grating discs that are orthogonal to each other. The probe is presented only in one eye. (d) Stimuli in the binocular boundary contour (BBC) condition. Both half-images carry identical gratings except that there is only one of the discs having the probe.



**Fig. 5.2.** Average results over three tracking durations (0–30 s, 30–60 s, & 60–90 s). (a) Predominance; (b) Average Duration of Dominance Phases; (c) Average Duration of Suppression Phases; (d) Frequency. There are 3 graphs in each column, corresponding to one disc size (1.50°, 2.25°, or 3.00°), respectively. Each graph summarizes the different stimulus conditions with separate curves: BBC (brown circle), BR (red square), MBC-disc (green triangle), & MBC-grating (blue triangle). Note that BBC is excluded in (b) and (c), due to generally lack of alternation within a 30-s tracking duration.

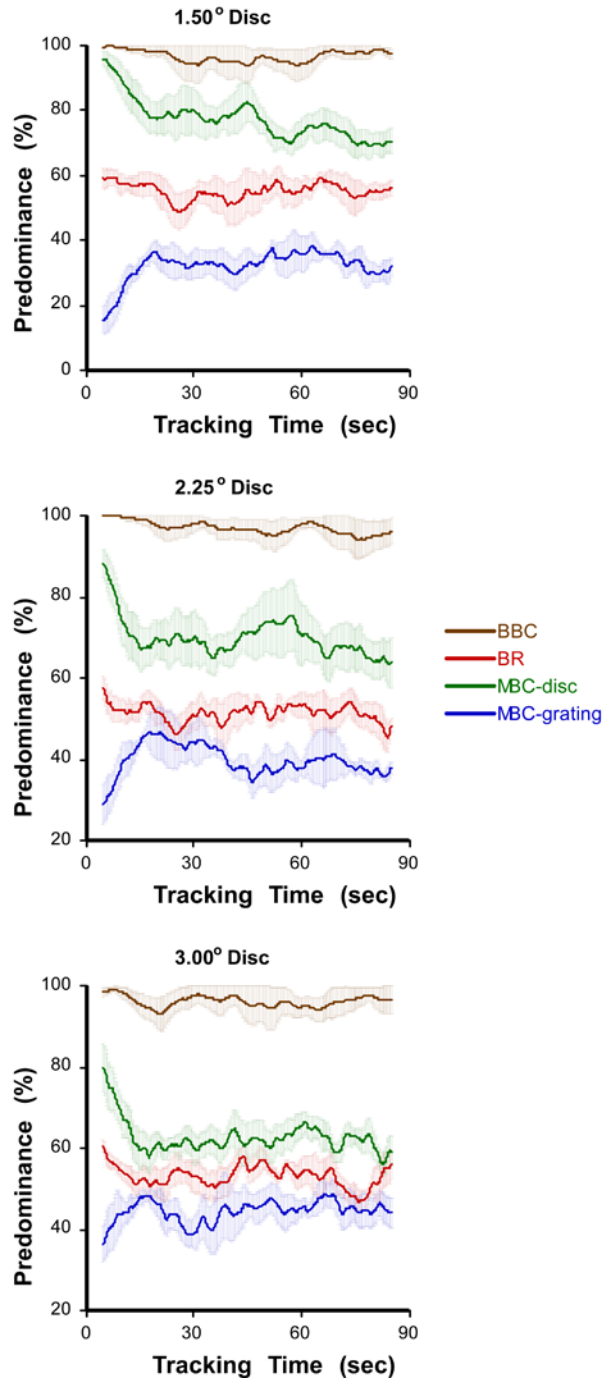


**Fig. 5.3.** Finer dynamic time courses of predominance. Each of the graphs is associated with one disc size (1.50°, 2.25°, or 3.00°), respectively, and each shows the four stimulus conditions separately: BBC (brown), BR (red), MBC-disc (green), & MBC-grating (blue). Each data point on a time course represents the average predominance over a 10-s time window that centers at that time point.

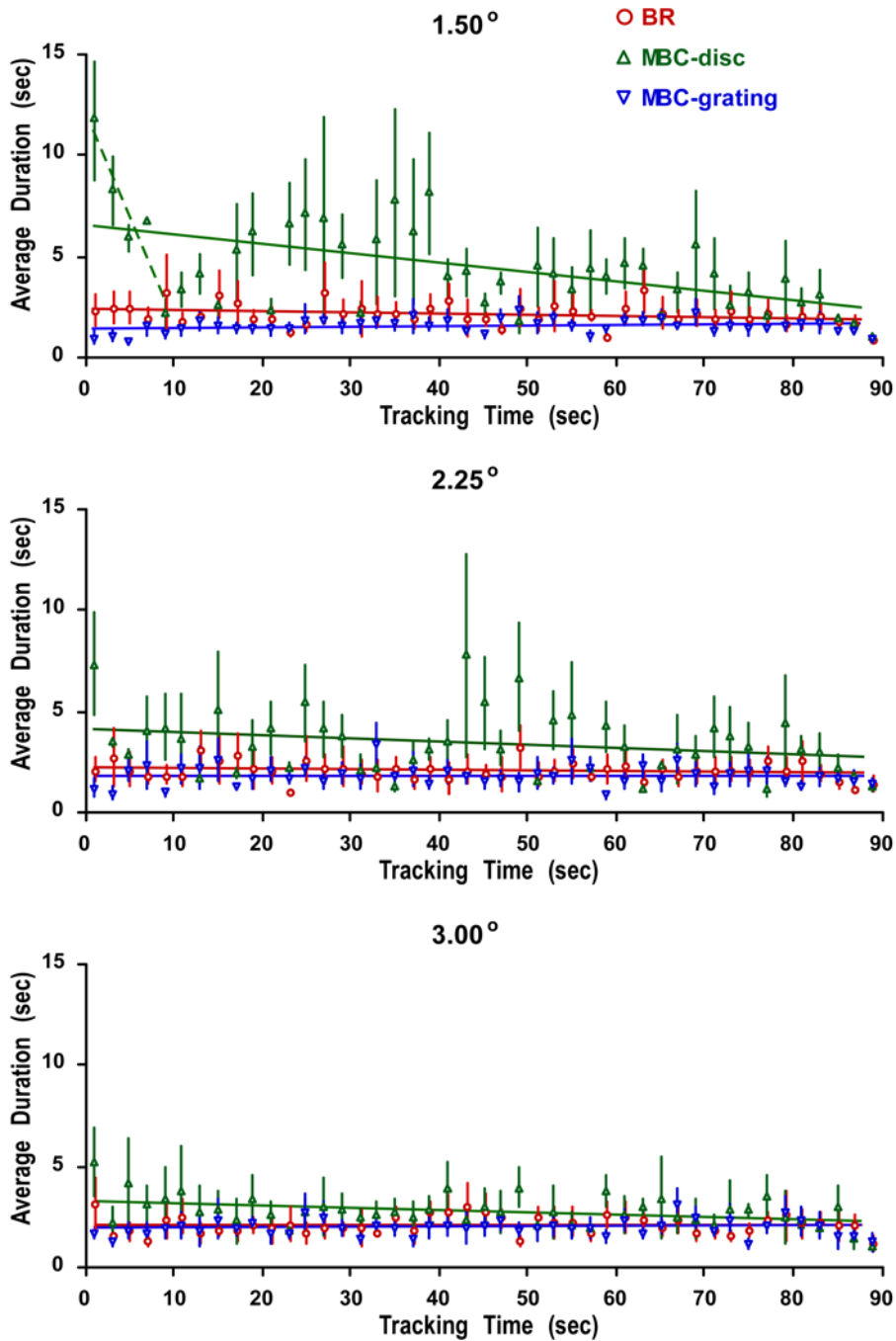


**Fig. 5.4.** Finer dynamics of average duration (dominance phases). Each of the graphs counts for one disc size (1.50°, 2.25°, or 3.00°), respectively, and represents three stimulus conditions separately: BR (red circle), MBC-disc (green triangle), & MBC-grating (blue triangle) (BBC not included). Each data point is the average duration of dominance phases summarized within a 2-s time window that centers at that time point (see Fig. 5.5 for more details).

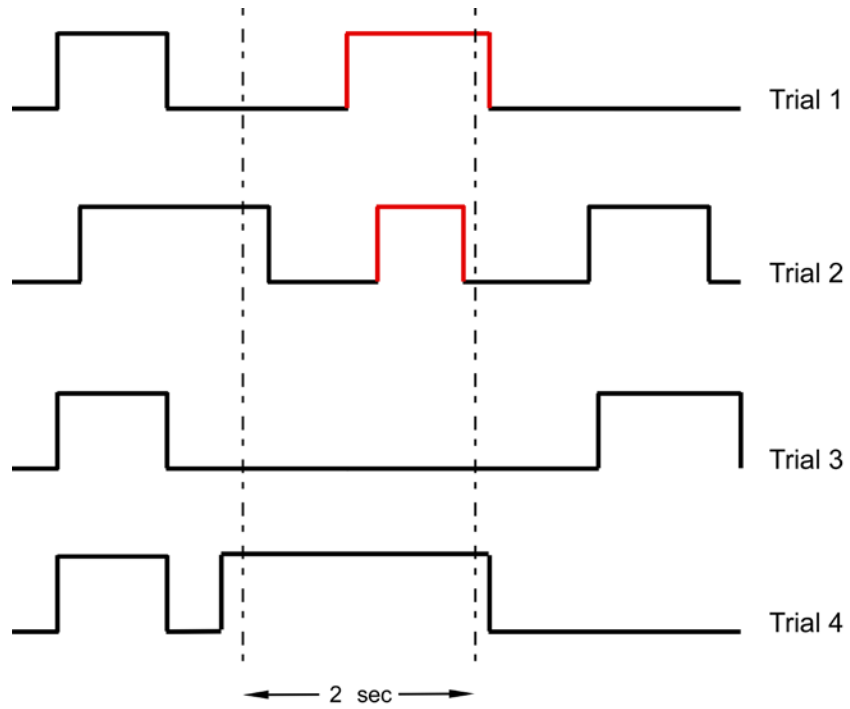


Fig. 5.5. Definition of time window for duration calculation. Only dominance phases starting within the 2-s time window contribute the average duration (aforementioned in Fig. 5.4) for that time window (red).

## Binocular Rivalry Condition

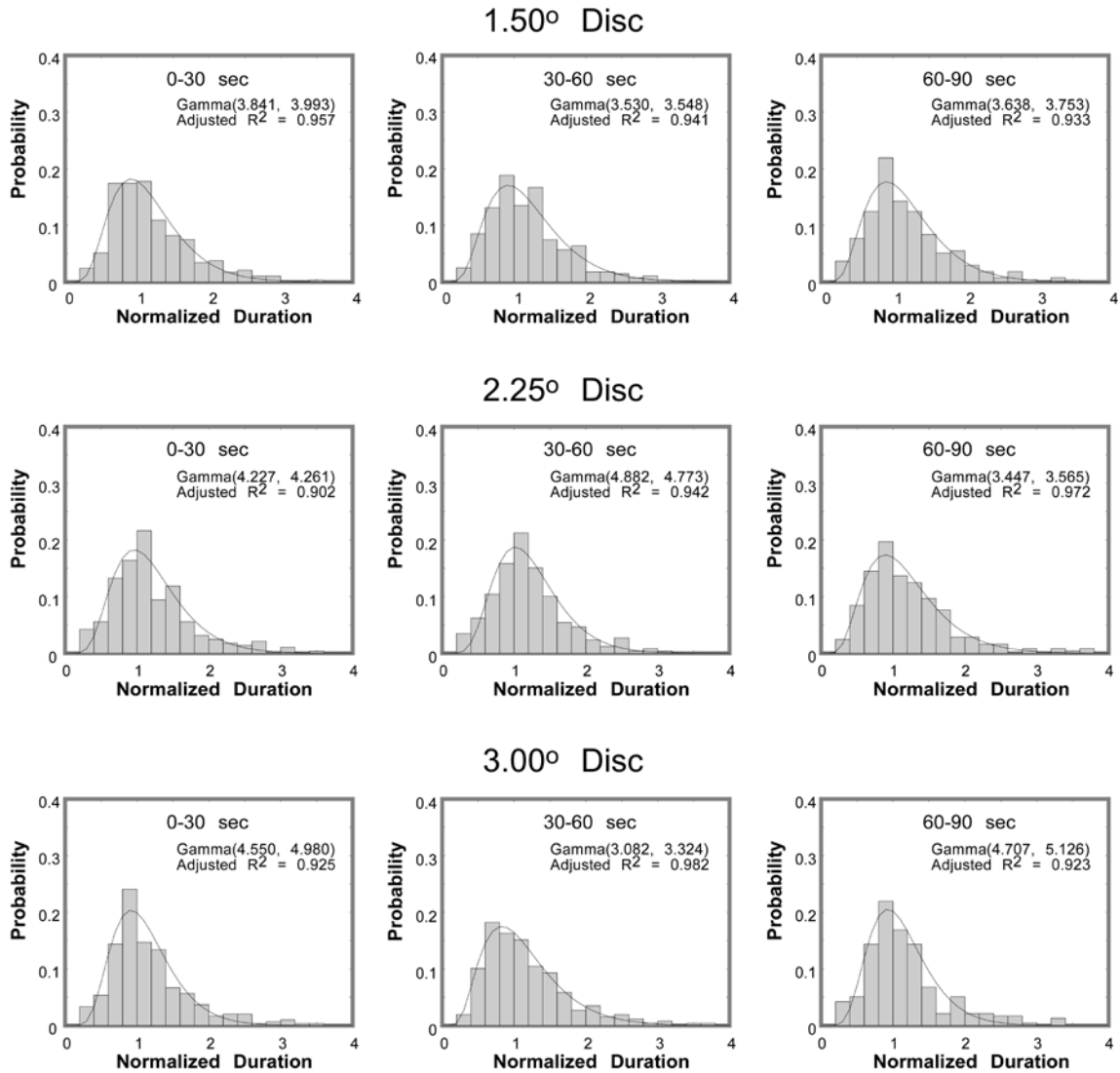
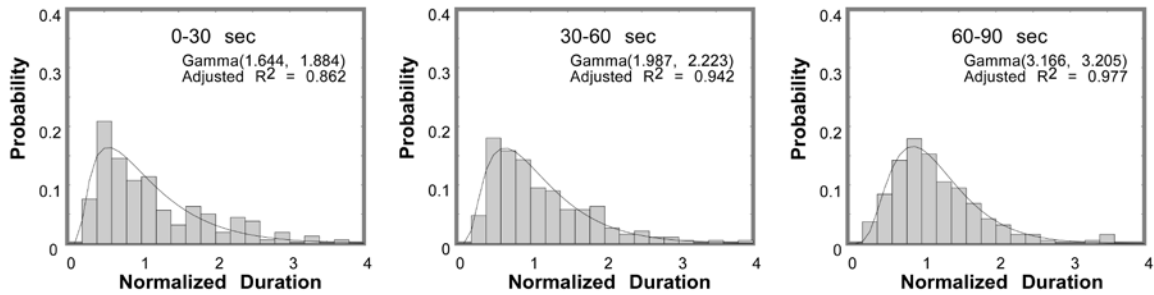


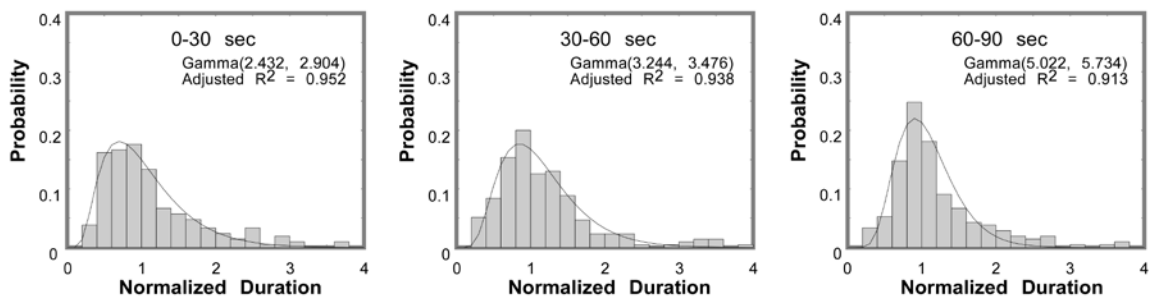
Fig. 5.6. Gamma distribution fitting (BR condition). Each row represents one disc size (1.50°, 2.25°, or 3.00°), respectively, and each column is associated with one of three tracking durations (0–30 sec, 30–60 sec, & 60–90 sec). There are nine graphs in total, which each shows the probability density of normalized duration data and the fitted Gamma distribution PDF.

## MBC-disc Condition

### 1.50° Disc



### 2.25° Disc



### 3.00° Disc

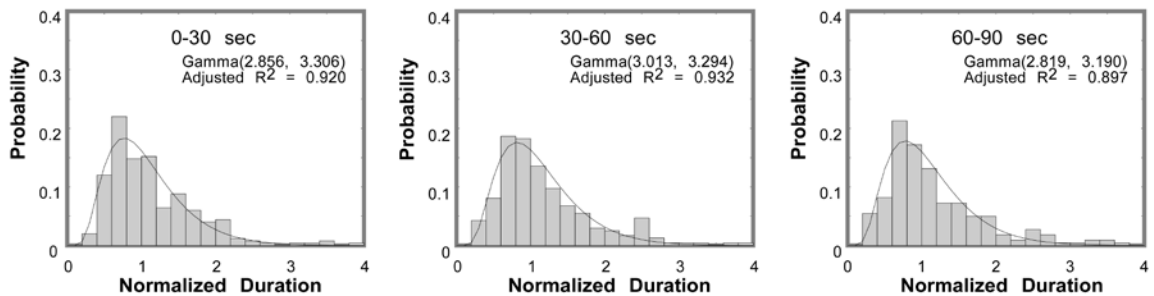


Fig. 5.7. Gamma distribution fitting (MBC-disc condition). Each row represents one disc size (1.50°, 2.25°, or 3.00°), respectively, and each column is associated with one of three tracking durations (0–30 sec, 30–60 sec, & 60–90 sec). There are nine graphs in total, which each shows the probability density of normalized duration data and the fitted Gamma distribution PDF.



## MBC-grating Condition

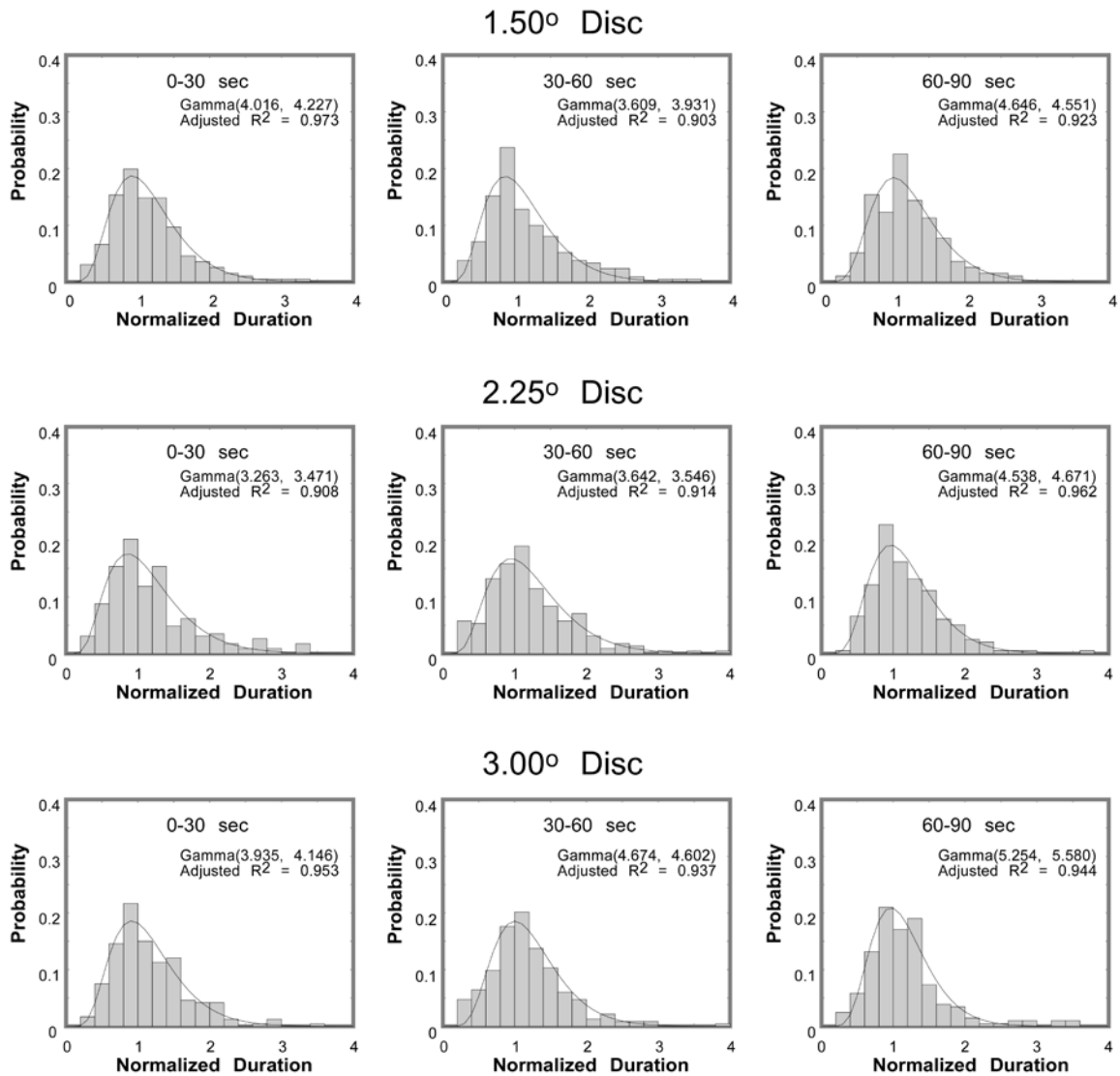


Fig. 5.8. Gamma distribution fitting (MBC-grating condition). Each row represents one disc size (1.50°, 2.25°, or 3.00°), respectively, and each column is associated with one of three tracking durations (0–30 sec, 30–60 sec, & 60–90 sec). There are nine graphs in total, which each shows the probability density of normalized duration data and the fitted Gamma distribution PDF.

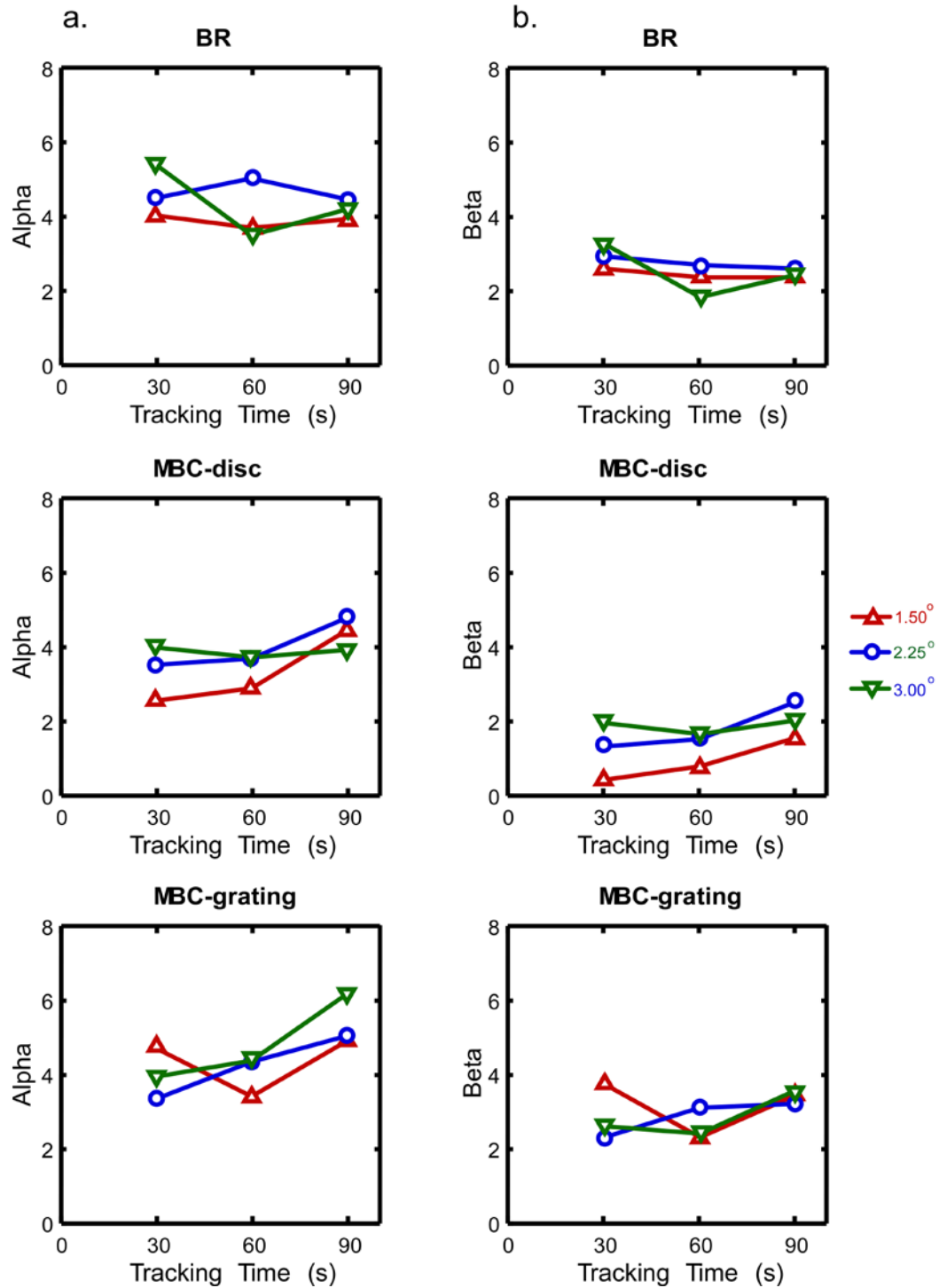


Fig. 5.9. Fitted Gamma parameters: (a) alpha and (b) beta. Each row represents one stimulus condition (BR, MBC-disc, or MBC-grating; BBC not included) and each column is for one distribution parameter. The results of the three disc sizes are plotted in the same graph: 1.50° (red triangle), 2.25° (blue circle), and 3.00° (green triangle).

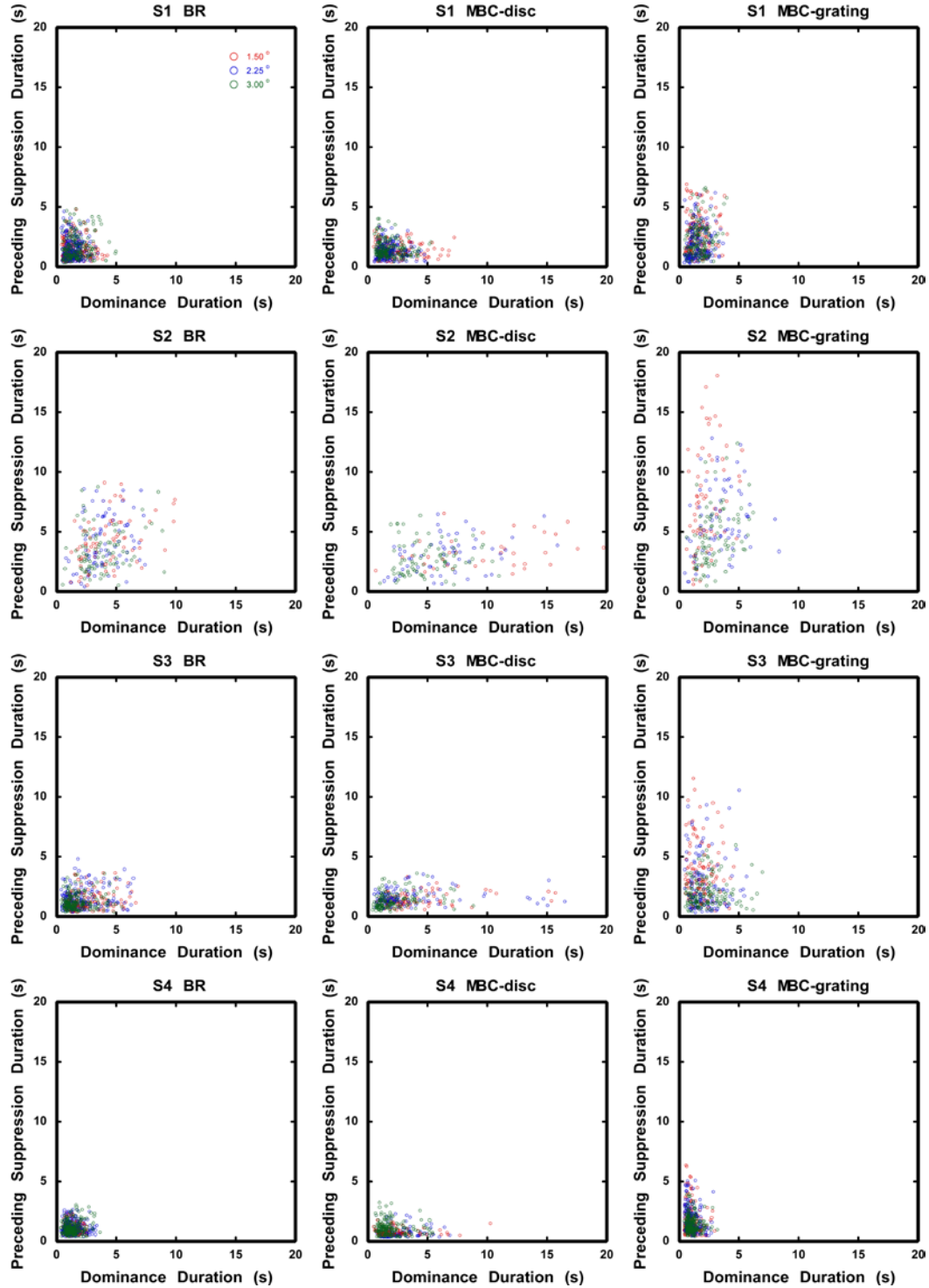
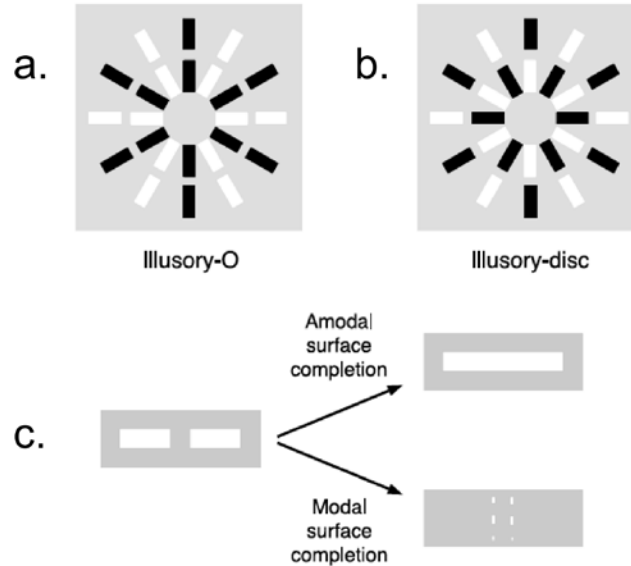
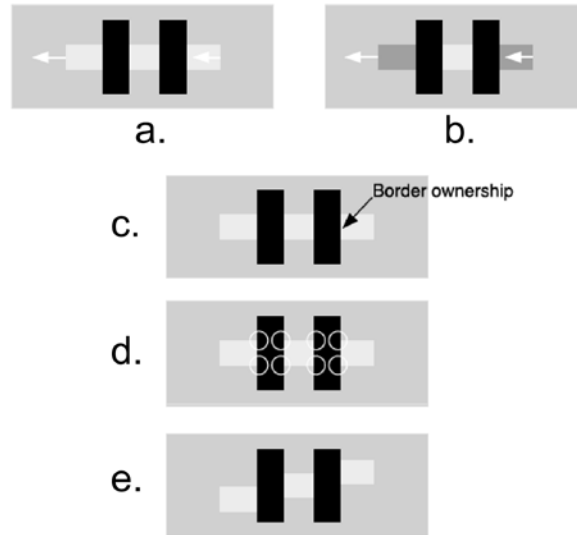


Fig. 5.10. Priming effect of Gamma distribution. The duration data of dominance phases (x-axis) are correspondingly plotted against the duration of their preceding suppression phases (y-axis), for all three disc sizes:  $1.50^\circ$  (red),  $2.25^\circ$  (blue), and  $3.00^\circ$  (green). The data are plotted separately for each observer (S1, S2, S3, or S4; one for each row) and each stimulus condition (BR, MBC-disc, or MBC-grating; one for each column; BBC not included).



**Fig. 6.1.** The effect of luminance contrast polarity on surface completion. Adjacent rectangular spokes along the same radial direction are rendered with either (a) the same or (b) opposite luminance contrast polarity. This leads to the perception of either (a) an illusory-O or (b) illusory-disc. (c) We hypothesize that the L-junctions (corners) of adjacent spokes with the same luminance contrast polarity are treated as implicit T-junctions, resulting in amodal and modal surface completion (illusory-O).



**Fig. 6.2.** (a) Three horizontal rectangular segments with the same luminance contrast polarity are seen as belonging to the same object (one longer horizontal rectangle) moving leftward in global motion. (b) The inner horizontal rectangular segment has an opposite luminance contrast polarity compared to the outer rectangular segments, leading to a failure in surface integration. The left outer rectangular segment is seen as expanding while the right outer rectangle compresses. (c–e) Analysis of the factors involved in surface completion.



Fig. 6.3. Separated rectangular segments with (a) same luminance contrast polarity and (b) opposite luminance contrast polarity. No real occluder exists between separated segments. The white arrows indicate the terminal edges that are rendered with local motion signals.

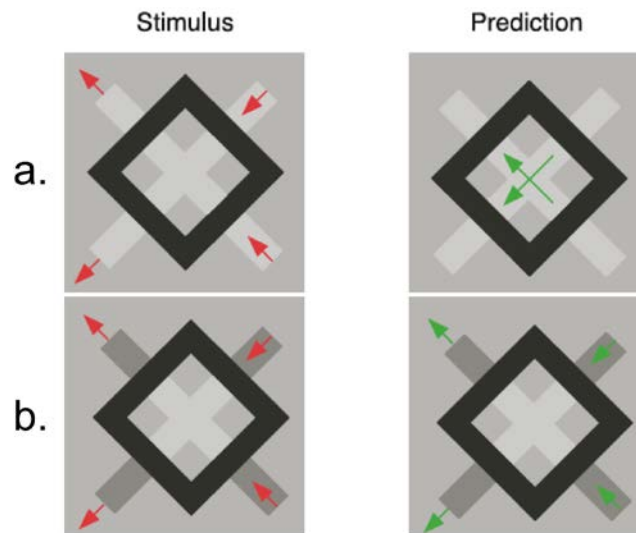


Fig. 6.4. The logic of Experiment 6.1. The terminal edges of stimuli (a) and (b) are rendered with local motion signals (arrows). All aspects of both stimuli are the same except for the luminance of the outer rectangular segments of stimulus (b), which leads to them having an opposite luminance contrast polarity relative to the inner rectangular segments. It is predicted that the inner rectangles in stimulus (a) with the same luminance contrast polarity are seen as sliding over each other (arrows) as they move together with the outer rectangles (global motion). In contrast, the inner rectangles in stimulus (b) with the opposite luminance contrast polarity are seen as stationary while the outer rectangles expand and compress.

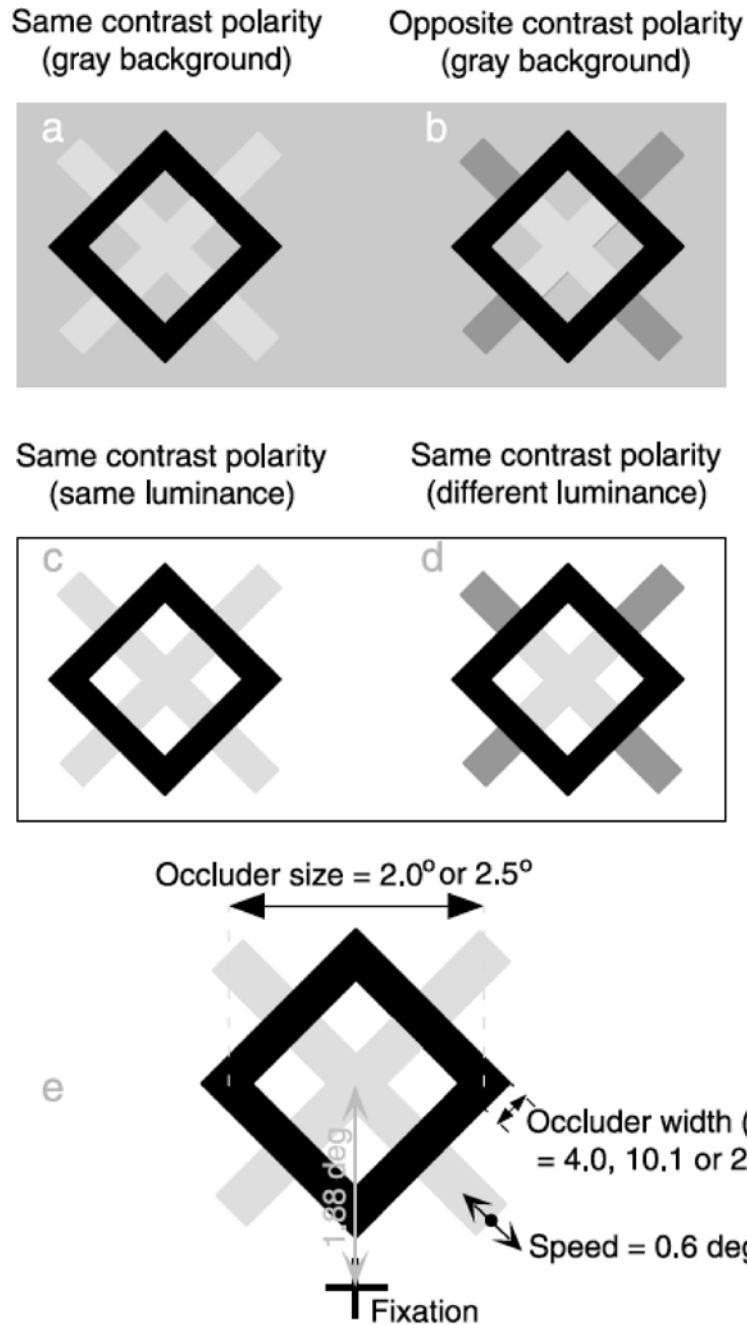


Fig. 6.5. The stimuli used in Experiment 6.1 (not drawn to scale). Stimuli (a) and (b) are the same as the ones in Fig. 6.4. Stimuli (c) and (d) are similar to (a) and (b) except for the background luminance. The general dimensions of the stimulus are specified in (e).

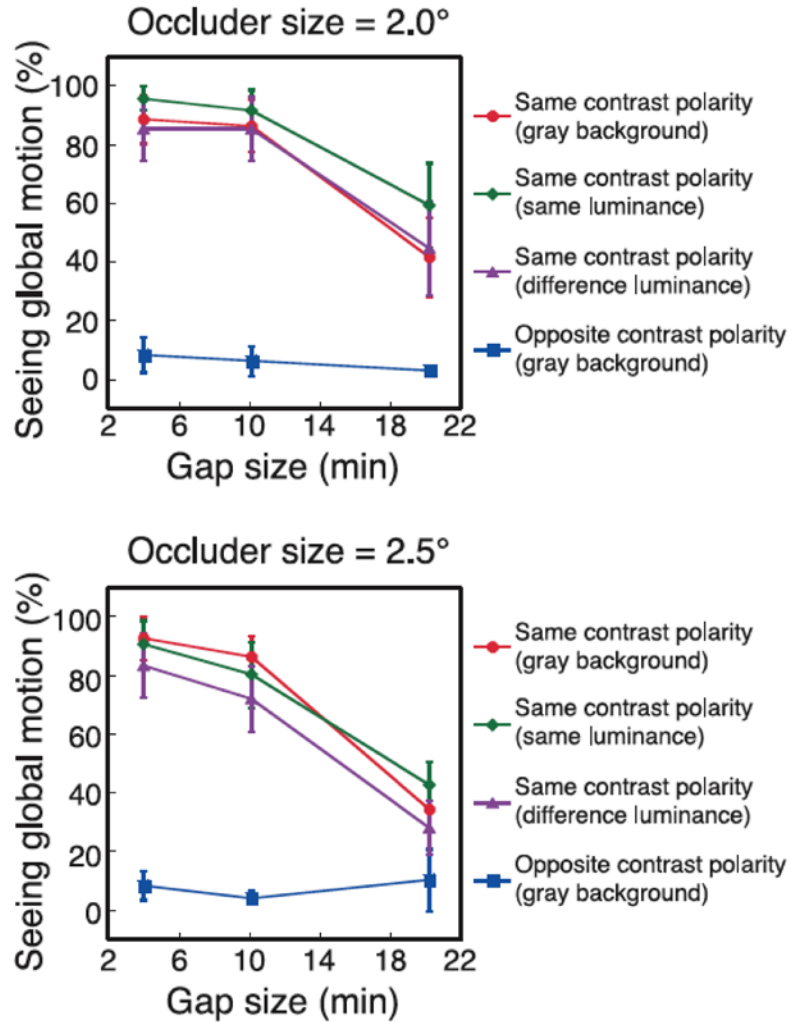
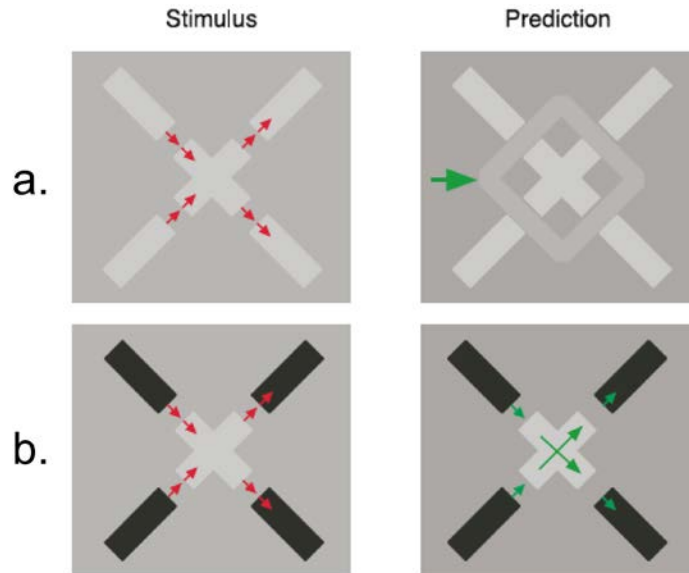


Fig. 6.6. Results of Experiment 6.1 for the stimuli with the small (upper graph) and large (lower graph) occluder sizes. Overall, motion integration (global motion) occurs in the conditions with the same luminance contrast polarity. But little global motion is perceived in the opposite luminance contrast polarity conditions.



**Fig. 6.7.** The logic of Experiment 6.2. The terminal edges of stimuli (a) and (b) are rendered with local motion signals (arrows). All aspects of both stimuli are the same except for the luminance of the outer rectangular segments of stimulus (b), which leads to them having an opposite luminance contrast polarity relative to the inner rectangular segments. It is predicted that the inner rectangles in stimulus (a) with the same luminance contrast polarity are seen as stationary, and an illusory diamond frame is seen as moving laterally (rightward arrow). In contrast, the inner rectangles in stimulus (b) with the opposite luminance contrast polarity are seen as sliding over each other (arrows), with their movements causing the outer rectangles to either compress or expand. During the experiment, we instructed the observers to report seeing either the inner rectangles as moving (no motion integration) or stationary (motion integration leading to global motion of the illusory diamond frame).



Same contrast polarity (gray background)      Opposite contrast polarity (gray background)



Same contrast polarity (same luminance)      Same contrast polarity (different luminance)

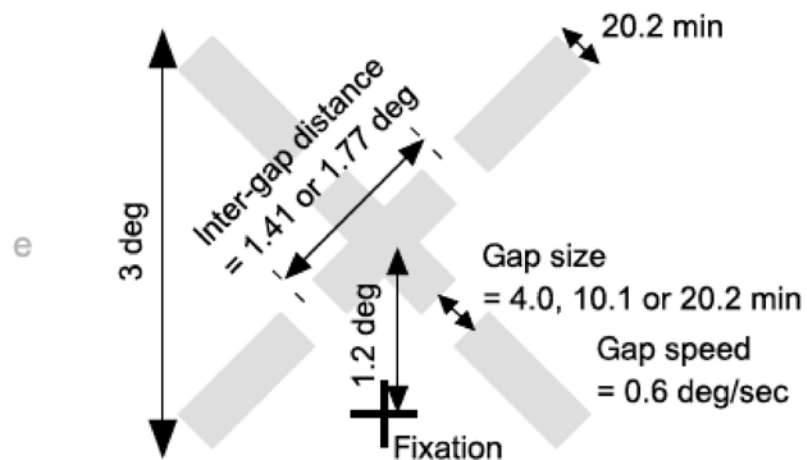
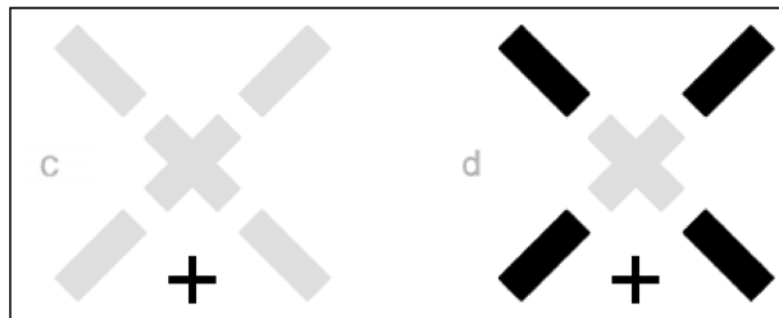


Fig. 6.8. The stimuli used in Experiment 6.2 (not drawn to scale). Stimuli (a) and (b) are the same as the ones in Fig. 6.7. Stimuli (c) and (d) are similar to (a) and (b) except for the background luminance. The general dimensions of the stimulus are specified in (e).

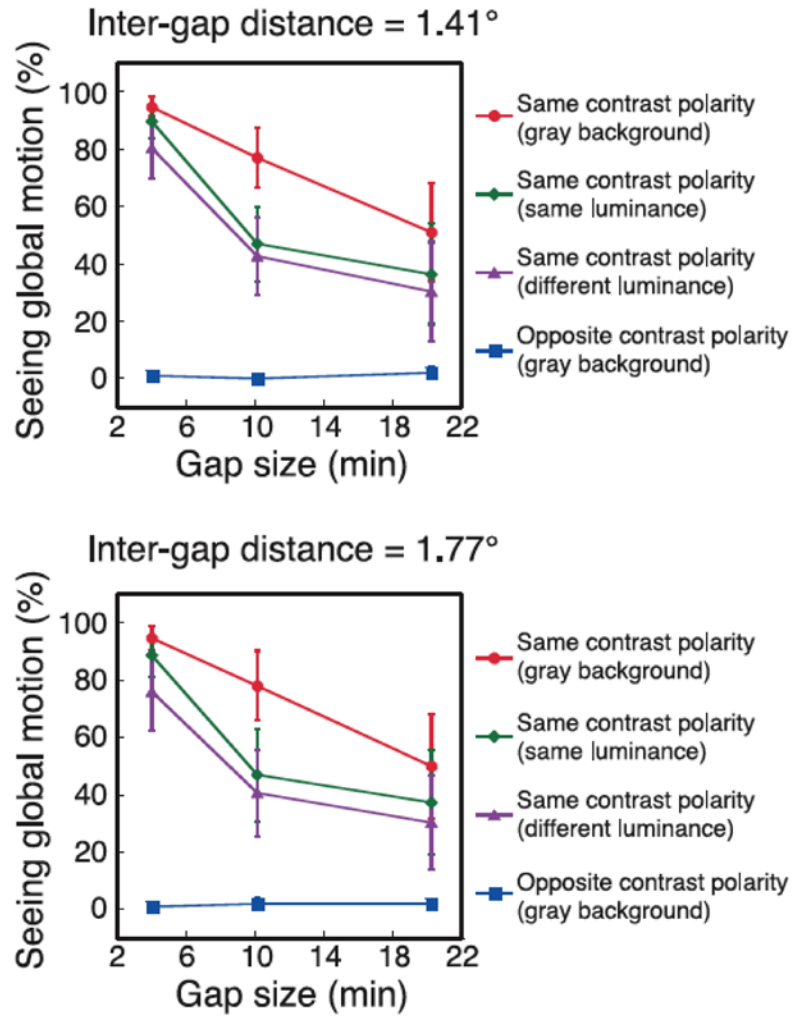
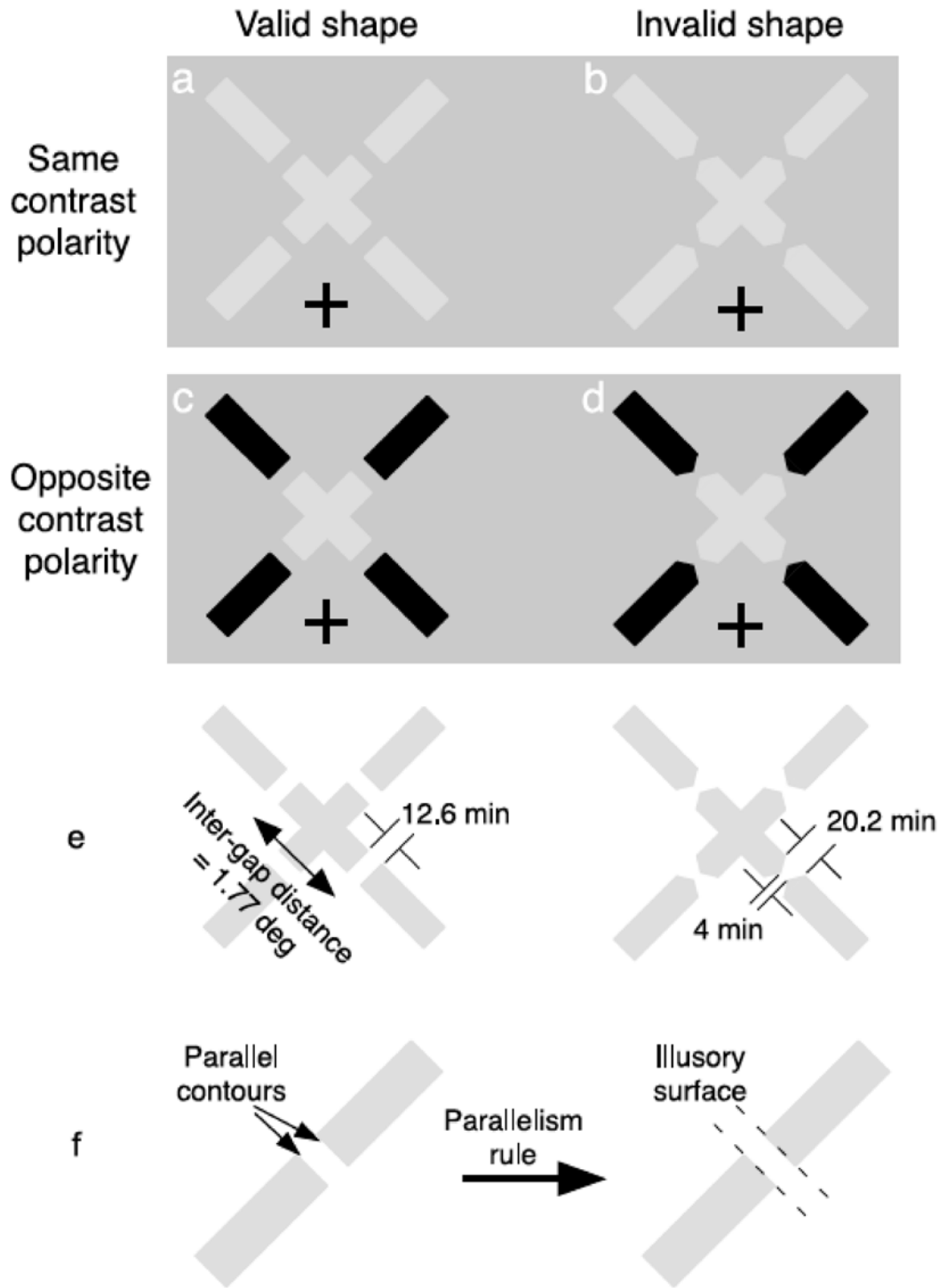


Fig. 6.9. Results of Experiment 6.2 for the stimuli with the small (upper graph) and large (lower graph) inter-gap distances. Overall, motion integration (global motion of the illusory diamond frame) occurs in the conditions with the same luminance contrast polarity. But little motion integration is perceived in the opposite luminance contrast polarity conditions.



**Fig. 6.10.** (a–d) The stimuli used in Experiment 6.3 (not drawn to scale). Luminance contrast polarity (a, b vs. c, d) and terminal shape (a, c vs. b, d) were varied. The stimuli (a, c) with the valid terminal shape have parallel/flat edges, while the stimuli (b, d) with the invalid shape have arrowhead edges. (e) The general stimulus dimensions of the valid and invalid shaped stimuli. (f) A depiction of the “parallelism rule,” which allows the formation of an illusory surface when there exists a gap with parallel edges.

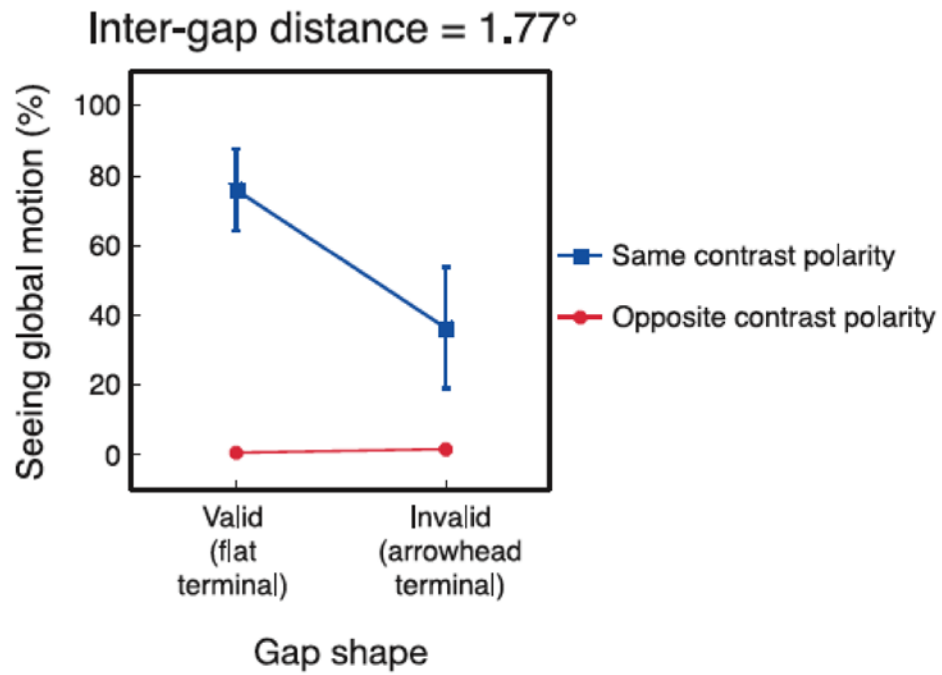
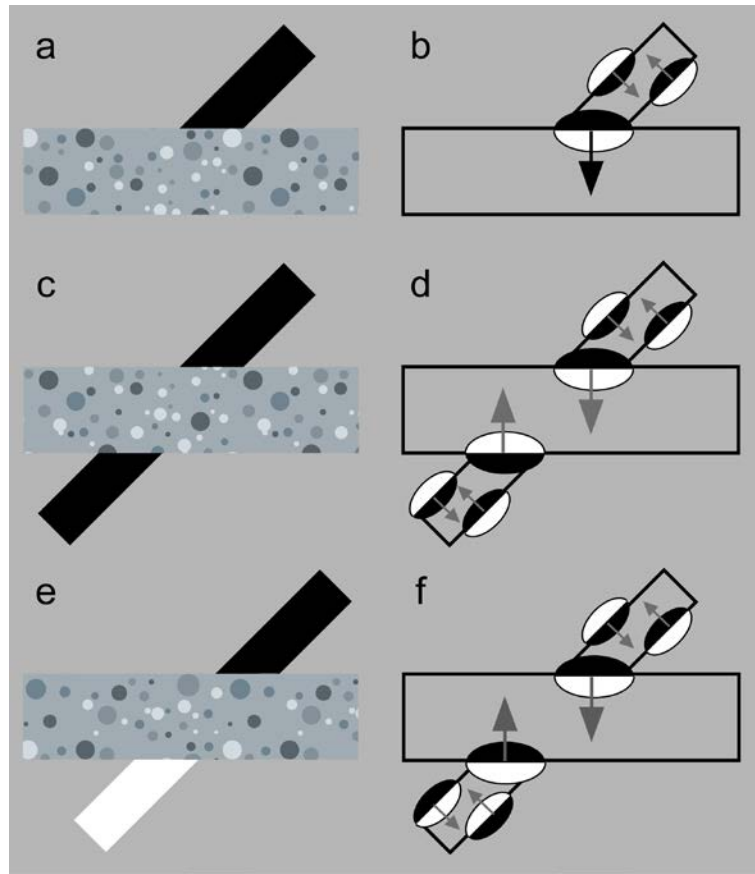


Fig. 6.11. Results of Experiment 6.3. Overall, motion integration (global motion of the illusory diamond frame) occurs predominantly in the condition with the same luminance contrast polarity and valid terminal shape (parallel/flat edge). As expected, little motion integration is perceived in the opposite luminance contrast polarity condition regardless of terminal shape.



**Fig. 7.1.** The hypothetical role of functional border ownership (BO) units in amodal surface completion. (a) A horizontal rectangle and an oblique segment intersect. (b) At the intersection, a functional BO unit (ellipse) is shown, which consists of a pair of BO neurons with the same receptive field properties but opposite directions of BO preference. The black and white halves of the ellipse indicate the unit's selectivity for luminance contrast polarity. A balance of responses between the two BO selective neurons determines the ultimate BO direction (von der Heydt et al, 2005; Zhou et al, 2000). At the border formed between the oblique segment and horizontal rectangle, the functional BO unit signals that the horizontal rectangle owns the border. This leads to the amodal extrapolation of the "unbound" oblique segment behind the horizontal rectangle. The functional BO units at the edges of the oblique segment also signal that the oblique segment owns the border over the gray background. (c) Two oblique segments with the same contrast polarity (CP) juxtapose the horizontal rectangle. (d) Following the explanation in (b), the functional BO units (ellipses) at the intersection provide consistent signals for amodal surface integration between the two oblique segments. (e) Two oblique segments with opposite CP juxtapose the horizontal rectangle. (f) Similar to (d), the functional BO units (ellipses) at the intersections have consistent BO information for amodal surface integration between the two oblique segments. However, their CP signals together with those of the oblique functional BO units indicate that the two oblique segments having opposite CP. We propose this prevents amodal surface integration of the two oblique segments from occurring.

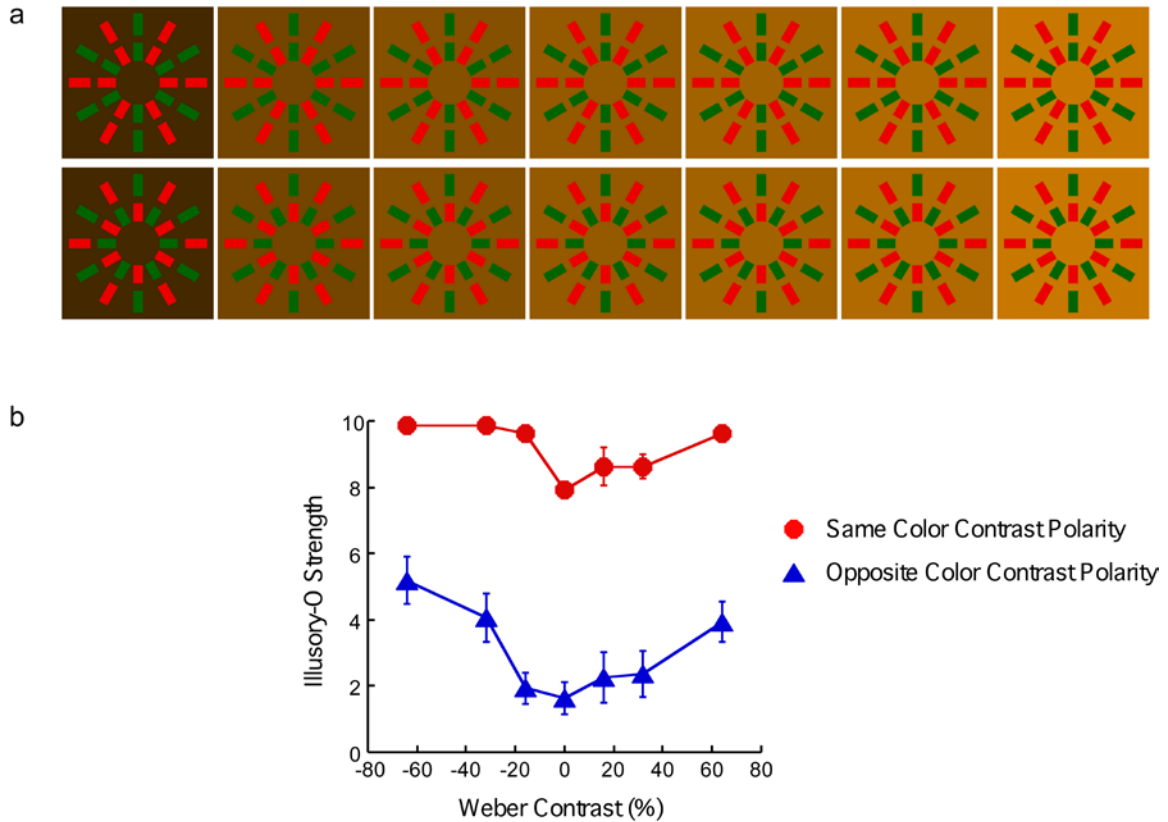


Fig. 7.2. Stimuli and results of Experiment 7.1. (a) The red and green radial spokes were set to equiluminance for individual observers using heterochromatic flicker photometry (HFP). The luminance level of the yellow background increases from the left to the right stimuli with the middle one being equiluminous with the spokes. The top and bottom row of stimuli have the same and opposite color contrast polarity, respectively. (b) The perceived Illusory-O strength as a function of the Weber contrast of the yellow background ( $n = 8$ ; 6 naïve observers and 2 authors). A positive value indicates the yellow background is brighter than the stimulus. Observers rated the strength as higher for the same color contrast polarity condition (red circles) than for the opposite color contrast polarity condition (blue triangles). For both conditions, the rating is lowest at equiluminance (Weber contrast = 0). The vertical bars indicate the standard errors.

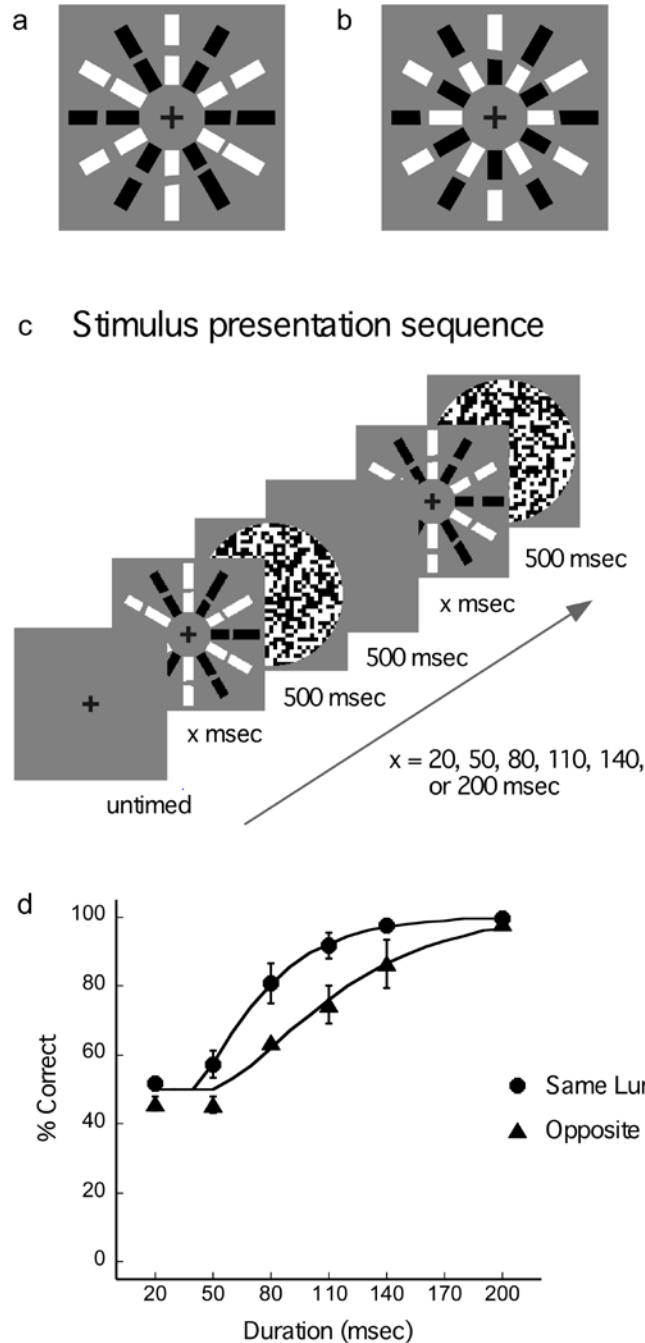


Fig. 7.3. Stimuli and results of Experiment 7.2. (a) Same luminance contrast polarity elliptical Illusory-O with the long axis oriented at  $45^\circ$ . (b) Opposite luminance contrast polarity elliptical Illusory-O with the long axis oriented at  $135^\circ$ . (c) The sequence of stimulus presentation in a trial. (d) The graph plots the percentage correct in discriminating the orientation of the elliptical Illusory-O for the same (circles) and opposite (triangles) luminance contrast polarity conditions ( $n = 4$ ; 3 naïve observers and 1 author). Performance increases with the stimulus duration, and is superior for the same luminance contrast polarity condition. The data points are fitted by the Weibull distribution functions. The vertical bars indicate the standard errors.

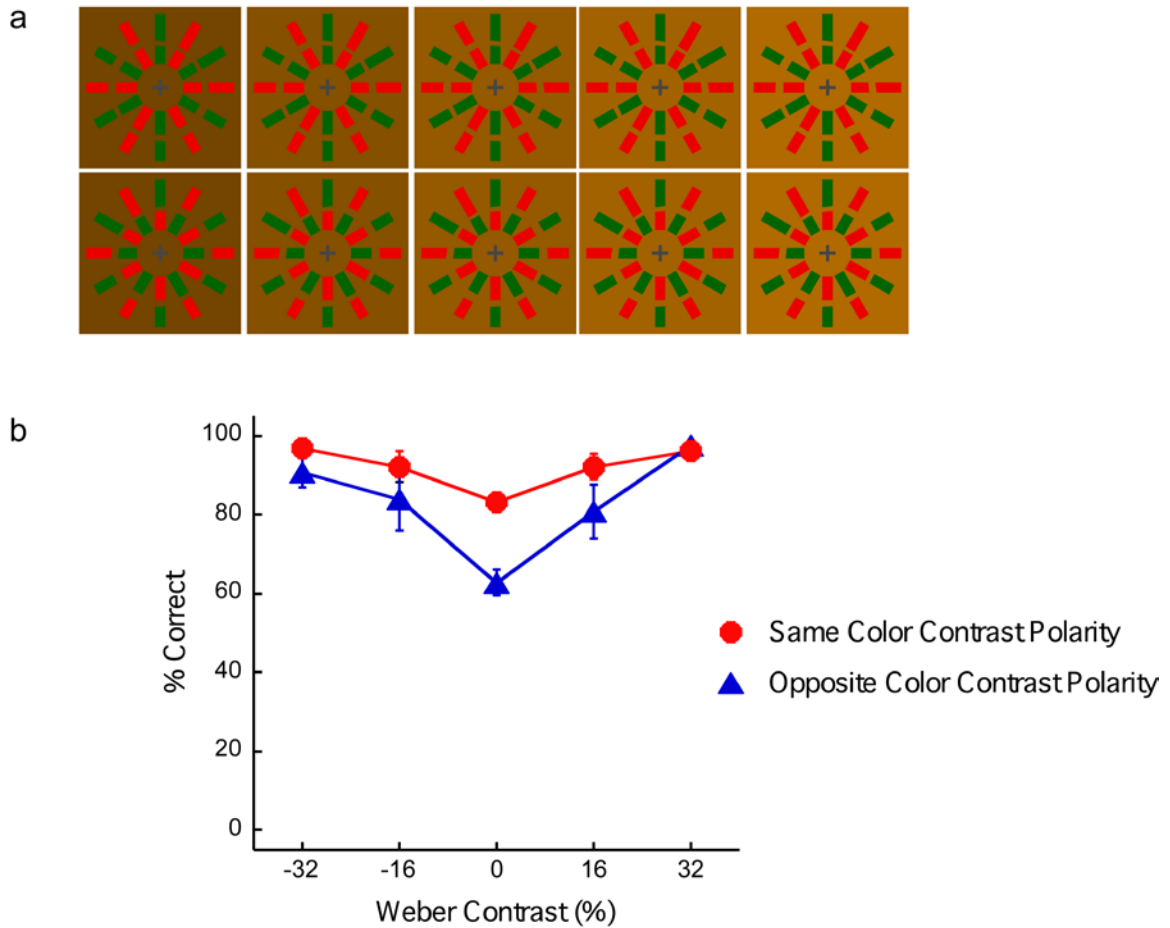
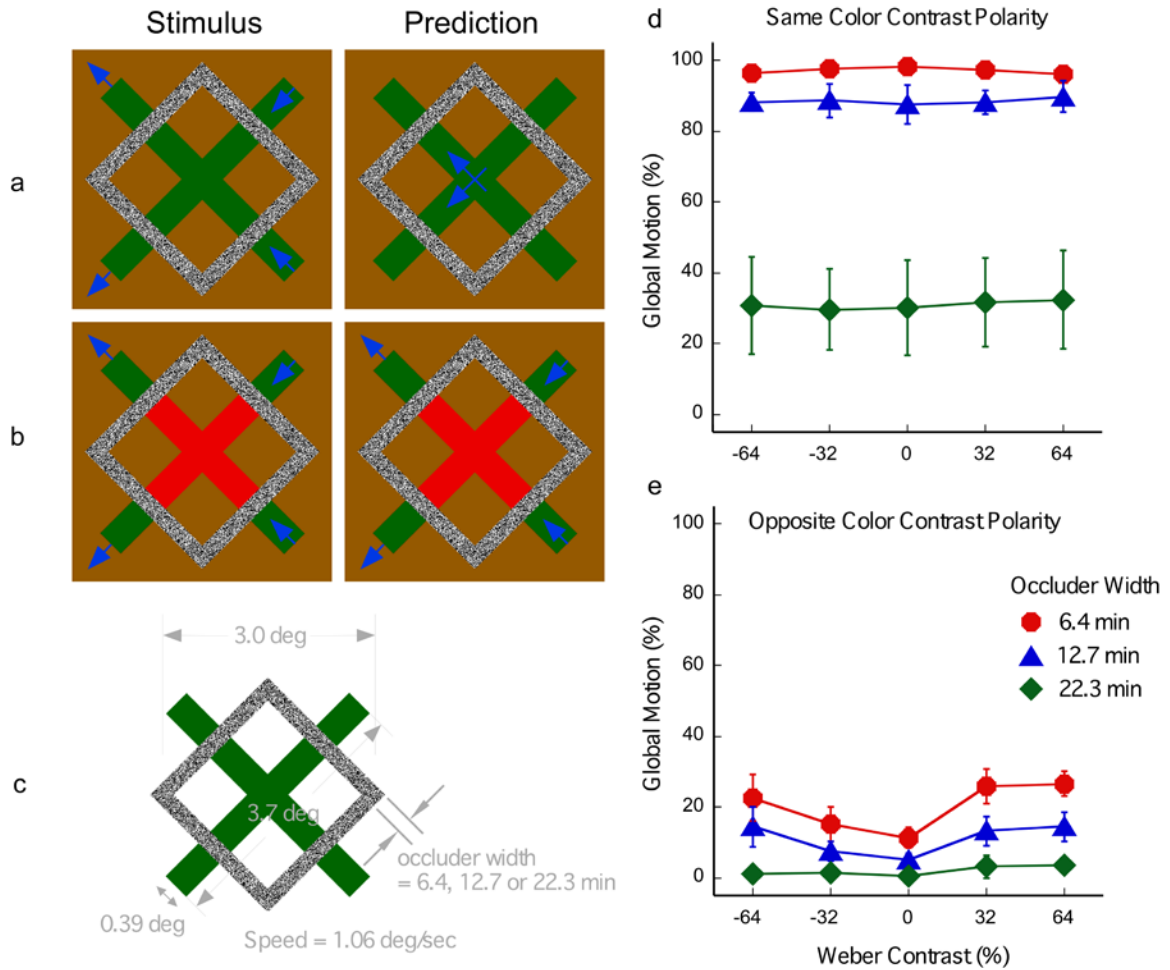
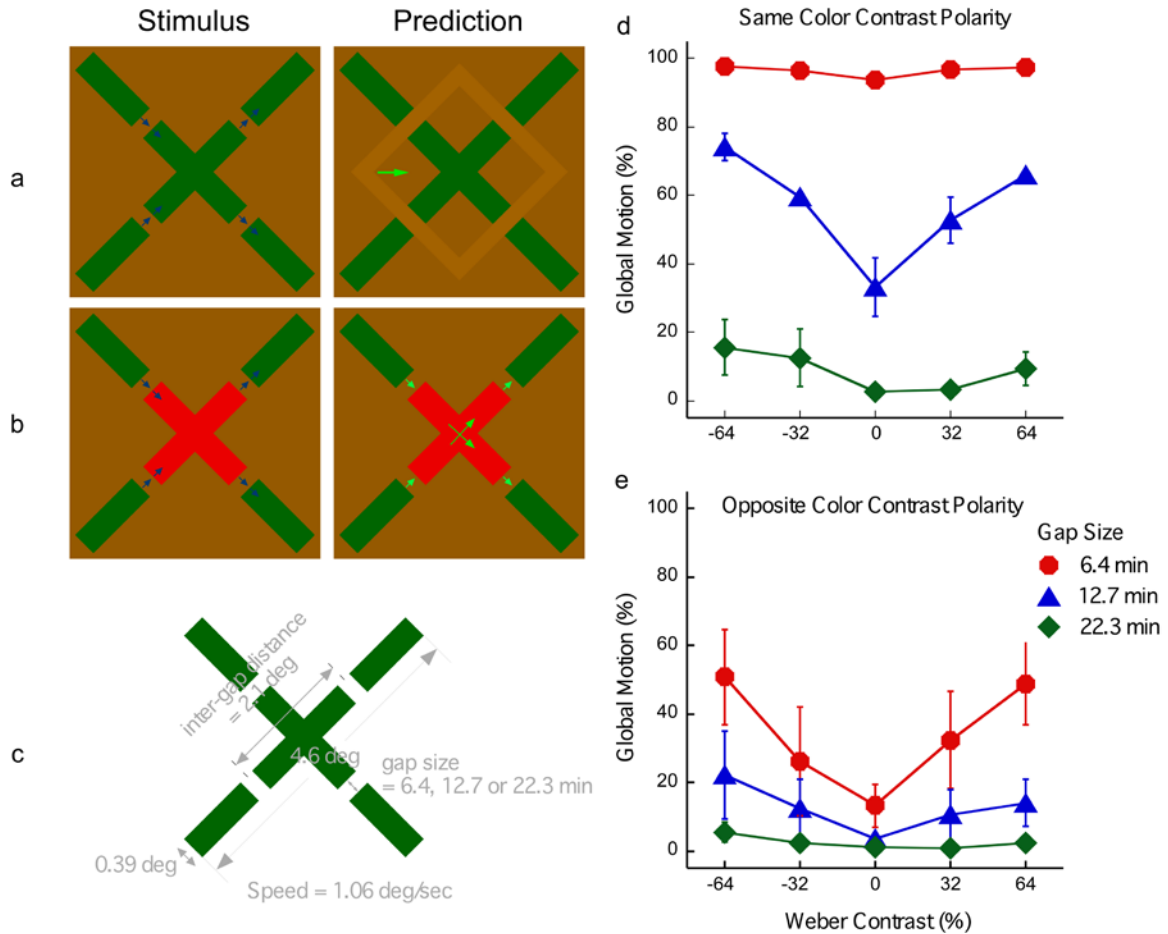


Fig. 7.4. Stimuli and results of Experiment 7.3. (a) The top-row stimuli have the same color contrast polarity and elliptical Illusory-O displays with the long axis oriented at  $135^\circ$ , while the bottom-row stimuli have opposite color contrast polarity with the long axis oriented at  $45^\circ$ . (b) The graph plots the percentage correct in discriminating the orientation of the elliptical Illusory-O for the same (red circles) and opposite (blue triangles) color contrast polarity conditions ( $n = 4$ ; 2 naïve observers and 2 authors). The data show a similar trend as the perceptual rating results in Fig. 7.2. The percentage correct is higher for the same than for the opposite color contrast polarity condition, with the largest difference occurring at equiluminance (Weber contrast=0). The vertical bars indicate the standard errors.





**Fig. 7.5.** Stimuli and results of Experiment 7.4. The basic stimulus design (left) comprises of oblique rectangular segments separated by a random-dot diamond frame (occluder). The inner rectangles and the diamond frame are static while the terminal endings of the outer rectangles have local motion signals (arrows). (a) In the same color contrast polarity condition the inner and outer rectangles have the same color, which can be either green or red (not shown). It is predicted (right) the aligned inner and outer rectangles are seen as a longer, partially occluded rectangle moving behind the diamond frame (arrows, global motion). (b) In the opposite color contrast polarity condition, the inner and outer rectangles have different colors. It is predicted (right) the outer rectangles are seen as compressing and expanding (arrows). (c) The dimensions of the stimulus. (d and e) The results, respectively, for the same color and opposite color contrast polarity conditions ( $n = 4$ ; 3 naïve observers and 1 author). For both conditions, the percentage of seeing global motion decreases with increasing width of the occluder (diamond frame). More global motion is seen in the same color contrast polarity condition (d) than in the opposite color contrast polarity condition (e). The vertical bars indicate the standard errors.



**Fig. 7.6.** Stimuli and results of Experiment 7.5. The basic stimulus design is similar to the one in Experiment 4 except with the diamond frame occluder removed to expose the four gaps. The terminals of the inner and outer rectangular segments facing the gaps carry the local motion signals (arrows). (a) In the same color contrast polarity condition (left) the inner and outer rectangles have the same color, which can be either green or red (not shown). It is predicted (right) the four gaps form an illusory diamond frame that moves laterally back and forth over a larger, partially occluded cross due to the amodal integration of the aligned inner and outer rectangular segments. (b) In the opposite color contrast polarity condition, the inner and outer rectangles have different colors. It is predicted (right) the two inner rectangular segments slide over one another while the outer segments facing the gaps expand and contract. (c) The dimensions of the stimulus. (d & e) The results, respectively, for the same color and opposite color contrast polarity conditions ( $n = 4$ ; 3 naïve observers and 1 author). The data for the mid-gap size in the same color contrast polarity condition and for the small-gap size in the opposite color contrast polarity condition exhibit an obvious V-shaped trend with its bottom at the equiluminous background setting (Weber contrast=0). Overall, for the same gap size, more global motion is seen in the same color contrast polarity condition (d) than in the opposite color contrast polarity condition (e). The vertical bars indicate the standard errors.

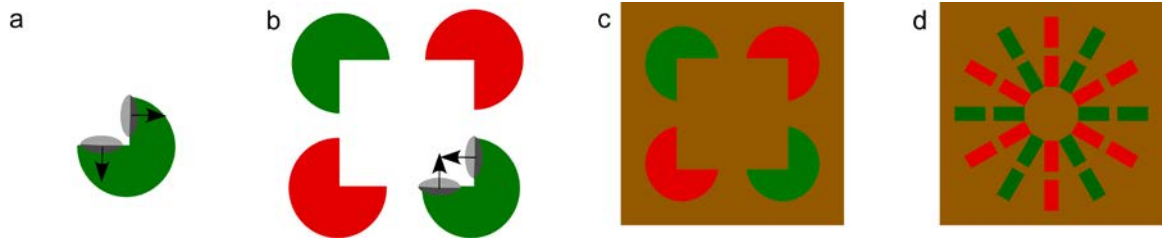


Fig. 7.7. (a) When a pacman element is seen by itself, the functional BO units at the horizontal and vertical edges signal that the pacman owns the borders. This is the basis in which the pacman is perceived as a figure in the foreground. (b) When the pacman is displayed in the vicinity of other pacmen that are aligned with it in the Kanizsa square formation, the functional BO units signal that the white square image, instead of the pacmen, own the borders. The “unbound” pacmen are thus amodally extended behind the white image patch (illusory surface). (c & d) Comparison of the Kanizsa illusory square and Illusory-O stimuli at equiluminance. The perceived illusion is stronger with the Illusory-O in (d) than with the Kanizsa illusory square in (c). We propose this is due to the Illusory-O stimulus having more contextual information than the Kanizsa square stimulus; namely, two aligned edges and small gaps that favor amodal surface integration.

APPENDIX II  
COPYRIGHT CLEARANCE

- A. The contents in chapter 1 were published on PNAS (Su, He, & Ooi, 2009; see *REFERENCES* for details). PNAS does not require authors to obtain permission for re-using the published material in their dissertations:

“Authors do not need to obtain permission for the following uses of material they have published in PNAS: (1) to use their original figures or tables in their future works; (2) to make copies of their papers for their classroom teaching; or (3) to include their papers as part of their dissertations. Please cite the original PNAS article in full when re-using the material. Because this material published after 2008, a copyright note is not needed.”

- B. The contents in chapters 2, 4, and 7 were published on Vision Research (Su, He, & Ooi, 2010c, 2011b, 2010b; see *REFERENCES* for details). The copyright clearances have been obtained, as attached in the following pages.

## ELSEVIER LICENSE TERMS AND CONDITIONS

Oo

This is a License Agreement between Yong Su ("You") and Elsevier ("Elsevier") provided by Copyright Clearance Center ("CCC"). The license consists of your order details, terms and conditions provided by Elsevier, and the payment terms and conditions.

**All payments must be made in full to CCC. For payment instructions, please see information listed at the bottom of this form.**

Supplier	Elsevier Limited The Boulevard, Langford Lane Kidlington, Oxford, OX5 1GB, UK
Registered Company Number	1982084
Customer name	Yong Su
Customer address	25 Washington Ln, Apt 516 WYNCOTE, PA 19095
License number	3498351207138
License date	Oct 29, 2014
Licensed content publisher	Elsevier
Licensed content publication	Vision Research
Licensed content title	The magnitude and dynamics of interocular suppression of monocular boundary contour and conflicting local features
Licensed content author	Yong R. Su, Zijiang J. He, Teng Leng Ooi
Licensed content date	24 September 2010
Licensed content volume number	50
Licensed content issue number	20
Number of pages	11
Start Page	2037
End Page	2047
Type of Use	reuse in a thesis/dissertation
Intended publisher of new work	other
Portion	full article
Format	both print and electronic
Are you the author of this	Yes

[Print This Page](#)

## ELSEVIER LICENSE TERMS AND CONDITIONS

Oc

This is a License Agreement between Yong Su ("You") and Elsevier ("Elsevier") provided by Copyright Clearance Center ("CCC"). The license consists of your order details, terms and conditions provided by Elsevier, and the payment terms and conditions.

**All payments must be made in full to CCC. For payment instructions, please see information listed at the bottom of this form.**

Supplier	Elsevier Limited The Boulevard, Langford Lane Kidlington, Oxford, OX5 1GB, UK
Registered Company Number	1982084
Customer name	Yong Su
Customer address	25 Washington Ln, Apt 516 WYNCOTE, PA 19095
License number	3498351398650
License date	Oct 29, 2014
Licensed content publisher	Elsevier
Licensed content publication	Vision Research
Licensed content title	Revealing boundary-contour based surface representation the time course of binocular rivalry
Licensed content author	Yong R. Su, Ziji Jiang J. He, Teng Leng Ooi
Licensed content date	1 June 2011
Licensed content volume number	51
Licensed content issue number	11
Number of pages	9
Start Page	1288
End Page	1296
Type of Use	reuse in a thesis/dissertation
Intended publisher of new work	other
Portion	full article
Format	both print and electronic
Are you the author of this	Yes

[Print This Page](#)

## ELSEVIER LICENSE TERMS AND CONDITIONS

Oo

This is a License Agreement between Yong Su ("You") and Elsevier ("Elsevier") provided by Copyright Clearance Center ("CCC"). The license consists of your order details, terms and conditions provided by Elsevier, and the payment terms and conditions.

**All payments must be made in full to CCC. For payment instructions, please see information listed at the bottom of this form.**

Supplier	Elsevier Limited The Boulevard, Langford Lane Kidlington, Oxford, OX5 1GB, UK
Registered Company Number	1982084
Customer name	Yong Su
Customer address	25 Washington Ln, Apt 516 WYNCOTE, PA 19095
License number	3498351283646
License date	Oct 29, 2014
Licensed content publisher	Elsevier
Licensed content publication	Vision Research
Licensed content title	Boundary contour-based surface integration affected by co
Licensed content author	Yong R. Su, Zijiang J. He, Teng Leng Ooi
Licensed content date	23 August 2010
Licensed content volume number	50
Licensed content issue number	18
Number of pages	12
Start Page	1833
End Page	1844
Type of Use	reuse in a thesis/dissertation
Intended publisher of new work	other
Portion	full article
Format	both print and electronic
Are you the author of this Elsevier article?	Yes

- C. The contents in chapters 3 and 6 were published on Journal of Vision (Su, He, & Ooi, 2011a, 2010a; see *REFERENCES* for details). ARVO is the copyright holder of these articles (including images, etc.). However, to re-use the materials in the primary author's own works is allowed without requiring any extra permission:

“Because you are the primary author of these manuscripts, we do not require you to seek permission to use your materials in your own works. We only require that you include a full citation which includes acknowledgement that ARVO is the copyright holder of these articles/images/etc.”



## CURRICULUM VITA

Yong Su

25 Washington Lane  
Apt 516  
Wyncote, PA 19095

### EDUCATION:

University of Louisville.....Louisville, KY  
Ph.D. in Experimental Psychology.....expected in 2014

University of Science and Technology of China.....Hefei, China  
Bachelor of Science in Bioscience.....1999  
Bachelor of Engineering in Computer Science and Technology.....1999

PROFESSIONAL SOCIETY: Vision Sciences Society

### PUBLICATIONS:

- Ooi, T.L., Su, Y., Natale, D., & He, Z.J. (2013). A push-pull treatment for strengthening the ‘lazy eye’ in amblyopia. *Current Biology*, **23**(8): R309–R310.
- Su, Y., He, Z.J., & Ooi, T.L. (2011). Revealing boundary-contour based surface representation through the time course of binocular rivalry. *Vision Research*, **51**(11): 1288–1296.
- Su, Y., He, Z.J., & Ooi, T.L. (2011). Seeing grating-textured surface begins at the border. *Journal of Vision*, **11**(1): 1–14.
- Su, Y., He, Z.J., & Ooi, T.L. (2010). The magnitude and dynamics of interocular suppression affected by monocular boundary contour and conflicting local features. *Vision Research*, **50**(20): 2037–2047.
- Su, Y., He, Z.J., & Ooi, T.L. (2010). Boundary contour-based surface integration affected by color. *Vision Research*, **50**(18): 1833–1844.
- Su, Y., He, Z.J., & Ooi, T.L. (2010). Surface completion affected by luminance contrast polarity and common motion. *Journal of Vision*, **10**(3): 1–14.
- Su, Y., He, Z.J., & Ooi, T.L. (2009). Coexistence of binocular integration and suppression determined by surface border information. *Proceedings of the National Academy of Sciences (USA)*, **106**: 15990–15995.

CONFERENCE ABSTRACTS:

- Ooi, T.L., Su, Y., & He, Z.J. (2011). Probe detection reveals a border-to-interior scheme for perceiving a grating-texture surface. *Journal of Vision*, **11**(11): 1054a.
- Su, Y., Ooi, T.L., & He, Z.J. (2010). Representing grating-texture surface begins with spreading of grating-texture from the surface boundary contour. *Journal of Vision*, **10**(7): 1180a.
- Ooi, T.L., Su, Y., & He, Z.J. (2010). Color contrast polarity of boundary edge affects amodal and modal surface completion. *Journal of Vision*, **10**(7): 1179a.
- Li, X., Su, Y., Ooi, T.L., & He, Z.J. (2010). Differentiating the contributions of surface feature and boundary contour strengths in binocular rivalry. *Journal of Vision*, **10**(7): 335a.
- Su, Y., Ooi, T.L., & He, Z.J. (2009). Binocular suppression in the monocular boundary contour display starts early ( $\leq 80$  msec). *Journal of Vision*, **9**(8): 305a.
- Ooi, T.L., Su, Y., Xu, J.P., & He, Z.J. (2009). On boundary contour and center-surround factors in binocular rivalry. *Journal of Vision*, **9**(8): 306a.
- Su, Y., Ooi, T.L., & He, Z.J. (2008). Incompatible local features are unnecessary for binocular suppression. *Journal of Vision*, **8**(6): 242a.
- Su, Y., Ooi, T.L., & He, Z.J. (2007). The speed and spreading of binocular rivalry dominance from boundary contours. *Journal of Vision*, **7**(9): 59a.
- Su, Y., He, Z.J., & Ooi, T.L. (2006). The critical role of boundary contours in the early temporal processing of binocular rivalry. *Journal of Vision*, **6**(6): 853a.
- Ooi, T.L., He, Z.J., & Su, Y. (2005). Binocular rivalry is affected by surface boundary contours. *Journal of Vision*, **5**(8): 5a.
- Su, Y., Ooi, T.L., & He, Z.J. (2004). Surface and motion integration determined by luminance contrast polarity. *Journal of Vision*, **4**(8): 888a.